Microparticle Adhesion in Model Metered Dose Inhalers

Karolina Charlotte Kjellberg
(née Barck)

This thesis is submitted in partial fulfillment of the requirements for the degree of Doctor of Philosophy

The School of Pharmacy
University of London

2010

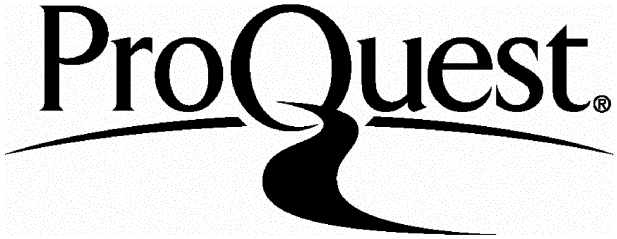

To my beloved husband, Jakob

Plagiarism statement

This thesis describes research conducted in the School of Pharmacy, University of London between October 2005 and October 2009 under the supervision of Professor Graham Buckton. I certify that the research described is original and that any parts of the work that have been conducted by collaboration are clearly indicated. I also certify that I have written all the text herein and have clearly indicated by suitable citation any parts of this dissertation that has already appeared in publication.

Signature

Date

Abstract

The factors that influence particle adhesion in model metered dose inhalers (MDI) have been investigated and models that predict the adhesion have been evaluated. Particle adhesion to the canister wall was correlated with Gibbs free energy of interaction based on surface energy parameters from sessile drop contact angle analysis, interaction parameters based on Hansen solubility parameters from Stefanis' group contribution method, forces of interaction from atomic force microscopy measurements and the physicochemical properties of the MDI components.

Non-pressurised model propellants were used throughout the study and simplified model formulations were studied consisting of two components, a powder compound (beclomethasone dipropionate, budesonide, terbutaline sulphate, polyacrylic acid and polyvinylalcohol) and a model propellant (2H,3H-perfluoropentane, perfluoroheptane and perfluorodecalin) that were filled into different canisters (polyethyleneterephtalate, aluminium, anodised aluminium, perfluoroalkane coated aluminium and glass).

The true adhesion of microparticles in model MDIs was studied with a method developed here and significant differences ($p<0.05$) in adhesion were found between the different MDI systems studied (0.02 - 47.6%w/w). It was also found that the adhesion reached a maximum within 60 minutes.

Among the methods for predicting interactions Gibbs free energy of interaction calculated using the surface component approach resulted in the best predictions of adhesion trends. It was found that even low polarity of materials involved had an important impact on the predicted interactions. Both apolar and polar energies of interactions were important to consider and the energy of interaction of particle-canister immersed in a liquid (ΔG_{132}) and the energy of interaction of particle-particle immersed in a liquid gave the best predictive model for the true adhesion in model MDIs since the interactions considered the intermaterial interactions in presence of the liquid. The linearity found when plotting the true adhesion of particles to a canister material against ΔG_{132} was considered good (R^2 0.6855 – 0.9987).

Acknowledgements

I would like to express my sincere gratitude to everyone who has made this thesis possible. In particular I would like to thank:

Prof. Graham Buckton, my first supervisor at the School of Pharmacy, for his profound knowledge and encouragement, experience, constructive criticism and willingness to answer all kinds of questions.

Dr. Philippe Rogueda, my previous supervisor at AstraZeneca, for his exciting ideas initiating this work, scientific guidance, interesting discussions, enthusiasm and kind spirit.

Dr. Simon Gaisford, my second supervisor at the School of Pharmacy, for his never failing enthusiasm, inspiration, positive attitude and encouragement.

AstraZeneca for financial support and Dr. Clive Washington, my current supervisor at AstraZeneca and colleagues at the Charnwood site in Loughborough, Dr. Agnes Colombani, Dr. Nayna Govind and Julien O'Brien for their scientific guidance and support.

Prof. Véronique Rosilio and her team at Université Paris-Sud, Department Physico-Chimie des Surfaces in Paris, France for great support and guidance in theoretical as well as experimental work in the area of surface energy analysis by contact angle and the ULLA consortium for the PhD grant that enabled my guest research in Paris.

My PhD student colleagues at the School of Pharmacy, Dr. Matthew Jones, Dr. Roy Turner, Dr. Ke Peng, Dr. Gabriela Oliveira, Dr. Tiago Sousa, Dr. Hisham Al-Obadi, Dr. Michael Pollit and many more who have been an enormous support in overcoming obstacles by discussing ideas and problems. Also staff at the School of Pharmacy, in particular Dr. David McCarthy for top quality SEM service, Rachael Bilginer and Catherine Baumer for impeccable organisation of everything surrounding the PhD and John Frost for building required equipment.

Finally my family, in particular my husband Jakob Kjellberg, for encouraging me to complete this work by being a constant source of support and inspiration giving me enthusiasm and drive to follow this work through.

Table of Contents

List of Figures

List of Tables

Abbreviations

a	– molar surface area of IGC probe
AFM	– atomic force microscope
AN	– Gutmann electron acceptor number
API	– active pharmaceutical ingredient
BDP	– beclomethasone dipropionate
CFC	– chlorofluorocarbon
COPD	– chronic obstructive pulmonary disease
δ_d	– dispersive contribution to Hansen solubility parameter
δ_p	– polar contribution to Hansen solubility parameter
δ_h	– hydrogen bonding contribution to Hansen solubility parameter
DN	– Gutmann electron donor number
ΔE^A	– internal energy of adsorption
ε	– dielectric constant
FDA	– food and drug administration
ΔG	– free energy of interaction based on surface energy parameters
ΔG^{LW}	– apolar free energy of interaction based on surface energy parameters
ΔG^{AB}	– polar free energy of interaction based on surface energy parameters
ΔG_{ij}	– polar free energy of interaction based on surface energy parameters, between compound *i* and compound *j*
ΔG_{ikj}	– polar free energy of interaction based on surface energy parameters, between compound *i* and *j* immersed in liquid *k*
γ	– surface free energy
γ^x	– surface free energy of material x
γ_{Ly}	– surface free energy of a liquid y
γ^{LW}	– dispersive component of surface free energy
γ^{AB}	– polar component of surface free energy
γ^+	– electron acceptor component of surface free energy
γ^-	– electron donor component of surface free energy
H	– contact angle hysteresis
HFA	– hydrofluoroalkane

HPLC – high-performance liquid chromatography

HPFP – 2H,3H-perfluoropentane

IGC – inverse gas chromatography

K_A – electron acceptor number

K_D – electron donor number

MDI – metered dose inhaler

μ – mean value

N – avogrado's number

N_i – amount first-order groups of type *i* in compound

C_i – first-order contribution of group *i*

N_j – amount second-order groups of type *j* in compound

C_j – first-order contribution of group *j*

PET – polyethyleneterephtalate

PFH – perfluoroheptane

PFD – perfluorodecalin

pMDI – pressurised metered dose inhaler

θ – contact angle

θa – advancing contact angle

θr – receding contact angle

R – gas constant

R_{RMS} – root mean squared roughness

SD – standard deviation

SEM – scanning electron microscopy

σ – standard deviation

T – absolute temperature

TGA – thermal gravimetric analysis

V_G – specific retention volume

V_N – net retention volume

V – molar volume

V_P – molar volume of IGC probe

VIF – variance inflation factor

XRPD – x-ray powder diffraction

ϕ – interaction parameter based on Hansen solubility parameters

Chapter 1: Introduction

Worldwide hundreds of millions of people are suffering from chronic respiratory diseases, which are considered the worlds 6th most common cause of death, more common causes of death are cardiovascular and communicable diseases, cancer and injuries (Bousquet and Khaltaev, 2007). Asthma and chronic obstructive pulmonary disease (COPD) are two common chronic respiratory diseases complicating people's everyday life worldwide and research to improve existing drugs as well as invent new ones is constantly advancing. Pulmonary delivery is very efficient for asthma and COPD active pharmaceutical ingredients (API) such as corticosteroids, β-agonists and anticholergenics since they are directly delivered on the target cells. It is also an effective delivery form for other diseases due to the rapid absorption and release in the bloodstream, minimized dose and minimised side effects compared to the same drug delivered orally (Dalby and Suman, 2003).

API delivery through the respiratory tract is also a popular research field for the treatment of diseases other than respiratory ones since the respiratory tract is considered a mild environment compared to the gastrointestinal tract. Degradation of compounds sensitive to the gastrointestinal tract's acidity, such as peptides and proteins, could be avoided if they were delivered through the respiratory tract, however there are problems like poor stability, side effects and short action (Bi and Zhang, 2007). Insulin for diabetes treatment is an example of how patient's life could be improved by replacing delivery through injections with pulmonary delivery and Pfizer was the first company to bring such a product, Exubera, to the market. Exubera was unfortunately withdrawn from the market due to the poor sales and the reasons for the poor sales have not been fully established (Bailey CJ 2007). Clinical trials had confirmed the short-term safety of the product but no long-term effect of the product had been investigated (Skyler et al., 2006, Rosenstock et al., 2004). Other issues with Exubera were the device shape and size and the low control in delivered dose compared to conventional injections of insulin. As a result several major institutions (National Institute for Health and Clinical Excellence, Diabetes UK, Association of British Clinical Diabetologists) and nurses' organisations did not recommend Exubera unless the patient had needle phobia since

they were not convinced of the benefits of inhalation of insulin over injections (Bailey CJ 2007).

1.1 Pulmonary Drug Delivery

1.1.1 Pulmonary Disease and the Respiratory Tract

In spite of asthma being a widely under-treated disease worldwide it is estimated to account for as much as 1-2 per cent of the total health care budget in developed countries (Shaya et al., 2008). An estimated number of people suffering from asthma in either mild, moderate or severe form is 300 million worldwide, 30 million in Europe and 10.1 million in the United Kingdom and Republic of Ireland (Masoli et al., 2004). Not all people suffering from the disease are diagnosed and therefore the number of asthmatics is greater than the numbers registered. When asthma is diagnosed and the patient is given the right medical treatment the symptoms are reduced significantly and the patient's life is improved. Asthma is a disease that could cause everything from slightly lower breathing capacity to death, though the death rate is fairly low compared to other chronic diseases. A patient suffering from asthma has an excess mucus production, airway inflammation and a reduced function of the ciliary clearance mechanism (World Health Organization, 2008a). Typical symptoms are cough, dyspnoea, wheezing, chest pain, chest tightness and sputum production and the asthma symptomes are worsen by environmental causes like dust, pollen, cigarette smoke, pet fur and pollution. Asthma is a well-known chronic disease first mentioned 3500 years ago in Egyptian Ebers Papyrus and in the first book on asthma, written by doctor Maimonides 1190 AD where he recommends a treatment consisting of a diet of large amounts of chicken soup together with refrain from sexual activity. Times have changed and asthma treatment has developed enormously since then and is today improving life for many asthmatics that would find everyday life unbearable without treatment.

COPD is a general name for chronic bronchitis, emphysema, chronic obstructive airway disease, chronic airflow limitation and some severe cases of chronic asthma (World Health Organization, 2008b). The world health organisation (WHO) reported in their annual world health report that approximately 210 million people worldwide suffer from COPD and around 3 million die from it each year (Masoli et al., 2004). A recent study has shown that the burden of COPD and asthma is significantly higher than the

burden of asthma alone (Shaya et al., 2008). The study showed that patients suffering from COPD or COPD and asthma were sicker and used medical services to a higher extent than asthma patients alone. The symptoms mentioned earlier for asthma are also symptoms of COPD but additional symptoms that are only seen in COPD patients are chronic bronchitis and lung emphysema. Further COPD is different from asthma since the condition is not fully reversible. COPD develops slowly, which is a major problem and as a result the patient is often unaware of the disease until the severe symptoms appear and the state is irreversible. The main cause of COPD is tobacco smoke but pollution could also cause COPD (World Health Organization, 2008b) and ceasing smoking improves the condition but does not cure it. A worldwide attempt to decrease deaths by COPD is the implementation of national smoking ban.

The lung volume of a healthy person is approximately six litres and air enters the respiratory system through the nose and is further transported to the lungs where gas exchange takes place. The upper airways include nose, mouth, nasal cavity and oropharynx, Figure 1.1a, while the lower airways include larynx, trachea, bronchus, bronchioles and alveolus, Figure 1.1b (Carr, 2008). In aerosol inhalation therapy the mouth is where air enters and passes the oropharynx, larynx, trachea and bronchus, bronchioles and finally to the alveolus where oxygen and carbon dioxide exchange takes place, Figure 1.1c. This is called the blood-gas barrier and is mainly built up by alveolar epithelium and capillary endothelium (Groneberg et al., 2006). Hence, the main responsibility of the respiratory system is to supply the blood with fresh oxygen and remove carbon dioxide from the blood stream.

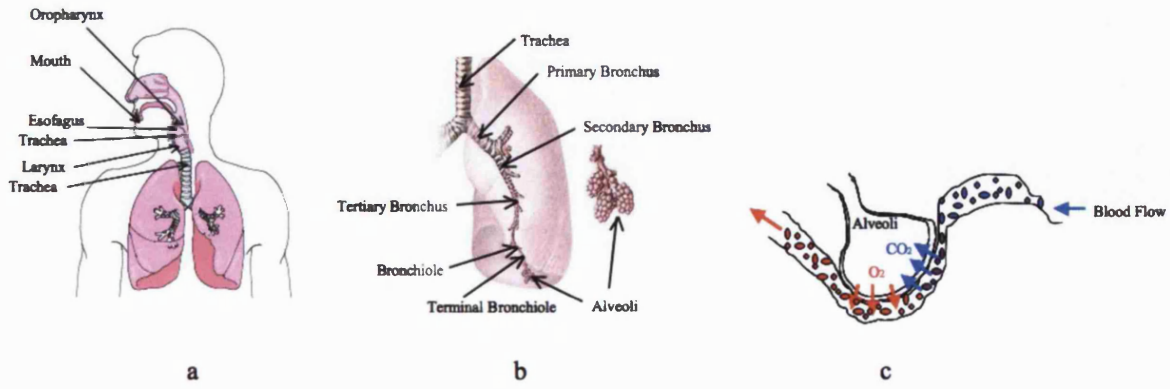

Figure 1.1 Images of: a) human respiratory tract, b) lower airways and c) carbon dioxide and oxygen exchange in an alveoli.

1.1.2 Particle Deposition in the Lung

During pulmonary drug delivery the drug is delivered through the respiratory tract with the aim of large particle deposition in the lower airways. A major disadvantage of drug delivery to the lungs is the large loss, around 70-95 % before the drug reaches the lower airways (Keller, 1999, Dolovich, 1995). The upper and lower respiratory tract are different in several aspects (Groneberg et al., 2006). First the upper airways have a smaller surface area and lower blood flow than the lower, secondly particles can easily be removed in the upper airways due to its high filtering capacity and finally the lower airways represents 95% of the lung's total surface area.

Several mechanisms need to be considered during particle deposition in the lungs (Groneberg et al., 2006). First inertial impaction, which is when large particles (3μm – up to more than 100 μm) of a certain velocity passes through the oropharynx and are deposited there and on the tongue because of their inability to follow the air stream. Hyperventilation can cause inertial impaction. Secondly sedimentation, when gravity affects particles (1-3μm) in the smaller airways and breath holding helps the mechanism. Thirdly diffusion, that leads to deposition of very small particles (0.5-1μm) in the bronchiole and alveolus, something that only affects a small percentage of the particles. Fourthly comes electrostatic precipitation that can cause adsorption of particles to the airways. Finally is the case when particles are very small and therefore exhaled before they have a chance to interact with the airways. To achieve deposition in the lower lung the particle size must be big enough to be affected by gravitational force but small enough to be absorbed in the alveolus. The final step to take into account in the lower respiratory tract is in the alveolus. The blood-gas barrier where the diffusion through alveolar epithelial cells is 10^3 times slower than through capillary endothelial cells, hence a rate limiting step (Groneberg et al., 2006). Regulation of airflow and particle size leads to an optimal delivery form and a good particle size for pulmonary delivery is 0.5-6 μm (Keller, 1999). It is hard to know the exact dose delivered since there is a large variation in inhalation ability leading to variations in drug deposition. Studies have shown that receptors for API groups, such as β-agonists, anticholinergics and corticosteroids are located in different parts of the lower airway. β-agonist receptors

are in large and small lower airways, anticholinergic receptors in the large and medium sized lower airways and corticosteroid receptors all over the lower airways including the small parts and alveolus (Terzano, 2001).

1.1.3 Pulmonary Delivery Devices

Pressurised metered dose inhalers (pMDI), dry powder inhalers (DPI) and nebulizers are the three main groups of devices on the market for pulmonary API delivery and amongst them pMDI are the most commonly used.

A DPI formulation consists of a dry powder blend where the most common blends consist of API and carrier particle such as lactose, which is there to minimize aggregation and enhance flow and dispersion (Telko and Hickey, 2005). DPIs are breath actuated and physicochemical properties such as particle size, shape and morphology has an impact on the aggregation, flow and dispersion and eventually the delivery to the lower airways (Telko and Hickey, 2005). There is a wide range of DPI devices available on the market and general issues and advantages with the devices will be discussed here. There are many advantages with DPIs since they are environmentally friendly, easy to use and only need to be activated by breath. Most devices indicate the remaining number of doses, but it is unfortunately rare that the DPI indicates if a dose has been properly inhaled (Richter, 2004). Device operation variations between manufacturers is another disadvantage, which could lead to confusion among patients (Terzano, 2001). Furthermore since DPIs are breath activated patients with lower respiratory capacity may have difficulties getting the right dose delivered to the target areas. The de-aggregation of particles and the delivered particle sizes are dependent on the inspiratory flow. The dry powder formulations are sensitive to humidity, which can cause problems both during manufacturing and the shelf life of the manufactured drug. It is also common that a DPI needs to be cleaned frequently and often it must be charged every time a dose is taken, which may be difficult for elderly arthritic patients. Finally it has been shown that only 60 per cent of patients manage to use a DPI properly (Terzano, 2001).

Nebulizers are suspension or solution based aqueous formulations that are aerosolised either by compressed gas or ultrasonic energy, then the aerosol is inhaled by the patient (Boulet et al., 1999). A nebulizer could be divided in two parts, the formulation and the

device; therefore the combination options are many, which enables purpose fit combinations for customers. The formulation is delivered through several breaths through a mask fitted to the face and since the dose varies with each breath the exposure time must be long to deliver a sufficient large dose to the lung, typically 10-15 minutes for a single dose (Dalby and Suman, 2003). Nebulizers are used for patients with limited inhalation capacity such as infants and young children, the elderly, those with severe asthma and COPD and emergency cases. Nebulizers are not as widely used as pMDI and DPI because of the high cost, long dose delivery time, low percentage of delivered dose, large device and need for cleaning. Even though nebulizers are bulky and not discrete for patients to use in their daily life they are highly suitable for hospital use where acute delivery of pulmonary APIs to patients is often required. Through a nebulizer APIs can be delivered easily to patients without training so very ill or injured patients who cannot inhale properly or handle handheld devices can be treated quickly.

1.1.3.1 Pressurised Metered Dose Inhaler

The most widely used pulmonary drug delivery devices are pMDIs and they have been on the market since 1959 (Dalby and Suman, 2003). In pMDIs the API is delivered to the respiratory tract by a high-speed aerosol. The API could either be dispersed or dissolved in a pressurised propellant. After actuation the formulation is pushed through the mouthpiece by the pressure in the canister, an aerosol spray is formed with fast-moving droplets containing particles that enter the airways, left image in Figure 1.2. The propellant evaporates and slow-moving particles proceed through the airways during inhalation, Figure 1.2.

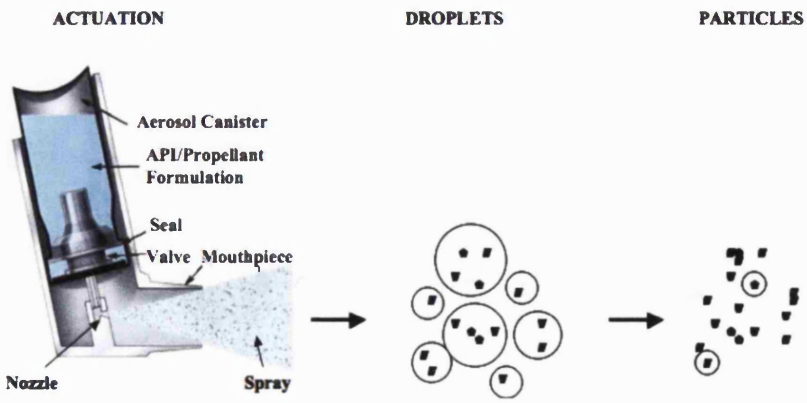

Figure 1.2. Particle delivery from a pMDI (Solvay, 2008).

A pMDI contains: drug, excipients, propellant, container, metered valve, actuator, nozzle and mouthpiece. The propellant used to be chlorofluorocarbons (CFC) but is nowadays hydrofluoroalkanes (HFA) because of environmental reasons. pMDI are very popular thanks to their efficient and quick drug delivery when used properly. Also different pMDI devices, independently of manufacturer, are operated in the same way (Terzano, 2001). Other factors making them popular are their small size, numerous doses of one device, long shelf life, low cost and microbial robustness (Keller, 1999). Even though there are many advantages with pMDIs there is room for improvements. More stable formulations could for example reduce the risk of particle caking, which may lead to dose variations. The adhesion to the pMDI valve components and container wall is an issue that can be resolved either by formulation optimization or coating the canister. The aerosol created determines the efficiency of the delivered dose and the aerosol nature is modified by the shape and size of the nozzle, actuator and valve.

Ironically the major issue with pMDI is that patients cannot use them properly, actually DPIs are considered easier to use. It has been reported that only 21 per cent of patients who had read the product instructions and 52 per cent who had been instructed by a health professional could use the pMDI correctly (Crompton, 2004). For a correctly delivered dose the patient first has to simultaneously actuate the pMDI and inhale deeply, then hold their breath for a few seconds to ensure sufficient delivery. The dose delivered varies between users and many devices still have no indication of remaining drug in the device. The introduction of spacers to enhance delivery has improved the pMDI delivery significantly. However due to the rapid transport of aerosol to the lungs a large drug deposition takes place in the oropharynx and is therefore swallowed. Also HFA causes a cold feeling in the oropharynx, the freon effect, which patients may find unpleasant. Even though there are numerous improvements to be made the pMDI is still the most popular delivery device for treatment of pulmonary disease (Crompton, 2004).

Generally the pMDI has not changed much since it was first introduced to the market. The major changes for pMDIs have been the introduction of spacers, breath-activated pMDIs and the change of propellants from CFC to HFA (Crompton, 2004). Seven years after the Montreal protocol was signed the two first HFA based pMDI were introduced to the market, proventil-HFA (3M Pharmaceuticals, St Pauls, Minnesota) and HFA albuterol sulphate (3M Health Care, Loughborough, UK) (Leach, 2005). Today's HFA

based pMDIs are superior to their CFC predecessors in many ways. The cold freon effect is reduced and lower doses can be delivered since the oropharyngeal deposit is significantly lower. Lower loss on the tongue and in the throat gives less systemic side effects. Further combination formulations where one pMDI contains both a corticosteroid and a β-agonist has been proven to give the same effect as inhaling them separately, where pMDI Symbicort® from AstraZeneca is a good example (Lyseng-Williamson and Simson, 2008). There is a constant competition between pMDI and DPI but pMDI remains the most popular device.

1.1.4 Suspension Formulation

An advantage with pMDI suspension formulations over pMDI solution formulations is that it is easier to control the stability of the API in suspension, since the API is more likely to degrade in solution (Smyth, 2003). As mentioned pMDIs generate aerosols and the advantages of delivering drugs as aerosols through the respiratory tract are numerous. Firstly the aerosol has a cooling effect and therefore irritation is reduced, secondly it minimises contamination and last the system is easy to control in terms of particle size, dose and physical form. An aerosol system consists of product concentrate and propellant. The product concentrate has active ingredients and excipients (i.e. antioxidants, surface-active agents and sometimes co-solvent).

1.1.4.1 Propellant

Stability in pMDI formulations is of great importance since instabilities could lead to significant dose variations. The pMDI market faced a great formulation challenge when the Montreal Protocol was signed in 1987 stating that substances like CFC, consuming stratospheric ozone should be phased out (UNEP, 2000). The change from CFC to HFA resulted in new and sometimes even better pMDIs (Leach, 2005). The existing CFC propellants, CFC 11, CFC 12 and CFC 114 were replaced by HFAs such as HFA 134a and HFA 227. These HFAs are also greenhouse gases but have lower ozone depletion potential than CFCs, Table 1.1, and are therefore considered less environmentally damaging and since they resembled the CFCs in terms of physicochemical properties they were approved as new propellants in pMDIs by the FDA. When CFCs were replaced by HFAs new formulation challenges, such as poor surfactant solubility, increased API solubility, particle size variations depending on actuator design and leaking seals appeared (McDonald and Martin, 2000). The higher solubility in HFAs for

many APIs lead to solution formulations replacing the more physically stable suspension formulations pMDIs in several cases (Lewis et al., 2005). Many of the issues that appeared when HFAs were first introduced as propellants in pMDIs have to a large extent been overcome today and new interesting delivery systems are available on the market and are being developed. Some examples are Pulmicort pMDI® from AstraZeneca, Clenil® from Chiesi Farmaceutici and Ventolin HFA® from GlaxoSmithCline.

Table 1.1. Physicochemical properties of propellants (McDonald and Martin, 2000, Smyth, 2003).

Physicochemical Property	CFC 11	CFC 12	CFC 114	HFA 134a	HFA 227
Boiling Point (°C)	23.7	-29.8	3.6	-26.5	-17.3
Vapour Pressure (psig @ 20°)	-1.8	67.6	11.9	68.4	56.0
Dielectric Constant	2.3	2.1	2.2	9.5	4.1
Density (g/ml)	1.49	1.33	1.47	1.21	1.41
Viscosity (mPas)	0.43	0.22	0.36	0.22	0.26
Ozone Depletion Potential	1	1	0.7	0	0

*Relative to CFC 11

The dielectric constant of propellants clearly indicates that the polarity of HFA is higher than CFC. This is due to fluorine being more electronegative than chlorine, which creates a distinct dipole on the hydrogen-carbon bonds in hydrofluoroalkanes (Vervaet and Byron, 1999). The propellant polarity will influence the behaviour of particles and molecules in the formulation. Further the boiling point and vapour pressure has an impact on device filling as well as API delivery. For instance in HFA based devices the cold freon effect is reduced thanks to higher spray temperature and less impact force in the oropharynx (Leach, 2005). The higher vapour pressure in HFA compared to CFC increases the plume velocity in the pMDI, which is positive since it leads to smaller droplets that can reach the whole respiratory tract. It has also been shown that a higher plume speed can contribute to reduced particle residue in the canister (Tiwari et al., 1998). The same study also showed that a higher plume speed leads to higher particle deposition in the oropharynx. Finally the smaller particle size makes inspiration flow less important, hence operation of pMDI easier.

1.1.4.2 Active Pharmaceutical Ingredient

Commonly used active pharmaceutical ingredients (API) for asthma and COPD treatment are anti-inflammatory corticosteroids and bronchodilatating β2-antagonists. Suspension has been preferred over solution formulation since it is considered more stable as API in solution is more sensitive to chemical degradation. However, instabilities in a suspension formulation could cause long- or short-term irreversible particle agglomeration and adhesion to the canister. The API in an ideal suspension formulation should be insoluble in the propellant. The API solubility in HFA can be decreased by altering salt, polymorphic form or the amount of amorphous content (Vervaet and Byron, 1999). The increase in polarity when using HFA causes increased solubility of API in suspension. Since many APIs are more soluble in HFAs processes such as Ostwald ripening (crystal growth), solvate and polymorph formation can occur and lead to increase in particle size, agglomeration and adhesion to the canister walls (Beausang, 2005). If solubility of an API is measurable in the propellant there is a high risk of crystal growth that will cause particle size increase upon storage (Vervaet and Byron, 1999). Crystal growth is also favoured if amorphous regions are present in crystalline materials. Often crystalline materials get amorphous regions during processing. When particles in a suspension are in the micrometer range the total particle surface area and also the surface free energy is large. Therefore the system tries to minimise its total surface free energy by particle agglomeration and adhesion to the canister surface (Parsons et al., 1992). In low API concentration suspensions this effect can cause significant dose variations and lead to insufficient API delivery following storage. However the crucial time when particle agglomeration must not occur is in the short term, between shaking and actuation of a pMDI.

1.1.4.3 Surfactant

Surfactants are used to enhance the dose uniformity in pMDI formulations by preventing irreversible particle agglomeration, adhesion to the canister and degradation of dissolved API (Michael 2001, Young 2003, Tiwari). They could also be used to enhance API solubility in the propellant. Nowadays surfactants major task is to enhance suspension stability by reducing caking since polymeric coatings mostly are used to prevent canister adhesion. Coatings including fluorinated polymers, such as polytetrafluoroethylene (PTFE), perfluoroalkoxy (PFA) or fluorinated ethylene propylene (FEP), are extremely successful at eliminating adhesion of salbutamol in

HFA134a and 227 metered dose inhalers (Britto, 2007). Much is required from a pMDI coating since it must resist the high-pressure environment without releasing any material or molecules over the life of the pMDI. Unfortunately there are parts in the pMDI that cannot be coated with the fluorinated coatings. In the valve and nozzle adhesion remains and surfactants are needed. Surfactants make a formulation more stable by covering the particles and sterically hindering them from strong inter-particulate interaction. There are several surfactants available for HFA formulations (Wu et al., 2008a, Wu et al., 2008b, Beausang, 2005). In order to stabilise a suspension the surfactant should preferably be soluble in the propellant. It was problematic when the surfactants used in CFC formulations turned out to be much less soluble in HFA propellants. However it has been shown that low surfactant solubility also stabilises the suspension (Byron, 1994). A surfactant could act as a flocculation enhancer and force particles to aggregate (Hickey et al., 1988). The purpose of adding a flocculation enhancer is to decrease the inter-particulate interaction forces between particles so the energy required for de-aggregation decreases. Another successful way of decreasing flocculation could also be to match the density of the propellant with the API by mixing propellants with various densities (Govind et al., 2000).

1.2 Interfacial Interactions

There are two main types of interactions between materials, cohesive and adhesive interactions. When materials of the same compound and size interact cohesion takes place and when materials of different compounds interact adhesion occurs. Secondary bonds are far less energetic than primary bonds but still play an enormously important role in colloid and interface science since they are long range. Primary bonds are covalent bonds (bond dissociation energy > 40 kJ/mol, typical energy is 300-700 kJ/mol) while secondary bonds are hydrogen bonds, ionic bonds and van der Waals bonds (bond dissociation energy < 40 kJ/mol) (Zeng et al., 2001). There are also electrostatic forces (Coulombic) that act between charged particles, though they are often disregarded in HFA suspensions due to their small impact compared to other interactions (Young et al., 2003, Ashayer et al., 2004).

In order to understand and improve existing and forthcoming products in the pharmaceutical, food, paint, detergent and oil industry amongst others it is essential to study particles behaviour at interfaces. In a colloidal system Liftzich-van der Waals

forces are the dominating interactions (Parsons et al., 1992). Mass transport in colloids can occur through ion transport around charged particles or in liquid junctions, also by thermal diffusion, which is a temperature gradient that creates a heat flux with a following mass flux. Brownian motion dominates particle motion in a colloidal system with no energy applied from the outside, where particles size < 1μm (Jones, 2006).

1.2.1 Surface Tension

Surface tension is the work required to create a unit area of a surface. Liquids possess a surface tension that is caused by attractive intermolecular forces in the liquid. The surface tension is the overall inward force on the liquid molecules at a liquid/vapour interface. If taking the example of a water-drop in air, the water molecules on the drop surface are more attracted to water molecules in the drop bulk than to the air molecules. The water molecules on the surface of the drop do interact with the air molecules but those interactions are very small compared to the intra-molecular interactions in the drop. The formation of a drop is therefore a result of the perpendicular surface tension force going from the surface and inwards to the liquid. At constant temperature and pressure the surface tension is defined by the following equation (Everett, 1988).

$$\Delta W = -\Delta G = -\gamma \cdot \Delta A \tag{1.1}$$

where ΔG is the surface free energy, ΔW thee work of adhesion, ΔA the area change and γ the surface or interfacial tension. Surface tension is often used for a liquid in contact with vapour and interfacial tension for two liquids or a liquid and a solid in contact. Further γ is called surface energy when talking about solids.

1.2.2 Surface Energy

Surface energy of a solid can be determined by contact angle formed by liquid drops on the solid surface. The relationship between the interfacial interactions was first described by Young (1805).

$$\gamma_{LV} \cos\theta = \gamma_{SV} - \gamma_{SL} \tag{1.2}$$

where θ is the contact angle in Figure 1.3 and γ_{LV}, γ_{SV} and γ_{SL} the interfacial tension between the liquid-vapour, solid-vapour and solid-liquid interfaces respectively. Measuring the contact angle of a drop on a surface is a quick and easy method to determine the wettability of the surface. The contact angle can be measured optically and the method gives a direct measurement of the contact angle, which is a great advantage. Though, if surface energy is required calculations must be done. It is of great importance that all surfaces involved in the experiment are clean and free from dust, otherwise it is hard to know if the true contact angle is measured or that of the contaminant.

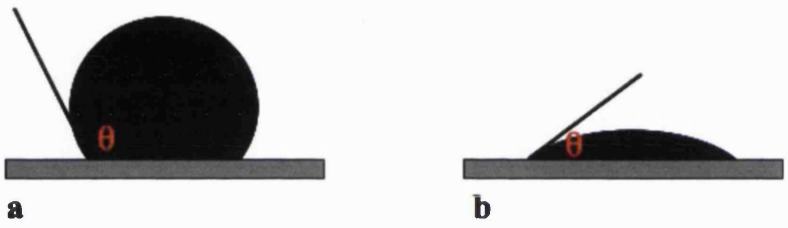

Figure 1.3. Contact angle between a drop and a solid surface. In a) $\theta > 90°$, wetting does not occur and b) $\theta < 90°$, wetting does occur.

Measuring contact angle is straight forward but one must consider a few things to get accurate results (Buckton, 1990, Buckton et al., 1995). First it is important to have a smooth surface to avoid hysteresis caused by physical surface heterogeneities that can give misleading contact angles. Second the drop has to be small enough to avoid the influence of gravitational forces on the shape. Third the viscosity of the liquid must be low enough to not affect the drop shape. Fourth if the powder compact is not saturated with the liquid used there is a possibility of the visible contact angle not being the real one, Figure 1.4b. Though saturating the powder compact may lead to swelling and deformation of the powder, which could also give inaccurate contact angle values. If the bed cannot be saturated another way of minimising the error in Figure 1.4 could be to measure the contact angle instantly after the drop forms.

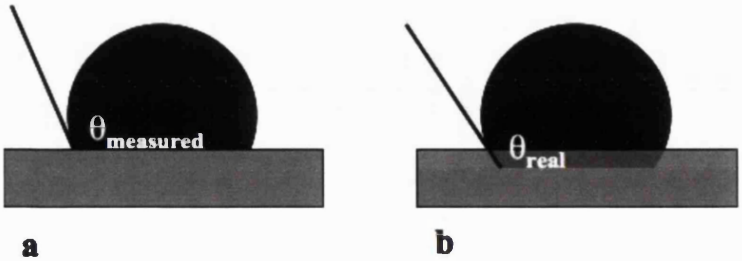

Figure 1.4. Contact angle error due to unsaturated powder bed, a) contact angle measured and b) real contact angle.

Fifth the drop is of dynamic nature which means that the contact angle changes with time. A way of getting around that problem is to always measure the contact angle at a certain time after drop deposition on the surface. Finally the preparation of compact discs may alter the powder's physical properties. Consequently the contact angle will not represent the powder before compaction. Even though all these errors exist contact angle is still a commonly used method, thanks to its simplicity.

The surface energy of solids can be calculated from the advancing contact angle from sessile drops. Surface energy parameters describing the polar and apolar nature of solid surface can be determined from contact angle and more details will follow in Chapter 4. Another very popular technique for surface energy determination is inverse gas chromatography, which will also be discussed in Chapter 4.

1.2.3 Apolar and Polar Interactions

Materials can be divided into two main groups, polar and apolar materials (Lyklema, 1991). Polar materials is the group name for Lewis acid-base compounds and apolar materials, also called Liftzich-van der Waals materials, is the group name for London dispersion forces, Keesome and Debye interactions (Lazghab et al., 2005). In non-aqueous pMDIs electrostatics are believed to have a less significant impact on the interactions between materials compared to Lewis acid-base and Liftzich-van der Waals interactions, which are believed to be the dominating interactions. London dispersion forces occur between non-polar molecules when their electrons are constantly moving and cause local charge imbalances. The interactions are complex, long range ($1 \cdot 10^{-9}$m), can be attractive or repulsive and a typical strength is 1 kJ/mol (van Oss et al., 1987). Keesome interactions (dipole - dipole) appears when two polar molecules (dipoles), one of opposite sign to the other (+ or -) interact and this is the dominating force when

hydrogen bonds are formed (van Oss et al., 1987). Debye interactions (dipole-induced dipole) occur when a dipole interacts with another molecule, which turns into an induced dipole and this is a temporary state where the side of the molecule facing the dipole's positive side becomes negative and vice versa (van Oss et al., 1987).

1.2.4 Capillary Interactions

When there are no particles present at a liquid interface it is flat but as soon as particles are present the surface deforms and capillary forces appear, the more the surface is deformed the stronger the capillary interactions become (Kralchevsky and Nagayama, 2000). Capillary flotation forces (particle radius > 5μm), Figure 1a-b, are driven by gravitational forces and therefore depend on the particle weight, the gravitational potential energy decrease as the particle inter-particulate distance decrease. Also the flotation forces decrease as the particle radius decrease. Two particles of the same size interact with attractive forces, Figure 1a, while two particles of different weight interact with repulsive forces, Figure 1b. Flotation forces no longer exist when the particle radius < 5μm, Figure 1c, since the thermal energy for such small particles exceeds the gravitational energy. For particles immersed in the liquid at the surface wetting drives the capillary immersion forces, Figure 1d, so the contact angle between the particle and the liquid determines the liquid surface deformation. As mentioned in Section 1.2.2 when the contact angle between the liquid surface and the immersed part of the particle is < 90° wetting occurs and if it is > 90° wetting does not occur. With increased interfacial tension the immersion forces increase and the flotation forces decrease, also when comparing the two forces immersion forces are much larger than flotation forces (Kralchevsky and Nagayama, 2000).

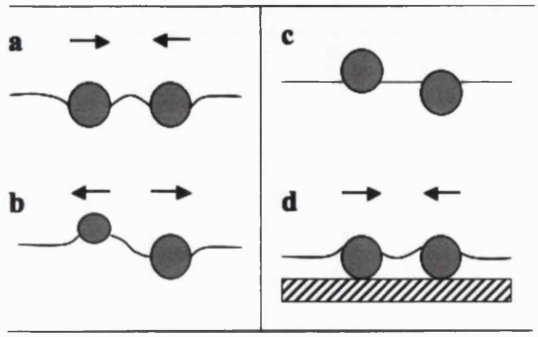

Figure 1.5. (Kralchevsky and Nagayama, 2000)

Floatation capillary forces by: a) attraction between two similar floating particles and b) repulsion between a heavy and a light floating particle, c) no flotation forces since no surface deformation or interaction for small floating particles in a liquid film, d) immersional capillary forces by attraction between two similar particles immersed in a liquid film on a solid substrate.

1.2.5 Heat and Mass Transfer

Heat transfer can take place through convection or conduction (Coulson et al., 1999). Heat transfer by conduction is when kinetic energy is transferred through a solid from a higher to a lower temperature. As high temperature matter collide with low temperature matter they transfer some of their kinetic energy, which results in a loss of kinetic energy (reduced speed) for the high temperature matter and gain of kinetic energy (increased speed) for the low temperature matter.

1.2.5.1 Convection

Convection can take place by heat or mass transfer and is when potential energy is transported through liquid or gaseous media by currents, Figure 1.6.

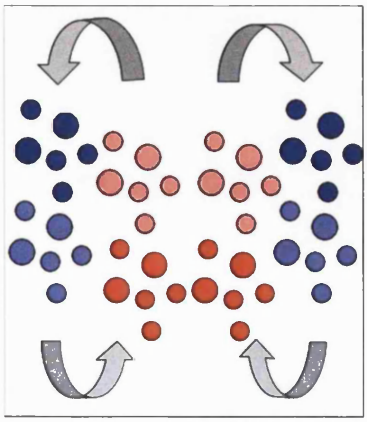

Figure 1.6. Schematic image of convection where red circles have lower density and blue circles have higher density.

Convection can either be natural or forced, natural convection is when no external source starts the convection and it starts by gravity differences. Forced convection is when an external source, such as a pump or a heater, starts the convection. Convection can be either thermal or solutal, the former is driven by density differences due to temperature gradients and the latter is driven by concentration gradients. When thermal convection acts on a system matter moves upwards by buoyancy forces since it is rising from a high temperature area, where the density is lower, to a low temperature area where the density is higher and matter sinks. When the high temperature matter meets the low temperature matter a heat exchange takes place. This is the most common form of convection and is called Rayleigh-Bénard convection (Coulson et al., 1999). If the convection is solutal matter move from a high to a low concentration area, causing interfacial turbulence and it has been well described and is called the Marangoni effect (Coulson et al., 1999). The Marangoni effect happens both when insoluble and soluble layers cover the surface (Cartwright et al., 2002). It may be induced by temperature, concentration and surface charge gradients through the interface (Morris and Parviz, 2006). If the surface tension decreases due to mass transfer, low surface tension areas will form and a spreading of dispersed material on the surface will occur. If the surface tension increases because of mass transfer the surface remains stable and no spreading takes place.

1.2.5.2 Particle Transport in Thin Films

In pMDI suspensions there is a pronounced particle activity at the liquid/gas/canister interface where the adhesion mainly takes place. Studies have shown that particle adhesion occurs above the fluid line in both sedimenting and creaming pMDI suspensions (Beausang, 2005). Section 1.2.5.1 described the driving forces for particle movements in a suspension and at the liquid/gas interface but other studies explaining the driving forces behind the activity by the liquid/gas/canister interface will be discussed here. The adhesion by the meniscus could be due to convective assembly that describes the agglomeration of particles in a wetting film by a solid surface due to lateral capillary forces driven by surface tension, Figure 1.7 (Nagayama, 1996). When convective assembly occurs first particles trapped in the film are attracted by each other through capillary immersion forces, then more particles from the suspension are dragged to the particles already trapped in the thin film regions. Hydrodynamic drag

forces are caused by the hydrodynamic flux created to compensate for the material loss due to evaporation at the thinner regions of the film. As long as there is a renewal of the liquid surface, in this case by more particles accumulating on the surface, mass transfer at the liquid-gas boundary will continue (Coulson et al., 1999). The particles trapped in the thinner film may crystallise when the liquid evaporates, which leads to adhesion. Particle transport in a suspension is driven by convection, Section 1.2.5.1, and effected by the wetting properties as well as the gas-liquid mass transfer by the liquid/gas/canister interface (Nagayama, 1996). When the surface tension of the liquid is lower the particles can easier deform the surface, which leads to higher capillary interactions (Nagayama, 1996). The propellants commonly used in pMDIs have low surface tension, which enables them to wet the canister surface well and they have low boiling point, leading to more liquid-gas mass transfer activity at the liquid/gas/canister interface (Rogueda, 2003, Coulson et al., 1999).

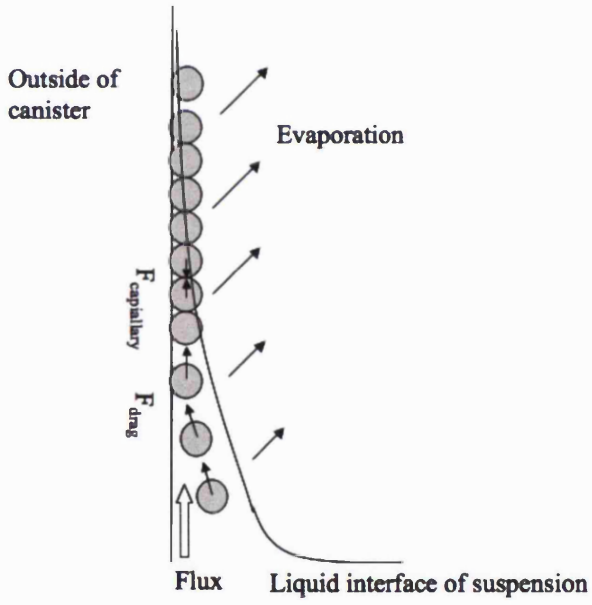

Figure 1.7. Possible convective assembly in a pMDI where cohesive capillary force $F_{capillary}$ and drag force F_{drag} is present.

Deegan explained the particle deposition by the liquid/solid/gas interface by the pinning effect by using the model of a coffee stain drying and forming a ring with high concentration of coffee on the outer edges of the stain (Deegan et al., 1997). Deegan studied the transport of solid material to the outer edges of a liquid drop optically (Deegan et al., 1997) and with a theory that predicts the flow velocity, rate of ring

growth and solute distribution within a drop (Deegan et al., 2000). The pinning effect appears due to the higher evaporation rate at the edges of a liquid drop compared to the centre, Figure 1.8, where the evaporation rate is lower due to the air above being saturated with vapour. To compensate for the material loss at the edges of the drop solid material is transported there and gradually a wall of solid material is built up at the edges. Finally when all liquid has evaporated a ring has formed due to the pinning effect.

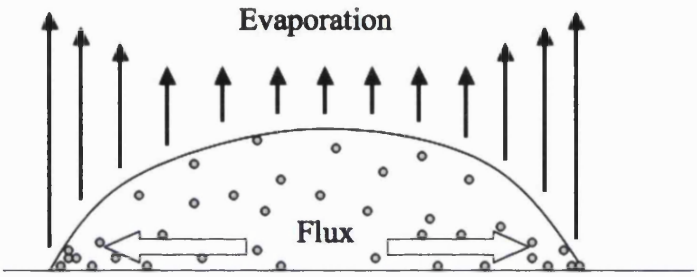

Figure 1.8. Pinning effect in a drop with particles.

1.3 Aim of Thesis

Pressurised metered dose inhalers are complex systems with a great variety of interactions, which needs to be considered to ensure optimal dose delivery and minimal adhesion to the canister wall. A deeper understanding of the interactions causing API loss by particle adhesion to the pMDI device would be helpful in a product design perspective in order to already at early stages create pMDI systems where minimal adhesion to the canister wall occur. Particle adhesion in pMDIs is a well-known problem that is currently mitigated by expensive canister coatings or surfactants in the formulation. The pMDI formulations have gone through significant development since the introduction of HFA propellants on the market and work has been done to explain the interactions that cause adhesion but more work is needed to get a good understanding of the interactions causing the adhesion in pMDIs since the systems are complex. Mostly when adhesion to pMDI canisters has been studied correlations have been made between adhesion in pMDIs and forces of interaction in model propellants that are liquid at room temperature. The reason for this is that many techniques used to study adhesive interactions in pMDIs cannot operate under pressurised conditions and therefore model propellants replace the propellants in pMDI formulations. However,

inaccurate correlations may be done when comparing pressurised MDIs with non-pressurised MDIs since the nature of the fluorinated liquid and pressure may have an impact adhesion.

The aim of this thesis was therefore to investigate non-pressurised MDIs based on model propellants throughout the study and look at when and where the adhesion occurs, find a suitable model to predict adhesion and evaluate what interactions has greatest impact on adhesion.

The areas in the model MDI systems focused on in this study were particle-canister, particle-liquid and particle-particle interactions. Due to the complexity of pMDI formulations simplified systems with three components were used in this study, including a powder compound, a fluorinated liquid and canister. Both theoretical and experimental approaches were evaluated to see how well they could predict and explain the true adhesion.

Chapter 2: Physicochemical Characterisation

In this chapter materials used in the model metered dose inhaler systems studied in this thesis were characterised. When comparing results a Student's t-test, two samples with same variance, was carried out with a significance level of 95% ($p < 0.05$).

2.1 Materials

In this study both polymer and API powders, hydrofluoroalkane and perfluoroalkane liquids and uncoated as well as coated canisters were used. The industrial grade polymers used were: polyacrylic acid (PAA) with an average molecular weight of 2 000 $g \cdot mol^{-1}$ (batch: 06107HD) was purchased from Sigma-Aldrich (UK), polyvinylalcohol (PVA) that was 98-99% hydrolyzed and had a molecular weight of 31 000 – 50 000 $g \cdot mol^{-1}$ (batch: 11329HD) was purchased from Sigma-Aldrich (UK) and polyvinylpyrrolidone K30 (PVP) with an average molecular weight of 30 000 $g \cdot mol^{-1}$ (batch: not available) was purchased from BASF (UK). The following micronised APIs were used: budesonide (batch: 05-000731AZ) and terbutaline sulphate (batch: 4103H) were donated by AstraZeneca (Charnwood, UK) beclomethasone dipropionate (BDP) (batch: 6661/M1) was purchased from Sicor, Italy. The following hydrofluoroalkanes were purchased from Apollo Scientific: 2H,3H-perfluoropentane (HPFP) with a purity of 98%, perfluoroheptane (mixed isomers) with a purity of 97% and perfluorodecalin (mixed E/Z isomers) with a purity of > 90%. Molecular structures of fluorinated liquids (Figure 2.1) and powders (Figure 2.2) are presented below. The boiling points of the liquids reported by the supplier were the following: HPFP 54°C, PFH 80-85°C and PFD 141°C.

All the fluorinated liquids used in this thesis were purified with molecular sieves, basic and acidic aluminium oxide, to remove organic impurities prior to experiments. The first purification step was to remove matter from the liquid by filtering it in a 0.2μm filter (sterilised Nalgene filter, Fisher Scientific UK). Secondly 25% w/v of basic aluminium oxide was added to the liquid, the mixture was shaken for 45 minutes and filtered through a new 0.2μm filter. Finally 2% w/v of acidic aluminium oxide was added to the liquid and the same procedure as for basic aluminium oxide was done. This method has earlier been proven successful for purification of fluorinated liquids

(Rogueda, 2003). The purity was confirmed by a stable surface tension in Section 2.11 and UV-spectra without drift in Section 2.13.

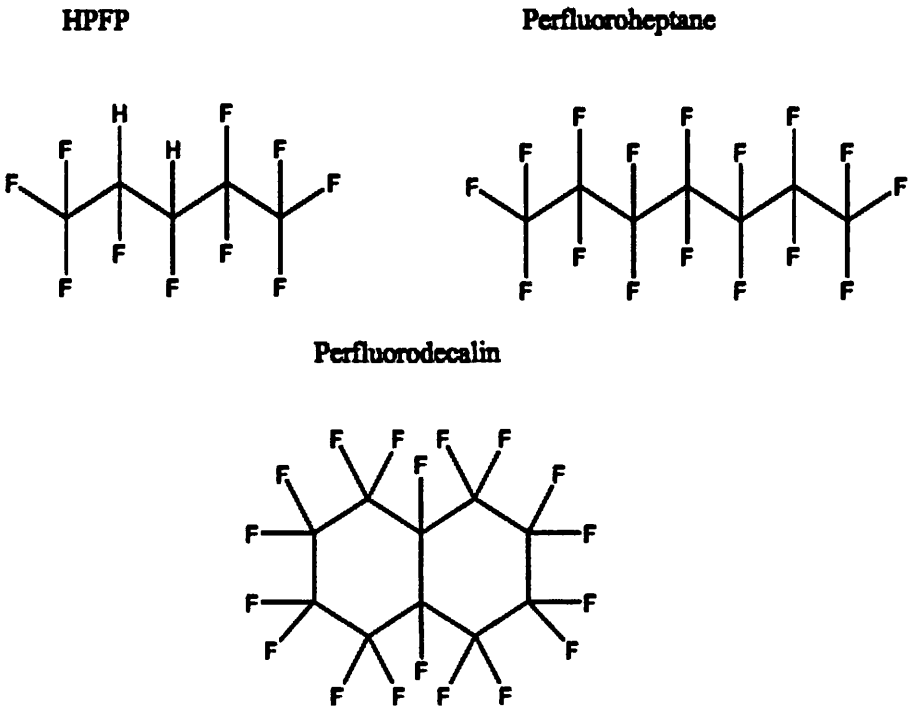

Figure 2.1. Molecular structure of fluorinated liquids.

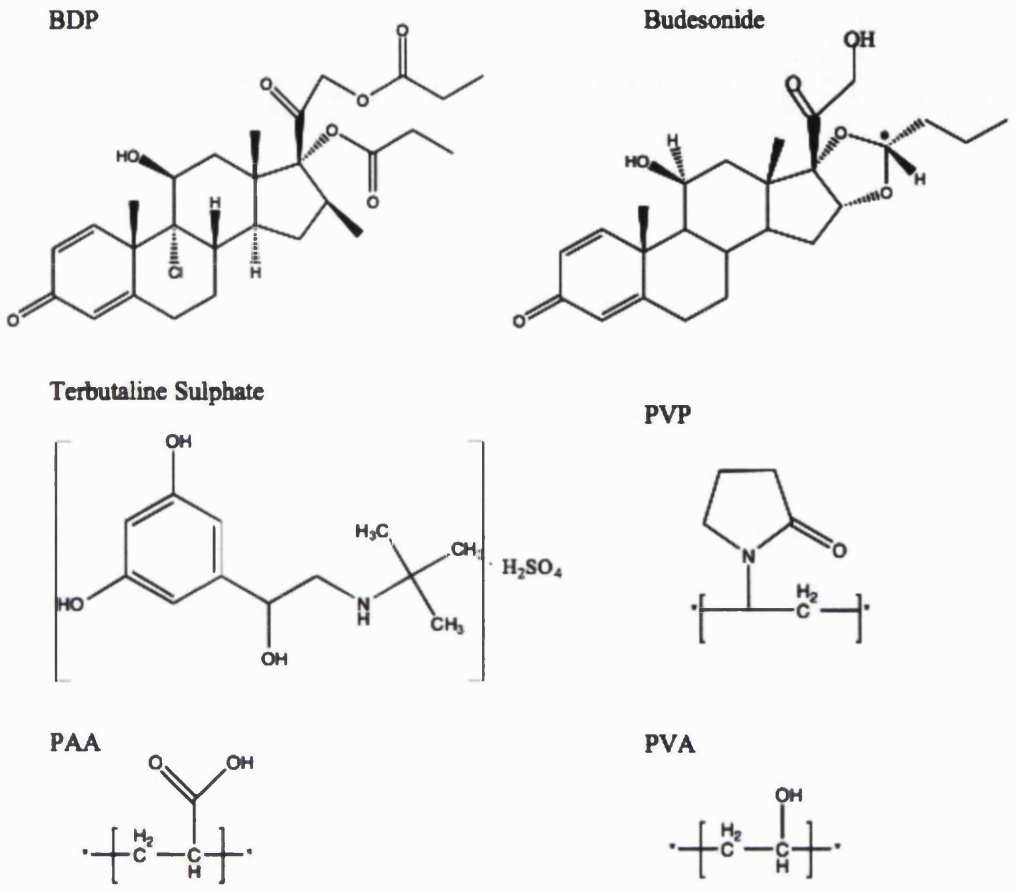

Figure 2.2. Molecular structure powder compounds used.

Four different canister inner wall materials were used in this study: polyethyleneterephtalate (PET), aluminium (AL), anodised aluminium (ALAN) and perfluoroalkane coated aluminium (ALPF). Continuous valves were used to seal the canisters. Canisters and valves were supplied by AstraZeneca, Charnwood, UK.

2.2 Scanning Electron Microscopy

2.2.1 Introduction

A scanning electron microscope (SEM) was used to visualise the morphology of powder particles and canister inner walls. SEM is a useful technique since it can produce very high-resolution three-dimensional images of surfaces as small as a few nanometres. A disadvantage is that the surface imaged must be conducting and therefore many materials needs coating that may alter the morphology. Furthermore coating of materials needs to be done in vacuum, which could also alter the surface shape. SEM images are created when a sample is bombarded with high-energy electrons in vacuum.

If a sample is not conductive it is coated with a very thin layer of conductive metal. The secondary electrons released from the sample are detected and processed into an image.

2.2.2 Materials and Methods

The morphology and size of powders: micronised BDP, budesonide, terbutaline sulphate and spray-dried PAA, PVP and PVA and canisters: PET, AL, ALAN, ALPF and glass was viewed and imaged at different magnifications using a SEM XL 30, FEI Company. The particles and canister surfaces were coated with gold by a K5-50 Sputter Coater, Emitech, for two minutes at 30 milliampere.

SEM images of particles after being stored in HPFP were taken to see if any changes in morphology had taken place. BDP, budesonide and terbutaline sulphate were suspended in HPFP and stored for 24 hours. Then the powders were filtered followed by drying at zero per cent relative humidity, for at least 24 hours prior to analysis, in a desiccator with potassium pentoxide.

2.2.3 Results and Discussion

According to the SEM images in Figure 2.3 the particle size of BDP, budesonide, PVP, PAA and PVA was below 5 μm. While looking at terbutaline sulphate some particles were larger than 5 μm. When the particle roughness was estimated from the SEM images it increased in the following order: PAA < PVA = PVP < BDP < budesonide < terbutaline sulphate. Furthermore the shape of spray-dried particles was spherical and the particle size quite similar while the micronised particles had irregular shape and a broad particle size distribution. The spray-drying process will be discussed in the next section.

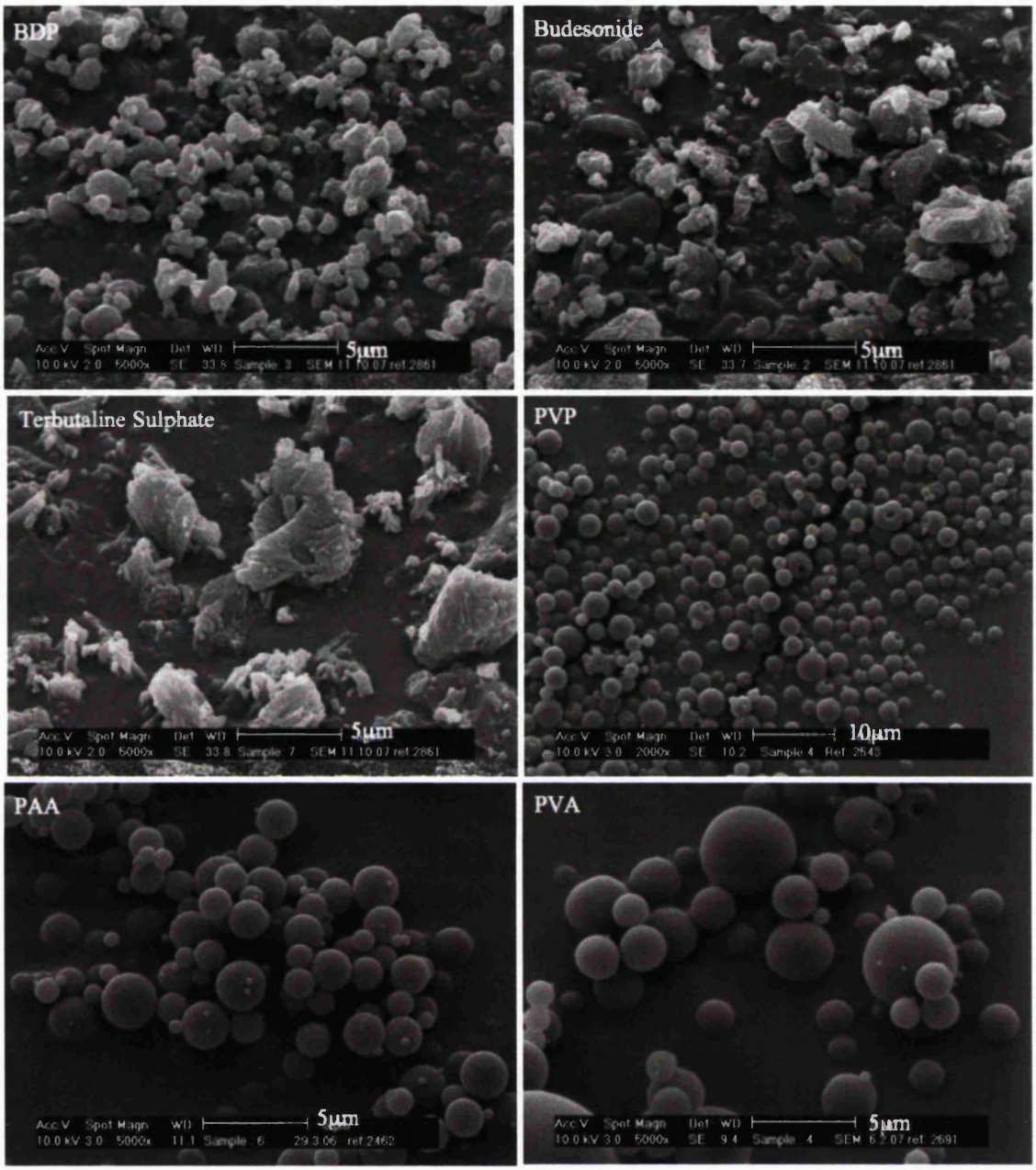

Figure 2.3. SEM images of micronised APIs (BDP, budesonide, terbutaline sulphate) and spray dried polymers (PVP, PAA and PVA).

In Figure 2.4 the SEM images show particles before and after having been stored in HPFP and no particular difference in morphology or size before and after could be detected by looking at the images. There may have been changes in fines that cannot be detected by eye but from the SEM images it is assumed that HPFP did not change the particle morphology or size significantly. However one must consider that those particles have been stored in the liquid, not at the fluid/gas/canister interface where the particles are more likely to change size due to for example Ostwald ripening since even

in closed systems at equilibrium gas exchange occur by the liquid/gas interface (Hickey et al., 1988).

In the literature it was found that the surface of large budesonide crystals changes over time when stored in HPFP (Traini, 2005). The change was visible when SEM images of a flat 50 × 50μm area of one crystal was studied, a large surface compared to the small particles showed here. The changes in surface morphology of the flat crystal were however not very large and such small changes may be hard to detect on the particles as in Figure 2.4. It may have been possible to detect morphology changes of the particles in Figure 2.4 if exactly the same particles in the same position would have been compared before and after storage in HPFP. There is also a possibility that surface dissolution occurred in HPFP but as the liquid was removed recrystallisation occurred, hence no visual surface change. A minor change would be for BDP that seems to agglomerate more after HPFP storage, which could be a result of surface changes when the particles were in contact with HPFP, caused by for example particles dissolving in HPFP. In Section 2.13 solubility in HPFP will be determined.

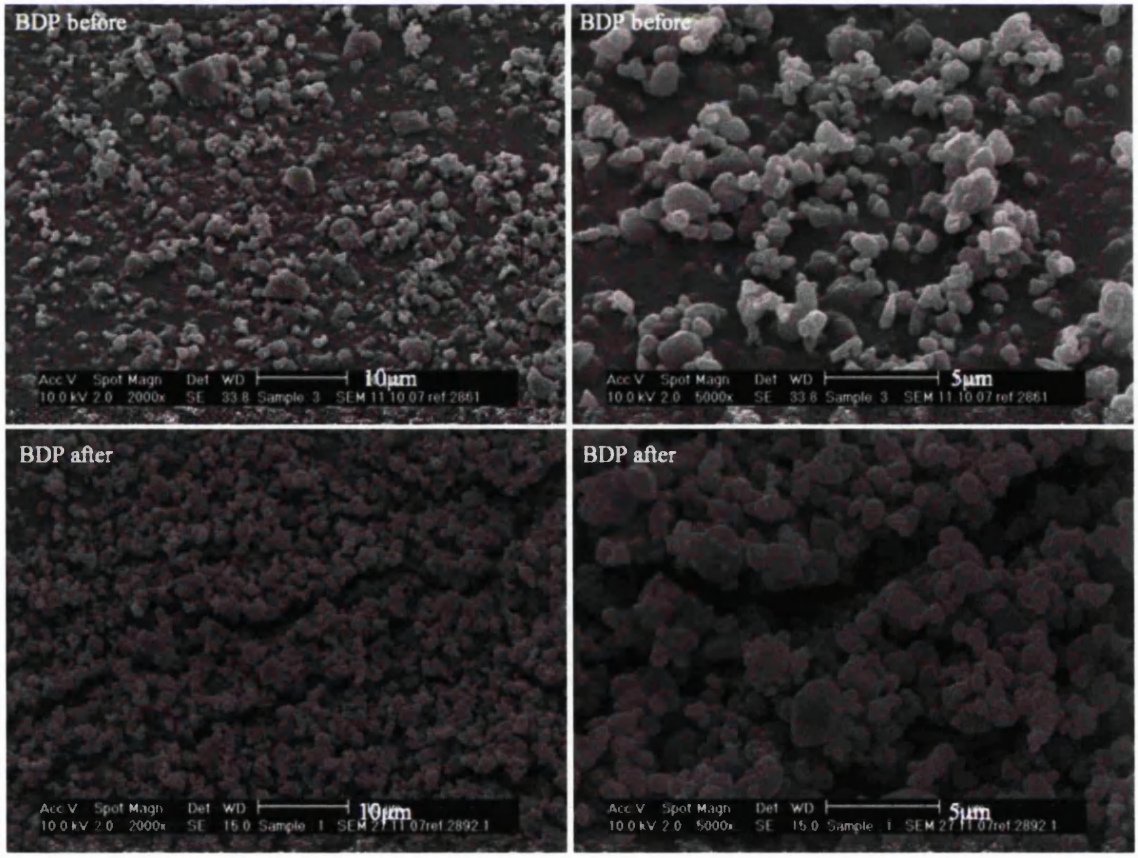

Figure 2.4 (continued on next page). SEM images of micronised APIs before and after storage in HPFP for 24 hours.

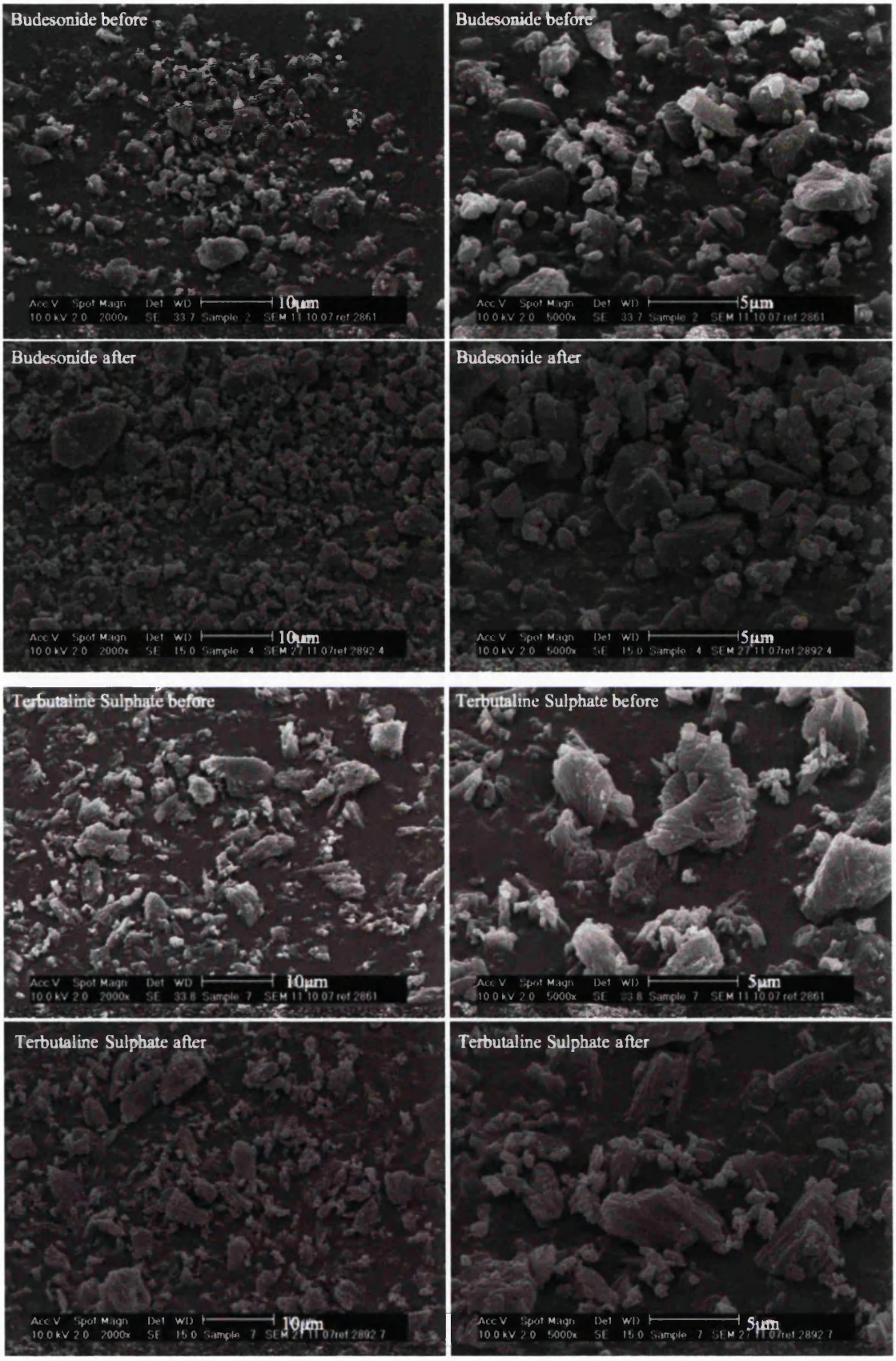

Figure 2.4 (continued from previous page). SEM images of micronised APIs before and after storage in HPFP for 24 hours.

In Figure 2.5 two SEM images of each canister material are presented, the left is less detailed than the right one. In the SEM images of canister materials it looks like the roughness of the surfaces followed the rank decrease: AL > ALPF > ALAN > PET > glass. The SEM images give an idea of what the surface morphology looks like but the roughness should be studied with another technique, such as atomic force microscope, to confirm the roughness visible here.

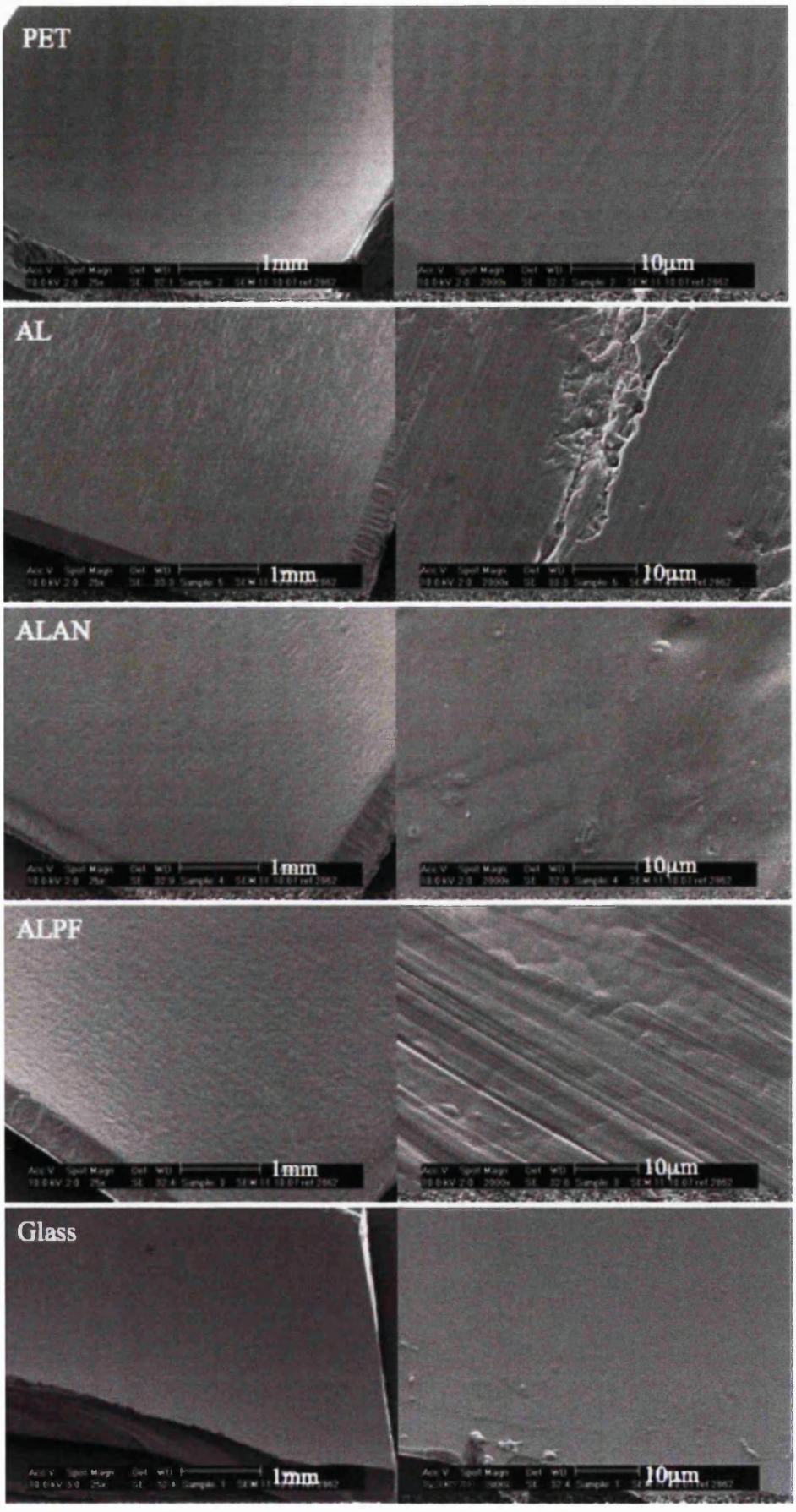

Figure 2.5. SEM images of canister inner surfaces.

2.3 Spray Drying

2.3.1 Introduction

Spray drying was used for the polymer powders to reduce the particle size to around 5μm and make the particle shape more uniform. Spray drying is commonly used in the pharmaceutical industry to dry drug products and to increase bioavailability by making crystalline materials more amorphous (Chen et al., 2004, Chidavaenzi et al., 2001, Yin et al., 2005). It is also used to control particle size, create microspheres, encapsulate materials (Gavini et al., 2006). Disadvantages with the technique are the risk of thermal degradation caused by the heat generated during processing, large material loss due to low yield and the operator may be negatively affected when inhaling toxic solvents and particles during processing.

The spray dryer consists of an atomizing feed, process gas supply, drying chamber, cyclone, bag filter and control system. A pneumatic feed pump transports the solution from the vial to the two-fluid nozzle. Compressed nitrogen atomizes the solution as it passes through the nozzle. The atomizer gas flow (p_{in}) and the nozzle atomizer gas pressure (p_{noz}) are controlled. The nitrogen is separated from air in a nitrogen generator. As the atomized flow enters the drying chamber it meets the hot process gas (nitrogen) and the liquid evaporates. The process gas chamber inlet flow (p_{out}) is controlled. Dry particles together with the process gas leave the process chamber and end up in the product bottle, fine particles continue to the filter unit. The process gas inlet temperature (T_{in}) is controlled and the process gas chamber outlet temperature (T_{out}) controls the feed rate to the nozzle.

Particle size, shape and the yield will be very dependent on the adjustable parameters, such as concentration, feed rate, solvent boiling point, nozzle pressure and gas flow in the spray-dryer. If the boiling point of a solvent is low, evaporation is rapid and the molecules have little time to arrange themselves in low energy positions, consequently decreased boiling point gives more amorphous particles. Collapsed particles are the result of too slow evaporation.

2.3.2 Materials and Methods

A Niro Spray dryer from Denmark fitted with a Maxigas nitrogen generator from Domnick Hunter was used for spray drying of PVP, PAA and PVA. Prior to spray drying the powder was dissolved in water, at room temperature and under magnetic stirring. The spray dryer settings used in this study are shown in Table 2.1.

Table 2.1. Spray-dryer settings.

Powder	Solvent	Concentration ($\%w \cdot v^{-1}$)	T_{in} (°C)	T_{out} (°C)	P_{in} ($kg \cdot h^{-1}$)	P_{out} ($kg \cdot h^{-1}$)	P_{noz} ($kg \cdot h^{-1}$)
PVP	Water	5	95	53	2	20	1.5
PAA	Water	10	95	59	2.5	25	1.9
PVA	Water	5	95	53	2	20	1.5

The spray-dried powders were stored at room temperature and zero percent relative humidity in a desiccator with potassium pentoxide to prevent physicochemical changes due to humidity.

2.3.3 Results and Discussion

Figure 2.6 show PVP, PAA and PVA particles created with the spray-drying conditions in Table 2.1. The majority of particles were spherical with a diameter of 1-5μm. For the supplied form of all three polymers the particle size and distribution was very large and the shape varied much compared to the micronised APIs and therefore it was necessary to spray-dry the polymers. In Figure 2.3 it is clear that the size of APIs in supplied form was quite uniform and in the desired range though the visual roughness was much higher than that of the spray dried particles in Figure 2.3. APIs were spray-dried to 1-5μm particles but the yield was very low and the materials expensive, therefore the supplied form was considered the most appropriate form to use in the following experiments.

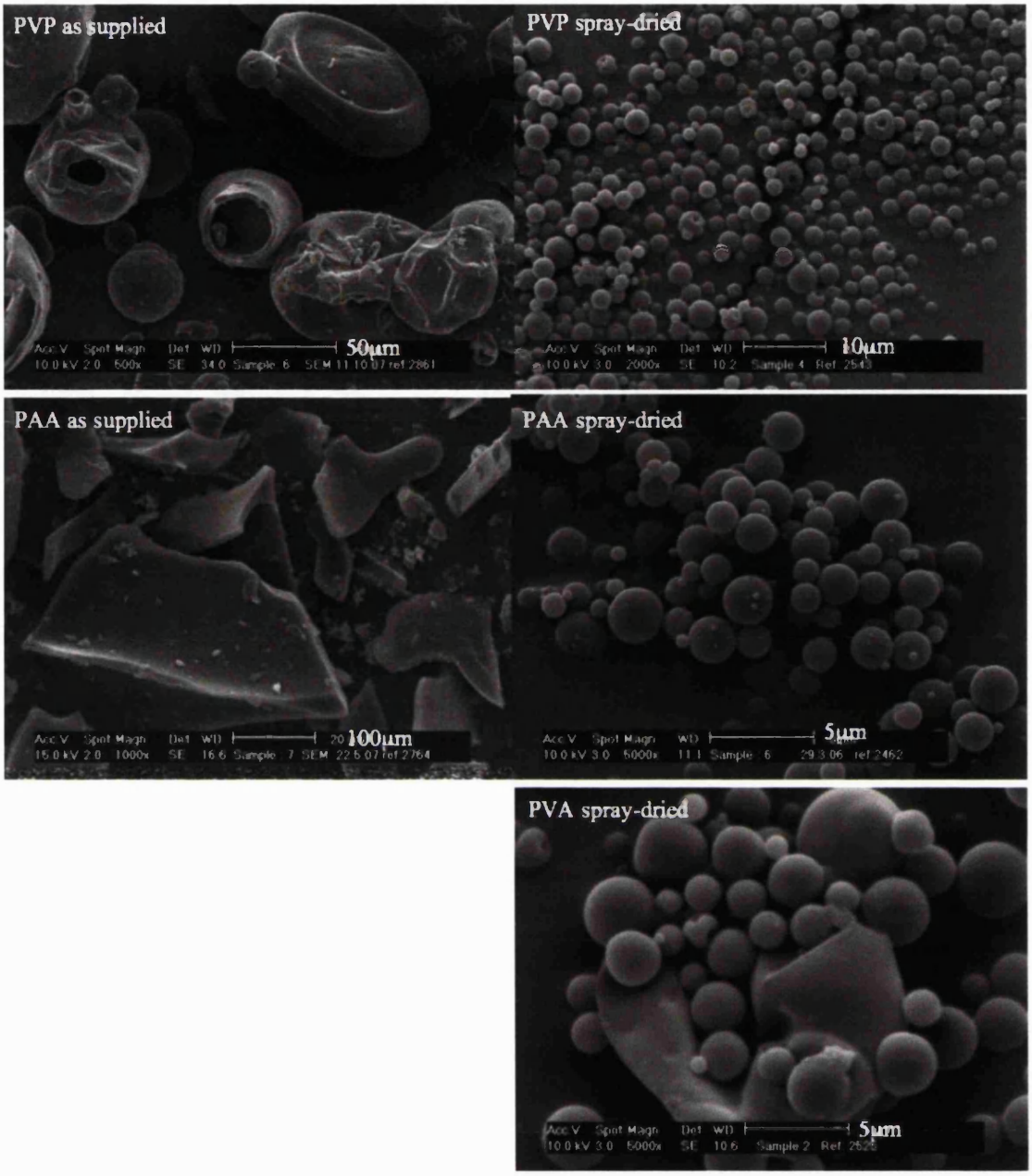

Figure 2.6. SEM image of PAA in: a) spray dried and b) supplied form.

2.4 Particle Size Analysis

2.4.1 Introduction

There are several techniques available for particle size determination. SEM in section 2.2, sieving and sedimentation are a few. Laser diffraction, where a measurement is quick and no calibration is required, was the method chosen in this study. The technique determines particle sizes by letting scattered laser light pass through a cell with particles in suspension and when the light hits particles the intensity and pattern of the scattered

lights is detected. Larger particles scatter light in smaller angles than small particles. In this study the particle size of interest was below 10 μm and above 0.05 μm and therefore, the Mie theory was used (Ruzer and Harley, 2005). The theory assumes that the particles are spherical, which is mostly not the case for particles. Further it assumes that the suspension analysed is dilute, which means that multiple scattering, caused by scattered light hitting particles, is neglected and only single scattering is assumed to reach the detector (Mitchell and Nagel, 2004).

2.4.2 Materials and Methods

A Malvern Mastersizer X equipped with a 45mm lens (Malvern Instruments Ltd., Malvern, UK) was used to determine particle size of BDP, budesonide, terbutaline sulphate and PAA in HPFP. The instrument had a small volume diffraction chamber equipped with a magnetic stirrer. Each sample was a suspension prepared freshly by adding approximately 1 mg of powder to HPFP. The particles were dispersed by sonication for one minute at room temperature prior to analysis and the sonication time was chosen since it was used in the adhesion study in Chapter 3. The particle size of three independent powder samples was measured three times each in the Mastersizer. During the method development the impact longer sonication time had on particle size was investigated and the only observed difference between 1 and 15 minutes sonication time was that the adhesion of particles to the canister wall increased, therefore the sonication time was kept at 1 minute, which is also a common time when preparing pMDI formulations. The suspension was added drop wise to an obscuration level of 10-20% and the particle size of each powder was measured three times.

2.4.3 Results and Discussion

In Table 2.2 the 10%, 50% and 90% cumulative percentile volumetric diameters of powders suspended in HPFP are shown. The median diameter ($D_{0.5}$) of BDP and budesonide were similar and that of terbutaline sulphate and PAA were similar. Though $D_{0.5}$ for the latter two was almost three times higher than $D_{0.5}$ for the former two. The results presented in Table 2.2 were only a part of the total particle size distribution. The reason for excluding parts of the size distribution was that there were particle agglomerates of around 100 μm present. Not even when the suspensions were sonicated for as long time as 20 minutes the agglomerates disappeared. Longer sonication time caused particles to adhere to the vial wall more rather than de-agglomerate. The SEM

images of dry powders in Figure 2.3 showed that the particle size for these four compounds was around 5μm, which further strengthen the observation of large particle clusters of around 100 μm, not single large particles, in HPFP when measuring size by laser diffraction.

Table 2.2. Particle size of powders in HPFP as measured by laser scattering (n=9).

	Particle Size in HPFP (μm)		
Powder	**$D_{0.1}$**	**$D_{0.5}$**	**$D_{0.9}$**
BDP	0.968 ± 0.103	2.808 ± 0.413	5.763 ± 0.386
Budesonide	0.852 ± 0.059	2.530 ± 0.343	5.348 ± 0.454
Terbutaline Sulphate	1.207 ± 0.110	7.600 ± 0.737	13.067 ± 1.102
PAA	1.108 ± 0.130	7.470 ± 1.447	14.377 ± 1.661

2.5 Density of Powders

2.5.1 Introduction

The true density of powders was measured with helium pycnometry. The technique determines the volume of a powder sample with a known mass by measuring the pressure change of helium in a calibrated volume. With that information it then calculates the true density of the powder. The technique is non-destructive and very accurate since helium is able to penetrate even the finest pores.

2.5.2 Method

A Helium AccuPyc 1330 Pycnometer (Micromeritics, USA) was used for density measurements. The powder samples were stored at room temperature in zero percent relative humidity for a minimum of 24 hours prior to analysis to ensure measurements were carried out on dry samples. Three independent samples of each powder were loaded into the $1cm^3$ sample cup and each samples density was measured five times. The true densities of BDP, budesonide, terbutaline sulphate and spray-dried PAA were determined.

2.5.3 Results and Discussion

The density of powders is presented in Table 2.3. All densities were quite similar and around 1.3 $g \cdot cm^{-3}$, a common density for pharmaceutical powders, although there was a significant difference between the densities and it increased in the following order: budesonide < terbutaline sulphate < BDP < PAA.

Table 2.3. True density of BDP, budesonide, terbutaline sulphate and PAA as measured by helium pycnometry (n=15).

Powder Sample	True Density ($g \cdot cm^{-3}$)
Micronised BDP	1.357 ± 0.011
Micronised Budesonide	1.292 ± 0.006
Micronised Terbutaline Sulphate	1.346 ± 0.002
Spray-dried PAA	1.383 ± 0.003

2.6 Differential Scanning Calorimetry

2.6.1 Introduction

Differential Scanning Calorimetry (DSC) is commonly used for determination of melting temperature, glass transition temperature and crystalline and amorphous content of powder compounds. DSC detects physical changes, such as melting and crystallisation and chemical changes, such as decomposition. It is advantageous that the mass required for analysis of a material is low and also that the measurements are quick. Changes are detected by measuring the temperature required to maintain a constant heat flow in the sample and reference during heating and cooling (Charsley and Warrington, 1992).

2.6.2 Materials and Methods

Micronised BDP, budesonide and terbutaline sulphate were analysed before and after the particles were suspended in HPFP in order to see if the melting point changed due to polymorphic changes. The samples were prepared as in Section 2.2.2. A temperature scan of 10°C/min from 20-300°C was carried out in a DSC-7 equipped with a TAC 7/DX thermal analysis controller (Perkin Elmer, UK). Dry powder samples (5-10 mg) were weighed into non-hermetically sealed aluminium pans that were crimped before loaded into the DSC. Three repeats were carried out for each powder. Calibration was done with indium at 10°C/min from 130-190°C prior to analysis.

2.6.3 Results and Discussion

The melting points (T_m) of the powders are presented in Table 2.4 and the DSC thermogram for BDP and budesonide can be found in Figure 2.7 and for terbutaline sulphate in Figure 2.8. The single endotherm for BDP and budesonide in the thermograms shown in Figure 2.7 confirmed the micronised APIs crystallinity and also correlated well with the literature (Vervaet and Byron, 1999, Tajber et al., 2009). The melting points of BDP changed after it had been stored in HPFP while the melting point of budesonide did not change after storage in HPFP, Table 2.4. The 3°C difference in melting point for BDP could be a sign of change in polymorphic form. Additional analytical techniques, such as x-ray powder diffraction and thermal gravimetric analysis, should be used to confirm the polymorph change. The melting peak for terbutaline sulphate shown in Figure 2.8 was followed by degradation and therefore no baseline followed and it was not possible to get an accurate enthalpy measurement. The melting temperature of terbutaline sulphate confirmed crystallinity of the API and agreed with the literature (Thi et al., 2008).

Table 2.4. Melting points of the APIs before and after storage in HPFP (n=3).

Powder	T_m [°C]	ΔH [$J \cdot g^{-1}$]
BDP	211.76 ± 0.32	74.75 ± 3.19
BDP stored in HPFP	214.66 ± 0.12	75.26 ± 2.65
Budesonide	258.77 ± 1.68	78.39 ± 5.33
Budesonide stored in HPFP	261.46 ± 1.68	83.64 ± 2.15
Terbutaline Sulphate	259.65	-

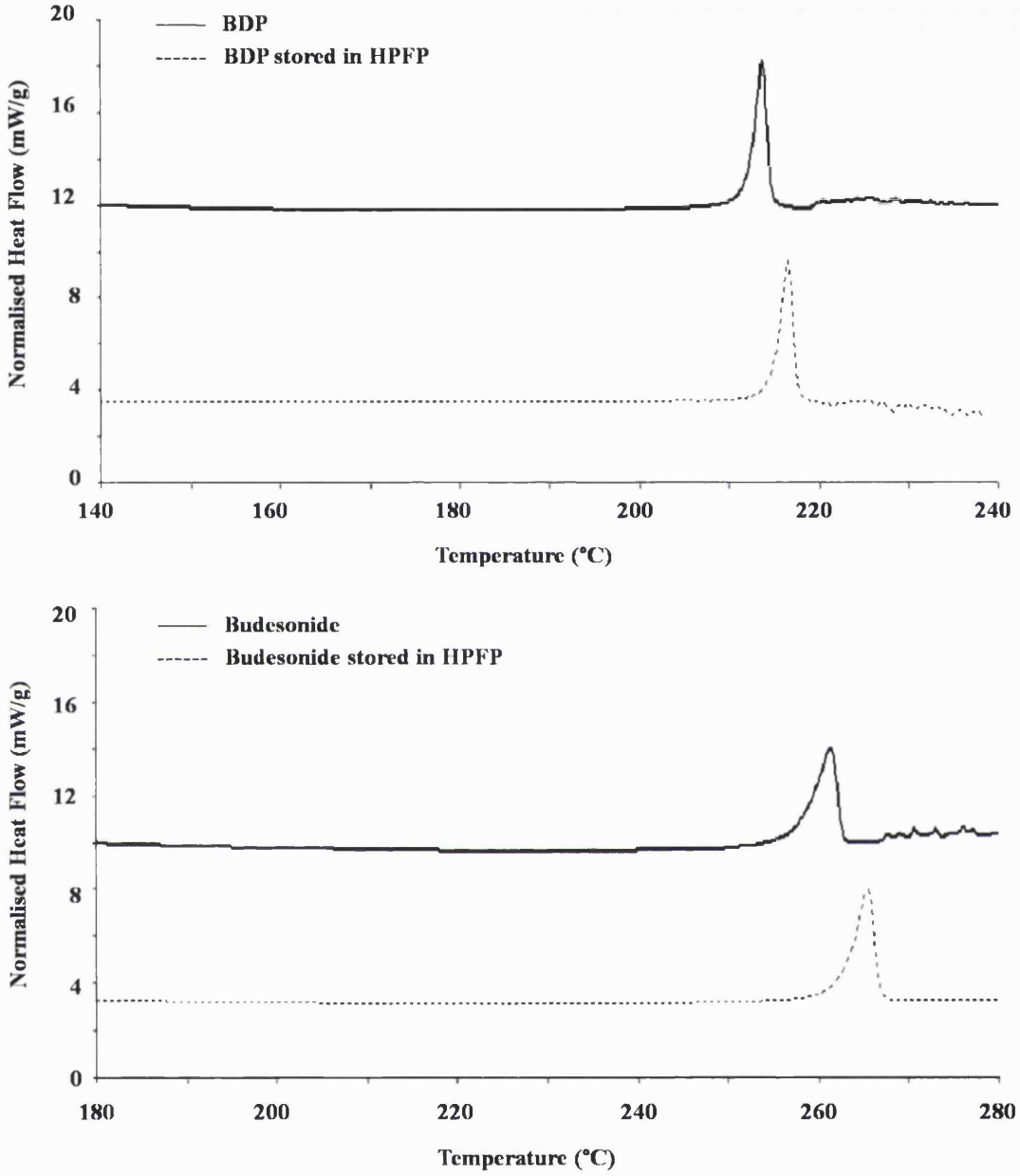

Figure 2.7. DSC thermograms of BDP and budesonide before and after stored in HPFP.

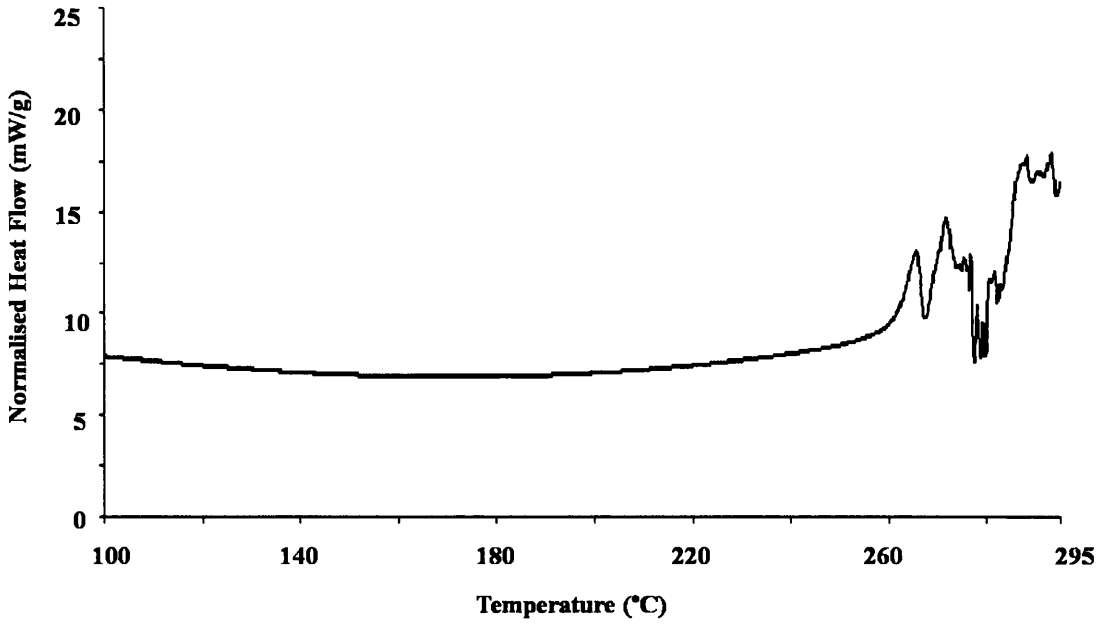

Figure 2.8. DSC thermogram of terbutaline sulphate.

2.7 X-ray Powder Diffraction

2.7.1 Introduction

X-ray Powder Diffraction (XRPD) was used to confirm the identity of APIs and to detect if polymorphic changes took place when powders were stored in HPFP. In the pharmaceutical industry it is common to determine polymorphic forms of crystalline materials with XRPD. The technique is popular since a measurement is non-destructive and quick.

2.7.2 Materials and Methods

XRPD diffractograms were generated with a Phillips analytical x-ray diffractometer, Cambridge, UK fitted with a 4 kW x-ray generator (PW3830) working at 45 kV and 30 mA. The samples were scanned from 5° diffraction angle 2θ to 40°, in three repeats. Powder samples stored in HPFP were prepared as in Section 2.2.2.

2.7.3 Results and Discussion

Each API diffractogram in Figure 2.9 showed no sign of amorphous content and correlated well with the corresponding diffractogram in the literature (Sakagami et al., 2002, Tajber et al., 2009, Rehman et al., 2004). The diffractogram before and after storage in HPFP overlapped well which was evidence that the interaction with the liquid

had caused no physical changes such as polymorphic form change or change in crystallinity.

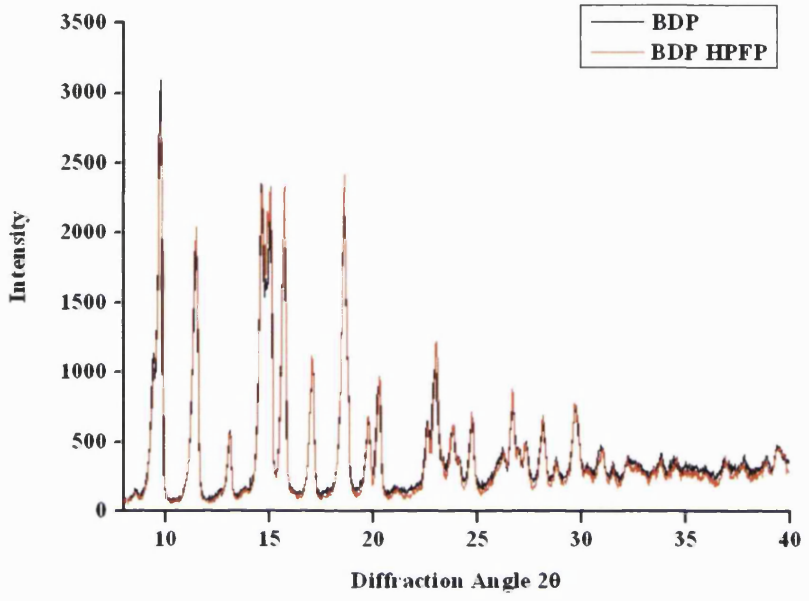

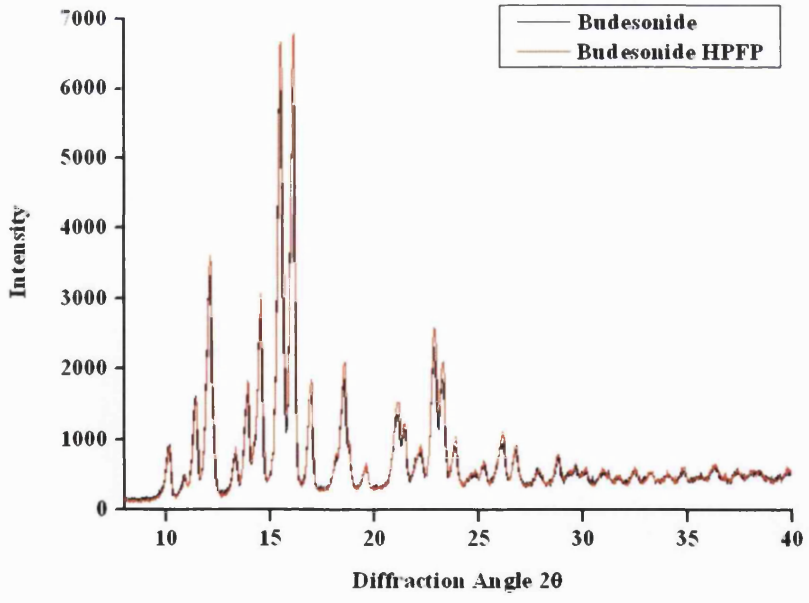

Figure 2.9 (continued on next page). X-ray powder diffraction spectra of APIs before and after storage in HPFP.

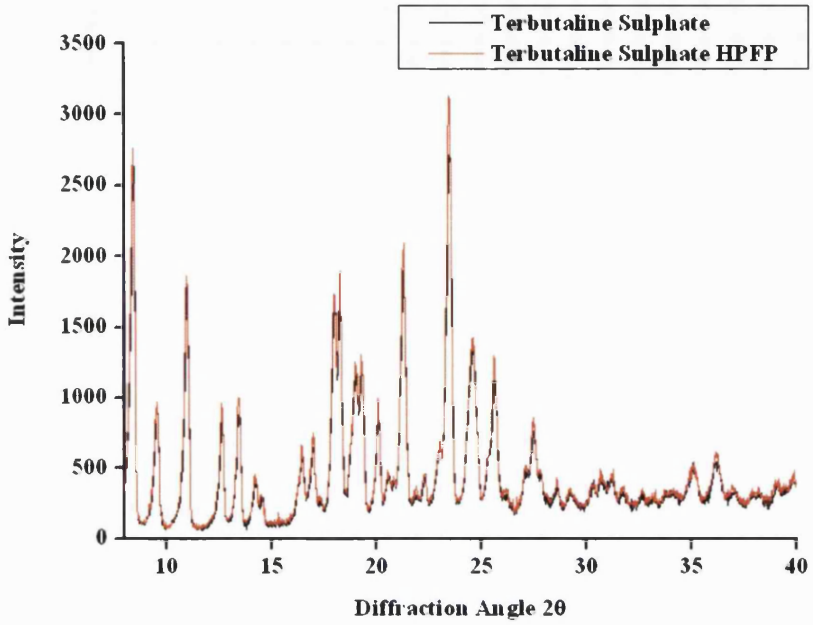

Figure 2.9 (continued from previous page). X-ray powder diffraction spectra of APIs before and after storage in HPFP.

2.8 Thermal Gravimetric Analysis

2.8.1 Introduction

Thermal Gravimetric analysis (TGA) was used to identify possible solvate formations in the APIs during storage in HPFP. TGA measures weight loss or gain, either as a function of increasing temperature or isothermally as a function of time. The technique is often used to detect chemical or physical changes, such as decomposition, evaporation, gas absorption and dehydration. It is a straightforward method where only a small sample is required for each experiment.

2.8.2 Materials and Methods

Micronised BDP, budesonide and terbutaline sulphate were analysed in triplicate with a Pyris 6 TGA from Perkin Elmer. In order to see if solvates were formed when powders interacted with HPFP they were analysed before and after storage in HPFP. Samples stored in HPFP were prepared as in Section 2.2.2. Ceramic pans were loaded with powder sample and the samples were heated at 10°C/minute starting at 30°C and ending at 260°C for budesonide and terbutaline sulphate and 220°C for BDP.

2.8.3 Results and Discussion

There were no significant differences in weight loss between the powder samples before and after storage in HPFP Table 2.5. Therefore HPFP did not form solvates with the powders during the 24 hours powders were stored in HPFP. The temperature range of interest was the one before the compound melted. The melting point of powders was presented in Table 2.4.

Table 2.5. Mass change of powders before and after storage in HPFP, as measured by TGA (n=3).

	Mass Change ($\%w \cdot w^{-1}$)	
Powder	**Before Storage in HPFP**	**After Storage in HPFP**
BDP	0.130 ± 0.034	0.091 ± 0.017
Budesonide	0.064 ± 0.012	0.045 ± 0.017
Terbutaline Sulphate	0.068 ± 0.018	0.067 ± 0.007

2.9 Density of Liquids

2.9.1 Introduction

Density measurements of fluorinated liquids were performed with a density meter based on oscillator technology. This is a quick method for density determination and the measurements are easy to perform.

2.9.2 Method

The density of fluorinated liquids was measured at five different temperatures: 15, 20, 25, 30 and 35°C with a DMA 35 hand held density meter from Anton Paar scientific, Austria. The density meter measured true density with accuracy of 0.001 $g \cdot cm^{-3}$. Prior to each measurement liquids and equipment were stored at least 1 hour in a controlled temperature unit to equilibrate at the desired temperature. At least 3 measurements were carried out at each temperature. The equipment was calibrated with water prior to analysis.

2.9.3 Results and Discussion

The densities of fluorinated liquids are shown in Table 2.6. The measured densities correlated well with the densities reported by the supplier of fluorinated liquids.

Table 2.6. Density of fluorinated liquids as measured by a density meter (n=3).

	Density ($g \cdot cm^{-3}$)		
Temperature (°C)	**HPFP**	**Perfluoroheptane**	**Perfluorodecalin**
15	1.603 ± 0.006	1.747 ± 0.006	1.949 ± 0.002
20	1.592 ± 0.007	1.731 ± 0.008	1.936 ± 0.005
25	1.578 ± 0.008	1.772 ± 0.010	1.927 ± 0.001
30	1.564 ± 0.011	1.712 ± 0.013	1.918 ± 0.001
35	1.550 ± 0.010	1.689 ± 0.013	1.909 ± 0.001

2.10 Viscosity

2.10.1 Introduction

A capillary viscometer was used to determine the true (dynamic) viscosity of fluorinated liquids. The experiment is straightforward and starts by filling the sample liquid into the tube, Figure 2.10. There sample volume should fill up the space between A and B. Then a vacuum raises the liquid to C and is then released. The time it takes for the liquid to travel from C to B is recorded manually and used to calculate the kinematic viscosity in Equation 2.1.

$$\nu = C \cdot t \tag{2.1}$$

Where ν is the kinematic viscosity, C the nominal constant and t the time. The dynamic viscosity can be calculated from the kinematic viscosity with Equation 2.2.

$$\mu = \nu \cdot \rho \tag{2.2}$$

Where μ is the dynamic viscosity and ρ is the density of the sample liquid.

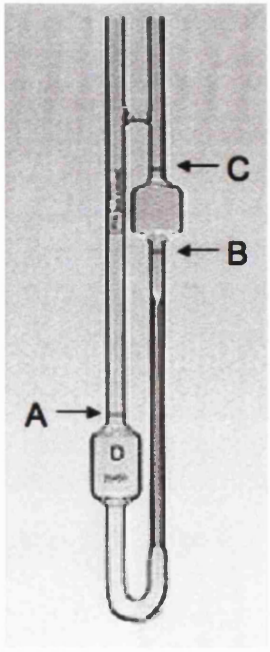

Figure 2.10. BS/U tube glass viscometer.

The disadvantage with this method is the human error in terms of timing accuracy and exactness in determining the point when liquid passes by the start and end point.

2.10.2 Materials and Methods

The densities of HPFP, perfluoroheptane and perfluorodecalin were determined in triplicate at five different temperatures: 15, 20, 25, 30 and 35 °C. Size O (C = 0.001) and A (C = 0.003) of BS/U tube glass viscometers, Figure 2.10, from Poulten Selfe & Lee Ltd were used. The viscometer filled with sample liquid was equilibrated for 30 minutes in a water bath at controlled temperature (± 0.1°C) prior to each measurement. All measurements were carried out in the same water bath. The time for the liquid to flow from C to B was measured with a digital stopwatch.

2.10.3 Results and Discussion

The dynamic viscosity of fluorinated liquids is presented in Table 2.7. It increased in the following order: HPFP < perfluoroheptane < perfluorodecalin.

Table 2.7. Dynamic viscosity of fluorinated liquids as measured by a U tube viscometer (n=3).

	Viscosity (mPa·s)		
T (°C)	HPFP	Perfluoroheptane	Perfluorodecalin
15	0.651 ± 0.001	0.942 ± 0.002	3.795 ± 0.000
20	0.605 ± 0.001	0.871 ± 0.000	3.264 ± 0.000
25	0.564 ± 0.000	0.805 ± 0.001	2.835 ± 0.003
30	0.525 ± 0.001	0.749 ± 0.001	2.490 ± 0.003
35	0492 ± 0.000	0.691 ± 0.001	2.180 ± 0.003

2.11 Surface Tension

2.11.1 Introduction

Surface tension of fluorinated liquids was measured with the Wilhelmy plate method, Figure 2.11. The Wilhelmy plate method is based on measuring the force created when a rectangular plate comes into contact with liquid. The plate is connected to a balance and the exact dimensions of the plate are known.

The tensiometer calculates the surface tension (σ) from Equation 2.3 (Wu, 1982).

$$\sigma = \frac{F}{P \cdot \cos\theta} \qquad (2.3)$$

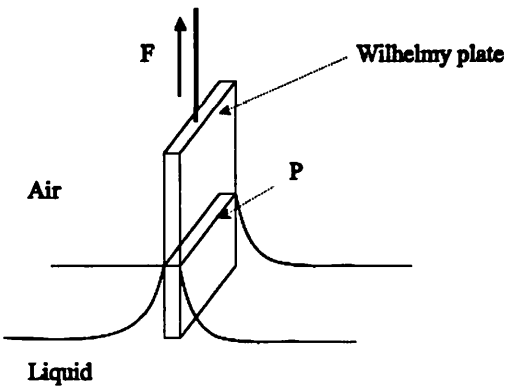

Figure 2.11. Schematic illustration of the Wilhelmy plate method.

Where F is the force the balance detects when the plate is in contact with the liquid, P is the perimeter of the plate, Figure 2.11 and θ is the contact angle of the plate. The platinum plate is optimally wetted and therefore θ is nearly zero, giving $cos\theta = 1$. Consequently the calculations of surface tension are only based on F and P. It is hard to measure surface tension properly since small quantities of contaminants could change the results significantly. The balance connected to the Wilhelmy plate is very delicate and sensitive, which enable accurate measurements.

2.11.2 Materials and Methods

The surface tension of fluorinated liquids was measured in triplicate at 20°C. A tensiometer from Krüss, Germany, equipped with a platinum Wilhelmy plate was used. Prior to each experiment both the plate and glassware was thoroughly cleaned (Rosilio, 2007). First the glassware was left in a mixture of TFD 4 detergent and hot water (15:85) for thirty minutes, then rinsed thoroughly with double distilled water and finally dried for at least 24 hours in an oven. The Wilhelmy plate was washed in a sulphochromic solution and rinsed in double distilled water prior to each experiment. Every day the equipment was calibrated with water before and after the experiments (Rosilio, 2007). When a measurement was carried out the value was recorded when the surface tension was stabilised, normally after ten minutes. Three repeats of each liquid was carried out.

2.11.3 Results and Discussion

The surface tension of fluorinated liquids is presented in Table 2.8 and the lower surface tension a liquid has the better it wets the surface. Though it has been reported that when surface tension decreases below 20 $mN \cdot m^{-1}$ the wettability is hardly changed (Rogueda, 2003). The surface tension of HPFP in Table 2.8 correlated well with values in literature (Rogueda, 2003).

Table 2.8. Surface tension of fluorinated liquids as measured by Wilhelmy plate (n=3).

	Surface Tension ($mN \cdot m^{-1}$)		
T (° C)	**HPFP**	**Perfluoroheptane**	**Perfluorodecalin**
22	13.391 ± 0.040	12.733 ± 0.058	18.056 ± 0.193

2.12 Dielectric Constant

2.12.1 Introduction

The dielectric constant of fluorinated liquids was measured. Measuring the dielectric constant of a liquid is straightforward and quick. It is an important physical property when studying suspension stability since the dielectric constant tells us how well a material concentrates an electric flux. Liquids with higher values, such as water with a dielectric constant of 78.85 (Floriano, 2004), are more easily polarised when an electric field is applied.

2.12.2 Materials and Methods

For dielectric constant measurements of fluorinated liquids a BI-870 dielectric constant meter from Brookhaven, USA was used. The measurements were performed at a frequency of 10kHz and at temperatures 10, 20 30 and 40°C respectively in triplicate. Furthermore the equipment and the liquids were stored in a controlled temperature unit and left to equilibrate for at least one hour at each temperature.

2.12.3 Results and Discussion

The dielectric constants of fluorinated liquids at different temperatures are presented in Table 2.9. It was observed that HPFP had much higher dielectric constant than both perfluoroheptane and perfluorodecalin, hence more likely to polarise under an applied electric field. Also it was observed that the dielectric constant decreased with increased temperature.

Table 2.9. Dielectric constant variations with temperature (n=3).

	Dielectric Constant		
T (°C)	**HPFP**	**Perfluoroheptane**	**Perfluorodecalin**
10	7.17	1.79	1.99
20	6.87	1.77	1.95
30	6.47	1.76	1.91
40	6.08	1.75	1.89

2.13 Solubility of API in 2H, 3H-perfluoropentane

2.13.1 Introduction

Solubility in pMDI suspension formulations is important to determine since it has been shown that partial solubility of micronised APIs in suspension formulations can cause crystal growth that can lead to instabilities in the formulation (Phillips et al., 1990). UV-vis spectroscopy was used to measure the solubility of APIs in HPFP. The technique is based on different molecules absorbing different wavelengths of UV or visible light. The sample is always analysed against a reference. Analysing samples is very quick while preparing solutions and calibration standards takes time.

2.13.2 Materials and Methods

The maximum solubility of BDP, budesonide and terbutaline sulphate in HPFP was determined with a UV spectrometer (Perkin Elmer, UK). Solubility of PAA and PVA could not be detected by UV spectroscopy since the compounds have no chromophore. However, solubility of PAA, PVA and PVP in HFAs was estimated from solubility values measured by others.

Solutions were prepared by sonicating 30 mg powder in 50 mL HPFP in a Turbula mixer for 1 day at 30°C. Sterile centrifuge tubes with screw lids were used to prevent HPFP to evaporate (Centrifuge tubes, PP, sterile, 15 mL, SuperClear™, VWR). The particles in the suspensions were filtered away prior to the analysis. One-centimetre quartz cells were used and the experiments were performed at room temperature. The cells were cleaned in the same way as the glassware in Section 2.11.2. Each sample with API/HPFP solution was measured against a blank reference containing HPFP only. The scans were performed at wavelength 240 nm for both BDP and budesonide and 276 nm for terbutaline sulphate.

Calibration standards were prepared by diluting stock solutions of BDP to 4, 8, 12, 17, 22, 25, 43, 49 $\mu g \cdot mL^{-1}$ and budesonide to 2, 10, 18, 26, 34, 42, 50 $\mu g \cdot mL^{-1}$ in the sterile centrifuge tubes with screw lids. The standard solutions were prepared from 3 stock solutions (0.5 mg powder in 10 mL HPFP) and the absorbance of each standard solution was measured three times, hence each calibration point was based on 9 measurements.

The method was validated by the ICH Q2B validation of analytical procedures. The parameters considered when validating the method were accuracy (> 99 %), limit of detection based on standard deviation of blank and slope (LOD = 1 μg/mL), linearity (R^2= 0.999) and stability.

2.13.3 Results and Discussion

HPFP was scanned to ensure that it had no signals interfering at the API wavelengths. The HPFP spectrum in Figure 2.12 showed a small signal < 230 nm. However, analysis in this study was done at 240 and 276 nm and therefore HPFP was highly appropriate for spectral studies of the APIs.

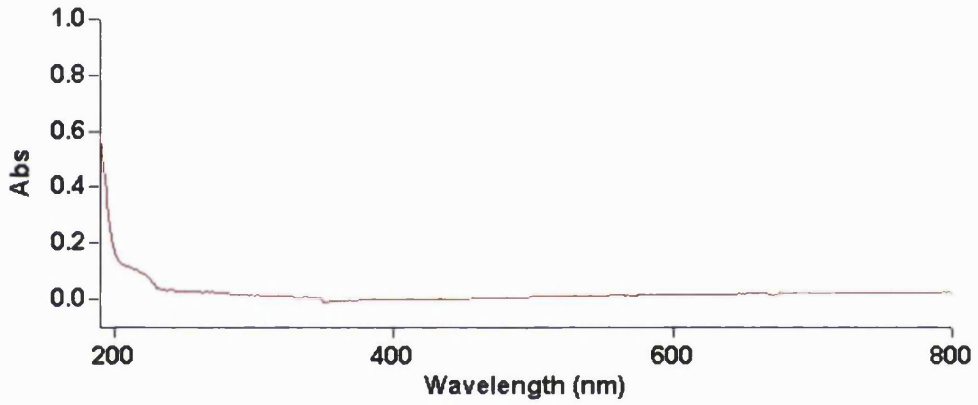

Figure 2.12. UV-vis spectra of: a) HPFP, b) perfluoroheptane and c) perfluorodecalin.

Solubility of a powder in a liquid is complex and is dependent on physicochemical properties such as morphology, crystalline and/or amorphous content, polymorphic forms, hydrophilic and/or lipophilic nature. One study showed that there can be a tenfold solubility difference in HPFP between two polymorphic forms of the same material (Cote et al., 2008).

In Table 2.10 the solubility of BDP was 1.5 times greater than the solubility of budesonide in HPFP. The solubility of terbutaline sulphate was very low. It was just above the limit of detection in its most concentrated solution. The absorbance was 0.03 and the detection limit was 0.025 (1μg/mL) therefore it was not possible to prepare calibration standards to enable quantification of terbutaline sulphate solubility in HPFP.

However since the solubility of terbutaline sulphate was right at the limit of detection the solubility was estimated to be 1μg/mL.

It has been shown by others that steroids are more soluble in hydrofluoroalkanes if they have higher lipophility and lower melting point (Williams et al., 1999). In Table 2.4 the melting point of BDP (211°C) was lower than that of budesonide (259°C). Consequently BDP should be more soluble in HPFP than budesonide, which is the case in Table 2.10. The API lipophility will be presented in Chapter 4. Another sign of BDP being more soluble in HPFP than budesonide and terbutaline sulphate is shown in Figure 2.4, where the morphology of particles before and after having been stored in HPFP was presented. There was a slight change in the morphology for BDP but not for budesonide and terbutaline sulphate.

It has been shown that HPFP is a good model propellant for HFA134a as compounds are dissolved similarly in the two HFAs (Ridder et al., 2005). PVP, PVA and PAA are biocompatible polymers that can be used as excipients in pulmonary formulations, for example PVP and PVA as stabilising agents (Jones et al., 2006a, Jones et al., 2006b) and PAA as mucoadhesive agent (Alpar et al., 2005). The solubility of PVP K30 in HPFP, PAA in HFA134a and 98% hydrolyzed PVA in HFA 134a are shown in Table 2.10. It has been shown in a study that amphiphilic polymers have similar solubility in HFA 134a and HPFP (Ridder et al., 2005) so therefore the assumption that the solubility of PAA and PVA respectively is similar in HPFP and in HFA 134a will be made in this study.

Table 2.10. Solubility of APIs in HPFP at 30°C (n=9).

	Solubility in HPFP ± SD ($\mu g \cdot mL^{-1}$)
BDP	132.749 ± 5.039
Budesonide	89.982 ± 4.531
Terbutaline Sulphate	1.0
PVP K30 (Rogueda, 2003) after 2 days	2700 ± 700
PAA (Columbano, 2000)	0.0*
PVA (Jones et al., 2006a)	0.0*

* in HFA134a

2.14 Conclusions

A thorough physicochemical characterisation of materials was undertaken and the results have been presented and discussed above. When studying adhesion of particles in MDIs particle properties such as size, morphology and density will have a direct impact (Hinds, 1999). The nature of liquids and canisters will also play an important role. Furthermore investigating if particles change when interacting with the liquid in a suspension is essential. In order to evaluate the most important factors in adhesion it is essential to know if particle surfaces are subject to changes like Ostwald ripening, dissolution or crystal growth (Vervaet and Byron, 1999). In Section 2.6-2.8 it was shown that no solvates were formed when powders were stored in HPFP. Therefore HPFP is a good candidate in the model MDI systems of this thesis. In this chapter, first differences in morphology, size, density, melting point, crystallinity and solubility of the powders were determined. Not unexpectedly the corticosteroids BDP and budesonide were very similar. The great difference between the three materials was the solubility. Moreover when physicochemical properties, such as density, viscosity, surface tension and dielectric constant were determined and differences were found between the various fluorinated liquids. The surface energies of powders and canisters are expected to vary from material to material and will be measured in the following chapter. Consequently materials with a range of properties will be used for studying adhesion in MDIs.

Chapter 3: Microparticle Adhesion

3.1 Introduction

The stability of metered dose inhaler suspensions is a major priority to ensure maximum device performance. Adhesion to the canister wall and valve components is one of many things that have an impact on the stability in pMDIs and in this study adhesion to the canister will be further looked into with the aim of understanding the phenomena better so adhesion can be minimized when developing new as well as existing pMDI devices. Others have looked at the adhesion to canister valve components (James et al., 2009, Jinks, 2008). Modifying the canister coating has been shown to reduce particle adhesion to the canister wall (Jinks, 2008). When pMDI propellants were changed from CFCs to HFAs the propellants physicochemical properties were changed (Chapter 1), which lead to less stable formulations that had to be reformulated. The instabilities were caused by issues such as decreased solubility of surfactants, increased solubility of APIs and enhanced adhesion to the canister wall (Parsons et al., 1992, Tiwari et al., 1998, Beausang, 2005). Partial solubility of APIs in a suspension formulation can lead to crystal growth due to Ostwald ripening, which can cause instabilities in the formulation, such as blockage of the nozzle and dose variations (Vervaet and Byron, 1999). Albuterol crystals in CFC suspensions have been shown to grow for as long as 38 weeks and a significant increase in crystal size was already observed after 3 days of storage in a CFC suspension (Phillips et al., 1990). The same study also showed that crystal growth was higher in liquids with higher polarity, so the crystals grew larger in CFC 11 than in CFC 12. Since HFAs are more polar than CFCs, showed by the dielectric constants for CFC and HFA propellants presented in Table 1.1, Section 1.1.4.1, crystal growth becomes a greater issue in the HFA formulation. In order to prevent adhesion in pMDIs a thorough understanding of the interactions causing it is essential. Others have shown that adhesion in pMDI depends on the API concentration, particle size, surface energy of particles, liquid and canister and the actuator dimensions (Vervaet and Byron, 2000, Parsons et al., 1992). The adhesion depends on the balance between particle-canister, particle-liquid and liquid-canister interactions, which will be discussed in more detail in Chapter 6. The adhesion can be altered by changing canister coating or the formulation and very efficient coatings (Britto, 2007) and formulations

(Lewis et al., 2008) for adhesion reduction are available on the market today. Unfortunately for many companies, but luckily for some, there are patents protecting the efficient coatings and formulations and therefore a further understanding of interactions between pMDI components and of adhesion is of great interest in an engineer perspective to enable development of new pMDI coatings.

There is an inconsistency in the literature where adhesive interactions in pMDIs are often predicted by experimental studies in non-pressurised systems. The ideal experimental setup would be to measure both the true adhesion and the predicted interactions in propellants such as HFA134a and HFA227 but many experiments are not possible to carry out under pressurised conditions. Correlating the true adhesion in pMDIs with predicted interactions in model HFAs does not consider the impact physicochemical differences between the propellants (mostly HFA 134a and HFA 227) and the model HFA (often 2H,3H-perfluoropentane) has on adhesion. Therefore non-pressurised systems will be used throughout this study for consistency and also to avoid errors in the correlations due to pressure and HFA nature. The interactions between particles and canister walls in pMDIs has in the past been determined directly by use of atomic force microscope (AFM) (Begat et al., 2004, Traini et al., 2006) or indirectly by for example contact angle or inverse gas chromatography (Beausang, 2005). The AFM experiments are generally not performed in pressurised environment and therefore model propellants, that are liquid at room temperature and pressure, have been used for such measurements (Traini et al., 2005, Traini et al., 2006). However the true adhesion in pMDIs is mostly measured in pressurised systems with propellants such as HFA 134a and HFA 227 (Jinks, 2008, Beausang, 2005, Tiwari et al., 1998). It has actually been shown that higher adhesion may be a result of higher internal pressure in the canister (Tiwari et al., 1998), which shows the importance of using the same HFA throughout studies to avoid errors in correlations between the true and predicted adhesion due to physicochemical differences between the propellants. Only one study could be found in the literature where a non-pressurised model CFC was used throughout the whole study when true adhesion was correlated with predicted interactions from contact angle (Parsons et al., 1992). Hence, there is a need to see how commonly used materials in pMDIs behave in terms of adhesion in non-pressurised model propellants. Especially in 2H,3H-perfluoropentane (HPFP), which is proven to be a suitable model propellant and has been widely used in experiments related to pMDIs (Rogueda, 2003, Traini et al.,

2006, James et al., 2009).

The true adhesion is mostly measured differently in pressurised and non-pressurised systems. For pressurised systems it is hazardous to empty the canister in other ways than by releasing doses by actuation, unless the canister is cut open and emptied at temperatures below the HFAs boiling point, which is -16.5°C and -26.3°C for HFA 227 and HFA 134a respectively (Rogueda, 2003). Once the pMDI is empty and the canister is cut open the HFA evaporates very quickly. In non-pressurised systems the canisters cannot be actuated since there is no pressure and must therefore be cut open and the suspension poured out, followed by rinsing of the canister with model propellant, Figure 3.1. Due to the different emptying methods the measured particle adhesion in pressurised systems give much larger adhesion (Dohmeier et al., 2009, Jinks, 2008, Tiwari et al., 1998) than the non-pressurised system (Parsons et al., 1992).

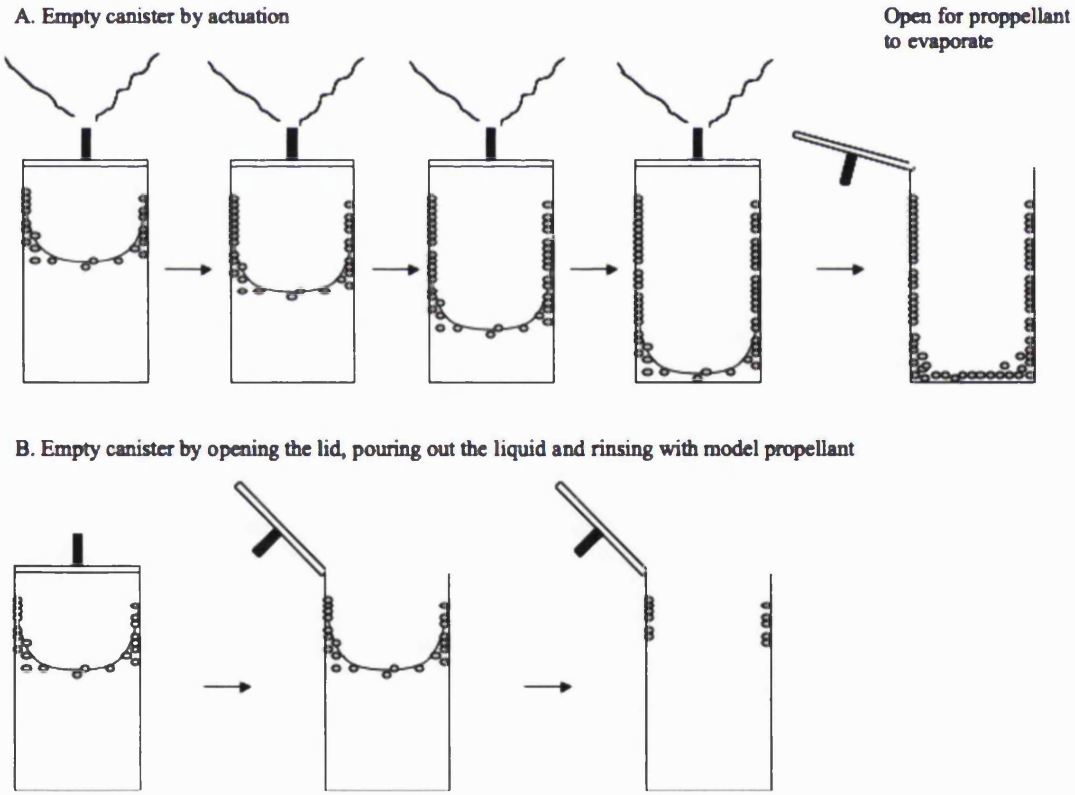

Figure 3.1. A schematic demonstration of the preparation of samples for adhesion analysis: A) pressurised canister and B) non-pressurised canister.

In this chapter the adhesion in model metered dose inhalers will be evaluated. Particle adhesion in pMDI varies a lot and is therefore not always easy to study (Beausang, 2005). Various factors that could affect adhesion, such as liquid and powder compound

chosen for the formulation, canister material, storage time, suspension concentration and filling volume will be looked into in this chapter.

3.2 Materials and Methods

Particle adhesion in model metered dose inhaler suspensions was studied visually, by weight and high-performance liquid chromatography (HPLC). The formulations were simplified and only API and fluorinated liquids that were in liquid form at room temperature and pressure were used. The formulations were creaming suspensions, since the density of the particles was lower than the density of the liquids. The simplified systems were used to enable easier comparison between the real adhesion, theoretical calculated interactions and interactions measured by atomic force microscopy.

The materials used were powders: beclomethasone dipropionate (BDP), budesonide, terbutaline sulphate, polyacrylic acid (PAA), polyvinylpyrrolidone (PVP) and polyvinylalcohol (PVA); liquids: 2H,3H-perfluoropentane (HPFP), perfluoroheptane and perfluorodecalin and canisters: glass, polyethyleneterephtalate (PET), aluminium (AL), anodised aluminium (ALAN) and perfluoroalkane coated aluminium (ALPF).

The true adhesion was investigated in four studies where a digital camera was used to record the visual adhesion, in addition the true adhesion was quantified by weight in study 2 and by HPLC in study 3. When comparing samples a t-test, two samples with same variance, was carried out with a significance level of 95% ($p < 0.05$).

3.2.1 Finding Powders that Adhere

The first study was carried out in order to find powders that adhered to canister walls when dispersed in fluorinated liquids and it was straightforward since adhesion was studied by eye. A range of micronised APIs and spray-dried polymers were suspended in HPFP in glass canisters with screw lids. A volume of 4 mL HPFP was added to the vial containing a spatula tip of API powder, the particles were suspended by manual shaking and put on storage at room temperature. When the canisters had been stored for 3 weeks at room temperature and emptied of suspension the adhesion was studied by digital imaging. The sample vial was put on a costume made stand, enlightened with a

photonic cold light source (PL3000, 150W, double gooseneck arm Brunel Microscopes Ltd, UK) and the adhesion at the former fluid line was recorded with a high resolution CCD digital camera (1.4 Megapixel CCD USB 2.0 Camera, Infinity 2-1, Digital Imaging Systems Ltd, UK) equipped with a zoom lens (Macro Video Zoom Lens, 18-108, F/2.5, Optem, Digital Imaging Systems Ltd, UK) mounted on the costume made camera stand at a fixed distance from the sample as in Figure 3.2.

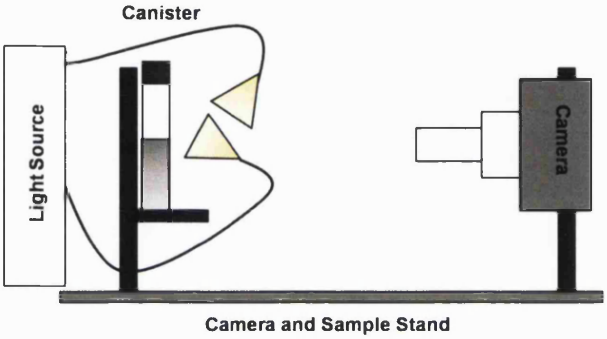

Figure 3.2. Set-up of imaging equipment (camera, light source, canister sample and stand) for recording adhesion.

The powders chosen were BDP, budesonide, terbutaline sulphate, PAA, PVA and PVP because the study required powders with a wide range of surface energies and polymers are known to have a lower surface energy compared to APIs (Jones, 2006). Also all compounds but PAA are commonly used in pMDI formulations and therefore interesting to study in the model propellants. BDP and budesonide are corticosteroids, terbutaline sulphate is a β-agonist and PVP and PVA are used as suspension stabilisers in pMDI formulations.

3.2.2 Adhesion Analysed by Weight

In the second study where adhesion was measured by weight, the two corticosteroids, BDP and budesonide and the polymer PVP were used. Adhesion of PAA was also studied but no adhesion was detected, therefore the adhesion of the compound was not. The adhesion in three different fluorinated liquids was investigated to understand the effect the nature of the liquid had on adhesion. The adhesion of BDP, budesonide and PVP in HPFP, perfluoroheptane and perfluorodecalin to glass canisters (7 ml squat form screw cap vials, Scientific Laboratory Supplies, UK) was measured as a function of time. The samples were stored for 0.5, 1, 230 and 450 hours and two additional sample

sets, budesonide and PVP in HPFP, were stored for 624 hours. Four repeat samples per measurement point were analysed. When true adhesion has been measured by others the adhesion after a week or longer has been looked at and therefore, to find the time required for maximum adhesion to be reached, time points earlier and later than a week were chosen. This explains the large gap between time points in this study. Suspensions of 2mg/mL concentration were prepared by adding 4ml liquid to 8mg powder. This is a commonly used concentration in pMDI formulations and has been used in other studies where true adhesion has been measured, which enabled comparison (Jinks, 2008, Beausang, 2005). One minute was the time chosen to shake the suspensions manually to allow time for the particles to disperse without losing too much time and each second the shaking movement in Figure 3.3 was performed.

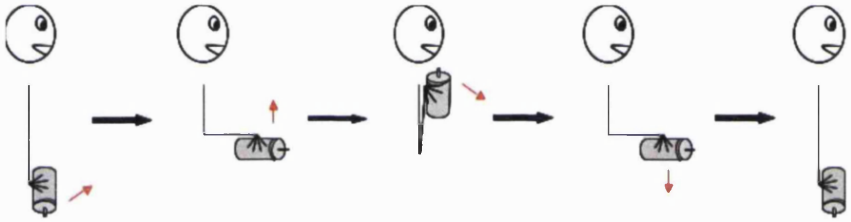

Figure 3.3. Method for manual shaking of a metered dose inhaler, 1Hertz.

The suspensions were stored at 30 ± 2 °C in a controlled temperature water bath. Due to high temperature variations in the laboratory caused by weather changes this temperature was chosen since it was the closest one to room temperature possible to control with good accuracy during the temperature fluctuations. Prior to analysis the vials were shaken ten times at the pace of 1 Hertz as in Figure 3.3 to remove loose particles, then the suspensions were poured out and canisters were rinsed with fluorinated liquid until there were no particles visible in the washing. When the liquid had evaporated the vials were weighed and adhered material was evaluated with the following equation.

$$W_{adhered\ material} = W_{vial\ with\ adhered\ material} - W_{empty\ vial} \qquad (3.1)$$

In order to get a visual idea of the adhesion digital images of the empty canisters with adhered material were taken with the camera used in Section 3.2.1.

3.2.3 Adhesion Analysed by HPLC

In the third study adhesion to canisters was determined with high-performance liquid chromatography (HPLC), which is an analytical technique that separates organic compounds by their affinity to the stationary phase. Not only the impact of storage time, powder and fluorinated liquid on adhesion was investigated but also the impact of canister material, suspension concentration and canister filling volume on adhesion were investigated.

The parameters were varied in the following way: storage time (1 hour, 1 and 2 days, 1, 2, 3, 4 and 5 weeks), powder (BDP, budesonide and terbutaline sulphate), fluorinated liquid (HPFP, perfluoroheptane and perfluorodecalin), canister material (PET, AL, ALAN and ALPF), suspension concentration (0.6, 2 and 4 mg/mL) and canister filling volume (3 and 6 mL for AL canisters, 5 and 10 mL for PET canisters). PAA was not included since it has no chromophore and therefore is not detectable by UV, which is the HPLC detector in this study. For each condition a repeat of five samples was done. Suspensions of 0.6, 2 and 4 mg/mL concentration were prepared in PET canisters by adding 10mL liquid to 6, 20 and 40 mg powder respectively and in AL-based canisters by adding 6mL liquid to 3.6, 12 and 24 mg powder respectively. For the study where adhesion by canister filling volume was looked into 10 and 5mL suspension was filled into PET canisters and 6 and 3mL suspension was filled into aluminium-based canisters at a concentration of 2mg/mL, which is a concentration commonly used in pMDI formulations. The canisters were sealed with crimped lids and either shaken at 1 Hertz as in Figure 3.3 for one minute or put in a sonication bath for one minute to disperse the particles. Further the samples were stored at 30°C ± 0.5 °C in a controlled temperature unit.

Prior to analysis the canisters were shaken ten times at 1 Hz as in Figure 3.3, emptied of suspension and rinsed with the fluorinated liquid used in the suspension until no particles remained in the fluorinated liquid disposed. When the fluorinated liquid in the canister had evaporated images of the transparent PET vials were captured with the camera settings used in Section 3.2.1. Then the adhered powder residue in the canister was dissolved, corticosteroids in ethanol and terbutaline sulphate in water, and the

washing was analysed by HPLC. The vials were rinsed twice with solvent to ensure all powder residue was dissolved, PET vials were rinsed with 3 mL and the aluminium-based vials with 2 mL each time respectively to obtain a washing with highest possible concentration. The washings were collected in syringes (disposable luer syringe, 2mL, Western laboratory solutions, UK) and filtered through 0.2μm filter units (Millipore express sterile polyetersulfone filter, 0.22μm pore size, Millipore, UK) before being analysed in the HPLC.

In the first part of this study adhesion of two different powders by time in the three different liquids was studied. BDP in perfluoroheptane and perfluorodecalin and budesonide in HPFP, perfluoroheptane and perfluorodecalin and PET canisters were used. Secondly adhesion by time of budesonide and terbutaline sulphate in HPFP was studied and PET, AL, ALAN and ALPF canisters were used. Thirdly the effect of suspension concentration and canister filling volume on adhesion was investigated but only for suspensions based on budesonide and HPFP in AL and PET canisters.

Images of adhesion of BDP, budesonide and terbutaline sulphate in HPFP to PET canisters after 2 weeks were captured with the camera used in Section 3.2.1.

3.2.3.1 HPLC Methodology

The adhesion to canisters was analysed with reverse phase isocratic HPLC. Reverse phase is when compounds are separated according to their hydrophobicity and an isocratic method is when the mobile phase composition is constant. An HPLC of the HP 1050 series (Hewlett-Packard, UK) was used, including an auto sampler, an isocratic pump and a variable wavelength UV-detector. The mobile phase passed through a solvent D-gasser 7600 series (Jones Chromatography, UK) prior to entering the HPLC. The system was controlled by and analysis of samples was carried out with PRIME version 4.2.0 software (HPLC Technology, UK). The HPLC methods used are detailed in Table 3.1. The samples were loaded into HPLC vials with screw lids (vials: HPLC screw vials, amber, 8 mm cap size, 2 ml and lids: black polypropylene with hole, seal in silicone/PTFE, Fisher Scientific, UK).

Table 3.1. HPLC methods.

	BDP	Budesonide	Terbutaline Sulphate
HPLC Column	Waters Symmetry C_{18}, 3.9 x150 mm, 5μm	Waters Symmetry C_{18}, 3.9 x150 mm, 5μm	Waters Symmetry C_{18}, 3.9 x150 mm, 5μm
Mobile Phase	Acetonitrile : Water 50 : 50	Acetonitrile : Water 40 : 60	Buffer : Methanol 75 : 25 + 1% w/v glacial acetic acid added to total volume Buffer: 5 mM sodium 1-hexanesulphonate in water.
Detection Wavelength (nm)	240	240	276
Flow Rate ($mL \cdot min^{-1}$)	1.0	1.0	1.0
Injection Volume (μL)	100	100	100
Run Time (min)	15	15	15
Retention Time (min)	2.4	2.0	3.7
Column Temperature (°C)	40	40	40

The mobile phases used to analyse the corticosteroids were prepared by mixing acetonitrile and water. The mobile phase used to analyse terbutaline sulphate was a mixture of a buffer and methanol and the buffer was prepared by first by mixing 1.0312g of sodium 1-hexanesulphontate into 1L water and then adding 10mL glacial acetic acid to the 5mM sodium 1-hexanesulphonate buffer followed by mixing. All mobile phases were sonicated for ten minutes to remove excess gas prior to entering the D-gasser and HPLC. All compounds used for preparing mobile phases can be found in Table 3.2.

Table 3.2. Compounds used for HPLC mobile phases

Compound	Supplier
Water HPLC gradient grade	Fisher Scientific
Acetonitrile HPLC gradient grade	Fisher Scientific
Methanol HPLC gradient grade	Fisher Scientific
Glacial Acetic Acid HPLC gradient grade	Fisher Scientific
Sodium 1-hexanesulphonate AnaL R grade	Fisher Scientific

Twenty-five samples were analysed at the time and prior to the analysis of each set of 25 samples the mobile phase was pumped through the HPLC system for 30 minutes followed by a blank injection to ensure a clean system. All samples were analysed in triplicate, right after preparation to prevent degradation of compounds in the solvent and

the analysis started with the samples that had been stored the shortest time and finished with the samples stored the longest, i.e. went from lower to higher concentration. Each analysis cycle of 25 samples started and ended with a blank run and every sixth vial was a calibration standard with known API concentration to ensure that the HPLC conditions had not changed.

Calibration standards were prepared from stock solutions made up in duplicate for each API by adding 0.012g of powder to 15 ml solvent (concentration = 0.8mg/mL). A series of calibration standards of 0.001-0.1mg/mL were prepared from the stock solutions for each API. Each sample was analysed in triplicate in the HPLC and consequently each point in the calibration curve was a mean of 6 measurements.

3.2.3.2 HPLC Method Validation

The analytical methods used were validated in terms of linearity, precision and accuracy according to the ICH Q2B validation of analytical procedures (CDER, 1994). Linearity is when the concentration of a sample within a specific range, in this study 0.001-0.1mg/mL, is directly proportional to the signal measured by the instrument. The linearity is obtained by calculating the linear regression of a curve, R^2 and if $R^2 < 0.999$ the curve is considered linear. The precision of the method shows the dispersion of the data and can be expressed by the standard deviation (σ) of the replicas

$$\sigma = \sqrt{\sum_{i=1}^{n} \frac{(x_i - \mu)^2}{n-1}} \tag{3.2}$$

where x_i represents the concentration of the i^{th} measurement, μ the mean of n replicas. Accuracy shows how close the experimental concentration is to the predicted concentration and if there is sample loss during preparation of the samples the accuracy will show it. The accuracy of the mean concentrations measured can be expressed as a percentage by using the following equation

$$Accuracy = \frac{\mu}{\mu_{est}} \cdot 100 \tag{3.3}$$

where μ and μ_{est} are the experimental and predicted mean concentrations respectively.

3.2.4 Short Time Adhesion

Finally in the fourth study the short time adhesion (< 24 hours) was studied visually with the camera setup used in Section 3.2.1. Due to the transparency of PET canisters they were used for the digital imaging. Close up images of BDP, budesonide and terbutaline sulphate particles in HPFP at the fluid line, Figure 3.4, were captured at various times (1, 5, 30, 60 minutes and 24 hours) within a day after the suspension was prepared. Timing started after the sample had been sonicated for 1 minute.

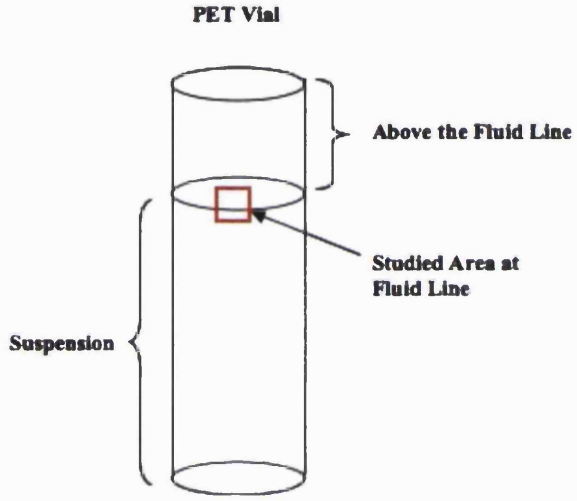

Figure 3.4. A schematic image of the area by the fluid line in PET canisters that was studied with a digital camera.

3.3 Results & Discussion

3.3.1 Finding Powders that Adhere

The adhesion of six powders to glass canisters after 3 weeks is shown in Figure 3.5. Four powders did adhere to glass (BDP, budesonide, terbutaline sulphate and PVP) and two did hardly adhere (PAA and PVA). The adhesion started very soon after the preparation of the suspensions and was considered irreversible since the particles adhered to the fluid line were not possible to remove by shaking the suspension. The corticosteroids BDP and budesonide were considered interesting for adhesion studies due to their physicochemical similarities. Among the four powders that did adhere in Figure 3.5 there were visual differences in the way the powders adhered. BDP and

budesonide showed distinct adhesion both through a ring formed in the area where the meniscus of the suspension had been and on the wall above the meniscus, BDP powder formed a more distinct ring than budesonide by the meniscus. PVP mainly adhered at the fluid line and formed a clear ring while terbutaline sulphate on the other hand did not form the ring but mainly adhered above the meniscus, which indicates that the adhesive interactions in HPFP are higher for the powders forming a ring than for terbutaline sulphate.

Since no visual adhesion of PAA and PVP was observed zero adhesion was assumed and the compounds zero adhesion will be included for comparison in other chapters.

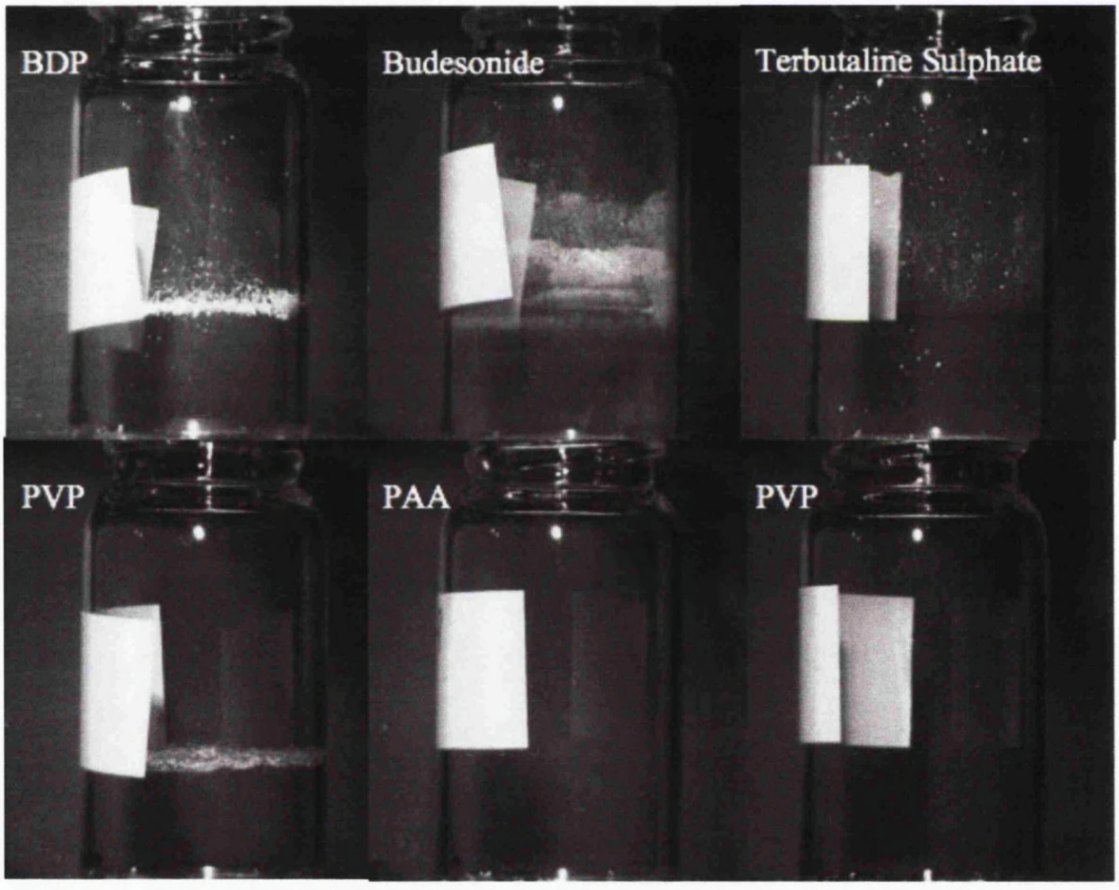

Figure 3.5. Adhesion of powders in HPFP to glass after 3 weeks. The images show canisters where suspensions had been poured out and HPFP evaporated.

In the adhesion presented in Figure 3.5 the powder mass in the suspension was not controlled since the main purpose of this experiment was to find powders that adhered

to the wall not to quantify the adhesion. A thorough comparison in the quantity adhered to the canister walls will be done in the following section.

3.3.2 Adhesion Changes in Various Model Metered Dose Inhaler Systems, Analysed by Weight

From the previous section it was shown that different powder compounds adhere to glass differently when dispersed in the same liquid. In this section the impact on adhesion when using hydrofluoroalkane compared to perfluoroalkane liquids will be studied. Adhesion results of various powders dispersed in hydrofluoroalkanes and perfluoroalkanes after 450 hours are presented in different ways quantitatively in Figure 3.6 and Figure 3.8 and visually in Figure 3.7. The adhesion of PAA was also studied here but no adhesion was detected by weight analysis, therefore zero adhesion of PAA was assumed.

The most apparent adhesion differentce was between PVP and corticosteroids in the liquids, Figure 3.6, where PVP adhered more than the corticosteroids at most of the time points in both HPFP and perfluoroheptane (2 sample t-test, $p < 0.05$). The trend observed in perfluorodecalin was different for the powders where there was no difference in adhesion of PVP and BDP and significantly lower adhesion than for budesonide up to 230 hours (2 sample t-test, $p < 0.05$). There was no difference in adhesion of BDP and budesonide in HPFP for all time points but 230 hours and in perfluoroheptane there was no difference for the first two time points then a significant difference (2 sample t-test, $p < 0.05$).

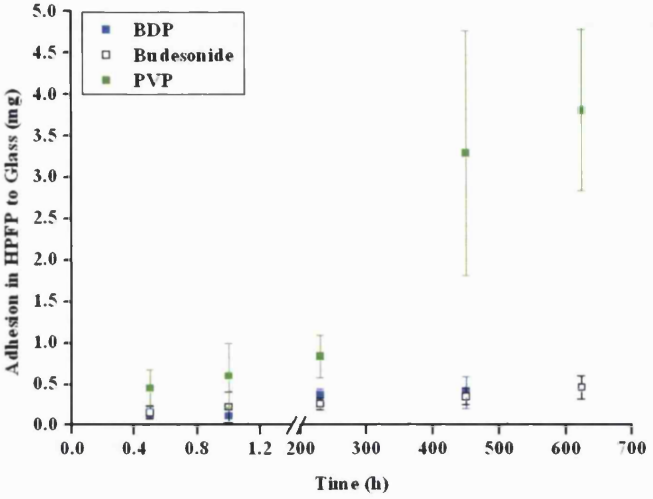

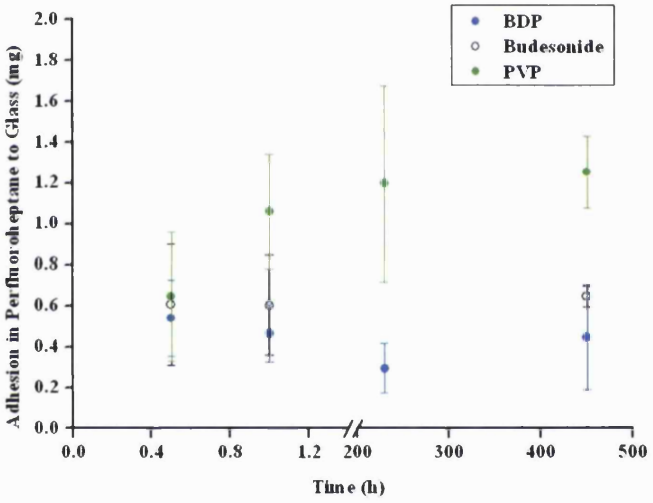

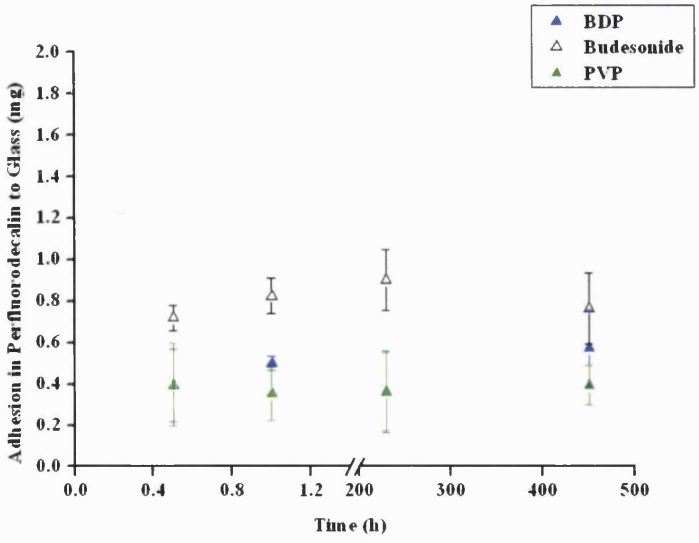

Figure 3.6. Adhesion of powders in HPFP, perfluoroheptane and perfluorodecalin to glass canister over time stored at 30°C as measured by weight (n=4).

A difference in particle adhesion between HPFP and the perfluorinated liquids was observed. The digital images in Figure 3.7 visually confirmed the differences in adhesion between powders in HPFP and perfluorinated liquids, but it was not visually clear that the adhesion of PVP in perfluoroheptane was higher than for the corticosteroids, which was shown in Figure 3.6. However, when looking at the amount adhered to the canisters the quantitative results in Figure 3.6 should be looked at. The total visual adhesion in HPFP increased like: BDP < budesonide < PVP, though the adhesion in the area of the meniscus was higher for BDP than for budesonide. The major adhesion of corticosteroids in HPFP was focused at and above the meniscus while it was spread over the entire canister wall in perfluorinated liquids. The adhesion of PVP was focused at and above the meniscus in HPFP and perfluorodecalin but not in perfluoroheptane where the adhesion seemed to occur at and below the meniscus.

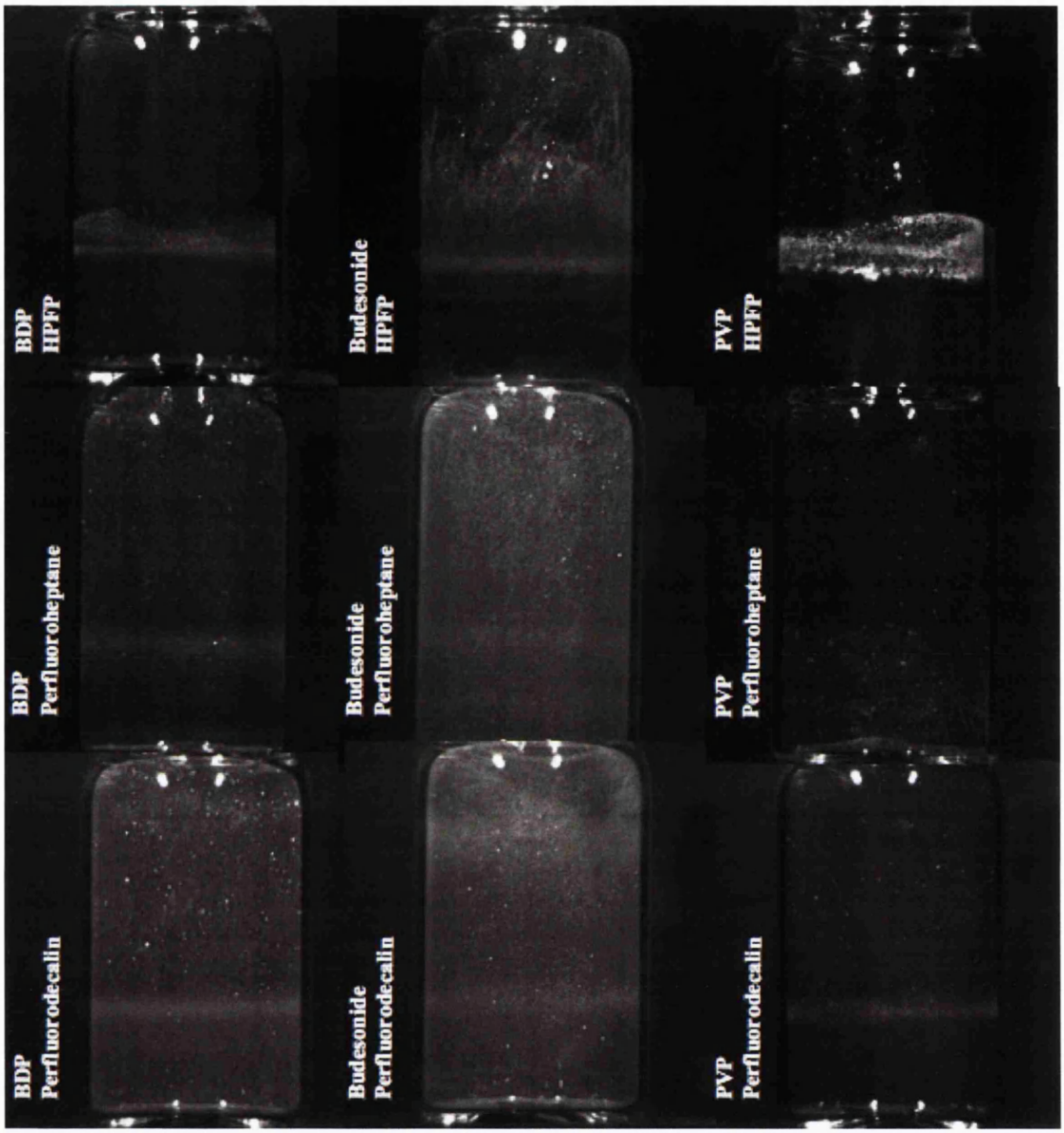

Figure 3.7. Digital images of adhesion of BDP, budesonide and PVP in HPFP, perfluoroheptane and perfluorodecalin to glass canisters after 450 hours. The images show canisters where suspensions had been poured out and HPFP evaporated.

Plots of adhesion for each powder in the fluorinated liquids are shown in Figure 3.8 and the figure shows that the adhesion over time increases in HPFP but not in perfluoroalkane liquids (2 sample t-test, $p < 0.05$). The adhesion of corticosteroids in HPFP was initially lower than in perfluorinated liquids but by time it approached the values of the perfluorinated liquids. Within 450 hours the adhesion of BDP in HPFP had reached the same adhesion as in the perfluorinated liquids but not budesonide, which remained lower (2 sample t-test, $p < 0.05$). In opposite to the corticosteroids adhesion behaviour the adhesion of PVP in HPFP ended up higher than in

perfluorinated liquids at 450 hours, also there was an increase in adhesion by time for PVP in perfluoroheptane (2 sample t-test, $p < 0.05$).

Since the visual adhesion followed similar rank order to adhesion analysed by weight the visual adhesion can be considered a quick way to fast analysis of adhesion.

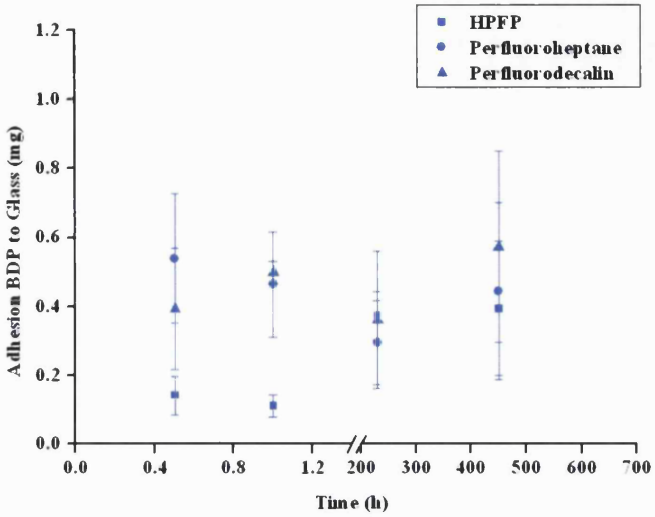

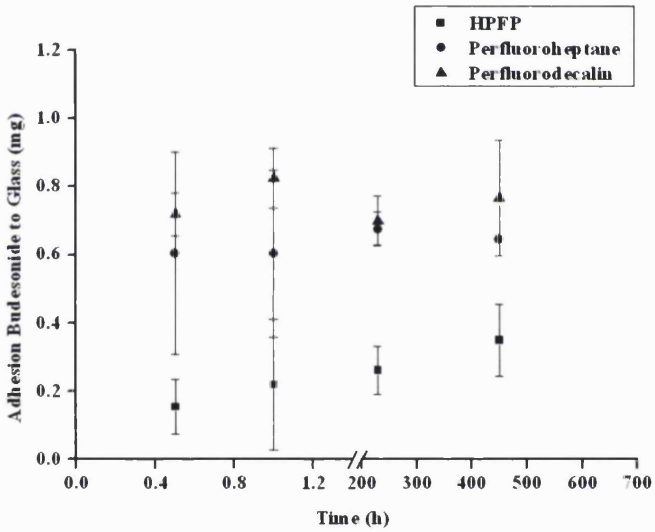

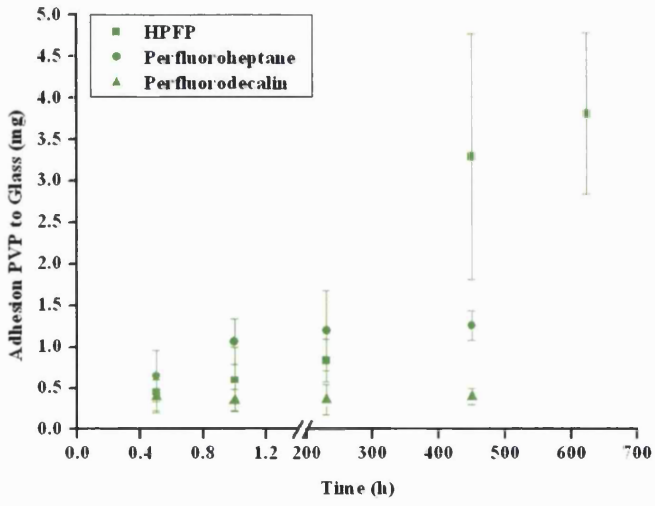

Figure 3.8. Adhesion of BDP, budesonide and PVP in fluorinated liquids to glass canister over time as measured by weight (n=4).

During the experiment the activity in the various suspensions was observed visually and there were clear differences between HPFP and the perfluorinated liquids. Particles were much more mobile and circulated quicker in HPFP compared to in the perfluorinated liquids. Also right after dispersing the powders in the perfluorinated liquids instant adhesion of particles all over the canister wall was observed, probably as a result of preferred adhesive interaction with the canister wall over the liquid interactions. These visual observations could be confirmed by a study in the literature where interactions between particles and fluorinated liquids were proven to be higher in HPFP than in perfluorodecalin due to hydrogen bonding (Jones et al., 2006a, Paul et al., 2005), which was shown by the oxygen atoms in the powder compounds hydrogen bonding with the hydrogen atoms in HPFP. Therefore the nature of the liquid has an impact on adhesion and there are several differences in physicochemical properties between the three fluorinated liquids used in this study, as summarised in Table 3.3. The hydrogen atoms in HPFP makes HPFP more polar than perfluorinated liquids, which is shown by the higher dielectric constant in Table 3.3 (Rogueda, 2003). The slower particle circulation in perfluorinated liquids, especially perfluorodecalin, is probably a result of the higher viscosity since the mass transfer in a more viscous liquids is slower (Coulson et al., 1999).

Table 3.3. Summary of the physicochemical properties of fluorinated liquids presented in Chapter 2.

Compound	Physicochemical Properties at 30°C			
	Density ($g \cdot cm^{-3}$)	Viscosity (mPa·s)	Surface Tension ($mN \cdot m^{-1}$)	Dielectric constant
HPFP	1.56 ± 0.01	0.53 ± 0.00	13.39 ± 0.04	6.47 ± 0.00
Perfluoroheptane	1.71 ± 0.01	0.75 ± 0.00	12.73 ± 0.06	1.76 ± 0.00
Perfluorodecalin	1.92 ± 0.01	2.49 ± 0.00	18.06 ± 0.19	1.91 ± 0.00

The increase in adhesion by time in HPFP is shown visually in the images in Figure 3.9 where the build up of adhered particles around the meniscus to form a ring over time is shown.

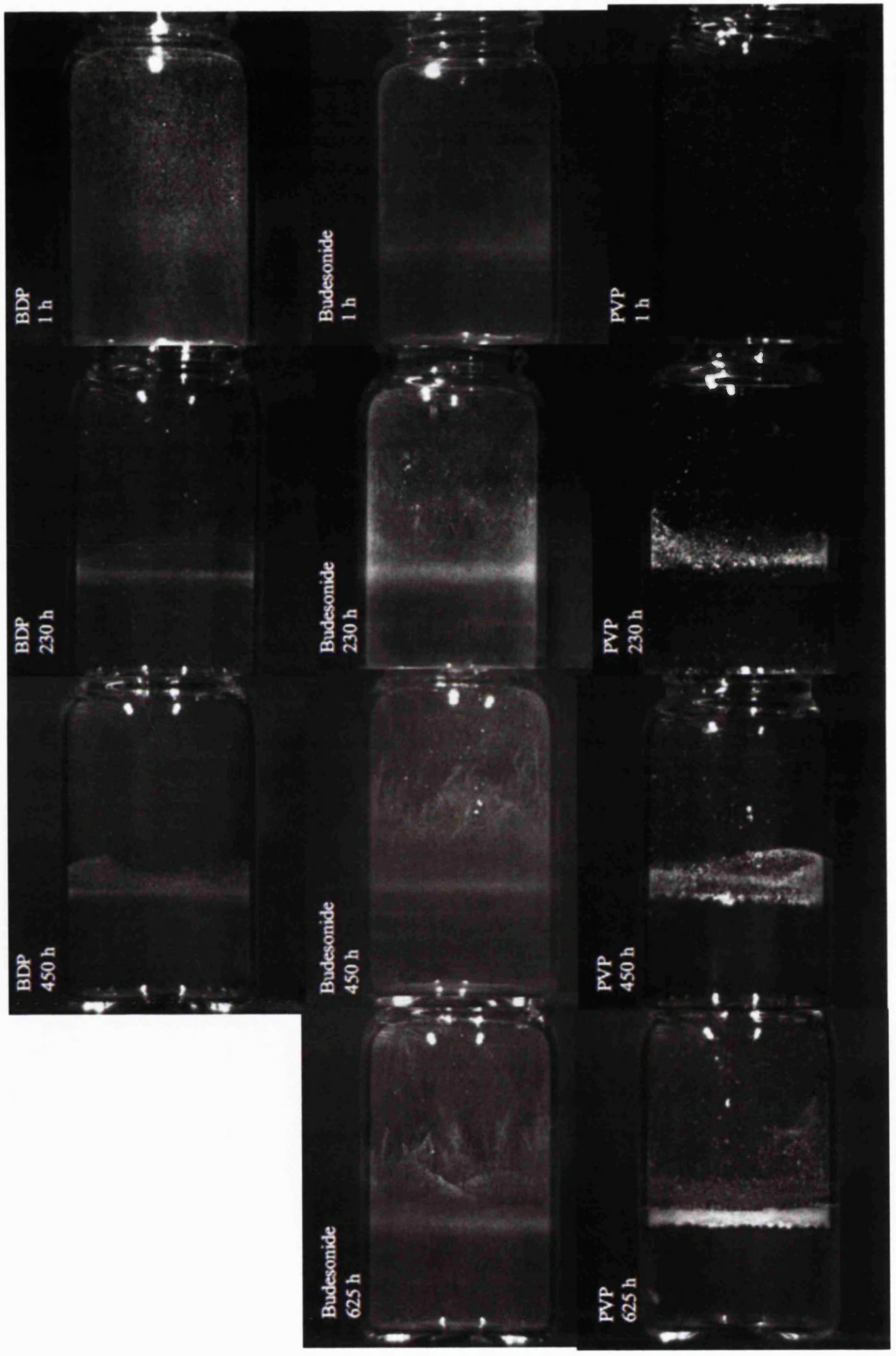

Figure 3.9. Adhesion of BDP, budesonide and PVP in HPFP to glass canisters by time. The images show canisters where suspensions had been poured out and HPFP evaporated.

Since the adhesion of PVP in HPFP over time was more than ten times higher than the adhesion of corticosteroids and the image of PVP in HPFP in Figure 3.7 show that adhesion primarily occurred by the meniscus for PVP there should be a build up of particles, likely first by adhesion to the canister and then by strong cohesive interactions between the particles in the suspension and already adhered particles. Since the canister area by the meniscus is limited the increase in adhesion is unlikely to be solely due to particles adhering to the canister wall but should also be due to other interactions, such as cohesion to already adhered particles. PVP is a polymer and therefore crystal growth is unlikely but polymers are known to swell when in contact with solvents and swelling of PVP particles could increase the contact area since the particles become smoother and softer, which could lead to higher adhesion (James et al., 2008). In HFA suspension systems there is a constant balance of interactions between particle-particle, particle-canister and particle-liquid that leads to more or less adhesion, which will be looked into in Chapter 6.

It was mentioned earlier that partial solubility of an API in a pMDI suspension is likely to lead to suspension instabilities, for small molecules the instabilities could be crystal growth. It was shown in Section 2.13.3 that PVP and the corticosteroids are partially soluble, terbutaline sulphate almost insoluble and PAA and PVA were considered insoluble in HPFP. The effect polymer solubility has on adhesion in HPFP has been shown by Paul et al. 2005a and 2005b where they looked at the ability of PVP and PEG (polyethyleneglycol) to adhere onto 3μm glass spheres in HPFP. It was shown that PVP, which was less soluble than PEG in HPFP adhered more to the glass spheres than PEG in HPFP, hence less polymer/liquid interaction resulted in a higher thermodynamic driving force for adhesion. It has been shown before, that adhesion is driven by the repulsive forces between the powder and the electron-dense HFA rather than by attraction between the powder and the wall (Vervaet and Byron, 1999). Since PVP is partly soluble in HPFP it is likely that its adhesion both depends on solubility and surface properties while the adhesion of the other two insoluble polymers, PAA and PVA, mainly depends on surface properties. If the suggested solubility/adhesion relationship, where adhesion increases with lower solubility (and powder-liquid interaction), would be applied to both PVP and APIs the adhesion would be higher for APIs, but it is the other way around. When looking at several of the partially soluble compounds in this study it is not only solubility that differ but they are also very

different in other physicochemical aspects, as presented in Chapter 2, therefore the adhesion differences cannot be explained solely by solubility. The general trend for all compounds investigated so far is that the ones that are soluble in HPFP, PVP, budesonide, BDP and terbutaline sulphate, adhered to the canister wall while the insoluble ones, PAA and PVA, did not.

Digital imaging turned out to be a useful tool for visual analysis of adhesion since it is quick and straightforward and gives a rough estimate of the material combinations that will lead to higher adhesion.

The adhesion by weight method used in this section for adhesion quantification showed some trends but was not considered accurate enough and two possible reasons were found. First analysing adhesion by weight with a five decimal balance was not considered accurate enough to detect differences in adhesion to glass of low amounts of powder (BDP and budesonide). This was most likely due to electrostatics being created when handling the samples with gloves that were used to prevent skin contact with the APIs. This was confirmed by weighing the same empty glass canister several times leading to considerable alterations in the readings in the fourth decimal of the balance. Secondly the screw lids for the vials used in this study were not providing a good enough seal, which led to evaporation of fluorinated liquid during storage. This was detected by a decrease in liquid levels after storage and it is likely that the variations in adhesion could have been a result of the evaporation increasing the mass transfer from the suspension to the canister wall, as described in Section 1.2.5.2. In the same section where mass transfer in thin films was discussed it was also explained that evaporation is known to have a driving effect on building up of particle deposits by the suspension/solid/gas interface.

Due to the inaccuracies in this method detected during the cause of the study it was not completed which lead to terbutaline sulphate data not being collected. In order to confirm if the adhesion differences in Figure 3.6 and 3.8 are representing true adhesion another more accurate analysis method such as HPLC should be used. It is important to confirm whether the large standard deviation was real or due to the use of a less suitable method before discussing the results in those figures more.

3.3.3 Adhesion Changes in Various Model Metered Dose Inhaler Systems, Analysed by HPLC

3.3.3.1 Method Validation

The retention time of the API peaks in the chromatogram corresponding to each API was ~2.4 minutes for BDP, ~2.0 minutes for budesonide and ~3.7 minutes for terbutaline sulphate.

Figure 3.10 shows the HPLC calibration plots of BDP and budesonide in ethanol and terbutaline sulphate in water for concentrations ranging from 0.001-0.1 mg/mL and the plots showed linearity in a linear regression analysis where $R^2 < 0.999$. Each calibration point is a mean of six measurements, based on two different stock solutions. There were no interfering peaks in the spectra, moreover after each calibration standard set was analysed the blank injected showed no residual sample from the previous run.

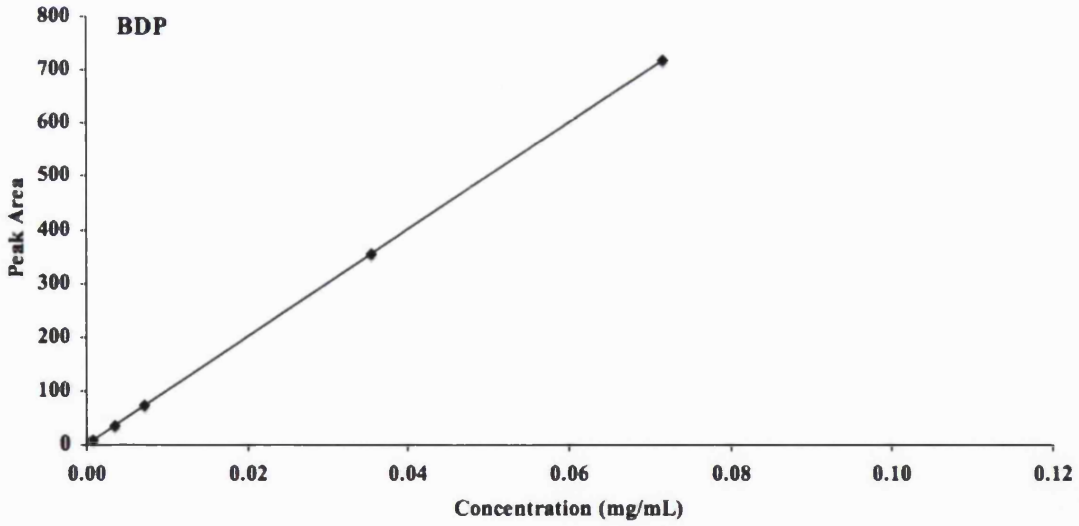

Figure 3.10. (continues on next page) Peak area against concentration. HPLC calibration plots for BDP (top), budesonide (middle) and terbutaline sulphate (below) (n=6).

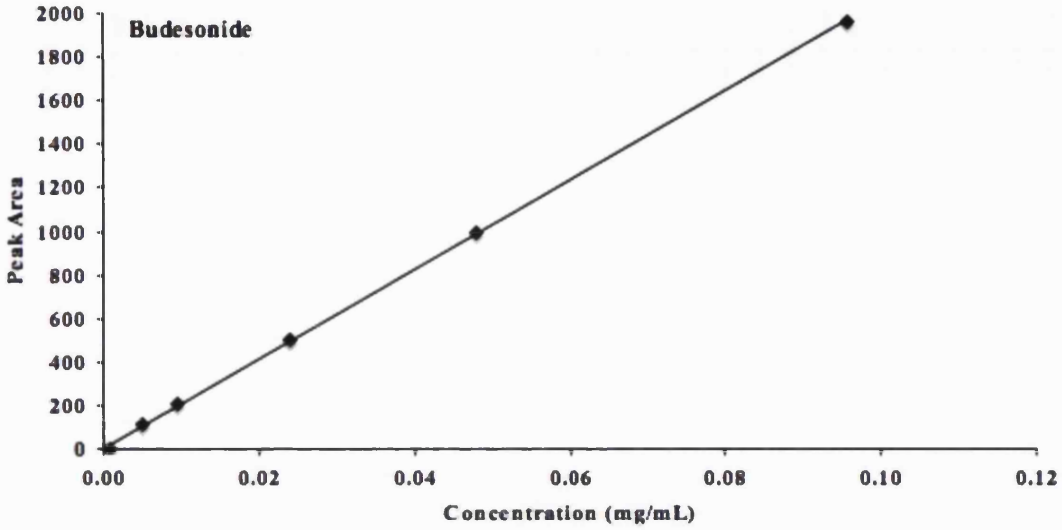

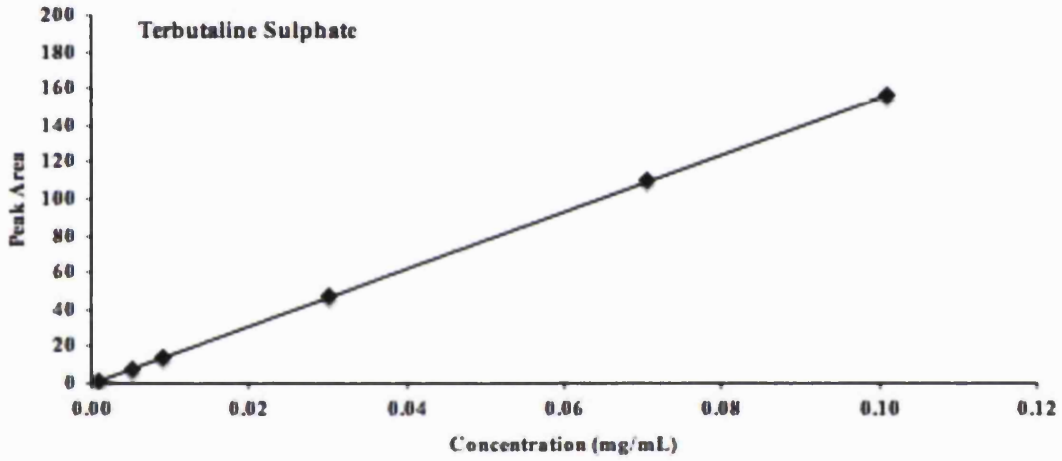

Figure 3.10 (continued from previous page)**.** Peak area against concentration. HPLC calibration plots for BDP (top), budesonide (middle) and terbutaline sulphate (below) (n=6).

Details of linearity, experimental and predicted concentration, precision and accuracy are presented in Table 3.4.

Table 3.4. Method validation details are presented: linearity (R^2), predicted concentration (μ_{est}), experimental concentration (μ), precision (SD) and accuracy for BDP, budesonide and terbutaline sulphate. (n=6)

API	R^2	μ_{est} (μg/mL)	μ ±SD (μg/mL)	Accuracy (%)
BDP	1.000	1	0.8 ± 0.05	81.3
		5	3.5 ± 0.1	69.4
		10	7.2 ± 0.1	71.7
		50	35.5 ± 0.8	71.1
		100	71.7 ± 1.2	71.7
Budesonide	0.9998	0.8	0.7 ± 0.002	91.4
		5.0	5.1 ± 0.1	101.3
		9.6	10.1 ± 0.5	105.3
		24.0	24.1 ± 0.8	100.5
		47.9	48.4 ± 2.7	101.0
		95.8	95.5 ± 4.3	99.7
Terbutaline Sulphate	1.000	1.0	0.9 ± 0.03	91.5
		5.1	5.0 ± 0.1	98.4
		9.1	9.1 ± 0.1	99.8
		30.3	30.5 ± 0.1	100.7
		70.7	70.8 ± 0.1	100.2
		101.0	100.9 ± 0.2	99.9

3.3.3.2 Adhesion Changes by Powder Compound, Fluorinated Liquid and Storage Time

Some of the trends shown in Section 3.3.2 were confirmed by this study and new trends appeared as a result of a more accurate analysis method. The impact of choice of powder, liquid, canister material, storage time, suspension concentration and canister filling volume had on adhesion was studied.

The results from the first part of this section are presented in Figure 3.11 where PET canisters were used and the suspensions were sonicated for one minute when prepared and stored in a water bath. The following parameters were varied: 1) powder compound, 2) fluorinated liquid and 3) storage time. If starting by looking at the effect the powder

chosen had on adhesion in Figure 3.10 there was a difference in adhesion between BDP and budesonide when the powders were suspended in the same liquid. Even though BDP and budesonide particles were very similar in terms of physicochemical properties and molecular structure (see Chapter 2), BDP adhered less than budesonide in perfluorinated liquids (2 sample t-test, $p < 0.05$). Looking back at the results in Figure 3.6 the adhesion of budesonide was also higher than the adhesion of BDP in perfluorinated liquids, which may be a result of BDP being more soluble in the liquids, hence a lower particle concentration in the suspension that leads to fewer particles available for adhesion to the canister wall. The impact of solubility on adhesion was possible to compare for the corticosteroids since solubility was the main physicochemical property difference between the two compounds that apart from solubility had very similar physicochemical properties and molecular structure as presented in Chapter 2. No solubility data for BDP and budesonide in perfluoroheptane and perfluorodecalin was available but since BDP was more soluble than budesonide in HPFP it is also likely to be more soluble than budesonide in the perfluorinated liquids.

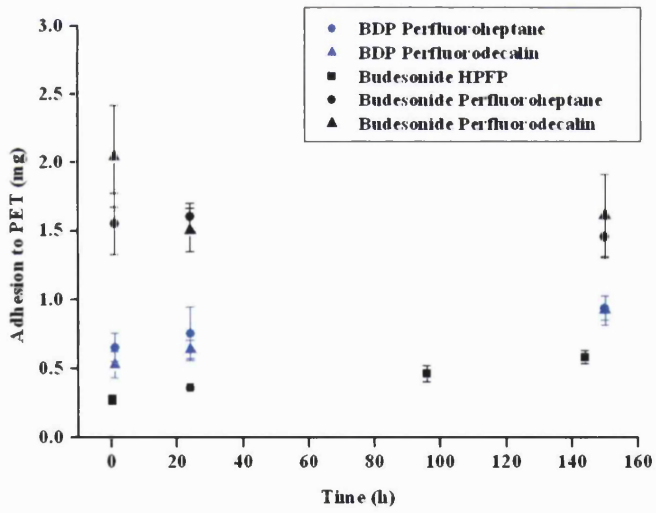

Figure 3.11. Powder adhesion to PET canisters over time as measured by HPLC (n=15).

Secondly when the adhesion differences between the fluorinated liquids in Figure 3.11 were compared, the vague trend shown in Section 3.3.2, where adhesion in perfluorinated liquids seemed higher than in HPFP for all compounds, was confirmed for budesonide in Figure 3.11 (2 sample t-test, $p < 0.05$). Furthermore there was no difference in adhesion of the same powder immersed in perfluoroheptane or perfluorodecalin (2 sample t-test, $p < 0.05$). The higher adhesion of budesonide in

perfluorinated liquids compared to HPFP is likely to be due to the lower powder-liquid attractive interactions in perfluorinated liquids, hence powder-canister adhesion is favoured over powder-liquid attractive interactions, as discussed in the previous section. Others have shown that when a compound that is able to hydrogen bond is in contact with HPFP and perfluorodecalin respectively there is hydrogen bonding between the compound and HPFP but not between the compound and perfluorodecalin (Paul et al., 2005). Therefore hydrogen bonding may be a reason for the higher attractive interaction between budesonide and HPFP. In perfluorinated liquids where repulsive rather than attractive powder-liquid interaction are likely to occur it could lead to the particles repelling from the liquid, resulting in more particles flocculating on the surface and adhering more to the canister walls (Paul et al., 2005, Purewal and Grant, 1997). The dielectric constant of fluorinated liquids in Table 3.3, Section 3.3.2, shows that HPFP has a dielectric constant approximately 3.9 times higher than the perfluorinated liquids, which shows that HPFP is more polar than the perfluorinated liquids (Rogueda, 2003). The influence of solubility on adhesion was discussed in the previous section. It has been shown that solubility of budesonide in fluorinated liquids increases with increased polarity of the liquids (Blondino and Byron, 1998) and since HPFP is more polar than the perfluorinated liquids the solubility of budesonide in HPFP is likely to be higher than in perfluorinated liquids. This could mean that the lower adhesion of budesonide in HPFP may also be a result of fewer particles in the suspension available to adhere since the solubility is higher. Propellants commonly used in pMDI are HFA227 and HFA134a with a dielectric constant of 4.07 and 9.46 respectively (Rogueda, 2003) that is considerably higher than those of the perfluorinated liquids, which is promising when aiming for minimal particle adhesion in suspension formulations.

Finally adhesion by time in Figure 3.11 will be looked into and similar to Section 3.3.2 the adhesion in perfluorinated liquids did not change significantly over time (2 sample t-test, $p < 0.05$), Figure 3.11 shows that maximum adhesion in perfluorinated liquids was reached within an hour. Adhesion of budesonide in HPFP increased over the time of the study (2 sample t-test, $p < 0.05$) and due to the length of the study it was not possible to see the time when maximum adhesion in HPFP occurred, therefore a study over longer time will be carried out. Others have shown that maximum adhesion for budesonide to PET canisters is reached within a day but that was for pressurised systems based on HFA 134a and HFA 227 (Beausang, 2005). Since there were

differences in the time when maximum adhesion was reached between suspensions based on different fluorinated liquids, showed both in Figure 3.11 and in Section 3.3.2, it cannot be assumed that the time for budesonide adhesion in HPFP to reach a maximum will be the same as in pressurised HFA systems.

3.3.3.3 Adhesion Changes by Powder Compound, Canister Material and Storage Time

The results from the second part in this section, where adhesion of budesonide and terbutaline sulphate in HPFP to PET, AL, ALAN and ALPF canisters was determined, are presented in Figure 3.12 and Figure 3.13 where the particles were dispersed by sonication and stored in an oven. The following parameters were varied: 1) powder compound, 2) canister material and 3) storage time. HPFP was chosen out of the three liquids used earlier in this section since it is a hydrogen substituted fluorinated liquid, such as the HFAs commonly used in pulmonary delivery (HFA 134a and HFA 227). According to the data presented so far there is a significant difference between adhesion in perfluorinated and hydrogen substituted fluorinated liquids and therefore HPFP was regarded the best model propellant of the three ones used in this study, also HPFP is commonly used as a model propellant for pMDI formulations when experiments cannot be performed in pressurised systems (Rogueda, 2003, Traini et al., 2005). BDP was not included in this part of the study as it was degraded by time when stored in HPFP and the adhesion was therefore not possible to analyse accurately by HPLC.

If starting by looking at particle adhesion to different canister materials, budesonide in Figure 3.12 and terbutaline sulphate Figure 3.13, and comparing the adhesion differences between the two APIs a significant difference in adhesion was found, where budesonide adhered more than terbutaline sulphate in all systems investigated (2 sample t-test, $p < 0.05$). This is also shown visually in Figure 3.14 where the images show that the adhesion of BDP and budesonide to PET was very similar and higher than terbutaline sulphate. This agrees with adhesion force measurements by AFM from the literature where budesonide has been compared to salbutamol sulphate, which is a compound similar to terbutaline sulphate, they have very similar molecular structure and physicochemical properties and it is therefore assumed here that salbutamol

sulphate and terbutaline sulphate behave similarly. In the AFM study the adhesion force between budesonide and AL and ALAN canisters in HPFP was shown to be stronger than the adhesion forces of salbutamol sulphate in the same systems (Traini et al., 2005). The same study also reported that the higher surface energy of budesonide compared to salbutamol sulphate could be a reason for higher adhesion. Terbutaline sulphate particles were larger than budesonide particles, which could affect adhesion through variations in contact area. Particle and canister roughness impact on adhesion has not yet been fully evaluated in pMDI systems, it has only been shown that roughness has an impact on adhesion (Young et al., 2003, Traini et al., 2006). Roughness impact on adhesion has been looked at in dry powder systems where adhesion of particles of the same compound but with different roughness have been evaluated and several studies have shown that adhesion decrease with increase in particle roughness (Paajanen et al., 2009, Adi et al., 2008a, Adi et al., 2008b). The adhesion differences may also be due to surface energy variance, which will be discussed in Chapter 4 and 6.

Secondly the adhesion differences between different canister materials in Figure 3.12 and Figure 3.13 was looked at and the amount of adhered material decreased in the following order for budesonide: PET > AL > ALAN > ALPF and for terbutaline sulphate: PET > ALAN > AL > ALPF. Studies found in the literature have shown that the force of adhesion decreases with increase in canister roughness when the canister roughness is in the submicron scale (Jiang et al., 2008) so if the canister materials roughness in this study is in the submicron scale roughness should have an effect on adhesion. So far the canister roughness has been evaluated visually by SEM in Section 2.2, not quantitatively, and it seemed to decrease in the following order: AL > ALPF > ALAN > PET > glass. There are signs in this study that the rougher aluminium based surfaces cause lower adhesion than the smoother PET and glass surfaces. Roughness and the chemical nature of the canister surfaces will be determined in detail in Chapter 4 and Chapter 5 and discussed in relation to true adhesion in Chapter 6.

Finally the time required for maximum adhesion of the powders to the various canister materials to be reached was studied in Figure 3.12 and 3.13. When comparing the suspensions in the different canisters no difference in adhesion over time was detected, the maximum adhesion had been reached after 7 days for all systems (2 sample t-test, p

< 0.05). The earlier time points, where budesonide and terbutaline sulphate adhered to AL canisters, show that the maximum adhesion level is reached already at the first time point, one day. Therefore the results in Figure 3.11, where the adhesion of budesonide in HPFP seemed to increase over a week may have been due to movements in the water bath that was used for temperature control. Each time a sample was removed from the water bath all samples moved which may have caused additional adhesion of particles above the fluid line.

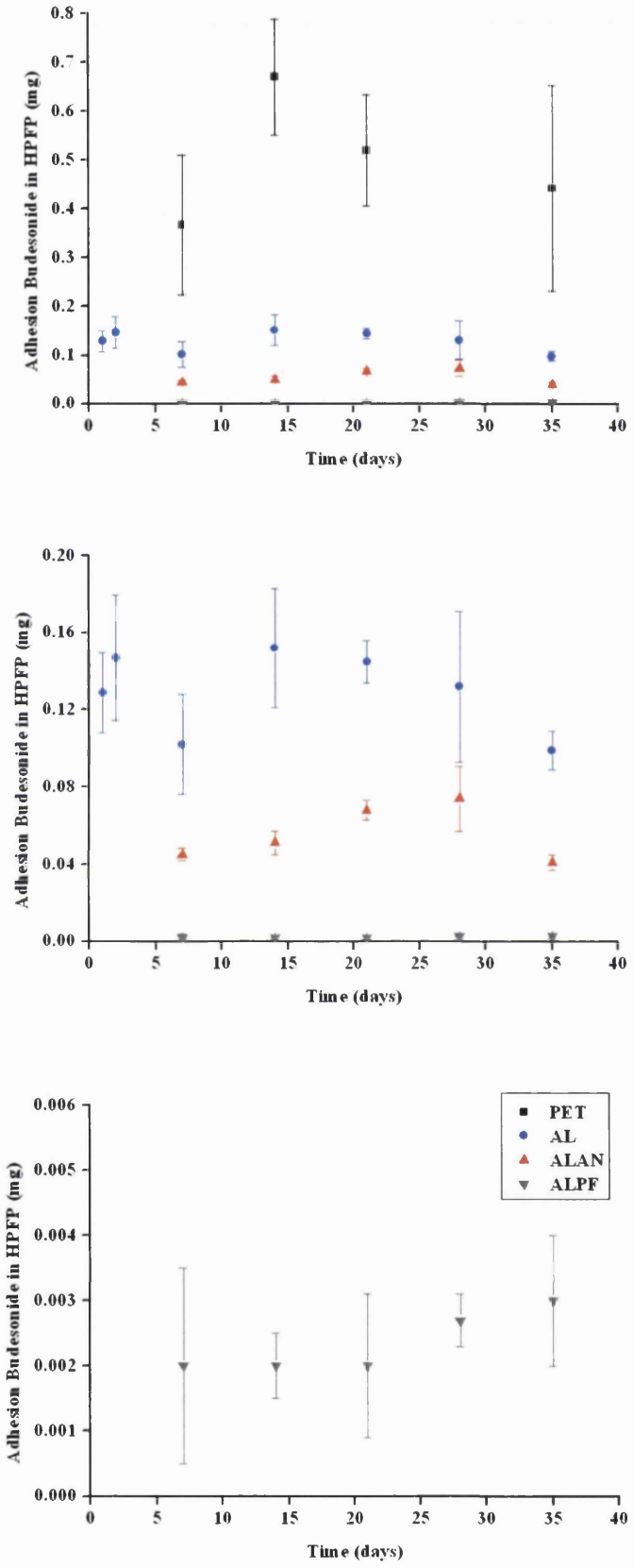

Figure 3.12. Adhesion of budesonide in HPFP to various canister materials by time as measured by HPLC (n=15).

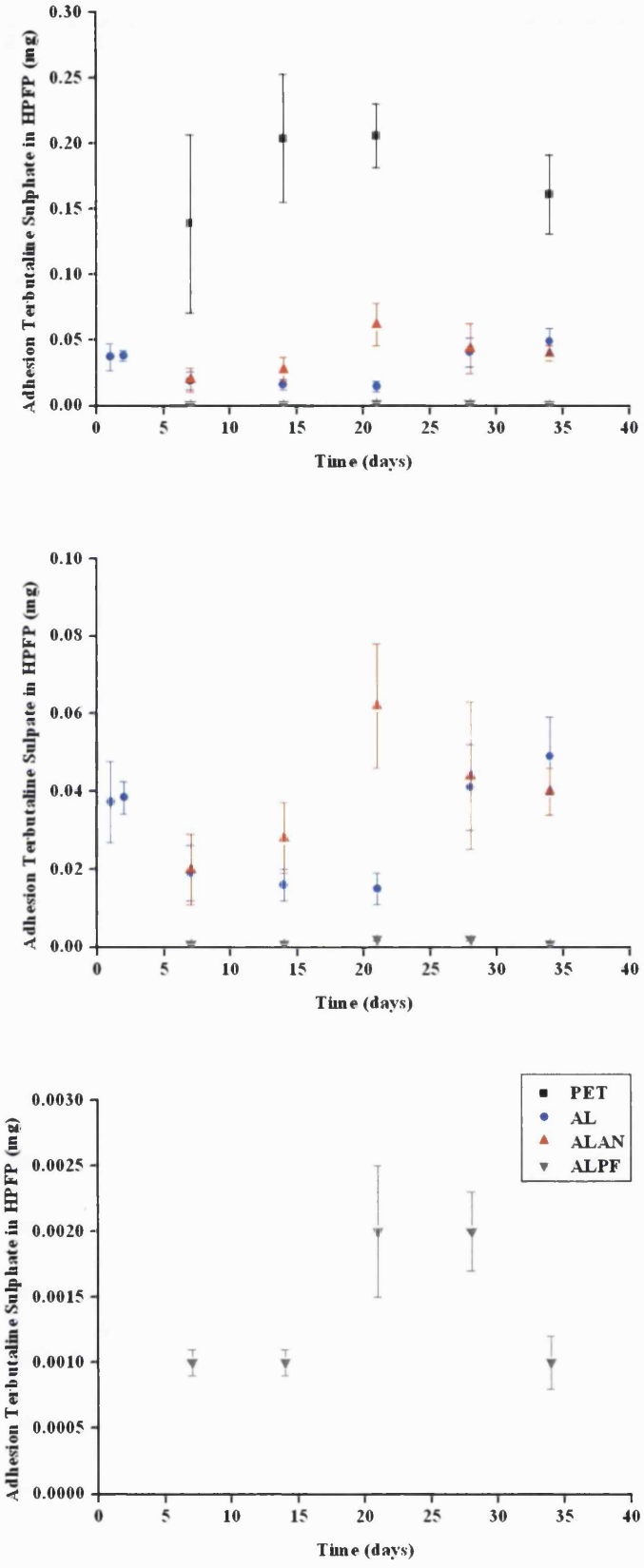

Figure 3.13. Adhesion of terbutaline sulphate in HPFP to various canister materials by time as measured by HPLC (n=15).

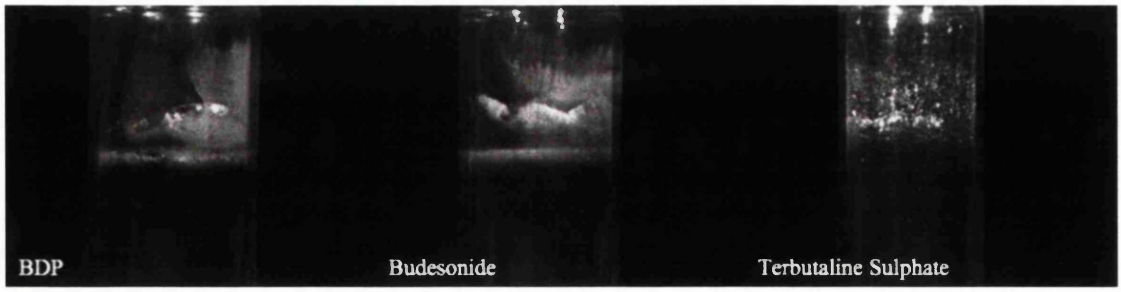

Figure 3.14. Digital images of adhesion to PET canisters from HPFP suspensions after 2 weeks. The canisters presented here contained no suspension.

The visual adhesion for BDP, budesonide and terbutaline sulphate to PET canisters shown in Figure 3.14 appears higher than the adhesion to glass canisters in Figure 3.5 and it also shows the pattern with a ring formed around the fluid line for BDP and budesonide, which was also shown in Figure 3.5. The quantitative adhesion for budesonide in HPFP to PET shown in Figure 3.11 was also higher than to glass shown in Figure 3.8. In Figure 3.14 the terbutaline sulphate adhesion to PET was pronounced around the fluid line, not only above the fluid line as for glass in Figure 3.5, Figure 3.7 and Figure 3.9, which indicates that the adhesive interactions with PET in HPFP are stronger than with glass.

3.3.3.4 Adhesion Changes by Suspension Concentration and Canister Filling Volume

In the final part of this study the effect suspension concentration and filling volume had on adhesion was investigated in a minor study. Figure 3.15 shows signs of that the amount of adhered material does increase with increased suspension concentration (2 sample t-test, $p < 0.05$), which correlates with the literature (Vervaet and Byron, 2000). In the results presented budesonide adhesion to PET canisters reached maximum adhesion at 2mg/mL but in AL canisters the maximum adhesion was not reached at 4 mg/mL. The data presented in Figure 3.15 show signs that the concentration of the suspension has an impact on adhesion but the adhesion should come to a stage when the canister area above the fluid line is saturated with particles and no more increase in adhesion occurs. This was shown in Section 3.3.2, Figure 3.8, where the adhesion in HPFP increased by time, which could be a result of evaporation due to leaking canister seals. Evaporation of the liquid automatically leads to higher powder concentration in

the suspension and if what is shown in Figure 3.15 is true a higher concentration gives an increase in adhesion by time. In Figure 3.16 there were no signs of adhesion increasing with increased filling volume (2 sample t-test, $p < 0.05$), hence based on that the size of the available canister wall area above the fluid line did not have an impact on adhesion. A larger set of samples is needed to confirm the trends shown in the brief study presented in Figure 3.15 and Figure 3.16.

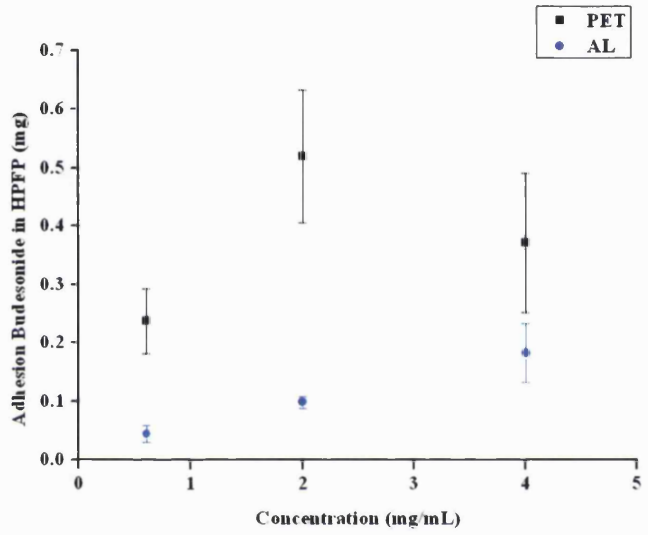

Figure 3.15. Plot of adhesion of budesonide in HPFP against concentration as measured by HPLC (n=12).

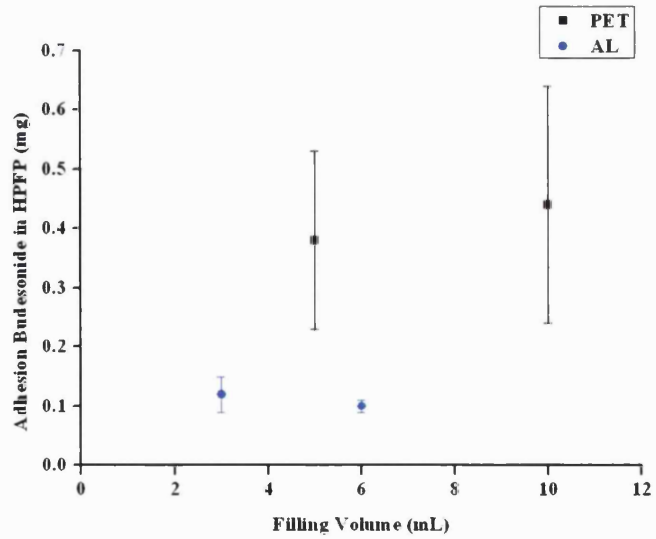

Figure 3.16. Plot of adhesion of budesonide in HPFP against filling volume as measured by HPLC (n=12).

3.3.4 Activity at Fluid Line

The previous section showed that maximum adhesion was reached within a day. Therefore this study will focus in detail on the adhesion by the fluid line within 24 hours to see when a maximum is reached and what that adhesion layer looks like. The advantage of digital imaging from the outside of the canister was that from the moment the suspension was prepared the activity at the fluid line in the suspension over time could be studied in detail. In previous experiments in this chapter the canisters have been emptied of the suspension before the adhesion has been analysed. Here the fluid interface was not disrupted when adhesion was registered, hence the particle activity at the liquid interface could be studied in real time. Looking at Figure 3.17 the major adhesion of all compounds to PET in HPFP took place within 60 minutes. If comparing the images at 60 minutes the adhesion of the three powder compounds decreased in the following order: BDP > budesonide > terbutaline sulphate. The images also show that a major part of the adhered BDP particles on the canister wall above the fluid line vanished between 60 minutes and 24 hours, probably due to particles dissolving in HPFP film at the meniscus over time. This was not as clear for budesonide as it was for BDP but as presented in Section 2.14 the solubility in HPFP after 24 hours was 1.5 times larger for BDP than for budesonide so probably budesonide particles in the meniscus did not dissolve to the same extent as BDP particles. Another observation in the BDP suspension was the increase in particle size in the meniscus area with time, which is likely to be crystal growth due to Ostwald ripening (Phillips et al., 1993). It has been observed in this study in Figure 3.17 that some particle adhesion is visible already after one minute and others have reported that microparticle adhesion in pMDI happens very quickly, within 5 minutes (Vervaet and Byron, 2000). It was mentioned earlier in this study that when APIs are partially soluble crystal growth can occur and cause adhesion to the canister (Vervaet and Byron, 1999). Another study investigated the crystal growth of albuterol in CFC propellants during 38 weeks and it showed that the crystal size had increased already after 3 days and continued to increase over the 38 weeks of the study. Albuterol and terbutaline sulphate are similar compounds in terms of physicochemical characteristics. Since the adhesion of terbutaline sulphate reaches a maximum within one hour in this study and Phillips *et. al* have shown that albuterol crystals in CFCs continues growing for 38 weeks it seems like an increase in particle size by crystal growth does not necessarily lead to an increase in adhesion. Even though

crystal growth may have an impact on the initial adhesion it does not seem to have an impact on the long term total adhered amount of particles, probably since smaller particles dissolves in favour of growth of larger particles, which does not change the total particle mass adhered. The particle growth may not have an impact on the adhesion to the canister wall but leads to larger particles that could get stuck in the nozzle and cause clogging of the MDI, which may end the device's life before the device is empty. A more polar liquid gives more crystal growth and since HFAs are more polar than CFCs crystal growth has become a more pronounced problem since HFAs were introduced to the market as more environmentally friendly propellants.

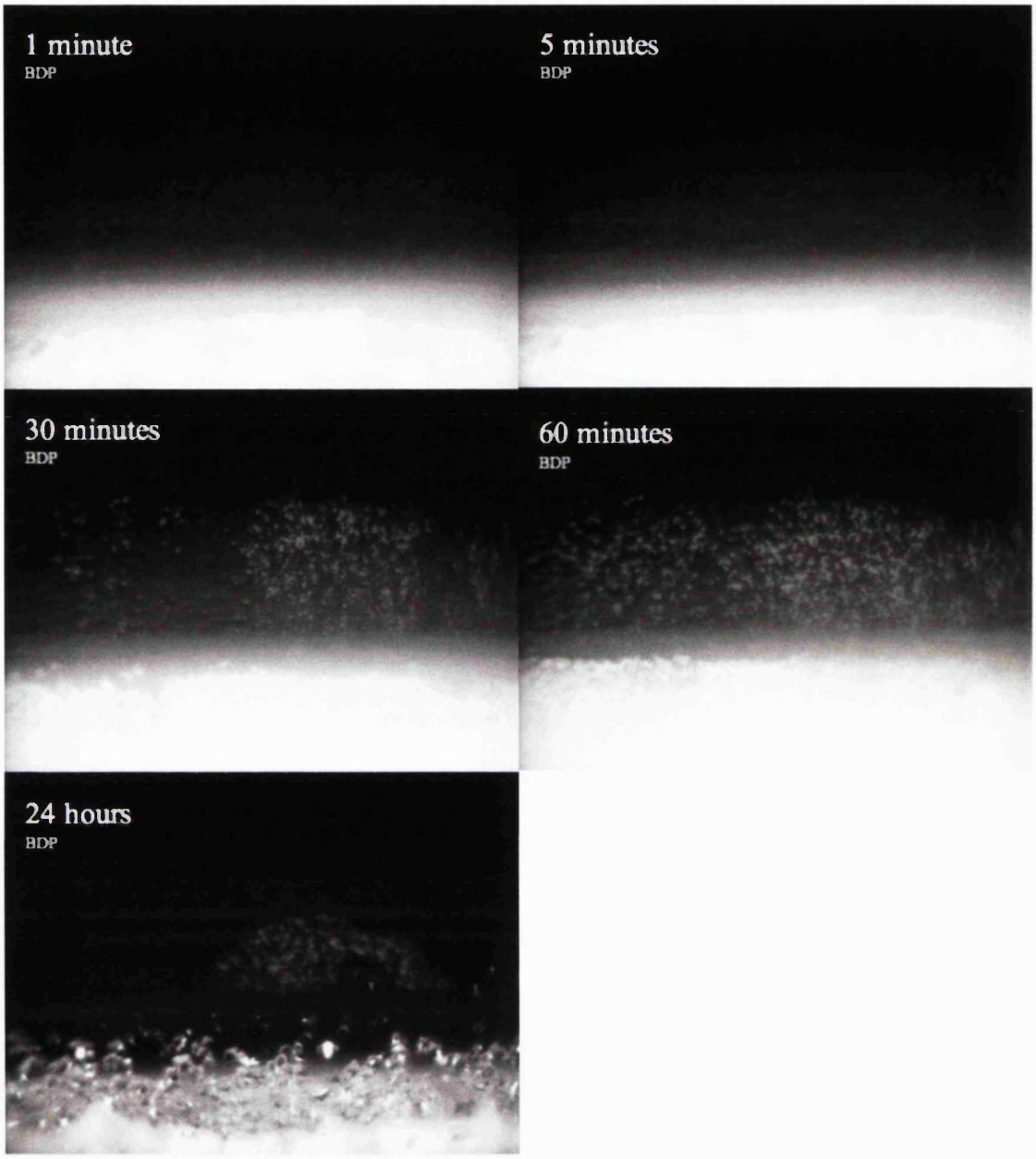

Figure 3.17 (continued on next page). Close up digital images of area at fluid line, described in Figure 3.4. PET canisters filled with suspension of BDP, budesonide and terbutaline sulphate particles in HPFP.

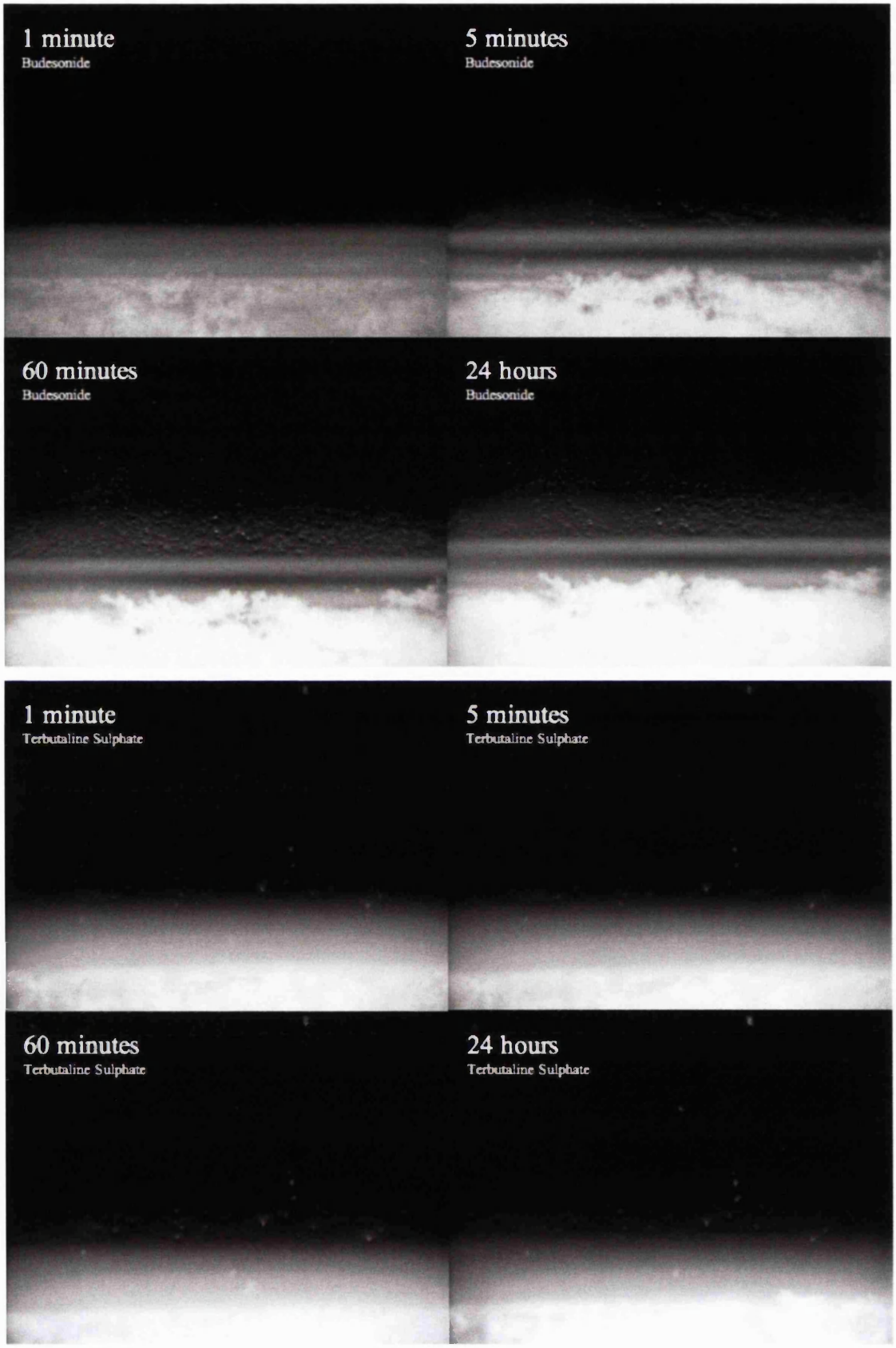

Figure 3.17 (continued from previous page). Close up images of area at fluid line, described in Figure 3.4. PET canisters filled with suspension of BDP, budesonide and terbutaline sulphate particles in HPFP.

3.4 Conclusions

A method for quantifying microparticle adhesion in model MDIs was developed and used in Chapter 3. When microparticle adhesion in model metered dose inhaler systems was measured it was evident that the adhesion in fluorinated systems is a complex mechanism influenced by various factors.

It was found that the way samples were prepared, stored and analysed had an impact on the adhesion results. First when preparing samples it was found that the systems must be properly sealed to avoid enhanced particle adhesion due to evaporation. Canisters with crimped valves were preferred over canisters with screw lids to avoid evaporation of the fluorinated liquid. Secondly it was found that the way powders were dispersed in the fluorinated liquids had an impact on the adhesion, dispersing by manual shaking did not give any visible adhesion during dispersing but so did dispersion by sonication and by using a longer sonication time higher adhesion during dispersion was observed. Despite the enhanced adhesion sonication was considered the best way to disperse the powders in the liquids. Thirdly the controlled temperature storage unit used had an impact on adhesion and it was found that an oven rather than a water bath should be used to avoid an increase in adhesion due to movements of the samples on storage when taking samples off storage. Finally the method used for analysis of the adhered amount was shown to be important where HPLC gave more accurate results than weighing and was therefore the preferred method. The analysis by weight was straightforward and did not require much sample preparation but the weighing results were affected by the electrostatics created when using protection gloves, which made the analysis method less accurate. Since the adhered material was only around 0.01% of the canister weight in some systems the mass was too low to accurately measure by weight when the electrostatics interfered. HPLC gave accurate results but involved more sample preparation and method development than weighing and since the HPLC was equipped with a UV-detector only molecules with a chromophore could be detected. Further the method could not be used to analyse adhesion samples where BDP had been stored in HPFP since BDP degraded over time and unknown bi-products were created. The best method for quantification of true adhesion in model MDI systems was regarded to be preparing the suspensions by dispersing particles through sonication in well sealed

canisters with crimped valves, storing the samples in a controlled temperature oven and analysing them by HPLC.

A straightforward and quick way to evaluate what material combinations leads to least adhesion is digital imaging. The adhesion could not be quantified by images but the images gave a good picture of the adhesion rank order between different systems. A disadvantage is that only transparent canister materials could be used. In this study only glass and PET canisters.

The adhesion varied between the different systems studied and there were variations in both amount adhered particles and the way the adhered particles were distributed on the canister wall where the latter indicated if the particle-wall adhesive interactions were favoured or not in presence of the liquid. Maximum adhesion was found to happen quickly, within an hour. Further it was found that the adhesion was higher in suspensions based on less polar fluorinated liquids, which could have been a result of the lower powder-liquid interactions leading to higher powder-wall adhesive interactions. Also the solubility of powder compounds in the HFA seemed to have an impact on adhesion where powders with low solubility, within μg/ml, adhered and the insoluble ones did not. It is known that the particle-canister adhesive interactions of compounds with low solubility is dependent on both solubility related changes such as crystal growth for small APIs and surface properties such as surface energy while adhesive interactions of insoluble particles mainly depends on the surface properties. Between the soluble compounds that adhered and had very similar physicochemical properties the more soluble adhered less, probably as a result of adhered particles dissolving in the HFA. Not only adhesive interactions seemed to be of importance to adhesion but also cohesive as there was a build up of particles by the meniscus. Finally there were indications that rougher surfaces caused lower adhesion, which would be due to lower powder-canister contact area in such systems.

In the model hydrofluoroalkane used, HPFP, particle loss due to adhesion of microparticles, APIs as well as polymers, ranged from 0.02% to 47.6% w/w. It was shown that microparticle adhesion is dependent on the choice of powder, liquid, canister material, storage time and suspension concentration. Furthermore during the development of an analytical method to quantify microparticle adhesion in MDI

canisters it was shown that preparation and analysis of samples had an impact on the adhesion results obtained. Finally the volume canisters were filled with seemed to have insignificant impact on particle adhesion. In these model MDI systems there seems to be a balance between particle-canister, particle-liquid and canister-liquid interactions, hence all possible adhesive and cohesive interactions must be considered and will therefore be looked at in more detail in Chapter 4 and Chapter 5 and correlated with the adhesion results from this chapter in Chapter 6.

Chapter 4: Surface Energy and Solubility Parameter

4.1 Introduction

In the pharmaceutical industry surfaces of various natures come into contact constantly. It could for example be contact between powder and the material of the equipment during processing, interactions between a surfactant and a propellant in a pressurised metered dose inhaler or contact between inhaled drug particles and human body tissue. In this study where metered dose inhaler suspensions are in focus the interactions of interest are between powder-powder, powder-liquid and powder-canister surfaces. Interactions between particles and various materials can be measured directly by, for example, atomic force microscopy but they can also be determined indirectly through calculations based on surface energy or solubility parameters (Rillosi and Buckton, 1995, Traini et al., 2005, Van Krevelen and Hoftyzer, 1997). First surface energy measured by inverse gas chromatography (IGC) and contact angle will be reported, and then solubility parameters measured by IGC and calculated by group-contribution. Finally surface energies and solubility parameters respectively will be used to calculate interactions between the materials used in this study. In this chapter the surface characteristics of the materials used in this study will be looked into by various methods. These methods were not included in the physicochemical characterisation in Chapter 2.

4.1.1 Surface Energy

Surface energy is a physicochemical property that describes the nature of a material surface and it plays an essential role for pharmaceutical powders in areas such as dissolution, dispersion, coating and granulation. For a liquid to adsorb onto a solid surface the interaction has to be strong enough to push away the already adsorbed gas molecules. The energy attracting the liquid to the solid surface must exceed the energy keeping the molecules in the liquid together and therefore determination of interfacial energy is essential. There are three main types of intermolecular bonds. First primary bonds, which are chemical bonds like covalent, ionic or metallic bonds, then secondary bonds, which include hydrogen bonds, van der Waals interactions (van Oss et al., 1987)

and last electron donor and electron acceptor bonds, which are Lewis acid and base respectively. The total surface energy is often divided into a dispersive (also called apolar or non-polar) and a polar part. Since London, Keesome and Dubye-Hyckel interactions are extremely small compared to hydrogen bond and acid-base interactions they are included in the dispersive part of surface energy (van Oss, 1994).

Wetting can take place through mechanisms such as spreading, capillary rise, condensation and immersion wetting (Lazghab et al., 2005) and surface energy can be determined by IGC, organic dynamic vapour sorption or contact angles from techniques such as sessile drop, the Wilhelmy gravitational method and the capillary intrusion technique (Buckton, 1990, Traini, 2005). The techniques all give indirect values of surface energy, i.e. the raw data must be processed by calculations based on various theories. Therefore measuring surface energy of the same material but with different techniques may be beneficial, since the results vary between different techniques, which gives a broader view of the nature of the surface of compounds (Jones, 2006, Traini et al., 2005). Surface energy values can be useful when predicting interactions between materials, something that will be done later on in this chapter.

4.1.1.1 Determination of Surface Energy and Free Energy of Interaction by Contact Angle

Measuring surface energy of solids by contact angle was introduced in Section 1.2.2 where it was mentioned that the advancing contact angle (θ_a), formed when a drop is placed on a solid surface, is used for surface energy calculations since it is considered more reproducible than the receding contact angle (θ_r) (Krüss, 2002). θ_r is formed when the volume of the liquid drop on the solid surface is reduced and is a measure of de-wetting of the solid surface. Contact angle hysteresis (H) is commonly used to determine surface heterogeneities, i.e. more or less wettable parts of the surface due to chemical or physical heterogeneities (Wolff et al., 1999).

$$H = \theta_a - \theta_r \tag{4.1}$$

An example of chemical heterogeneity is if the contact line of a water drop on a surface would reach an area more hydrophilic, then the contact angle would decrease and the

contact line would move forward quicker. An example of physical heterogeneity is if the drop contact line should reach a rough spot of the surface, which would cause the contact line motion forwards to slow down and create a larger contact angle. It has been shown that when the surface roughness is less than 100 nm it does not affect the contact angle (Buckton et al., 1995). When measuring contact angle on compressed powder discs there is often both chemical and physical heterogeneity.

It has been shown that macroscopic variations of surfaces can be detected by H and microscopic variations by the contact angle variance ($\Delta\theta$) which is the range between the lowest and the highest contact angle value (Wolff et al., 1999). If the heterogeneities are uniformly distributed $\Delta\theta = 0$ and $H \neq 0$ and if the heterogeneities are non-uniformly distributed $\Delta\theta \neq 0$ and $H \neq 0$ (Wolff et al., 1999). Moreover distribution of high and low surface energy sites on a surface can be described by looking at $\Delta\theta_a$ and $\Delta\theta_r$. When $\Delta\theta_a < \Delta\theta_r$ a mainly low surface energy area has defects of high surface energy areas and when $\Delta\theta_a > \Delta\theta_r$ a mainly high surface energy area has defects of low surface energy areas (Wolff et al., 1999).

The apolar and polar nature of materials can be determined from θ_a in the following way. The relationship between contact angle, surface tension of a solid and a liquid respectively and the solid/liquid interfacial tension was first described by Young (Young, 1805). In another century Fowkes work became the base for parting surface energy into polar and dispersive components (Fowkes, 1963). Interaction between two materials was described by the Dupré equation (van Oss, 1994). It was shown that it is only by luck that predictions based on interactions from dispersive and polar surface energy parameters correlates with reality (Fowkes et al., 1990). Van Oss showed the great importance of the electron donor and acceptor character of a material when predicting interactions (van Oss et al., 1987). A material with electron donor character could also be called a Lewis acid (γ^-) and electron acceptor character could be called a Lewis base (γ^+). Hence, van Oss stated that any material could be described by the following three parameters: apolar (Lifshitz-van der Waals), electron acceptor and electron donor parameters with symbols: γ^{LW}, $\gamma^+$and γ^- respectively.

In order to determine the surface energy of a solid surface the contact angle of at least three different liquids, one apolar and two polar, must be determined. The surface components approach express the surface energy as the sum of γ^{LW} and γ^{AB} respectively.

$$\gamma = \gamma^{LW} + \gamma^{AB} \tag{4.2}$$

where the polar component could be divided into $\gamma^{+}$and γ^{-}

$$\gamma^{AB} = 2\sqrt{\gamma^{+}\gamma^{-}} \tag{4.3}$$

The free energy of interaction between two materials *i* and *j* is determined by the Dupré equation in the following way:

$$\Delta G_{ij} = \gamma_{ij} - \gamma_i - \gamma_j \tag{4.4}$$

where

$$\gamma_{ij}^{LW} = \left(\sqrt{\gamma_i^{LW}} - \sqrt{\gamma_j^{LW}}\right)^2 \tag{4.5}$$

and

$$\gamma_{ij}^{AB} = 2\left(\sqrt{\gamma_i^{+}\gamma_i^{-}} + \sqrt{\gamma_j^{+}\gamma_j^{-}} - \sqrt{\gamma_i^{+}\gamma_j^{-}} - \sqrt{\gamma_i^{-}\gamma_j^{+}}\right) \tag{4.6}$$

which results in

$$\gamma_{ij} = \left(\sqrt{\gamma_i^{LW}} - \sqrt{\gamma_j^{LW}}\right)^2 + 2\left(\sqrt{\gamma_i^{+}\gamma_i^{-}} + \sqrt{\gamma_j^{+}\gamma_j^{-}} - \sqrt{\gamma_i^{+}\gamma_j^{-}} - \sqrt{\gamma_i^{-}\gamma_j^{+}}\right) \tag{4.7}$$

The free energy of interaction between two compounds, *i* and *j,* submerged in a liquid, *k,* could also be described by the Dupré equation.

$$\Delta G_{ikj} = \gamma_{ij} - \gamma_{ik} - \gamma_{jk} \tag{4.8}$$

Further the free energy of interaction between two particles or molecules of the same compound, *i*, submerged in a liquid, *k*, is given by:

$$\Delta G_{iki} = -2\gamma_{ik} \tag{4.9}$$

If $\Delta G > 0$ repulsion between materials occur and if $\Delta G < 0$ attraction occur.

If the surface free energy parameters (γ, γ^{LW}, γ^{+}, γ^{-} and γ^{AB}) of a solid (*S*) shall be determined θ of one apolar (*LA*) and two polar liquids (*L1* and *L2*) on the surface must be measured. It is done by first calculating γ_S^{LW} by using the contact angle of the apolar liquid in:

$$\gamma_L(1+\cos\theta_L) = 2\left(\sqrt{\gamma_S^{LW}\gamma_L^{LW}} + \sqrt{\gamma_S^{+}\gamma_L^{-}} + \sqrt{\gamma_S^{-}\gamma_L^{+}}\right) \tag{4.10}$$

and no polar parameters are present for the apolar liquid, hence:

$$\gamma_{LA}(1+\cos\theta_{LA}) = 2\left(\sqrt{\gamma_S^{LW}\gamma_{LA}^{LW}}\right) \tag{4.11}$$

that by rearrangement gives an expression where γ_S^{LW} is the only unknown parameter:

$$\gamma_S^{LW} = \frac{\gamma_{LA}{}^2(1+\cos\theta_{LA})^2}{4\gamma_{LA}^{LW}} \tag{4.12}$$

The following equations were developed from Equation 4.10 and they only have one unknown parameter each, $\gamma^{+}{}_S$ in Equation 4.13 and $\gamma^{-}{}_S$ in Equation 4.14. It does not matter what one of the two polar liquids that is chosen as *L1* or *L2* since it results in the same $\gamma^{+}{}_S$ and $\gamma^{-}{}_S$ values. If not, another set of polar liquids must be chosen.

$$\gamma_S^+ = \left(\frac{\sqrt{\gamma_{L2}^+}\left(\gamma_{L1}(1+\cos\theta_{L1}) - 2\sqrt{\gamma_S^{LW}\gamma_{L1}^{LW}}\right) - \sqrt{\gamma_{L1}^+}\left(\gamma_{L2}(1+\cos\theta_{L2}) - 2\sqrt{\gamma_S^{LW}\gamma_{L2}^{LW}}\right)}{\left(2\sqrt{\gamma_{L1}^-\gamma_{L2}^+} - 2\sqrt{\gamma_{L2}^-\gamma_{L1}^+}\right)} \right)^2 \quad (4.13)$$

$$\gamma_S^- = \left(\frac{\sqrt{\gamma_{L2}^-}\left(\gamma_{L1}(1+\cos\theta_{L1}) - 2\sqrt{\gamma_S^{LW}\gamma_{L1}^{LW}}\right) - \sqrt{\gamma_{L1}^-}\left(\gamma_{L2}(1+\cos\theta_{L2}) - 2\sqrt{\gamma_S^{LW}\gamma_{L2}^{LW}}\right)}{\left(2\sqrt{\gamma_{L1}^+\gamma_{L2}^-} - 2\sqrt{\gamma_{L2}^+\gamma_{L1}^-}\right)} \right)^2 \quad (4.14)$$

4.1.1.2 Surface Energy Determination by Inverse Gas Chromatography

IGC is a surface analysis technique that has many advantages. The technique is not dependent on the sample morphology, the instrument has a high sensitivity and reproducibility and also the powder sample does not need to go through preparation that could lead to changes in the surface properties (Voelkel et. al, 2009). Moreover most probe liquids can be used in the IGC and since the method is non-destructive the powder can be reused after measurements.

In conventional gas chromatography the stationary phase is known and the mobile gas phase unknown, whilst in IGC it is the other way around, Figure 4.1. The injected gas will only result in one peak and the time it takes for that peak to elute is registered. IGC measures the net retention time, t_r, for of each probe running through a powder column.

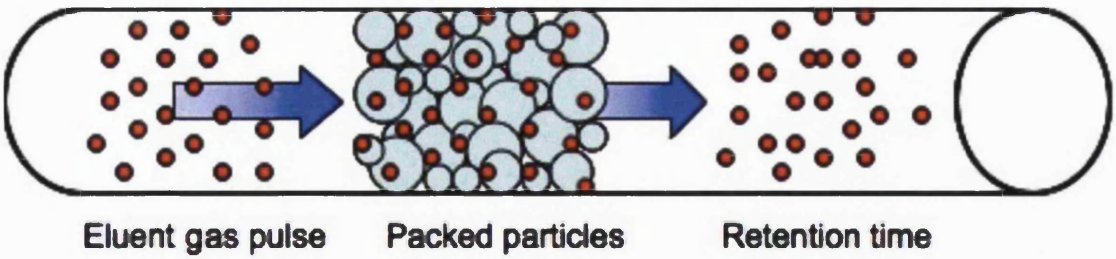

Figure 4.1. Scheme of when a known mobile phase passes through an unknown stationary phase in IGC.

The calculations leading to dispersive surface energy and acid-base components have been described in detail by Tong (Tong et al., 2002). The powder $\gamma^{LW}{}_S$ is obtained from the slope of the straight line that appears when $RTlnV_N$ is plotted against $a(\gamma^{LW}{}_L)^{1/2}$.

$$RT\ln V_N = 2N\left(\gamma_S^{LW}\right)^{\frac{1}{2}} a\left(\gamma_L^{LW}\right)^{\frac{1}{2}} + C \qquad (4.15)$$

where R is the gas constant, T the temperature in Kelvin, V_N the retention volume, N Avagrado's number (the definition of a mole), a the molar surface area of the probe, $\gamma^{LW}{}_L$ the dispersive surface energy of the probe and C a constant.

The retention volume, V_N, can be obtained from t_r in the following equation.

$$V_N = \frac{j}{m} \cdot w\left(t_R - t_0\right) \cdot \frac{T_S}{T_{ref}}$$

Where j is the correction factor for pressure drop in the column, m the sample mass, w the exit flow rate at 1 atm and the reference temperature, t_R and t_{ref} the retention time of the probe and the probe where no interaction occurs respectively.

The most frequently used way of calculating the acid-base constants of the powder was first described by Schultz, Equation 4.16, where the extent of interaction with each polar probe is represented by the Gibbs free energy of adsorption (ΔG_A). Each polar probe is plotted in the $RTlnV_n$ to $a(\gamma^{LW}{}_L)^{1/2}$ plot and the vertical distance between the alkane line and the polar probe equals its ΔG_A (Tong et al., 2002).

$$-\Delta G_A = RT\ln\left(\frac{V_N}{V_N^{ref}}\right) \qquad (4.16)$$

The electron acceptor number (K_A) and the electron donor number (K_D) can be determined through the following equation.

$$\Delta G_A = K_A DN + K_D AN^* \qquad (4.17)$$

where DN and AN^* of the probes can be found in literature. If $\Delta G/AN^*$ is plotted against DN/AN^* the gradient of the straight line is K_A and the intercept is K_D. IGC experiments could be run at infinite or finite dilution but mostly the former is used. Infinite dilution is when a very low probe concentration is injected in the column, which leads to the

probe molecules only interacting with the high-energy sites of the powder sample. In a powder there is surface heterogeneity, which means that a property like surface energy varies and when running measurements at infinite dilution interaction with mainly high-energy sites occur, which is a way of controlling the energy measured. Finding infinite dilution can either be done by altering the probe injection concentration or by altering the sample mass. For infinite dilution the experiments must be run in the Henry region, Figure 4.2, which is the region where the results are not influenced by probe-probe interactions and there is a linear relationship between the amount adsorbed and the probe concentration in this region (Mukhopadhyay and Schreiber, 1995).

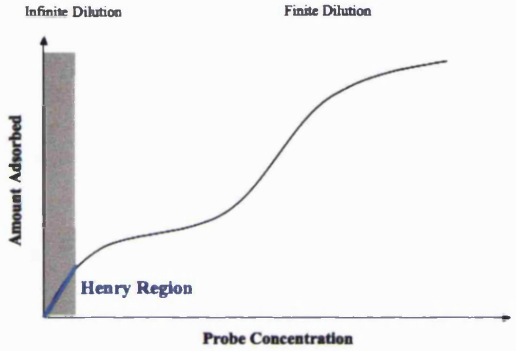

Figure 4.2. Graph showing that infinite dilution is in the Henry region.

However there are limitations with IGC, firstly by running the experiments at infinite dilution the method measures probe/powder interaction at the higher energy sites of the powder, i.e. with respect to the mean the surface energies measured by IGC are overestimated (Jones, 2006, Traini, 2005). Furthermore it is not possible to compare the dispersive and polar contributions since the former are measured in $mJ \cdot m^{-2}$ and the latter are dimensionless.

4.1.2 Solubility Parameters

Solubility parameters are frequently used to predict the compatibility between different materials in terms of intermolecular interactions. With solubility parameters it is possible to predict miscibility, adhesion and wetting but they give a better prediction for liquids and semi solids than for solids (Voelkel et al., 2009). A great advantage with solubility parameters is that they can be determined based on the molecular structure of compounds only. Also it gives detailed information about the apolar, polar and hydrogen bonding character of a material. In this study solubility parameters will be

used to predict intermolecular interactions between various components in model metered dose inhaler formulations but there is a drawback. It has been shown that solubility parameters are non-predictive of the differences in polarity of HFAs solvent properties (Dickinson et al., 2000) which may make them less suitable for interaction prediction in fluorinated metered dose inhalers. However in this thesis it will be investigated how well adhesive interactions can be predicted based on Hansen solubility parameters since it is a theoretical approach that can be useful when limited quantities of material is available. Surface energy parameters will also be evaluated in the same way and then the two approaches will be compared.

Hildebrand first defined the solubility parameter by stating that if the cohesive energy density (*CED*) of a material is known the solubility parameter can be determined with the following equation (Hildebrand et al., 1970):

$$\delta = (CED)^{\frac{1}{2}} = \left(\frac{\Delta E_v}{V}\right)^{\frac{1}{2}} \tag{4.18}$$

where δ represents the solubility parameter, ΔE_v the internal energy of vaporisation and V the molar volume. The cohesive energy of a material indicates the attraction a materials atoms or molecules have for each other and it represents the energy required to separate the materials atoms or molecules to an infinite distance (Hancock, 1997). Intermolecular interactions that are included in the cohesive energy are van der Waals forces, ionic bonds, hydrogen bonds and electrostatic interactions. Physicochemical properties of a material, such as boiling and melting point and solubility depend on the cohesive energy of the material. The more similar solubility parameter two materials have the stronger the intermolecular interactions between them are.

Hansen divided the total Hildebrand solubility parameter into partial solubility parameters. The Hansen solubility parameters were included in an equation expressing the Hildebrand solubility parameter in terms of Hansen's dispersive (δ_d), polar (δ_p) and hydrogen bonding (δ_h) partial solubility parameters (Hansen, 2000).

$$\delta^2 = \delta_d^2 + \delta_p^2 + \delta_h^2 \tag{4.19}$$

The Hansen solubility parameters are useful, since they give a detailed description of the nature of materials and also enable calculations of interactions between materials. Another advantage with solubility parameters is that they can be determined theoretically, which is useful if for example the right equipment is not available or if there is not enough material for experimental determination of solubility parameters. It could also work as a control to ensure experiments have been performed correctly.

Hansen solubility parameters can be determined experimentally by: sublimation, vaporisation, IGC, solubility, partition, calorimetry or surface tension and theoretically by calculations from a group contribution method (Hancock, 1997, Hoy, 1989, Stefanis and Panayiotou, 2008, Van Krevelen and Hoftyzer, 1997). The choice of technique depends on the nature of the compound, whether it is an organic or a metallic compound, a polymer or a small molecule. It also depends on the amount of material available and the time available to carry out experiments.

However when characterising the nature of materials by solubility parameter there are limitations that must be considered (Hansen, 2000). First the solubility parameter theory is based on liquids and therefore the approximation that gases are liquids and solids super-cooled liquids has been done. For solids where the molecules are arranged differently on the surface than in the bulk the interactions between materials may not be the same when predicted with solubility parameters. Also the solubility parameter is dependent on temperature and molecular shape and size. Further there are interactions not included in the Hansen solubility parameters, such as induced dipole, metallic and electrostatic, which are not considered. Also the solubility parameter theory work best for non-polar compounds that interact with weak dispersion forces and finally measuring solubility parameter is often laborious (Adamska and Voelkel, 2005).

4.1.2.1 Determination of Hansen Solubility Parameters by Inverse Gas Chromatography

When determining Hansen solubility parameters by IGC the same advantages and disadvantages as for surface energy measurements are present. Further there are general limitations with the solubility parameter discussed in Section 4.1.2. The raw data from

IGC that the solubility parameters calculations are based on is the probe retention volumes V_N that were measured by IGC (Tong et al., 2002). The internal energy of adsorption, ΔE^A, for polar systems was determined with the following equation.

$$\ln V_G = -\left(\frac{\Delta E^A}{RT}\right) + K_G \tag{4.20}$$

where V_G is the specific retention volume that is calculated by dividing V_N by the sample mass. Further R is the gas constant, T the absolute temperature and K_G a constant. ΔE^A was determined by plotting lnV_G to $1/T$. The solubility parameters are related to ΔE^A as presented in Equation 4.20.

$$-\Delta E^A = V\left(\delta_d^P \delta_d^S + \delta_p^P \delta_p^S + \delta_h^P \delta_h^S\right) \tag{4.21}$$

where V is the molar volume of the probe, δ_d^P, δ_p^P, δ_h^P the dispersive, polar and hydrogen bonding Hansen solubility parameters of the probe. Values for these parameters are available in the literature. The unknown parameters in Equation 4.21 are δ_d^S, δ_p^S, δ_h^S that are the dispersive, polar and hydrogen bonding contribution to Hansen solubility parameter of a material. They are determined by multiple linear regression through the origin.

4.1.2.2 Determination of Hansen Solubility Parameters and Interaction Parameters by Group Contribution

As mentioned earlier solubility parameters can be determined theoretically through calculations based on group contribution methods, where each molecular group or atom in a compound contributes with a certain value, which is used in the calculations that give solubility parameters. As long as the molecular structure of a compound is known the Hansen partial solubility parameters (δ_d, δ_p and δ_h) can be calculated by group contribution. In group contribution methods the standard values for different atoms and molecules have been determined experimentally. There are many different methods available for calculations of the total solubility parameter but only a few for the Hansen solubility parameters. Hansen solubility parameters are mostly calculated by Hoftyzer and van Krevelen's or Hoy's method (Van Krevelen and Hoftyzer, 1997, Hoy, 1989).

Out of the methods available for solubility parameter calculations over the last decades these two methods have been the ones that are covering the widest range of molecular groups and that enables calculations of the partial Hansen solubility parameters. The van Krevelen method works best for organic compounds and polymers while the Hoy method is best for solvents. However, in this study a new approach covering even more molecular groups and atoms will be used.

Recently a new approach to calculate the Hansen solubility parameters was published by Stefanis et. al (Stefanis and Panayiotou, 2008). This new group-contribution method is for organic compounds and considers both first-order (conformation) and second-order groups (configuration). The first-order groups account for every molecule or atom in the compound while the second-order groups only cover the fragments in the compounds that cannot be described accurately enough by first-order contributions (Kang et al., 2002). Not all compounds have second-order contributions but for compounds who have them isomers and polyfunctional compounds can be distinguished thanks to second-order contributions. In contrast to first-order group contributions the same molecule or atom can be included in several second-order group contributions in the calculations. The major advantage with this method compared to previous ones is that it considers second-order group-contributions. Moreover each Hansen solubility parameter is calculated by one equation only, which minimises the risk of calculation errors. Stefanis' group contribution method is under development and therefore the values used here are a combination between published values and new yet not published values received directly from Stefanis (Stefanis, 2008). Finally a major advantage with Stefanis' method is that it includes a very large number of molecular groups and atoms.

The equations necessary for calculations of the Hansen solubility parameters by the Stefanis method are presented below. Calculation examples are shown in Appendix 1.3.

$$\delta_d = \left(\sum_i N_i C_i + W \sum_j N_j C_j + 16.9981 \right) \tag{4.22}$$

$$\delta_p = \left(\sum_i N_i C_i + W \sum_j N_j C_j + 7.6134 \right) \tag{4.23}$$

$$\delta_h = \left(\sum_i N_i C_i + W \sum_j N_j C_j + 7.7004 \right) \quad (4.24)$$

where N_i is the amount first order groups of type i in the compound and C_i is the first-order contribution of group i while N_j is the amount second-order groups of type j in the compound and C_j is the second-order contribution of group j. Equation 4.23 and Equation 4.24 are only valid when $\delta_p > 3$ MPa$^{1/2}$ and $\delta_h > 3$ MPa$^{1/2}$.

If $\delta_p < 3$ MPa$^{1/2}$ the following equation must be used.

$$\delta_p = \left(\sum_i N_i C_i + W \sum_j N_j C_j + 2.7467 \right) \quad (4.25)$$

If $\delta_h < 3$ MPa$^{1/2}$ the following equation must be used.

$$\delta_h = \left(\sum_i N_i C_i + W \sum_j N_j C_j + 1.3720 \right) \quad (4.26)$$

A limitation with Stefanis' method is that some groups, especially fluorinated ones, are not fully represented in this method. Some groups are only represented in terms of apolar group-contribution not polar or hydrogen bonding. Further there are several limitations when calculating Hansen solubility parameters from group-contribution methods no matter what method is used. First of all it gives an estimation of solubility parameters not real values, secondly it does not consider the physical form of materials, such as amorphous content, crystallinity, shape or roughness. Finally the approximation that all molecular compounds are evenly distributed in the material is done, which is not true since molecules often tend to arrange differently at a surface of a material than in the bulk.

As mentioned earlier the interaction between two materials can be calculated from solubility parameters and will be used to predict adhesion. The interaction parameter (ϕ) based on Hansen solubility parameters between two materials, A and B, is calculated in the following way (Rowe, 1988).

$$\phi = 2\left[\frac{{}^{A}x_d \cdot {}^{B}x_d}{{}^{A}x_d \cdot g_1 + {}^{B}x_d \cdot g_2} + \frac{{}^{A}x_p \cdot {}^{B}x_p}{{}^{A}x_p \cdot g_1 + {}^{B}x_p \cdot g_2}\right] \tag{4.27}$$

where x_d is the fractional non-polarity and x_p the fractional polarity defined in Equation 4.28 and Equation 4.29 respectively. The constants g_1 and g_2 are defined in Equation 4.30 and Equation 4.31 respectively.

$${}^{A}x_d = \left[\frac{{}^{A}\delta_d}{{}^{A}\delta}\right]^2 \tag{4.28}$$

$${}^{A}x_P = 1 - {}^{A}x_d \tag{4.29}$$

$$g_1 = \frac{{}^{A}\delta^2 \cdot {}^{A}V^{\frac{1}{3}}}{{}^{B}\delta^2 \cdot {}^{B}V^{\frac{1}{3}}} \tag{4.30}$$

where V is the molar volume ($V=M_W/\rho$).

$$g_2 = \frac{1}{g_1} \tag{4.31}$$

The closer ϕ is to unity the higher the intermolecular interactions between the two materials will be (Rowe, 1988). With lower ϕ cohesive interactions will be favoured over adhesive interactions.

4.2 Materials and Methods

The nature of compounds surfaces was determined in this study, first by surface energy from contact angle (powders, canisters) and IGC (powders) measurements and then by solubility parameters from IGC measurements (powders) and Stefanis' group contribution method (powders, liquids and canisters).

The materials characterised were powders: beclomethasone dipropionate (BDP), budesonide, terbutaline sulphate, polyacrylic acid (PAA) and polyvinylpyrrolidone (PVP); liquids: 2H,3H-perfluoropentane (HPFP), perfluoroheptane and perfluorodecalin and canisters: glass, polyethyleneterephtalate (PET), aluminium (AL), anodised aluminium (ALAN) and perfluoroalkane coated aluminium (ALPF).

When comparing samples a student's t-test, two samples with same variance, was carried out with a significance level of 95% ($p < 0.05$).

4.2.1 Surface Energy Calculated from Measured Contact Angles

The surface energy of powders and canisters was determined by measuring the advancing contact angle (θ_a) of various liquid drops on the solids. The surface energy parameters were obtained through calculations where θ_a was used as the raw data and detailed calculations can be found in Appendix 1.1.

Contact angles were measured with a DSA-10 drop shape analysis system (Krüss, Germany) and the results were recorded with DSA1 v.1.80 software (Krüss, Germany). Liquid drops (3-5μL) were automatically released from a syringe fitted with a needle (0.5 mm diameter) and put on the surface and a camera recorded either snap shots of the drop shape or a video. Then the software measured the contact angle between the liquid and the solid surface as in Figure 1.3. The surfaces investigated were powders: BDP, budesonide, terbutaline sulphate and PAA and canisters: PET, aluminium, anodised aluminium and PFA coated aluminium. Glass was not included in this study due to experimental issues. Three liquids, commonly used for contact angle measurements, were used for both powders and canisters. To cover both the apolar and polar characteristics of the surfaces two polar and one apolar liquid was used where the apolar was diiodomethane and the two polar were ethylene glycol and water. Depending on the spreading rate of the drop, either a video or snapshots were recorded. The measurements were performed at 20°C. Further the surface tension of all three liquids was measured by the Wilhelmy plate technique method described in Section 2.11. It was done to enable an accurate choice of surface energy parameters from literature for the surface energy calculations.

The advancing contact angle of ten drops of each liquid on each material surface was recorded immediately after the drop was formed. The receding contact angle (θ_r), formed when the liquid drop was reduced, was measured for canisters but not for powders because the liquid had modified the powder surface substantially during the advancing contact angle measurements preventing θ_r from being measured. Finally the variation between contact angles ($\Delta\theta_a$ & $\Delta\theta_r$) and the hysteresis for canisters was determined.

The powder samples were prepared by compressing approximately 250 mg in a 13 mm die with a force of 10 kN in an IR-press (Traini et al., 2005). The compacts were kept at zero per cent relative humidity at least 24 hours prior to analysis. Small pieces of canister samples were prepared. The aluminium canisters were cut into smaller pieces and flattened out but due to the stiffness of PET it was not possible to flatten out the PET canisters and therefore they were simply cut into small pieces. The analysis software was able to measure contact angle of curved surfaces. PET canister pieces were cleaned with ethanol for 30 minutes and then left to dry for four days to ensure all ethanol had left the material. All surfaces were kept in a dust free box when not analysed to avoid contamination of surfaces.

Table 4.1. Surface Energy Components and Parameters (20°C) of liquids used for calculations in contact angle measurements (van Oss, 1994).

	Surface Energy Components and Parameters ($mJ \cdot m^{-2}$)				
Liquid	γ^{LW}	γ^{+}	γ^{-}	γ^{AB}	γ
Diiodomethane	50.80	0.00	0.00	0.00	50.80
Ethylene Glycol	29.00	1.92	47.00	19.00	48.00
Water	21.80	25.50	25.50	51.00	72.80

The surface energy parameters were calculated from the advancing contact angle with Equations 4.2, 4.3, 4.12, 4.13 and 4.14.

4.2.2 Surface Energy Calculated from IGC Measurements

The dispersive surface energy, K_A and K_D of powders were determined by IGC. The retention volume of the inert apolar probes was used to calculate γ^{LW} with Equation 4.15 and the retention volume of the inert polar probes was used to calculate K_A and K_D with

Equation 4.16 – Equation 4.17. Detailed calculations of K_A and K_D can be found in Appendix 1.2.

An IGC (Surface Measurement Systems, UK) was used to investigate the surface energy of powders: BDP, budesonide, terbutaline sulphate and PAA. Between 50 and 150 mg of powder was loaded in a silanized and washed glass column with 3 mm inner diameter (Surface Measurement Systems, UK). The column was tapped for 20 minutes to evenly distribute the powder loaded into the column and then it was put in the IGC for analysis. First the column was conditioned for 2 hours at 30°C and zero percent relative humidity to remove moisture then the probes were run through the column. Two columns for each material were analysed three times, which resulted in a total number of six runs for each powder.

Nine inert probes were chosen. Five were apolar hydrocarbons of varying carbon chain length: decane, nonane, octane, heptane and methane. Four were polar probes: acetonitrile, acetone, ethyl acetate and 1,4-dioxane. The polar probes were different in terms of electron donor and acceptor properties according to the electron acceptor number (AN^*) and donor number (DN) in the Gutmann acid-base scale Table 4.2 (Gutmann, 1978).

Table 4.2. Gutmann numbers for polar probes in IGC (Gutmann, 1978).

Probes	Character	AN^*	DN
Acetone	amphoteric	2.5	17
Acetonitrile	amphoteric	4.7	14.1
1,4-dioxane	basic	4.32	14.8
Ethyl acetate	amphoteric	1.5	17.1

The following method was used to determine infinite dilution. Each column was filled with as much powder as possible but not more than for the decane peak (the largest probe molecule with longest retention time) to come out within 30 minutes. Then probes were injected at five different concentrations and a concentration was chosen, where the retention time of decane did not change by concentration and was as short as possible.

4.2.3 Solubility Parameter Calculated from IGC Measurements

The solubility parameters of BDP, budesonide, terbutaline sulphate and PAA were determined by IGC (Surface Measurement Systems, UK).

The solubility parameter nature of the powder compounds was evaluated in the IGC with the following five probes, inert to all four powders: decane, cyclohexane, acetonitrile, 1.4-dioxane and ethyl acetate. These five were specifically for solubility parameter measurements and the probes mentioned in Section 4.2.2 for surface energy measurements and since the SMS IGC allows up to 10 probes to be used at one time surface energy and solubility parameters could be determined during the same experimental run. It was considered best to use the same set of probes for all powders since that enabled better comparison of the surface characteristics between the powders.

The probes were injected at four different temperatures: 30, 40, 50 and 60 °C. For each column measurements were carried out in three cycles, each cycle starting at the lowest and ending at the highest temperature, to ensure that the material surface did not change when exposed to increased temperature. Two columns for each powder were analysed three times resulting in six runs in total for each powder. The Hansen partial solubility parameters for the probes used are available in Table 4.3.

Table 4.3. Hansen partial solubility parameters (Huu-Phuoc et al., 1986, Huu-Phuoc et al., 1987a, Huu-Phuoc et al., 1987b).

	Solubility Parameter Data ($kPa^{1/2}$)		
Probe	δ_d	δ_p	δ_h
Decane	499.53	0.00	0.00
Cyclohexane	529.29	0.00	0.00
Acetonitrile	485.29	569.4	194.10
1,4-Dioxane	601.76	58.20	232.90
Ethyl Acetate	481.41	168.20	291.20

4.2.3.1 Selecting Polar Probes for Solubility Parameter Measurements in IGC

In order to find the optimal combination of probes enabling a minimum number of experiments that gives a maximum accuracy and precision the experimental matrix optimization technique by Huu-Phuoc et al. was used (Huu-Phuoc et al., 1986, Huu-

Phuoc et al., 1987b, Huu-Phuoc et al., 1987a). This is a statistical method that is used to find the most optimal set of probes that will give the most information of the powder character by getting as good partial solubility parameter values as possible by IGC. In this study the experimental matrix optimization will be used to find an optimal set of probes for determination of the Hansen solubility parameters of the powders, BDP, budesonide, terbutaline sulphate and PAA by IGC.

The equation used to determine solubility parameters by IGC was Equation 4.21, presented in Section 4.1.2.1 and below.

$$-\Delta E^A = V_i\left(\delta_d^i\delta_d^j + \delta_p^i\delta_p^j + \delta_h^i\delta_h^j\right) \tag{4.21}$$

Where $-\Delta E^A$ is the internal energy of adsorption of the probe to the powder, V_i is the molar volume of the probe, δ^i_d, δ^i_p and δ^i_h represents the known probe dispersive, polar and hydrogen bonding solubility parameters respectively and δ^j_d, δ^j_p and δ^j_h the unknown solubility parameters of the powder.

From Equation 4.21 the following matrix system is created where the number of probes used corresponds to the number of equations in the matrix.

$$\begin{pmatrix} -\Delta E_1^A \\ -\Delta E_n^A \\ -\Delta E_N^A \end{pmatrix} = \begin{pmatrix} V_1\delta_{1d} & V_1\delta_{1p} & V_1\delta_{1h} \\ V_n\delta_{nd} & V_n\delta_{np} & V_n\delta_{nh} \\ V_N\delta_{Nd} & V_N\delta_{Np} & V_N\delta_{Nh} \end{pmatrix} \times \begin{pmatrix} \beta_d \\ \beta_p \\ \beta_h \end{pmatrix} + \begin{pmatrix} \varepsilon_1 \\ \varepsilon_n \\ \varepsilon_N \end{pmatrix} \tag{4.32}$$

In Equation 4.32 N is the number of rows representing the various probes and the three columns represent the molar volume multiplied with the dispersive, polar and hydrogen bonding partial interaction parameter for these probes, β represents the unknown partial solubility parameters of the powder and finally ε represents the experimental errors created by N equations.

The IGC probes evaluated by the experimental matrix optimization method are in a group of molecular probes with known Hansen solubility parameters and molar

volumes (Huu-Phuoc et al., 1987a). All these probes are volatile at low temperatures and cover the possible interactions between the probes and the stationary phase.

The first step in this method is to identify and exclude the unsuitable probes from the group, which are the probes that absorbs to the stationary phase, causes degradation of IGC seals and has too low boiling point. When these probes had been excluded from the group of molecular probes 12 remained and their molar volumes and partial solubility parameters that will be used in the calculations in Equation 4.32 are shown in Table 4.4.

Table 4.4. The Hansen values for molar volume and partial solubility parameters of the organic solvents included in the experimental matrix optimisation method (Huu-Phuoc et al., 1987a).

	Molecular probe	V	Partial Solubility Parameters ($cal^{1/2} \cdot cm^{-3/2}$)		
		($ml \cdot mol^{-1}$)	δ_d	δ_p	δ_h
1	Hexane	131.60	7.24	0.00	0.00
2	Heptane	147.40	7.42	0.00	0.00
3	Octane	164.00	7.55	0.00	0.00
4	Nonane	180.00	7.65	0.00	0.00
5	Decane	195.90	7.72	0.00	0.00
6	Cyclohexane	108.70	8.18	0.00	0.00
7	Toluene	106.80	8.80	0.70	1.00
8	Ethyl acetate	98.00	7.44	2.60	4.50
9	Chloroform	81.00	8.65	1.50	2.80
10	Acetone	74.00	7.58	5.10	3.40
11	Acetonitrile	52.60	7.50	8.80	3.00
12	1,4-dioxane	86.00	9.30	0.90	3.60

In the second and third steps in the matrix optimisation method the accuracy and precision will be calculated by using the statistical software Minitab 15.

The second step of this method is to determine the accuracy was determined by calculating the variance inflation factor (*VIF*) for the partial solubility parameters of this group of 12 molecular probes and *VIF* ensures that the parameters are independent and that there is no severe multicollinearity, for this *VIF* must be between 1 and 10 (Huu-Phuoc et al., 1987a, Huu-Phuoc et al., 1987b, Huu-Phuoc et al., 1986). The multicollinearity is considered low when VIF < 4 (Lewis et al., 1999). The results were $VIF_{\delta d}$ = 1.063, $VIF_{\delta p}$ = 1.784 and $VIF_{\delta h}$ = 1.708 for the 12 probes in Table 4.4, which

showed low multicollinearity and therefore the experimental matrix was fine in terms of accuracy.

The third step is to determine precision by calculating the D-optimality, which is when the normalized determinant $|M|$ of the information matrix X is maximized for different molecular probes with *VIF* between 1 and 10 (Huu-Phuoc et al., 1987a, Huu-Phuoc et al., 1987b, Huu-Phuoc et al., 1986).

$$|M| = \frac{|X'X|}{N^p} \tag{4.33}$$

where $|X'X|$ is the determinant and p the number of coefficients in the model equation, in this case p=3 for $V{\cdot}\delta_d$, $V{\cdot}\delta_p$ and $V{\cdot}\delta_h$. The quality of the information per probe is reflected by $|M|$ and the higher value of it the better the experiment is. Since 9 probes is the maximum number of probes that can be used in an SMS IGC, submatrices of 4 to 9 probes were considered.

In Table 4.5 the statistical calculations for various submatrices of the probes from Table 4.4 are presented. The calculations were made based on the V, δ_d, δ_p and δ_h values for the probes presented in Table 4.4.

Table 4.5. Results from calculations of optimal probe method by Minitab 15. Molecular probe number are related to probe numbers in Table 4.4.

		D-optimality	Variance Inflation Factors		
N° Probes (N)	Molecular Probes	|M|	$VIF_{\delta d}$	$VIF_{\delta i}$	$VIF_{\delta h}$
4	5, 8, 11, 6	$1.63{\cdot}10^{14}$	3.391	3.731	1.457
5	5, 8, 11, 6, 12	$1.78{\cdot}10^{14}$	2.927	2.706	1.319
6	1, 5, 6, 8, 11, 12	$1.73{\cdot}10^{14}$	2.591	2.632	1.375
7	1, 4, 5, 6, 8, 11, 12	$1.76{\cdot}10^{14}$	2.785	2.721	1.511
8	1, 4, 5, 6, 8, 10, 11, 12	$1.78{\cdot}10^{14}$	3.193	3.118	3.193
9	1, 4, 5, 6, 8, 9, 10, 11, 12	$1.65{\cdot}10^{14}$	2.978	2.764	1.625

Table 4.5 show that using five probes gives a good precision since $VIF < 4$ for all three solubility parameters and $|M|$ is maximised. D-optimality is the parameter to rely on according to Huu-Phuc (Huu-Phuoc et al., 1986, Huu-Phuoc et al., 1987a, Huu-Phuoc et al., 1987b). By using 5 probes measurements of surface energy and solubility parameter

could be done in the same run, which made the experimental design efficient time wise. This was how the optimal probes for solubility parameter determination were chosen.

4.2.4 Solubility Parameter Calculated by Stefanis' Group Contribution Method

The Hansen solubility parameters were calculated by Stefanis' group contribution method for powders: BDP, budesonide, terbutaline sulphate and PAA, canisters: PET and ALPF and finally liquids: HPFP and perfluoroheptane. Since the Stefanis group contribution method only applies to organic compounds the sulphate molecule in terbutaline sulphate was excluded from the calculations. For the same reason solubility parameters for aluminium canisters were not calculated. It was possible to predict Hansen solubility parameters for ALPF and perfluoroheptane though not all group contribution values were available, which may have given accurate values. Generally calculating solubility parameters by group contribution is known to be less suitable for fluorinated liquids and therefore experimental determination of such compounds is preferred to get accurate values (Hoye et al., 2008). The electron dense nature of fluorine atoms has a significant impact on the nature of fluorinated liquids and since that is not accounted for in the predictions based on the molecular structure the accuracy of theoretical solubility parameters for compounds containing fluorine is considered low. However since it was not possible to determine the solubility parameters experimentally in this study it was still considered interesting to calculate the solubility parameters of fluorinated liquids here in order to compare interactions based on solubility parameters with those based on surface energy.

4.2.5 Interactions Calculated from Surface Energy and Solubility Parameters

Theoretical determination of interactions between materials is a quick method when time-consuming experiments, such as atomic force microscopy, cannot be performed. Here interactions between materials were first calculated from surface energy and then from Hansen partial solubility parameters. The free energy of interaction was calculated from surface energy based on contact angle measurements. Surface energy values of materials were used in Equation 4.4 - 4.7 and 4.9 to calculate energy of interaction in binary systems (ΔG_{12} and ΔG_{121}) and in Equation 4.8 to calculate energy of interaction in ternary systems (ΔG_{132}). The error limit calculated was the range between the highest and lowest ΔG value. Further the interaction parameters (ϕ) based on solubility

parameters were calculated from values from Stefanis' method. The interaction parameters were calculated from Equation 4.27 – 4.31. When calculating ϕ for PET and ALPF the materials densities and molecular weights were unknown and therefore common values of for such polymers were chosen and the same density and molecular weight was set for PET and ALPF, density of 1.4 $g \cdot cm^{-3}$ and a molecular weight of 65 000 $g \cdot mol^{-1}$.

4.3 Results and Discussion

4.3.1 Surface Energy from Contact Angle Data

The mean values of contact angles measured with three liquids on powder compacts and canister surfaces are presented in Table 4.6. A detailed calculation example can be found in Appendix 1.1. Among the powders in Table 4.6 BDP and budesonide were more hydrophobic than terbutaline sulphate and PAA. Similarly PET was more hydrophobic than AL and ALAN. However, all canister surfaces but ALPF were wetted to some extent by the three liquids since $\theta < 90°$. ALPF was not hydrophilic since $\theta_{Water} > 90°$ and $\theta_{Diiodomethane} < 90°$ but very close to 90° and therefore not very hydrophobic either. Higher hydrophobicity was shown by the lower contact angles of the apolar liquid diiodomethane and the higher contact angles of water on the surfaces.

Table 4.6. Advancing contact angle for compact powder discs and canister surfaces (n = 10).

	Advancing Contact Angle ± SD (°)		
Powder	**Diiodomethane**	**Ethylene Glycol**	**Water**
BDP	22.7 ± 2.9	49.1 ± 2.8	69.0 ± 2.9
Budesonide	24.2 ± 1.9	31.3 ± 3.0	58.8 ± 2.9
Terbutaline Sulphate	37.7 ± 2.4	27.6 ± 3.5	29.4 ± 2.9
PAA	47.0 ±1.1	23.5 ± 2.1	25.6 ± 2.6
PET	29.9 ± 2.7	51.5 ± 2.9	78.8 ± 1.8
AL	46.6 ± 1.9	54.0 ± 4.2	70.8 ± 3.3
ALAN	49.1 ± 1.0	51.0 ± 4.8	65.6 ± 5.0
ALPF	82.3 ± 1.7	88.7 ±1.9	113.1 ± 3.1

The advancing and receding contact angle variation ($\Delta\theta_a$ and $\Delta\theta_r$) and hysteresis for canisters is shown in Figure 4.3 and 4.4 respectively. Hysteresis can show both physical and chemical heterogeneity (Wolff et al., 1999) and if the surface roughness is less than 100 nm the physical heterogeneity has no impact on hysteresis (Buckton et al., 1995). A

quantitative study of the canisters surface roughness will be done by atomic force microscopy in Chapter 5 and then it will be known if the canister roughness has an impact on the contact angle. These results will therefore be discussed in more detail in Chapter 5.

Figure 4.3 and Figure 4.4 show that there are contact angle variations and hysteresis respectively for all three liquids on the four canister surfaces, which confirms that the surface heterogeneities are non-uniformly distributed at the surface, since $\Delta\theta \neq 0$ and $H \neq 0$ as described in Section 4.1.1.1. When looking closer at the contact angle variance, which gives a more microscopic view of the surface, in Figure 4.3 $\Delta\theta_a < \Delta\theta_r$ for the majority of the sessile drops on the canister surfaces. This means that there are mainly low surface energy areas with defects of high surface energy areas. In Figure 4.3 a clear difference between AL and ALAN canisters, that could not be detected by θ_a only in Table 4.6, was found where there was a great difference between $\Delta\theta_a$ and $\Delta\theta_r$ for diiodomethane for ALAN but not for the polar liquids and vice versa for AL. In Figure 4.4 the macroscopic view of the surface is shown by the hysteresis, which is much lower for ALPF and PET canisters than for AL and ALAN canisters meaning that the former surfaces are smoother.

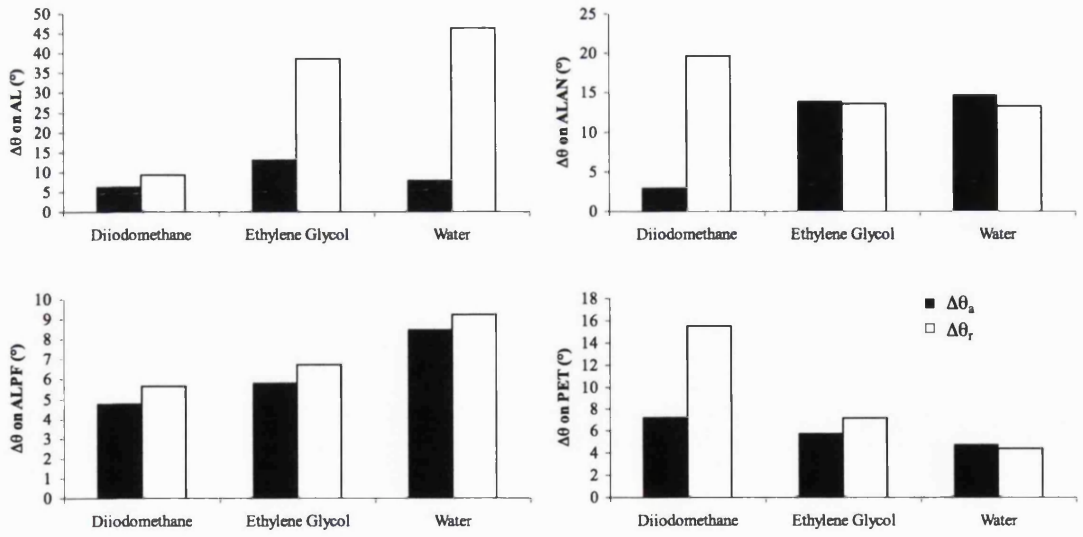

Figure 4.3. Contact angle variance ($\Delta\theta$) of sessile drops on canisters: AL (top left), ALAN (top right), ALPF (bottom left) and PET (bottom right), (n=10).

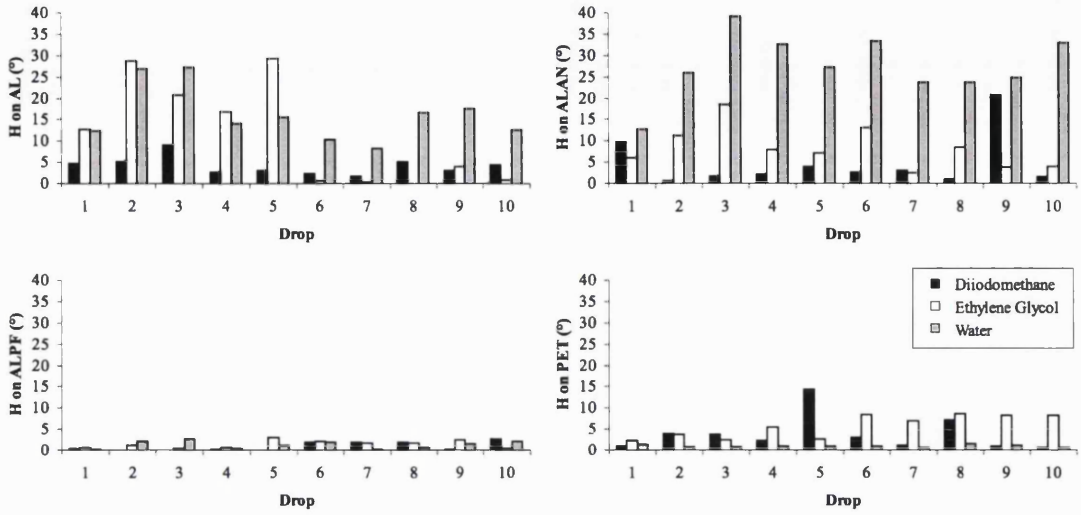

Figure 4.4. Contact angle hysteresis (H) of sessile drops on canisters: AL (top left), ALAN (top right), ALPF (bottom left) and PET (bottom right).

In Table 4.7 the surface energy components of powders, canisters and HPFP are shown. The HPFP values used were available in the literature (Beausang, 2005). The surface energy parameters in Table 4.7 were calculated from the mean contact angles and the error limits calculated were the range and not the standard deviation. The range was based on the difference between the highest and the lowest calculated surface energy value for each material.

When looking at the results from this study in Table 4.7 there are clear variations between the materials. The dispersive surface energy (γ^{LW}) of powders can be ranked: BDP = budesonide > terbutaline sulphate > PAA and canisters: PET > AL = ALAN > ALPF. The change in polar parameters of the materials show that the electron accepting character (γ^{+}) increases: terbutaline sulphate < budesonide < BDP < PAA and the electron donor character (γ^{-}) increases like: BDP < budesonide < terbutaline sulphate < PAA. A general comparison of the surface energy character of APIs and polymers in Table 4.7 shows that the polymers are of more polar and less apolar nature than the APIs. Where surface energy values for the materials characterized here were found in the literature a comparison was done but the values correlated poorly, which was likely since the materials from studies in the literature originating from different sources than the materials used in this study.

Table 4.7. Surface energy components of powders, canisters and HPFP from contact angles (n=10).

Material	Surface Energy Components and Parameters from Contact Angle ± Range ($mJ \cdot m^{-2}$)				
	γ^{LW}	γ^{+}	γ^{-}	γ^{AB}	γ
BDP	46.9 ± 1.9	0.130 ± 0.03	14.6 ± 3.9	2.8 ± 0.03	49.7 ± 2.0
Budesonide	46.4 ± 1.3	0.064 ± 0.01	19.3 ± 4.5	2.2 ± 0.4	48.7 ± 1.6
Budesonide (Traini et al., 2006)	49.1 ± 0.4	0.34 ± 0.4	22.5 ± 3.8	4.6 ± 2.9	--
Terbutaline Sulphate	40.8 ± 2.3	0.005 ± 0.003	56.5 ± 2.5	1.1 ± 0.4	41.8 ± 2.6
PVP (Cayakara et al., 2006)	28.3	1.2	51.0	15.3	43.6
PAA	35.9 ± 1.2	0.196 ± 0.02	59.7 ± 3.3	6.8 ± 0.2	42.8 ± 1.1
PET	44.3 ± 2.2	0.003 ± 0.01	6.3 ± 0.8	0.3 ± 0.6	44.6 ± 1.7
AL	36.2 ± 2.1	0.001 ± 0.01	15.9 ± 3.5	0.2 ± 0.5	36.4 ± 2.5
AL (Traini et al., 2006)	40.4 ± 0.2	0.8 ± 0.2	16.1 ± 1.7	--	47.7 ± 1.2
ALAN	34.8 ± 1.1	0.022 ± 0.06	21.0 ± 7.7	1.4 ± 2.2	36.1 ± 3.3
ALAN (Traini et al., 2006)	43.4 ± 0.8	0.5 ± 0.2	24.7 ± 2.2	--	50.5 ± 0.5
ALPF	16.3 ± 1.6	0.12 ± 0.03	0.09 ± 0.34	0.2 ± 0.4	16.6 ± 2.0
ALPF (Traini et al., 2006)	17.3 ± 0.8	0.4 ± 0.1	10.4 ± 0.9	--	21.5 ± 0.2
HPFP (Beausang, 2005)	8.26	2.50	1.00	3.16	11.42

4.3.2 Surface Energy Results from Inverse Gas Chromatography

In the IGC experiments the surface properties of BDP, budesonide, terbutaline sulphate and PAA were examined with apolar and polar probes. For each powder compound representative surface energy plots and Gutmann acid-base number plots are shown in Figure 4.5 and Figure 4.6 respectively. A detailed calculation example of how K_A and K_D were obtained can be found in Appendix 1.2.

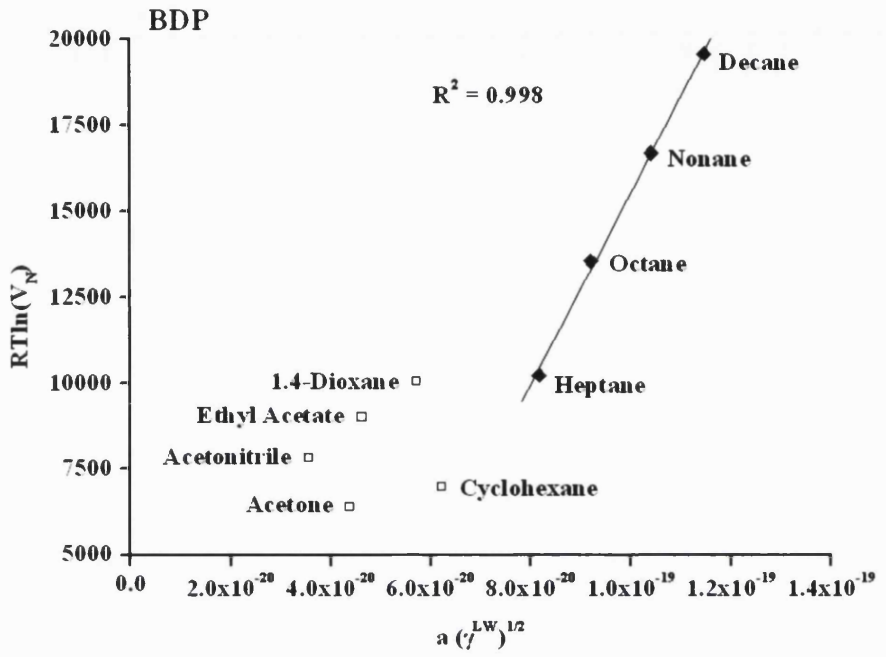

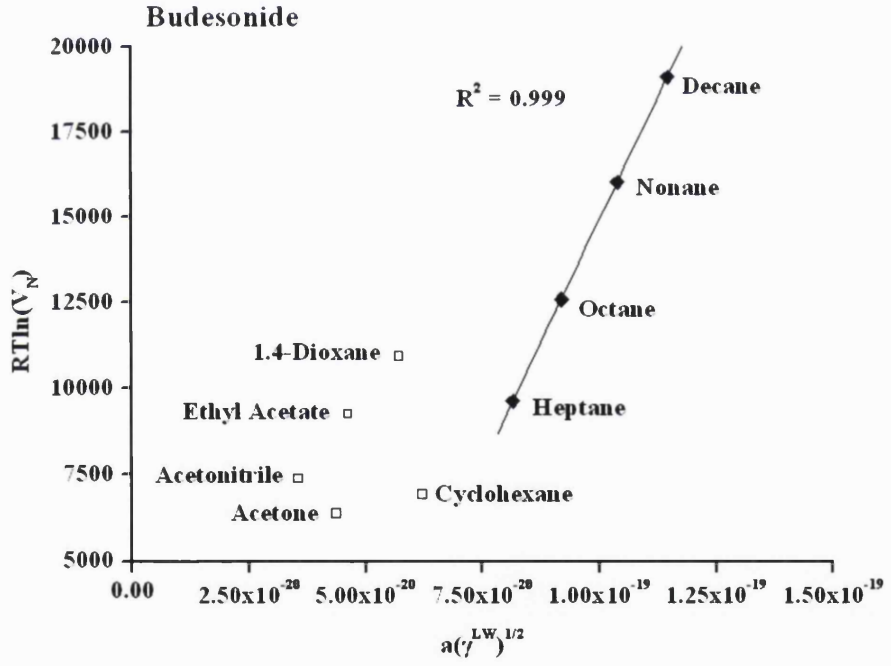

Figure 4.5 (continued on next page). Representative surface energy plots of: BDP, budesonide, terbutaline sulphate and PAA at 30°C (n=6).

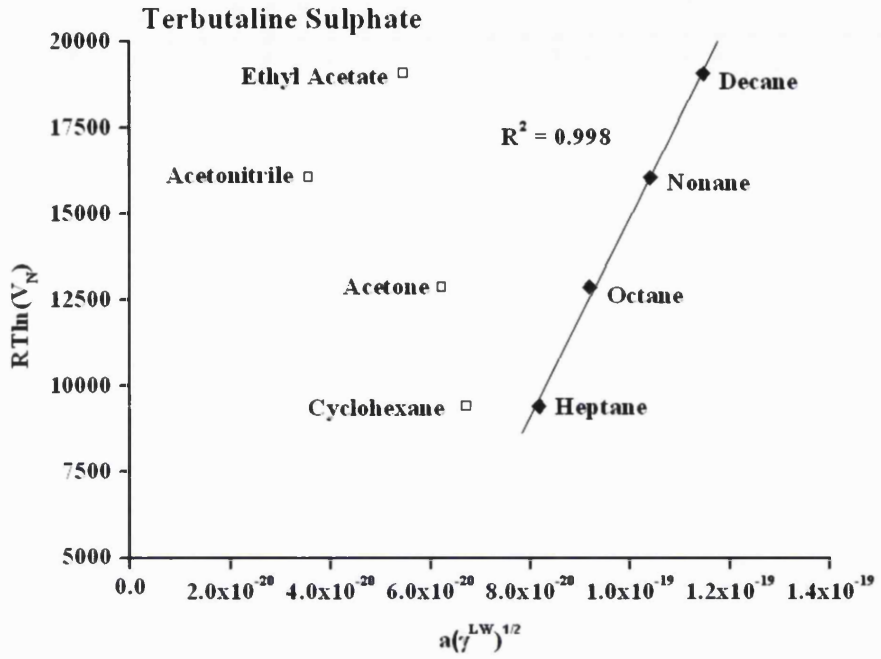

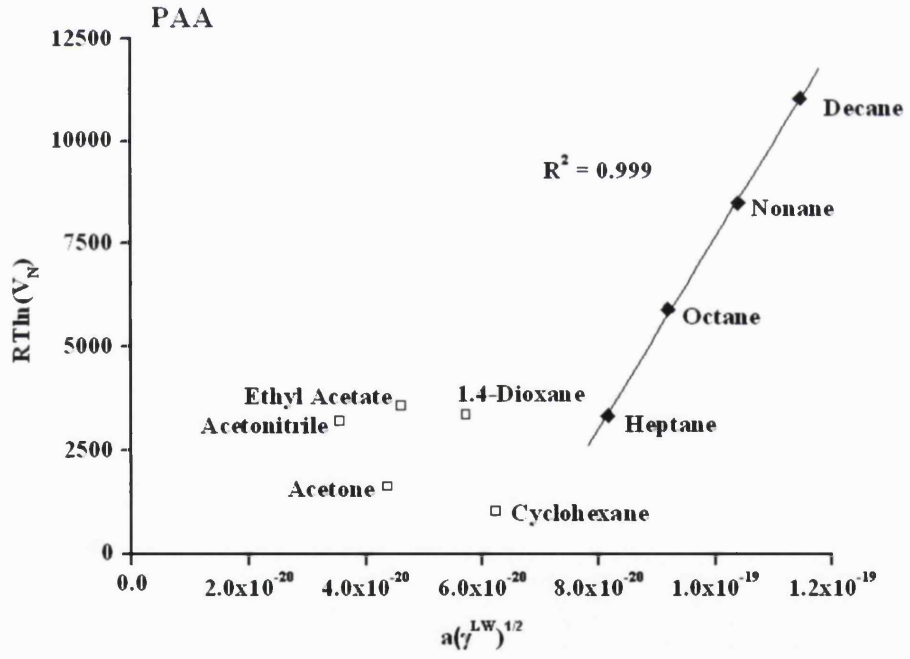

Figure 4.5 (continued from previous page). Representative surface energy plots of: BDP, budesonide, terbutaline sulphate and PAA at 30°C (n=6).

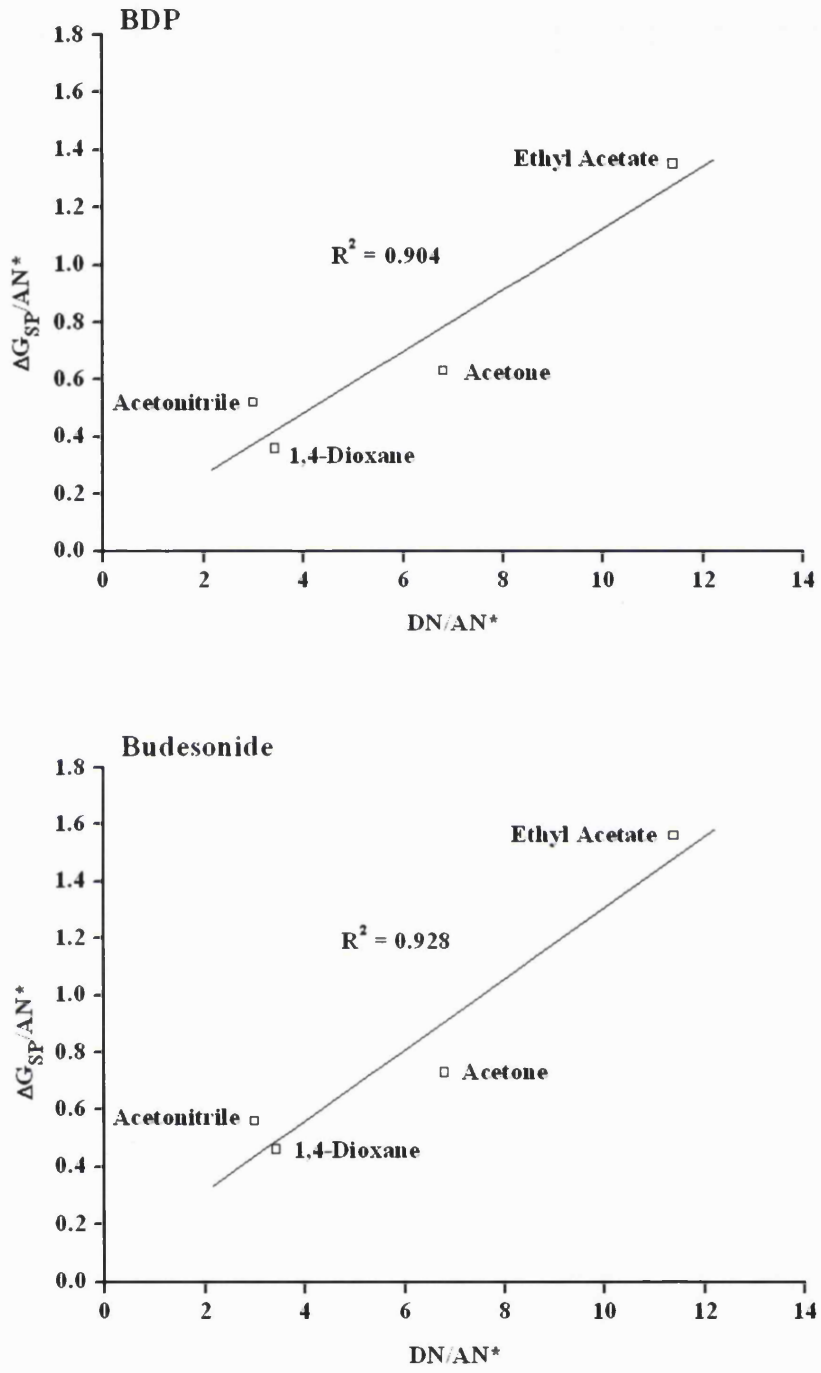

Figure 4.6 (continued on next page). Representative Gutmann acid-base number plots of: BDP, budesonide, terbutaline sulphate and PAA at 30°C (n=6).

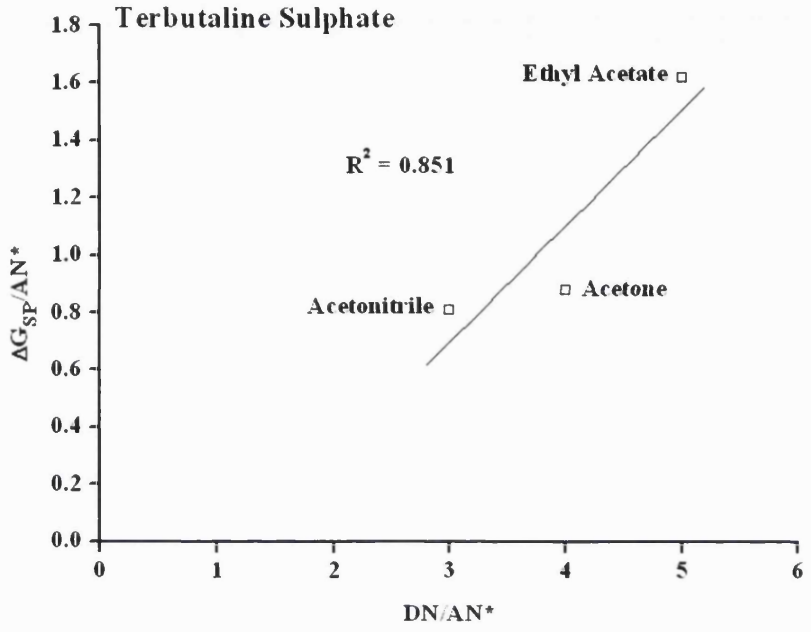

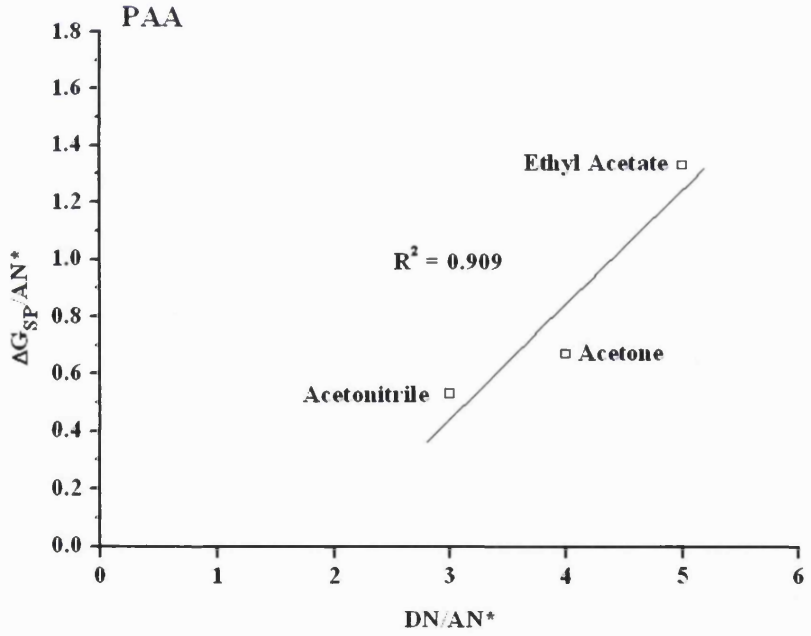

Figure 4.6 (continued from previous page). Representative Gutmann acid-base number plots of: BDP, budesonide, terbutaline sulphate and PAA at 30°C (n=6).

In Table 4.8 the mean values of the surface energy components obtained for the powders are presented.

Table 4.8. Surface free energy components of powders as measured by IGC (n=6).

	Dispersive Surface Energy and Polar Parameters from IGC (± SD)		
Compound	γ^{LW} (mJ·m^{-2})	K_A	K_D
BDP	53.8 ± 1.2	0.108 ± 0.001	0.049 ± 0.003
Budesonide	57.9 ± 2.0	0.123 ± 0.001	0.065 ± 0.005
Terbutaline Sulphate	56.8 ± 0.8	0.098 ± 0.001	0.411 ± 0.004
PAA	37.2 ± 0.4	0.101 ± 0. 006	0.162 ± 0.020

The dispersive surface energy from IGC varied in the following way: budesonide = terbutaline sulphate > BDP > PAA. The IGC results for APIs differed from the contact angle results in Table 4.8, where the dispersive surface energy of budesonide was equal to BDP and higher than terbutaline sulphate.

Determination of surface energy by IGC and contact angle respectively has both experimental and theoretical differences, which can make comparison of the results difficult. In Figure 4.10 dispersive surface energies originating from contact angle and IGC respectively are compared. The error limit presented is the range rather than the standard deviation in Table 4.8, since it was the only error limit possible to calculate for γ^{LW} from contact angle.

From Figure 4.7 it is clear that γ^{LW} of the APIs obtained from IGC were higher than those from contact angles (2 sample t-test, $p < 0.05$), which is commonly but not always the trend between the two methods (Buckton and Gill, 2007). PAA was an exception since there was no difference between γ^{LW} from contact angle and IGC (2 sample t-test, $p < 0.05$). The variation between methods could be due to surface heterogeneity in terms of surface energy. As mentioned earlier IGC measurements were performed at infinite dilution, hence γ^{LW} of mainly high-energy sites of the powder was measured. The reason for PAA γ^{LW} to be similar from IGC and contact angle may be since the powder had been spray-dried, which may have caused a more even surface energy distribution on the surface compared to micronised powders.

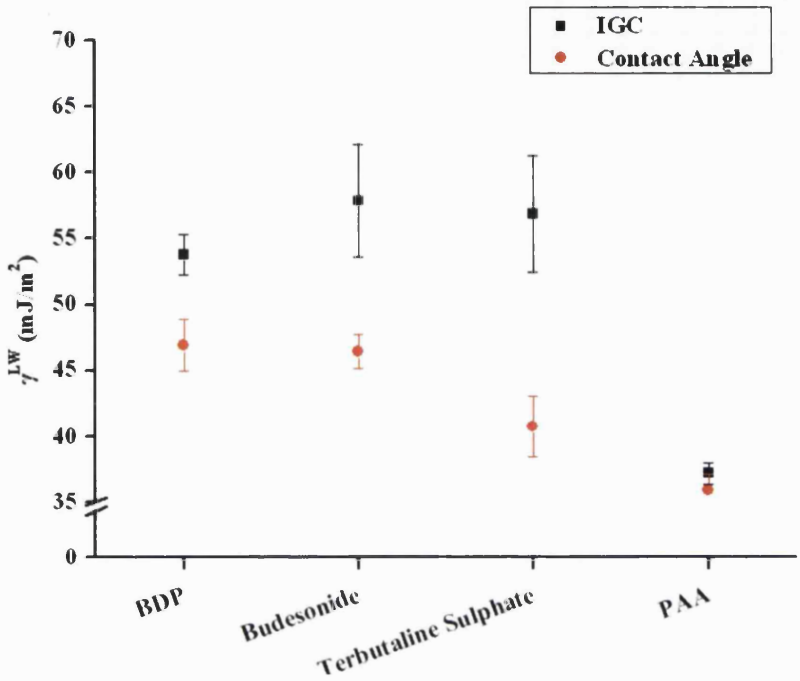

Figure 4.7. Comparison of dispersive surface energy obtained from IGC (n=6) and contact angle (n=10). The error limit presented is the range.

In Figure 4.8 the dimensionless numbers K_A and K_D from IGC are compared with γ^+ and γ^- from contact angle. Even though the electron acceptor and donor parameters have not got comparable units the electron acceptor and donor character of materials can be compared and Figure 4.8 showed that it varied between methods. The consistency that appeared between the methods was that the electron donor character of BDP and budesonide was lower than for terbutaline sulphate and PAA. The literature stated that it is common for materials to have strong electron donor character and hardly any electron acceptor character, which was the case in this study shown in Table 4.7 (van Oss et al., 1987).

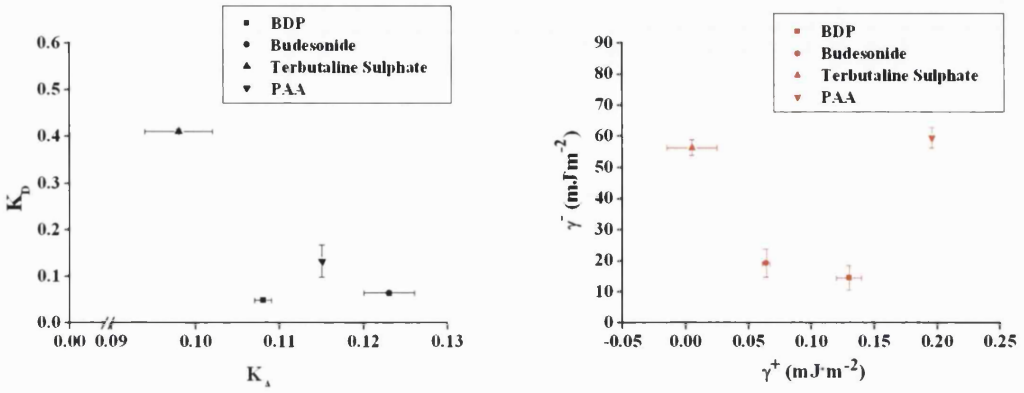

Figure 4.8. Comparison of surface energy parameters obtained from IGC (n=6) and contact angle (n=10).

Over all γ^{LW} was consistent between the results from this study and the literature but the acid and base parameters varied. K_A and K_D for budesonide correlated well with the majority of the literature values, Table 4.9. When comparing K_A and K_D of BDP and terbutaline sulphate with the literature the values did not correlate. K_A and K_D for BDP were not the same in this study and the literature but the relation between the parameters in each study was $K_A > K_D$ in all four different studies presented in Table 4.9. For terbutaline sulphate the internal order of K_A and K_D did not even correlate in the various studies compared. In the results from this study $K_A < K_D$ but in the Beausang study $K_A > K_D$ for terbutaline sulphate. This is likely to be due to the poor fit of the line originating in the calculation technique chosen, which was the most commonly used one first described by Schultz (Jones et al., 2008). There are various ways of calculating K_A and K_D and it has been shown that the Schultz method may be an unsuitable approach for some pharmaceutical materials since it can give a poor fit of the line and therefore misleading K_A and K_D values (Jones et al., 2008).

Table 4.9. Surface energy parameters, measured values from Table 4.8 (n=6) compared to literature values and the liquids used to measure K_A and K_D. The Schultz technique was used for determination of K_A and K_D. Error limit is the standard deviation (SD).

Powders	γ^{LW} (mJ·m^{-2})	K_A	K_D	Acetone	Ethyl Acetate	Acetonitrile	1,4-Dioxane	Ethanol	Chloroform	Methanol	Benzene	Tetrahydrofuran
BDP	53.77 ± 1.15	0.108 ± 0.001	0.049 ± 0.003	x	x	x	x					
BDP (Columbano, 2000)	52.3	0.12	0.015		x				x		x	x
Budesonide	57.86 ± 2.03	0.123 ± 0.001	0.065 ± 0.005	x	x	x	x					
Budesonide (Beausang, 2005)	59.4 ± 0.3	0.141 ± 0.002	0.053 ± 0.007	x	x			x	x			
Budesonide (Jones, 2006)	60.21 ± 0.27	0.131 ± 0.001	0.053 ± 0.007	x	x	x		x		x		
Budesonide (Traini, 2005)	62.9 ± 1.7	0.113 ± 0.002	0.013 ± 0.001	x	x			x	x			
Terbutaline Sulphate	56.84 ± 0.81	0.098 ± 0.001	0.411 ± 0.004	x	x	x						
Terbutaline Sulphate (Beausang, 2005)	56.6 ± 0.2	0.200 ± 0.003	0.027 ± 0.004	x	x			x	x			

4.3.3 Solubility Parameters from Inverse Gas Chromatography

Hansen solubility parameters can be used to predict adhesion (Voelkel et al., 2009) and the solubility parameters of BDP, budesonide, terbutaline sulphate and PAA were obtained from IGC and the mean values are presented in Table 4.10. IGC can only be used for powders therefore the solubility parameters for canisters and fluorinated liquids could not be determined by IGC. The solubility parameters in Table 4.10 show great similarities between the corticosteroids, BDP and budesonide, while PAA is different. Since the standard deviations of the terbutaline sulphate solubility parameters were so large it was not compared with the other powder compounds. The reason for the large standard deviation in the calculated δ_d was explained earlier by the exceptionally long retention time of 1,4-dioxane.

Table 4.10. Hansen solubility parameters of powders calculated from IGC (n=6).

	Solubility Parameter Data ± SD ($MPa^{1/2}$)			
Powder	δ_d	δ_p	δ_h	δ
BDP	18.2 ± 2.6	13.2 ± 2.6	8.1 ± 5	23.9
Budesonide	18.9 ± 2.9	10.5 ± 5.0	13.0 ± 9.2	25.2
Terbutaline Sulphate	21.9 ± 10.3	13.8 ± 18	55.0 ± 32.7	60.8
PAA	13.1 ± 0.8	2.0 ± 1.4	13.9 ± 2.5	19.2

The solubility parameter indicates how likely intermolecular interactions through dispersive, polar or hydrogen bonding interactions are, the more similar solubility parameters the more likely intermolecular interaction are. The compatibility of two compounds is determined by calculating the interaction parameter (ϕ), as described in Section 4.1.2.2 by Equation 4.27. Further on in this Chapter the calculated solubility parameters of powder compounds from this section and canisters will be used to calculate ϕ,.

4.3.4 Solubility Parameters from Stefanis' Group Contribution Method

Stefanis' group contribution method was used to determine the Hansen solubility parameters for the various model metered dose inhaler components and this is a theoretical approach where only the molecular structure of the compound is required to determine the solubility parameters. The solubility parameters of powders: BDP, budesonide, terbutaline, PAA; canisters PET and ALPF and liquids: HPFP were calculated and detailed calculation examples can be found in Appendix 1.3.

In Table 4.11 the Hansen solubility parameters calculated from Stefanis' group contribution method are presented. The solubility parameters for BDP, budesonide and PAA correlated well with the experimental IGC values for the same compounds shown in Table 4.10. That shows that Stefanis' group contribution method and IGC are compatible methods even though Stefanis' predictions did not include the group contribution of some molecules for compounds containing fluorine, such as ALPF, HPFP and perfluoroheptane and inorganic molecules, such as the sulphate in terbutaline sulphate, which was discussed in Section 4.2.4.

Table 4.11. Solubility parameters of powders calculated from Stefanis' Group Contribution Method.

	Solubility Parameter Data ($MPa^{1/2}$)			
Powder	δ_d	δ_p	δ_h	δ
BDP	23.0	19.7	10.6	32.1
Budesonide	22.6	14.0	17.8	32.0
Terbutaline Sulphate	18.8	8.5	26.7	33.7
PVP	21.5	12.0	10.0	27.0
PAA	17.3	8.6	11.0	22.2
PET	19.2	13.7	7.0	24.6
ALPF*	14.1	9.0	6.3	17.8
HPFP*	15.7	4.6	4.7	17.0
Perfluoroheptane	11.7	3.7	4.8	13.1

*not all group contributions were available in Stefanis' group contribution method

In Figure 4.9 the Hansen solubility parameters from IGC are plotted against those from Stefanis' group contribution method. Since Stefanis' were theoretical values no standard deviation is shown. In Figure 4.9 there is a trend showing that the Hansen solubility parameters from Stefanis' method were either equal to or slightly higher than the IGC values. The correlations between the two methods were surprisingly good when looking at the linearity in Figure 4.9. For terbutaline sulphate the results were excluded when determining the linearity since there were issues mentioned earlier with δ^{IGC} that caused the large standard deviation. The linear relationship between solubility parameters from IGC and Stefanis' method was $R^2_{\delta d} = 0.975$, $R^2_{\delta h} = 0.176$, $R^2_{\delta p} = 0.911$, $R^2_{\delta} = 0.955$, where δ_d and δ_p showed a nice correlation but not δ_h.

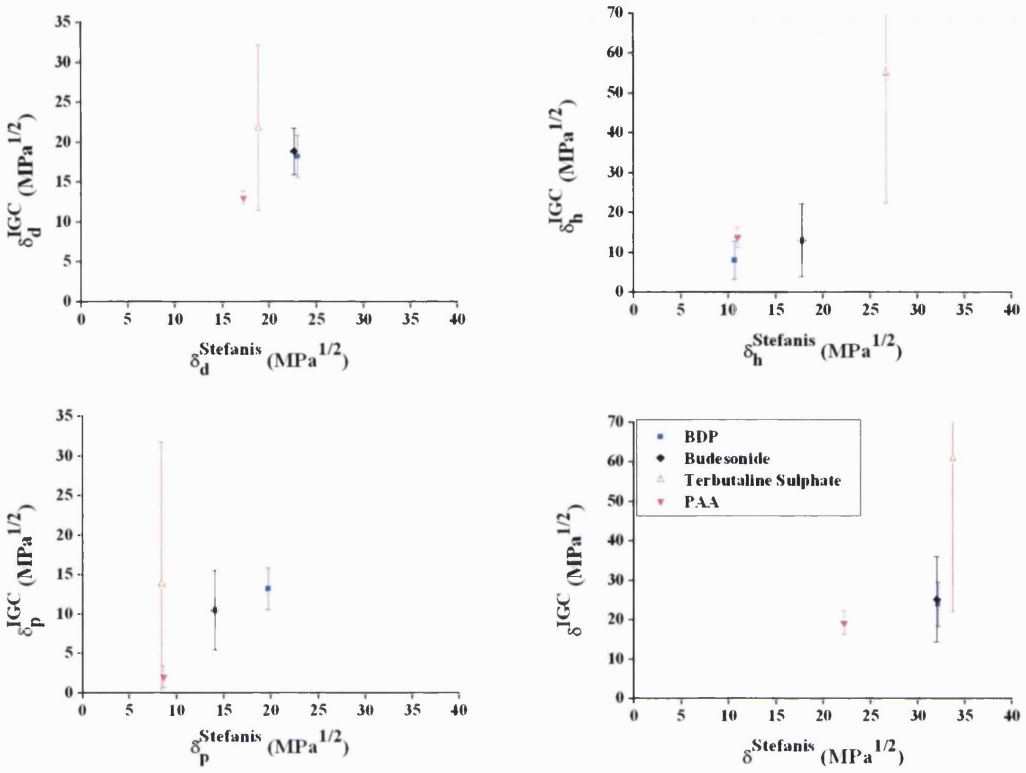

Figure 4.9. Comparison of solubility parameters obtained from Stefanis' group contribution method and IGC (n=6).

4.3.5 Interactions Between Particles, Canister and Fluorinated Liquids

The interactions that are presented in this section originated from two different sources, first the free energy of interaction (ΔG) based on surface energy parameters and then interaction parameter (ϕ) based on solubility parameters. It was investigated how well the two ways of calculating correlated.

4.3.5.1 Interactions from Surface Energy

ΔG based on surface energy parameters for various material combinations are presented in Table 4.12 – Table 4.15. A detailed calculation example can be found in Appendix 1.4.1. The error limit presented is the range, i.e. the difference between the highest and the lowest calculated values.

First in Table 4.12 ΔG_{12} is presented, which is the free energy of interaction between powder and canister. All ΔG_{12} values in the table are negative, which means that there

should be attraction between the canister surfaces and the powders, the more negative ΔG_{12} the higher attraction there is. For instance BDP and budesonide are compared to terbutaline sulphate and PAA more attracted to PET, while there was no difference in ΔG_{12} between powders in each of the other canisters (2 sample t-test, $p<0.05$). Further the powder-canister attraction in Table 4.12 for each powder decreased with canister material like: PET > AL = ALAN > ALPF (2 sample t-test, $p<0.05$), a similar trend was also shown by others through the surface free energy of interaction (γ_{12}) between materials (Traini, 2005).

Table 4.12. Free energies of interaction for binary systems, powder (1) and canister (2). Based on surface energy parameters from contact angle measurements (n=10).

	ΔG_{12} ± Range (mJ·m^{-2})				γ_{12} (mJ·m^{-2})
	BDP	Budesonide	Terbutaline Sulphate	PAA	Budesonide (Traini, 2005)
PET	-93.4 ± 3.3	-92.4 ± 2.8	-86.2 ± 3.0	-82.8 ± 1.7	-
AL	-85.5 ± 4.5	-84.2 ± 4.3	-77.8 ± 5.4	-76.1 ± 4.3	32.02
ALAN	-85.2 ± 4.9	-84.0 ± 4.9	-78.2 ± 6.9	-77.0 ± 6.2	30.87
ALPF	-58.3 ± 4.4	-58.3 ± 3.8	-56.9 ± 3.7	-54.1 ± 3.3	13.10

Table 4.13 first show the free energy of interaction between powders and HPFP (ΔG_{13}) and then canisters and HPFP (ΔG_{23}). From ΔG_{13} it is shown that BDP and budesonide are less attracted to HPFP than terbutaline sulphate and PAA, which makes sense since the two latter are hydrophilic while the two former are hydrophobic. Probably the higher interaction is due to hydrogen bonding between the powders and the hydrogens in HPFP. From ΔG_{23} it is shown that HPFP is much less attracted to ALPF than to the other canister materials. HPFP has a dominating electron acceptor site (γ^+) and PET, AL and ALAN have dominating electron donor sites (γ^-), hence interaction should be favoured. In ALPF neither γ^+nor γ^- dominates and both parameters are very low, Table 4.7.

Table 4.13. Free energy of interaction for binary systems. First between powder (1) and HPFP (3) and then between canister (2) and HPFP (3). systems, powder (1) and canister (2). Based on surface energy parameters from contact angle measurements (n=10).

	ΔG_{13} ± Range ($mJ \cdot m^{-2}$)		ΔG_{23} ± Range ($mJ \cdot m^{-2}$)
BDP	-52.2 ± 2.3	PET	-46.3 ± 1.3
Budesonide	-53.6 ± 2.2	AL	-47.3 ± 2.5
Terbutaline Sulphate	-60.6 ± 1.6	ALAN	-48.7 ± 3.6
PAA	-59.8 ± 1.2	ALPF	-24.9 ± 2.9

In Table 4.14 the interaction between two particles of the same compound immersed in HPFP (ΔG_{131}) is shown. Table 4.14 shows that BDP particles immersed in HPFP were more attracted by each other than budesonide, i.e. more cohesive. It also shows that terbutaline sulphate particles repelled each other more than PAA when immersed in HPFP. In general the steroid particles were attracted by each other while terbutaline sulphate and PAA particles were repelled by each other when immersed in HPFP. The results presented in Table 4.13 and Table 4.14 suggest that since the corticosteroids interact less with HPFP through hydrogen bonding their cohesiveness is larger than the cohesiveness of terbutaline sulphate and PAA.

Table 4.14. Free energy of interaction between two particles of the same compound (1) immersed in HPFP (3). systems, powder (1) and canister (2). Based on surface energy parameters from contact angle measurements (n=10).

	ΔG_{131} ± Range ($mJ \cdot m^{-2}$)			
	BDP	Budesonide	Terbutaline Sulphate	PAA
HPFP	-17.9 ± 0.8	-13.0 ± 1.1	14.7 ± 2.1	11.2 ± 0.3

In Table 4.15 the free energy of interaction between powder and canister immersed in HPFP (ΔG_{132}) is shown. ΔG_{132} is a suitable parameter to predict the interactions in the model metered dose inhaler systems studied in this thesis, since it considers the interactions between the three interacting materials, powder-canister-liquid, of the system. In Table 4.15 there are both negative and positive ΔG_{132} values. The negative ΔG_{132} shows that BDP and budesonide is attracted to all canister materials. Further the positive ΔG_{132} shows that PAA is repelled from all materials and terbutaline sulphate from all materials but PET. It is also clear from Table 4.15 that the interaction between a powder and the canisters increase in the following order: ALPF < aluminium canisters

< PET. These interactions will be discussed in relation to true adhesion in Chapter 6. To conclude all ΔG results presented here it seems like the less a compound interacts with the liquid the more cohesive it is and also more adhesive to the canister wall.

Table 4.15. Free energy of interaction for tertiary systems, powder (1) and canister (2) immersed in HPFP (3), powder (1) and canister (2). Based on surface energy parameters from contact angle measurements (n=10).

	ΔG_{132} ± Range ($mJ \cdot m^{-2}$)			
	BDP	Budesonide	Terbutaline Sulphate	PAA
PET	-17.8 ± 0.3	-15.4 ± 0.7	-2.1 ± 0.1	0.4 ± 0.8
AL	-8.9 ± 0.3	-6.3 ± 0.4	7.2 ± 1.3	8.1 ± 0.6
ALAN	-7.2 ± 1.1	-4.6 ± 0.9	8.3 ± 1.6	8.6 ± 1.4
ALPF	-4.1 ± 0.9	-2.7 ± 1.2	5.7 ± 0.8	7.7 ± 0.8

4.3.5.2 Interactions from Solubility Parameter

In this section the interaction parameter based on Hansen solubility parameters (ϕ) have been calculated and a detailed calculation example can be found in Appendix 1.4.2. It has been shown by others that Hansen solubility parameters (δ_d, δ_p, δ_h) give a poor prediction of interactions between materials in fluorinated liquids (Dickinson et al., 2000). However, since it was possible to calculate δ_d, δ_p, δ_h based on the molecular structure of all three materials in the model metered dose inhalers studied the interactions between two materials could be calculated and it was considered of interest to see if the interactions based on surface energy parameters and solubility parameters respectively correlated. Chapter 6 contains an evaluation of what method correlates best with the adhesion studies from Chapter 3. In case it would be possible to predict adhesion in fluorinated systems by ϕ there would be a purely theoretical way to foresee undesired interactions in such systems, which would be a simple and cheap method. In Table 4.16 and Table 4.17 ϕ between various compounds is shown. No error limit is presented in the tables since the values are not experimental but based on purely theoretical calculated δ_d, δ_p, δ_h.

In Table 4.16 ϕ between powders and the same canister decreased in the order: BDP > budesonide > terbutaline sulphate > PAA, which was similar to ΔG_{12} (free energy of

interaction between powder and canister) where the predicted interaction for corticosteroids was higher than for terbutaline sulphate and PAA. When ϕ is closer to 1 it means that the two materials are more compatible, hence more likely to interact, in this case through adhesion. When looking at ϕ of the same powder to various canisters the interaction with ALPF was higher than with PET and in Chapter 3 the adhesion to ALPF was much lower than the adhesion to PET. By purely studying δ_d, δ_p and δ_h in Table 4.11 it was expected that ϕ should be lower for ALPF and higher for PET since for ALPF compared to PET δ_d, δ_p and δ_h values were much lower and further away from the values of APIs, hence ALPF should lead to lower adhesive interactions. This inconsistency is likely to be due to the assumptions made in the ϕ calculations where density and molecular weight of the compounds are included. Since the real density and molecular weight values were not available for ALPF and PET common values for these polymers were used and the same values were assumed for both polymers. When the density and molecular weight in the calculations was altered, as a trial to see the impact it had on ϕ different ϕ were obtained. This shows that using the real density and molecular weight of compounds involved in the calculations is of great importance and if these values are hypothetical it could give misleading values. Therefore the predicted interactions of the same powder with PET and ALPF respectively by ϕ will not be compared only the predicted interactions for different powders in contact with the same canister material.

When comparing ϕ of powders in Table 4.16 to the same liquid the following was true: PAA > terbutaline sulphate > budesonide > BDP, which agreed well with the results for ΔG_{13} (free energy of interaction between powder and liquid) from contact angles. Further the comparison of ϕ for liquids to the same powder gave: HPFP > perfluoroheptane. This means that powders generally interact more with HPFP than perfluoroheptane, probably since there is hydrogen bonding between hydrogen bonding sites in the powder compounds and the hydrogen atoms in HPFP, something that is not possible with perfluoroheptane since the perfluorinated compound has no hydrogen atoms (Alison et al., 2005). In Chapter 3 it was shown that the adhesion from HPFP suspensions was lower than from perfluoroheptane and perfluorodecalin and a possible explanation was the lack of hydrogen bonding interactions in the perfluorinated liquids.

Table 4.16. Interaction parameter for binary systems. Based on solubility parameters calculated from Stefanis' group contribution method. systems, powder (1) and canister (2).

	ϕ			
	PET	ALPF	HPFP	Perfluoroheptane
BDP	0.602	0.898	0.395	0.273
Budesonide	0.576	0.876	0.413	0.287
Terbutaline Sulphate	0.535	0.799	0.417	0.298
PAA	0.456	0.758	0.529	0.374

Finally in Table 4.17 it is shown that the interactions between canisters and HPFP are larger than between canisters and perfluoroheptane. This means that HPFP compared to perfluoroheptane easier wets the canister wall and since the adhesion was lower from HPFP compared to perfluoroheptane suspensions this indicates that adhesion is lower in a liquid that easier wets the canister surface.

Table 4.17. Interaction parameters for binary systems, canisters/HPFP. Based on solubility parameters calculated from Stefanis group-contribution method.

	ϕ	
	HPFP	PFH
PET	0.272	0.184
ALPF	0.263	0.177

The two ways of calculating interactions, first from surface energy parameters and then from solubility parameters, agreed surprisingly well for the systems studied. There were discrepancy between the methods when it came to the predicted interaction between the canisters, ALPF an PET and a powder. However, due to assumptions made in ϕ calculations ΔG were considered closer to reality in that case. The good correlations are surprising since the solubility parameter calculations included two major shortcomings. Firstly incomplete solubility parameter values for HPFP and perfluoroheptane due to the lack of some polar and hydrogen bonding group contributions in Stefanis method. Secondly the molar volume assumptions for PET and ALPF since no experimental values existed. The data in this chapter will be discussed in relation to adhesion in Chapter 6.

4.4 Conclusions

It can be concluded that surface characteristics can be determined through various techniques, in this study experimentally by contact angle by sessile drop and IGC and theoretically through Stefanis' group contribution method. However, choosing the best technique is not straightforward and depends on the materials that will be investigated. Contact angle for example is more suitable for solid materials with smooth surfaces, such as the canisters, where there is little chance for variation in contact angle. In order to measure contact angle of powders the surface must be modified to become smooth, in this case compressed to discs and the contact angle on compressed discs may not represent the "real" powder since the physical form may have been altered during compression. IGC is more suitable for powders since it is non-destructive and the powder can be analysed without modifying the surface, however it often gives overestimated results. Another limitation is that IGC is only for powders and therefore the canister surfaces could not be analysed by IGC. Also the IGC calculations does not give the same units for the apolar and polar surface energy parameters. Another method, apart from contact angle, that could predict the nature of all materials was the group contribution method that gave a purely theoretical estimation. Even though Stefanis' group contribution method covers more molecular groups than any other group contribution method it lacks information about some fluorinated molecules and is not applicable to in-organic materials such as aluminium and glass.

In this chapter both surface energy and solubility parameters of materials were determined. Contact angle and IGC were used to determine surface energy and IGC and Stefanis' group contribution method were used for solubility parameters. There was a good correlation between the powder solubility parameters determined by IGC and Stefanis' group contribution method. Since experimental results from IGC and theoretical results from Stefanis' group contribution method correlated well the theoretical approach can be viewed as a suitable alternative when solubility parameters cannot be determined experimentally, which was the case for canisters and HPFP in this study.

The dispersive surface energy parameters from contact angle and IGC were compared. It is widely known that the dispersive surface energy from IGC at infinite dilution is

overestimated since predominantly the high-energy sites of a powder are measured. Hence, also in this study contact angle measurements resulted in lower dispersive surface energy values than IGC. There was no correlation between the electron donor and acceptor parameters originating from contact angle (γ^+ and γ^-) and IGC (K_A and K_D).

Finally the major two different ways of predicting interactions correlated surprisingly well. The first approach was the free energy of interactions (ΔG) based on surface energy parameters (γ^{LW}, γ^+, γ^- and γ) from contact angle and the second approach was the interaction parameters (ϕ) based on Hansen solubility parameters (δ_d, δ_p, δ_{hb} and δ) calculated from Stefanis group contribution method. It was possible to determine interaction in ternary systems, between powder and canister immersed in a liquid by ΔG but not by ϕ. ϕ was only for binary systems but mainly correlated well with the binary ΔG results. A brief overview of the predicted interactions from calculated ΔG values showed that more hydrophilic compounds interacted more with the model HFA and less with the canister wall and its own particles. The compounds interacting more with the canister wall also had stronger cohesive forces when immersed in HPFP. Finally there were signs that a higher predictive liquid-canister interaction leads to lower particle adhesion to the canister wall. In Chapter 6 these interaction predictions will be correlated to the adhesion from Chapter 3.

Chapter 5: Interactions by Atomic Force Microscopy

5.1 General Introduction

Atomic force microscopy (AFM) is a powerful instrument commonly used in solid dosage formulation development, including inhalation formulation development of DPIs particularly and also pMDIs. AFM can give detailed surface information, such as roughness, force of interaction with other materials, surface energy, mechanical properties, to a great level of detail that is not possible to get with conventional bulk methods, it can measure forces down to 10pN (Roberts, 2009). As previously stated interactions between materials commonly used in pMDIs are of interest to this study therefore AFM was used to determine the roughness of canisters and also adhesive particle-canister interactions of some material combinations. The force of adhesion measured by AFM is well established in the area of inhalation and has been used to gain a better understanding of interactions in pMDI systems (James et al., 2009, Traini et al., 2007, Traini et al., 2005, Ashayer et al., 2004, Young et al., 2003) as well as DPI systems (Adi et al., 2008b, Jones et al., 2006a, Young et al., 2006). It is advantageous that minimal quantities of material is required for AFM experiments. However the results does only represent some areas of the sample and in force of adhesion measurements only a limited number of particles are represented.

5.2 Atomic Force Microscopy

The AFM is equipped with a laser, cantilever probe, piezoelectric scanner, photo detector and feedback loop controller as shown schematically in Figure 5.1. Depending on the AFM mode chosen different cantilevers can be used and the cantilever is a spring like rectangular silicon or silicon nitride base acting under Hook's law in Equation 5.1 with a tip mounted in the centre of one side.

$$F=-k\Delta D \qquad (5.1)$$

where F is the force, k the spring constant of the cantilever and ΔD the cantilever

deflection. The cantilever has a tip radius of curvature in the nanometre range, which enables measurements in the nanoNewton range (Jones, 2006). In order to focus on the desired area on the surface a light microscope is used and by moving the scanner along three different axes (x, y, z) the right sample areas for analysis can be found and the tip and sample surface can be brought into contact to measure adhesion forces. The photo detector registers variations in the laser beam from cantilever deflection, Figure 5.1. Finally the feedback loop controller is there to prevent collisions between tip and surface and it constantly adjusts the distance between tip and surface.

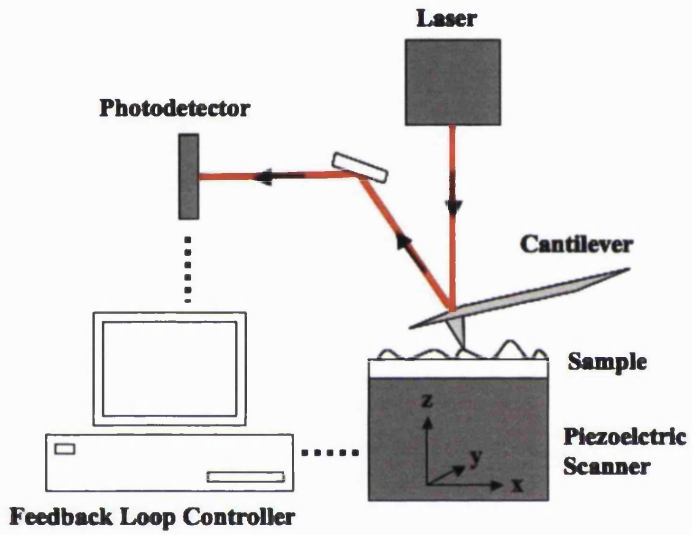

Figure 5.1. A schematic image of the atomic force microscope.

5.2.1 Tapping Mode AFM

Tapping mode AFM can be used to determine the roughness of surfaces. A cantilever with a stiff crystal silicon tip is used for such measurements and it is externally oscillated at or close to its own specific resonance frequency. To maintain the set amplitude for the oscillating tip the surface is constantly automatically adjusted in the z-axes, the necessary adjustments are recorded by the feedback loop system that register the tip-sample force of interaction and adjusts the sample. The surface topography of a specific area is mapped when the cantilever tip is raster scanned across the area by moving the piezoelectric scanner in the x and y directions. From the same raw data a quantitative analysis of the roughness can be done by calculating the root mean square roughness (R_{RMS}) with Equation 5.2 in the AFM software.

$$R_{RMS} = \sqrt{\frac{1}{n_p}\sum_{i=1}^{n} y_i^2} \qquad (5.2)$$

where n_p is the number of points in the image and y_i is the longest distance from the central line, as shown in Figure 5.2.

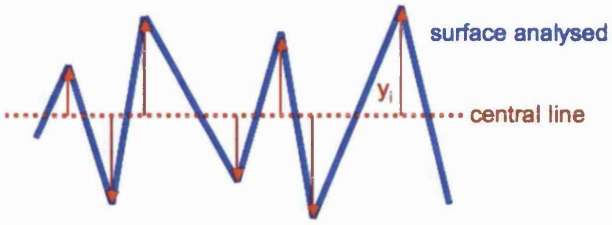

Figure 5.2. Topography profile of a substrate to support Equation 5.2.

5.2.2 Force-Distance Measurements

Through force-distance measurements the force of adhesion between a particle and a surface can be obtained as a direct measurement. An AFM colloidal probe is used, which is when a single micrometer-sized particle is attached to a tipless silicone nitride cantilever.

The force of adhesion between the particle and the substrate is measured from the deflection of the cantilever when the substrate is brought into contact with the particle and then retracted. The surface that the particle will interact with is attached to the piezoelectric scanner and the laser and photo detector monitors the cantilever deflection during the interaction. After the experiment SEM analysis of the colloidal probe is undertaken to ensure the particle is still attached to the tip and this analysis can only be performed after the measurement since the SEM sample coating alters the surface characteristics of the tip.

5.3 Materials & Methods

AFM was used to determine the topography of canisters and the force of adhesion between microparticles and canisters.

The materials used were powders: budesonide and terbutaline sulphate and canisters: polyethyleneterephtalate (PET), aluminium (AL), anodised aluminium (ALAN), perfluoroalkane coated aluminium (ALPF) and glass.

When comparing results a Student's t-test, two samples with same variance, was carried out with a significance level of 95% ($p < 0.05$).

5.3.1 Analysis of Canister Roughness

The roughness of canister surfaces, PET, AL, ALAN, ALPF and glass, was determined with Tapping Mode AFM by using a Multimode AFM, J-scanner, NanoScope IV controller and NanoScope 5.12b control software (all from Vecco, Cambridge, UK) and a silicon tip (model number: OMCL-AC249TS, Olympus, Japan). The canister areas were analysed in triplicate with the following settings: scan size 10×10 μm, scan rate 1.0 Hz, resolution 512×512 pixels. Based on Equation 5.2 R_{RMS} was calculated by the AFM software.

5.3.2 Preparation of Colloidal Probes and Canister Substrates

Micronised budesonide and terbutaline sulphate microparticles were glued onto tipless cantilevers (Vecco NanoProbe^{TM}, spring constant 0.58 $N \cdot m^{-1}$, model number: NP-OW, Vecco Instruments SAS, Dourdan, France) by using epoxy resin (Araldite Precision, Bostik Ltd, Leiceter, UK) by the micromanipulation method described by Traini (Traini, 2005). Purpose built cylindrical glass cover slip holders were attached to an optical light microscope 10×lens, the cantilever was placed in a purpose made holder below the microscope lens and could be moved along the x, y and z axes to approach the slip. As shown in Figure 5.3 first the resin was transferred to the cantilever, (1), then the microparticle was transferred, (2), and finally the colloidal probe was left to cure for at least 48 hours prior to use in an experiment, (3).

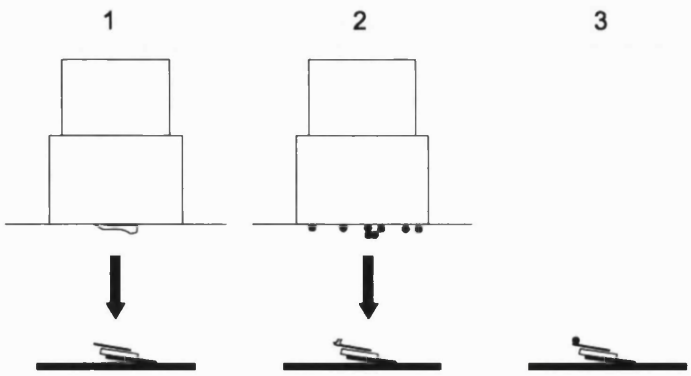

Figure 5.3. Method for preparing colloidal probes, above a cylindrical glass cover slip holder and below the cantilever in a cantilever holder. (1) Glue is applied to the cantilever, (2) particle is attached to glue and (3) colloidal probe is left to dry for at least 48 hours.

An optical microscope with incident illumination was used to confirm a successful colloidal probe preparation with only one particle attached and no resin covering the particle.

The canister surfaces were cut into small pieces that were a few millimetres wide and long. In order to mimic the canisters used in Chapter 3 no solvent was used to clean the surfaces, it was only ensured that no dust was present on the surface.

5.3.3 Force of Adhesion between Particle and Canister

The force of adhesion between particles, budesonide and terbutaline sulphate, and canister surfaces, AL, ALAN and ALPF was determined by force-distance measurements at zero per cent relative humidity by using a Multimode AFM, J-scanner, NanoScope IV controller and NanoScope 5.12b control software (all from Vecco, Cambridge, UK) and the colloid probes prepared in Section 5.3.2. Smoother canister areas were chosen for analysis in order to avoid damage of the colloidal probe and force-distance curves were collected over 5×5 μm areas (n=256) with a z-scan rate of 4.07 Hz and a nominal compressive force of 11.6 nN.

The force of adhesion between budesonide and PET was too high and could therefore not be measured. Force-distance curves were collected for each colloidal probe by running it on one canister surface at the time, starting with the roughest, in the

following order: AL, ALAN, ALPF and finally AL again to confirm that the particle of the colloidal probe was intact after the analysis. The force of adhesion was obtained by processing the force-distance curves in the custom made AFM analysis software ForceCat 2007.

After the force of adhesion measurements a SEM XL 30, FEI Company was used to capture SEM images of the colloidal probe to confirm that the particle had not fallen off the cantilever because it would have made the results invalid. The colloidal probes were coated with gold by a K5-50 Sputter Coater, Emitech, for two minutes at 30 milliampere.

5.4 Results and Discussion

5.4.1 Canister Roughness

It is necessary to evaluate the roughness of surfaces when carrying out AFM measurements because roughness has an impact on adhesion measurements (Price et al., 2002, Young et al., 2004). In Section 2.2 visual canister roughness was estimated with SEM and the images are shown again for comparative reasons in Figure 5.4 with a roughness decrease of: AL > ALPF > ALAN > PET > glass. Compared to the flat glass surface PET had small wavelike patterns along the surface. The ALPF surface had an evenly distributed wavelike pattern like PET but much more pronounced and including small hills. If comparing AL and ALAN in Figure 5.4 the roughness appears different, ALAN looks less rough and with roughness more uniformly distributed than AL. Anodising of aluminium surfaces is done through an electrochemical process that makes the natural oxide layer of aluminium thicker and tougher, aluminium canisters for pMDI use are anodised prior to coating to make the polymeric coating adhere better.

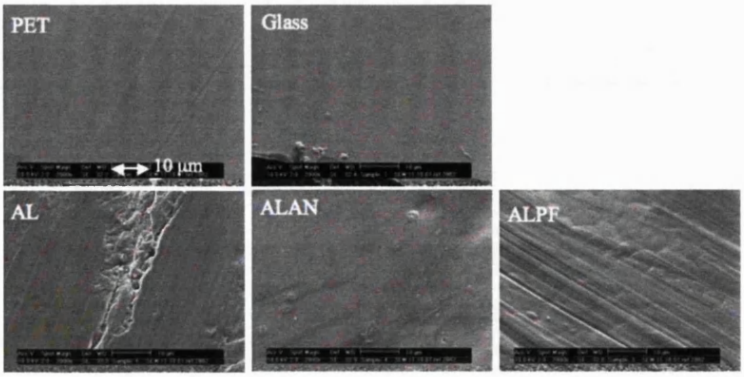

Figure 5.4. SEM images of canister surfaces from Section 2.2.

In Figure 5.5 AFM images of the canister topography are shown and the differences shown by SEM were more detailed by AFM where the visual roughness decrease was: AL = ALPF > ALAN > PET > glass. The visual roughness determination of canister surfaces by SEM and AFM were complimentary since SEM showed larger areas (6.3 mm × 4.7 mm in Section 2.2 and 63 µm × 47 µm in Figure 5.4) with a lower level of detail and AFM showed smaller areas (10 µm × 10 µm in Figure 5.5) with a greater level of detail. The wavelike pattern for the two polymer surfaces in the SEM images was not visible at the same level of detail in AFM; instead PET showed unevenly distributed low roughness and ALPF the hill like topography that was shown by SEM, which was probably due to a less optimal PFA coating process. Both AL and ALPF have a high roughness in Figure 5.5 but the topography is not at all alike, the peak distance is shorter for AL than for ALPF and AL has sharper peaks while ALPF has rounder peaks. Roughness as well as peak distance has been shown to have an impact on the force of adhesion measured by AFM, since the value of those parameters will have an impact on the contact area between the probe and the substrate (Zhou et al., 2003). For the AFM images smoother areas were chosen since those would be the ones used for force of adhesion measurements and that may have lead to an underestimated roughness for AL since the AFM topography in Figure 5.5 only represents the smoother areas of AL seen in Figure 5.4.

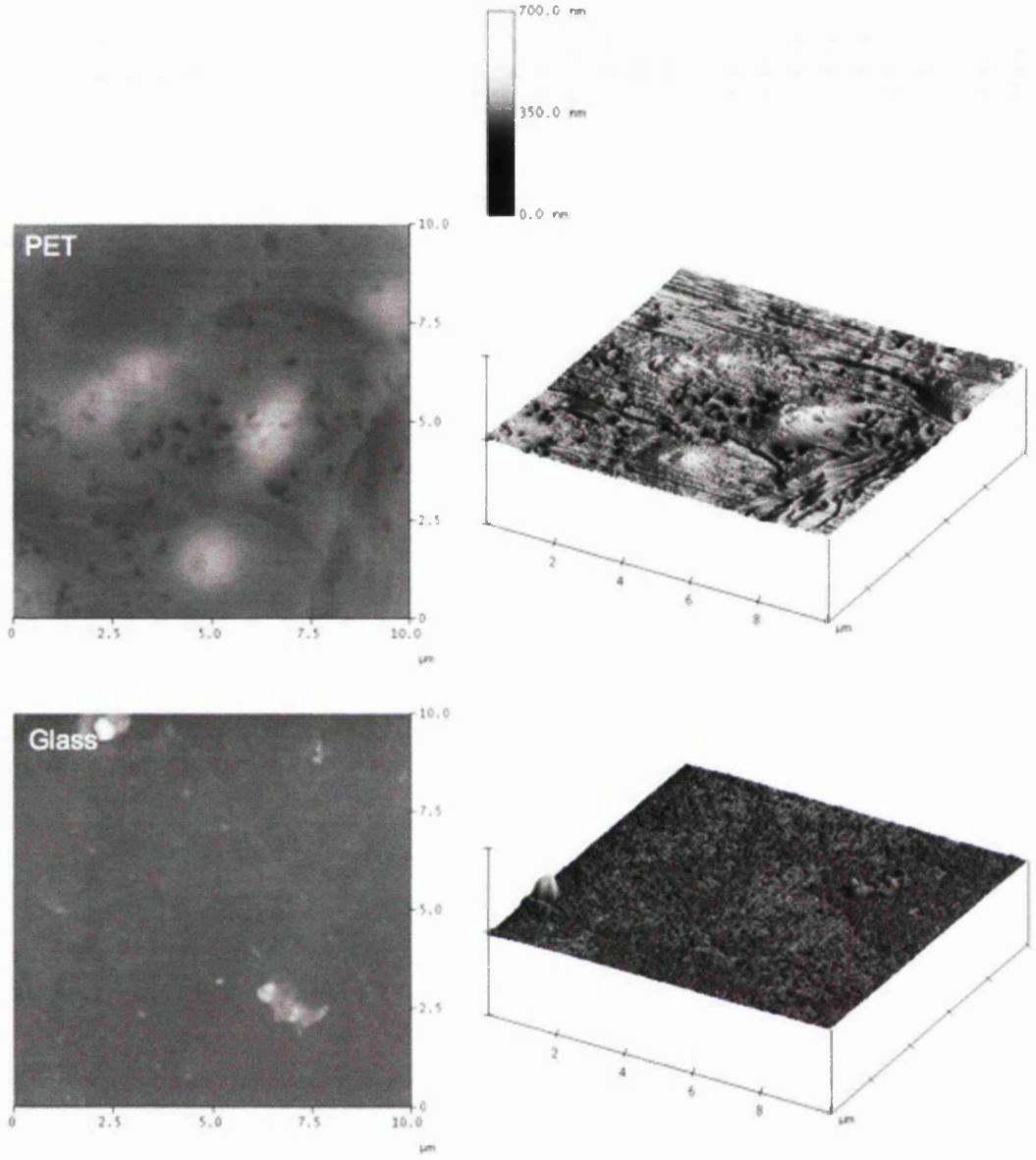

Figure 5.5. (Continues on next page) Representative topographical images of square areas (10 μm x 10 μm) of the canisters inner wall from tapping mode AFM. The z-scale colour grading for the 2D-images is shown above. The z-scale for the 3D images is 700μm/division.

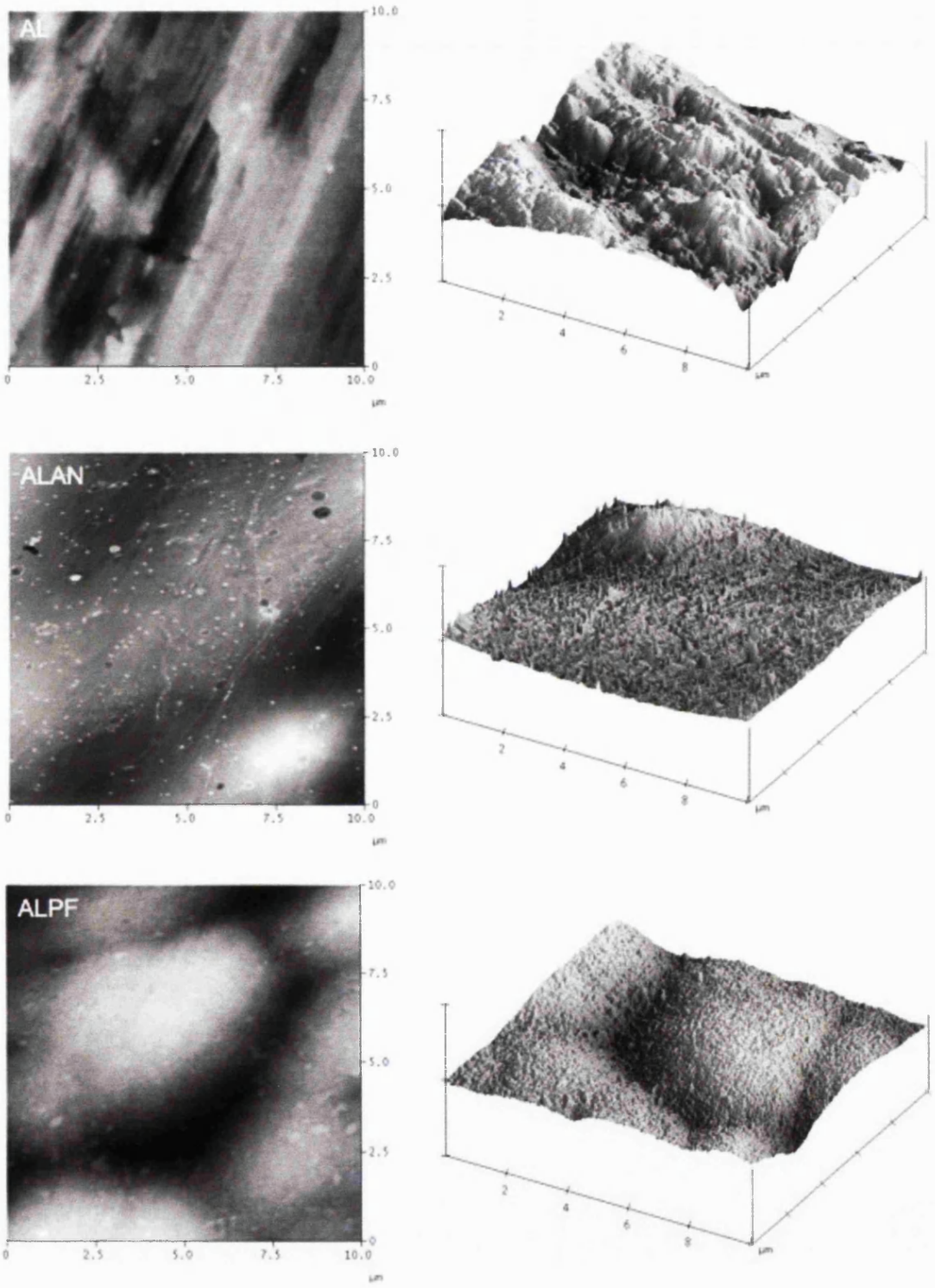

Figure 5.5. (Continues from previous page) Representative topographical images of square areas (10 µm x 10 µm) of the canisters inner wall from tapping mode AFM. The z-scale colour grading for the 2D-images is shown above. The z-scale for the 3D images is 700µm/division.

In Table 5.1 R_{RMS} values for the canisters are shown and the surfaces can be considered rough compared to crystal surfaces commonly used in F_{adh} experiments. The surface roughness preferred to obtain reproducible results are often R_{RMS} < 2nm (Traini et al., 2005). However R_{RMS} and its standard deviation for the canisters are of reasonable size for the canister materials in this study (Traini et al., 2006). R_{RMS} varied in the order: AL = ALPF = ALAN > PET = Glass (2 sample t-test, $p < 0.05$). The standard deviation in Table 5.1 shows a rank decrease for roughness distribution of AL > ALPF > ALAN > PET > glass, which explains the visual roughness shown in Figure 5.4 and Figure 5.5 better than the mean R_{RMS}.

Table 5.1. R_{RMS} of canister surfaces measured by AFM. (n=3)

Canister	R_{RMS} (nm) 10 μm x10 μm ± SD
PET	9.4 ± 3.5
Glass	9.0 ± 1.7
AL	65.1 ± 27.3
ALAN	31.0 ± 9.8
ALPF	50.9 ± 14.2

In Chapter 4 the canister heterogeneity was investigated by contact angle and the results showed heterogeneities but since the roughness was not measured it was not possible to establish if the heterogeneities were physical or chemical. Roughness impact on surface energy is still under discussion but it has been shown that a roughness below 100 nm would not have an impact on surface energy (Buckton et al., 1995) and therefore, since R_{RMS} < 100 nm for the canister surfaces in Table 5.1 the surface heterogeneities presented in Chapter 4 should mainly be due to chemical heterogeneities, not physical. The canister surface heterogeneities relation to true adhesion of particles will be discussed in Chapter 6.

Investigating surface roughness by several techniques was useful since the canisters inner wall was large and even though a statistical test of the results in Table 5.1 did not show any difference in R_{RMS} between AL, ALAN and ALPF differences were found when the standard deviation of the numerical values were studied together with the images from AFM and SEM. In total when combining the results from AFM and SEM the roughness of the canisters decreased like: AL > ALPF > ALAN > PET > glass.

5.4.2 Force of Adhesion between Particle and Canister

A representative light microscope image of a terbutaline sulphate colloidal probe with one particle attached is shown in Figure 5.6.

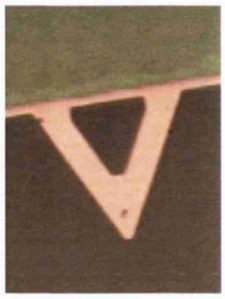

Figure 5.6. Light microscope image of a terbutaline sulphate colloidal probe.

Figure 5.7 shows SEM images of the same terbutaline sulphate colloidal probe after it had been used for F_{adh} measurements and the images confirm that the particle was undamaged and had not fallen off the cantilever tip during the experiments.

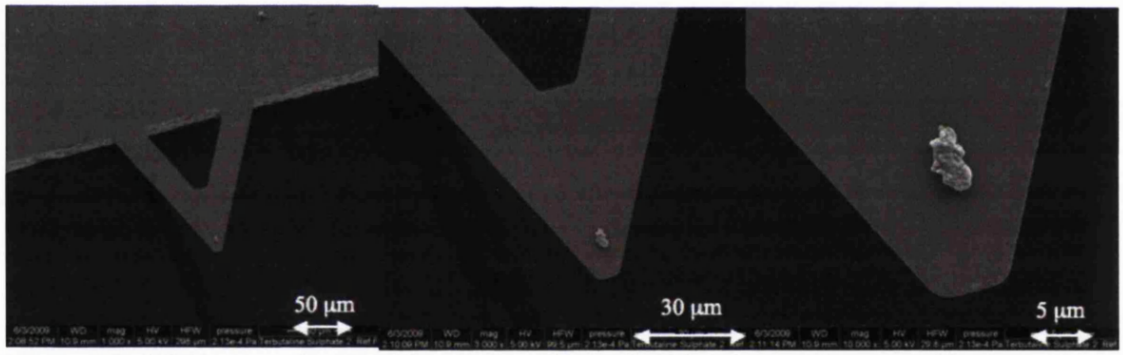

Figure 5.7. SEM images of a terbutaline sulphate AFM colloidal probe at various magnifications.

The force of adhesion (F_{adh}) for budesonide and terbutaline sulphate interacting with AL, ALAN and ALPF canisters is shown in Table 5.2. When budesonide interacted with PET F_{adh} was too high to measure, it was therefore assumed to be too high to measure for terbutaline sulphate as well so no F_{adh} for budesonide and terbutaline sulphate with PET is presented in Table 5.2. The standard deviation was very large in all cases, but the data points presented are significantly different (2 sample t-test, $p < 0.05$), such large error is common in F_{adh} measurements where the substrate roughness is high (Götzinger and Peukert, 2003). The data in Table 5.2 suggest a rank decrease in ${F_{adh}}^{PET} > {F_{adh}}^{ALPF} > {F_{adh}}^{AL} > {F_{adh}}^{ALAN}$ for budesonide and terbutaline sulphate. It is only possible to compare measurements of the same particle with different canister surfaces since one must ensure that the same contact area is used each time.

Table 5.2. Force of adhesion between microparticle: budesonide and terbutaline sulphate and canister: PET, AL, ALAN and ALPF as measured by AFM (n=256).

	Force of Adhesion mean [nN]		
	Budesonide Tip 1	**Budesonide** Tip 2	**Terbutaline Sulphate** Tip 1
PET	Too high to measure	Too high to measure	Not measured
AL	291.04 ± 114.72	262.73 ± 133.36	204.27 ± 50.72
ALAN	28.32 ± 41.60	66.84 ± 82.56	115.58 ± 47.90
ALPF	349.11 ± 55.49	365.79 ± 132.28	216.36 ± 99.47

The force of adhesion obtained has been shown to be dependent on many factors such as surface energy, hardness, roughness (James et al., 2009, Adi et al., 2008b, Traini et al., 2005, Young et al., 2003, Zhou et al., 2003).

Table 5.3 shows the free energy of interaction (ΔG_{12}) for binary systems, budesonide and terbutaline sulphate interacting with the canister materials. The values are taken from Section 4.2.5.1, Table 4.13 and repeated here for convenience. The data in Table 5.3 show a rank decrease of $\Delta G_{12}^{ALPF} > \Delta G_{12}^{ALAN} = \Delta G_{12}^{AL} > \Delta G_{12}^{PET}$ for budesonide and terbutaline sulphate confirming attractive interactions since ΔG_{12} is negative, the lower ΔG_{12} the more attractive energy of interaction. $\Delta G_{12}^{PET} < \Delta G_{12}^{AL} = \Delta G_{12}^{ALAN}$ shows that the powders are more attracted to PET and it correlates with the AFM results that showed stronger force of adhesion between powders and PET. This was also the case when the powders interaction with PET was compared with ALPF since $\Delta G_{12}^{PET} < \Delta G_{12}^{ALPF}$ and $F_{adh}^{PET} > F_{adh}^{ALPF}$. The same relation between ΔG_{12} and F_{adh} was not shown for power interactions with ALPF compared to AL and ALAN since $\Delta G_{12}^{AL} = \Delta G_{12}^{ALAN} < \Delta G_{12}^{ALPF}$ and $F_{adh}^{ALPF} > F_{adh}^{AL} > F_{adh}^{ALAN}$. It may mean that other factors than surface energy, such as surface roughness have an impact on F_{adh}.

Table 5.3. Free energies of interaction for binary systems (ΔG_{12}), powder (1) and canister (2). Based on surface energy parameters from contact angle measurements from Chapter 4 (n=10).

	ΔG_{12} ± Range ($mJ \cdot m^{-2}$)	
	Budesonide	**Terbutaline Sulphate**
PET	-92.4 ± 2.8	-86.2 ± 3.0
AL	-84.2 ± 4.3	-77.8 ± 5.4
ALAN	-84.0 ± 4.9	-78.2 ± 6.9
ALPF	-58.3 ± 3.8	-56.9 ± 3.7

Some studies in the literature have shown that surface roughness has an impact on F_{adh} measured by AFM (Adi et al., 2008a, Traini et al., 2006, Zhou et al., 2003, Young et al., 2003) while others showed that surface energy, in particular the polar contribution, but not roughness had an impact on F_{adh} (James et al., 2009). Some studies showed that a higher F_{adh} is a result of a lower R_{RMS} due to larger contact area (Adi et al., 2008b, Young et al., 2003) and an example of that here is that $F_{adh}^{PET} > F_{adh}^{ALPF,\ AL,\ ALAN}$ and $R_{RMS}^{PET} < R_{RMS}^{ALPF,\ AL,\ ALAN}$ since F_{adh}^{PET} was not recorded it is not included in Figure 5.8 but it was higher than all F_{adh} presented.

Since the following rank order, $F_{adh}^{ALPF} > F_{adh}^{AL} > F_{adh}^{ALAN}$, could not be explained by ΔG_{12} it will be explained by looking closer at the roughness and peak distance of the canister surfaces. First the chemically similar canister surfaces AL and ALAN were compared $F_{adh}^{AL} > F_{adh}^{ALAN}$, $R_{RMS}^{AL} = R_{RMS}^{ALAN}$. The higher F_{adh}^{AL} may be explained by looking closer at the topography of the canister since as mentioned earlier not only R_{RMS} is important when looking at the impact of roughness on F_{adh}, but also the peak distance (λ) of the rough surface (Zhou et al., 2003). Zhou *et al.* found that when two chemically similar aluminium surfaces 1 and 2 were compared $F_{adh}^{AL\ 1} > F_{adh}^{AL\ 2}$, $R_{RMS}^{AL\ 1} < R_{RMS}^{AL\ 2}$ and $\lambda_{AL\ 1} > \lambda_{AL\ 2}$ and it was explained that a higher λ enabled particles to position themselves between the peaks and therefore the contact area became higher when λ was larger and R_{RMS} was smaller, Figure 5.8 (Zhou et al., 2003).

Figure 5.8. Left is a schematic image of a smoother surface with longer peak-to-peak distance, right is a rougher surface with shorter peak to peak distance and left the smoother surface with longer peak-to-peak distance.

$\lambda^{AL} > \lambda^{ALAN}$ could explain why $F_{adh}^{AL} > F_{adh}^{ALAN}$ when $R_{RMS}^{AL} = R_{RMS}^{ALAN}$ because a micron sized particle may get a larger contact area when in contact with AL than with ALAN since the large peak distance on AL surfaces enables microparticles to fit between the peaks. The same implies for ALPF when compared to ALAN where $F_{adh}^{ALPF} > F_{adh}^{ALAN}$, $R_{RMS}^{ALPF} = R_{RMS}^{ALAN}$ and $\lambda^{ALPF} > \lambda^{ALAN}$. Other studies where interactions by AFM in model metered dose inhaler systems have been looked into have

shown similar trends but also that the surface energy has a great impact on F_{adh} (Traini et al., 2006, Young et al., 2003, James et al., 2009). As discussed earlier not only physical heterogeneities has an impact on F_{adh} but also chemical nature and heterogeneities of the materials involved. This will be discussed in more detail in Chapter 6.

James *et al.* showed that the hardness of materials may have an impact on F_{adh}, they showed indications of softer materials giving higher F_{adh} (James et al., 2007). A softer surface makes the particle on the cantilever sink into the surface more when it is approached and therefore gets harder to pull off, which could lead to a higher force of adhesion. Since the polymer coated ALPF should be a softer material than AL and ALAN the softness may also have had an impact on the higher F_{adh}^{ALPF}. It is well known that the process of anodising aluminium makes aluminium harder so where $F_{adh}^{AL} > F_{adh}^{ALAN}$ one cannot exclude the possibility that hardness has an impact on the result.

5.5 Conclusions

The surface roughness was studied in detail by AFM and together with the SEM results from Chapter 2 the following rank decrease was found for the canister surface roughness: AL > ALPF > ALAN > PET > glass.

It was found that the force of adhesion between particles and canisters measured by AFM could be explained by the free energy of interaction, roughness and hardness of the canisters. Only a few of the systems looked at in Chapter 3 were studied here and it was found that the force of adhesion varied significantly for the same particle interacting with different canister materials and that it is most likely due to both chemical and physical differences in the surface characteristics, something that will be discussed in more detail in Chapter 6.

Chapter 6: Predicting Interactions in Model Metered Dose Inhalers

6.1 Introduction

From an engineer perspective in early development of metered dose inhaler systems it would be advantageous to be able to predict what material combinations would cause more or less adhesion and identify the physicochemical properties of materials that are of importance for adhesion. The impact of physicochemical properties such as surface energy and roughness on microparticle adhesion in MDIs has been looked into by others (James et al., 2009, Dohmeier et al., 2009, Jinks, 2008, Traini et al., 2006, Tiwari et al., 1998, Parsons et al., 1992) but since MDIs are complex systems more work in the field needs to be done to gain a good understanding that can help developing pMDIs with minimal adhesion. Measuring adhesion to canisters in MDIs is a time consuming process, often done when the formulation is already developed, which limits the changeable parameters. Studies have shown that adhesion can be reduced through changing the canister coating (Jinks, 2008), coating particles (Paajanen et al., 2009) or altering the particle roughness (Adi et al., 2008a, Adi et al., 2008b).

The primary aim of this chapter is to evaluate data from previous chapters to find the most suitable method(s) for predicting microparticle adhesion to canisters and secondly it is to gain a further understanding of what interactions drive adhesion. In previous chapters the adhesion of microparticles in model metered dose inhalers (creaming suspensions) was investigated, true adhesion was measured in Chapter 3 and Chapter 5 and theoretical interactions were determined in Chapter 4.

6.2 Predicting Adhesion

The true adhesion data presented in this chapter results from the adhesion in model MDI systems analysed by HPLC in Section 3.3.3, with two exceptions, first the adhesion to glass data that was analysed by weight and originates from Section 3.3.2 and secondly the adhesion of PAA to glass data that was measured visually resulting in zero adhesion, Chapter 3. Also analysis of PAA adhesion by weight gave no adhesion. The

assumption that adhesion of PAA to all canister materials in this study was zero was therefore done. Since the HPLC was equipped with a UV detector and PAA has no chromophore PAA was excluded from the HPLC study. Adhesion after one week was the time point chosen to present here since it was fairly short but still long enough for maximum adhesion to be reached in all systems, for this reason the largest set of data was collected for this time point. The time point closest to one week for glass canisters was adhesion after 10 days, which is the one that will be presented here. This study focused on creaming suspensions but other studies have shown that adhesion to the canister also occur in suspensions that sediment (Beausang, 2005).

The materials used were powders: beclomethasone dipropionate (BDP), budesonide, terbutaline sulphate, polyacrylic acid (PAA), polyvinylpyrrolidone (PVP) and polyvinylalcohol (PVA); liquids: 2H,3H-perfluoropentane (HPFP), perfluoroheptane and perfluorodecalin and canisters: glass, polyethyleneterephtalate (PET), aluminium (AL), anodised aluminium (ALAN) and perfluoroalkane coated aluminium (ALPF).

When comparing data a Student's t-test, two samples with same variance, was carried out with a significance level of 95% ($p < 0.05$).

6.2.1 Adhesion by Energy of Interaction Based on Surface Energy from Contact Angle

Previous studies have shown that adhesion increase with increased dispersive surface energy of powders (Beausang, 2005, Traini, 2005, Parsons et al., 1992). In addition the same studies have shown that interactions in suspensions cannot only be explained by the materials individual surface energies but the interactions between the two materials in the liquid must also be considered. Gibbs free energy of interaction (ΔG) based on the van Oss theory for interfacial forces in non-aqueous media (Chapter 4), i.e. the surface component approach (SCA) was used to predict and understand the apolar and polar energy of interactions that drive microparticle adhesion in the model metered dose inhaler formulations in this study. It is an advantage that the theory includes both apolar and polar contributions when predicting energy of interaction since it has been proven to be important to include both when predicting adhesion in pressurised metered dose inhalers (James et al., 2009, Traini et al., 2005). The majority of powder compounds in

this study are poorly soluble in HPFP and therefore their interactions are highly dependent on surface energy (Jones et al., 2006a).

In Chapter 4 ΔG (Gibbs free energy of interaction) was determined based on surface energy parameters from contact angle measurements, which were measured by drop shape analysis, a conventional and widely used method for investigating surface energy of solid materials. The main advantage of measuring surface energy by contact angle from drop shape analysis is that it, unlike surface energy and solubility parameters from IGC and Stefanis' group contribution method, enabled determination of surface energy parameters of all materials used in this study. HPFP was an exception that was not analysed here since surface energy values for the HPFP used in this study were available in the literature (Beausang, 2005). Figure 6.1 shows the interactions in the model MDI that could be predicted by ΔG. The adhesion and cohesion in HPFP vapour may be different from in air but the calculations did not allow considering the presence of other vapours than air when determining ΔG_{12} (energy of interaction of particle-canister) and ΔG_{11} (energy of interaction of particle-particle) so the effect of HPFP vapour on predicted interactions was not included in this study.

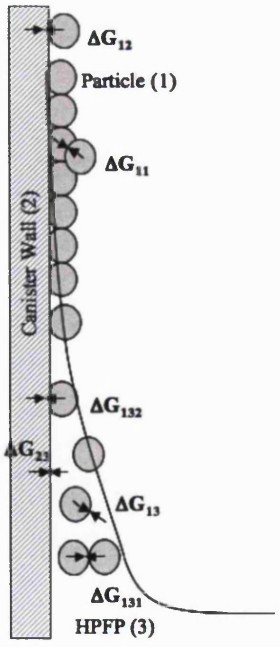

Figure 6.1. Image of the interactions in the MDI canister calculated by the SCA, where ΔG_{12} – particle-wall interaction, ΔG_{11} – particle-particle interaction, ΔG_{132} – particle-wall interaction in liquid, ΔG_{23} – canister-liquid interaction, ΔG_{13} – particle-liquid interaction and ΔG_{131} – particle-particle interaction in liquid.

The ΔG_{132} value best mimics the adhesion in the meniscus area in the canisters since it represents the energy of interaction between particles (1) and the wall (2) immersed in a liquid (3) and the systems are creaming suspensions where the particle concentration is high in the meniscus area. In Figure 6.2 the correlation between true adhesion to canisters in HPFP and ΔG_{132} for budesonide and terbutaline sulphate respectively is presented. In the budesonide graph in Figure 6.2 a linear relationship between adhesion and ΔG_{132} was observed (R^2 0.8990) and the plot shows that attractive particle-wall interactions occur ($\Delta G_{132} < 0$) in HPFP and higher attraction should lead to higher adhesion. When the point representing adhesion to glass, which was an outlier, was excluded from the plot R^2 became 0.9985 and the improvement in linearity is explained by ΔG_{132} for glass being based on theoretical glass surface energy values from the literature rather than values measured of the glass canisters used in this study and the true adhesion was measured by weight not by the more sensitive HPLC method, which could explain why glass did not follow the same trend as the other canisters. The linearity for terbutaline sulphate was lower than for budesonide (R^2 0.8783) but only the particle-wall interactions with PET were attractive ($\Delta G_{132} < 0$) and the interactions with AL, ALAN and ALPF were repulsive ($\Delta G_{132} > 0$).

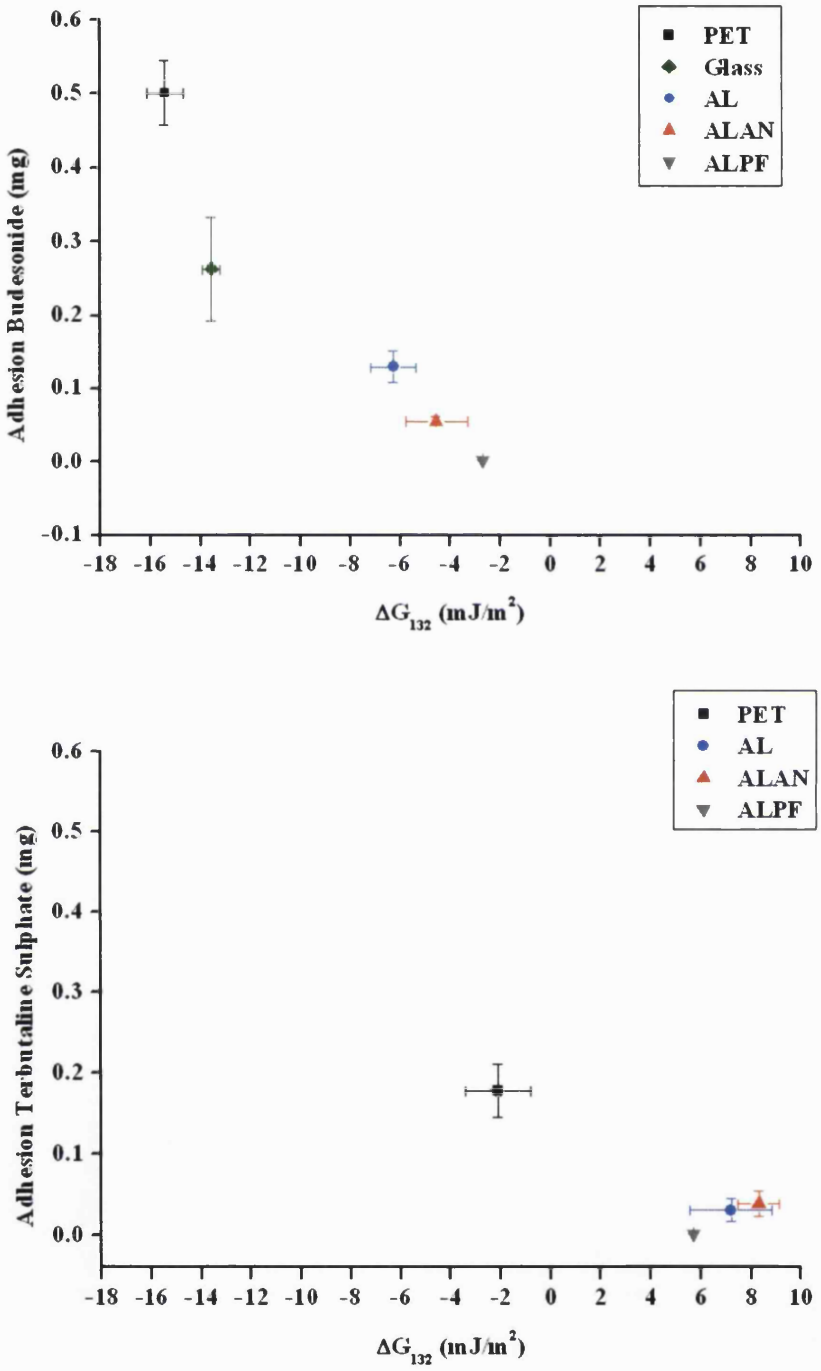

Figure 6.2. Adhesion of budesonide and terbutaline sulphate in HPFP suspensions after 1 week against ΔG_{132}.

If correlating the results in Figure 6.2 with adhesion images from Chapter 3 shown again in Figure 6.3 the trend that a ring of adhered material in the meniscus area appear due to higher adhesion for the systems where $\Delta G_{132} < 0$ appear. When $\Delta G_{132} > 0$ no

such ring is formed due to much lower adhesion in the meniscus area, which is probably since the particles are repelled from the canister wall when immersed in the liquid. This was true for most systems but more experiments are needed to fully confirm the trend.

In Figure 6.3 the ring in the former meniscus area appeared for budesonide in both PET and glass canisters while for terbutaline sulphate no such adhesion appeared in glass only slightly in PET canisters. In Figure 6.2 the ΔG_{132} value for budesonide predicted higher attraction to PET in the meniscus area than ΔG_{132} for terbutaline sulphate, which is also shown by the more pronounced ring by the meniscus in Figure 6.3. No quantitative adhesion analysis was done for terbutaline sulphate in glass canisters, therefore it is not represented by a point in Figure 6.2, however the predicted ΔG_{132} value for terbutaline sulphate to glass was -9 mJ/m^2, which contradicts the above argument that $\Delta G_{132} < 0$ leads to the ring like pronounced adhesion in the meniscus area, since such low ΔG_{132} should lead to more adhesion to glass than PET in the meniscus area. On the other hand the images of PVP adhesion in Figure 6.3 confirms the statement, since adhesion of PVP to glass in HPFP was 0.83 mg and focused around the meniscus area with a ΔG_{132} = -13 mJ/m^2, though ΔG_{132} was not based on measured values of the PVP and glass materials used in this study but values from the literature and therefore ΔG_{132} may be misleading.

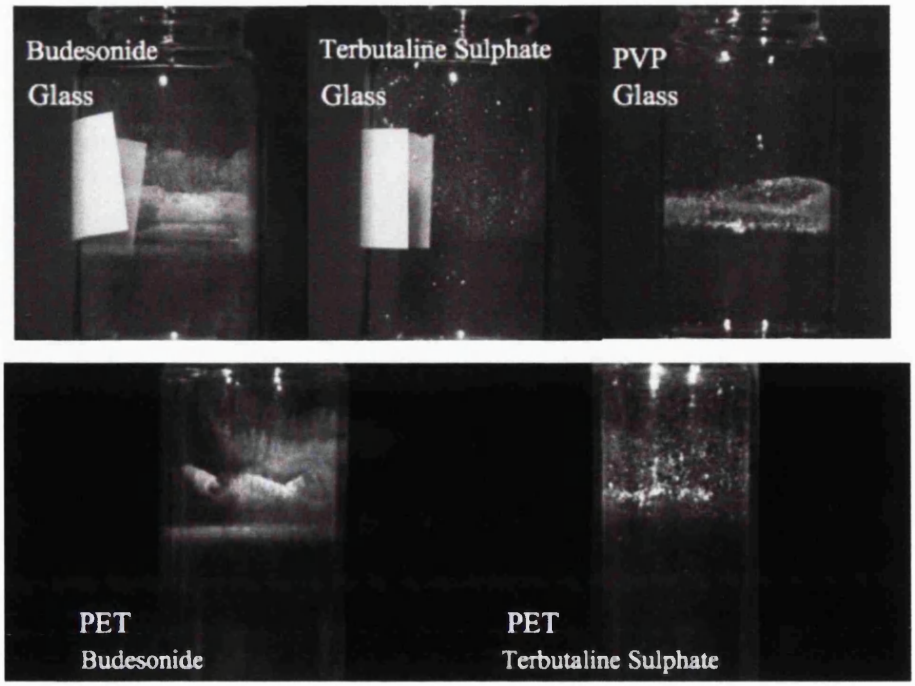

Figure 6.3. Digital images of empty glass and PET canisters with adhered particles after 3 weeks in HPFP suspensions.

In the MDI systems studied there will be a constant balance between the energy of interaction of the various materials involved, ΔG_{12} (energy of interaction of powder-canister), ΔG_{13} (energy of interaction of powder-liquid) and ΔG_{23} (energy of interaction of canister-liquid). In theory if ΔG_{12} is higher ΔG_{13} will be lower, which should lead to particle adhesion to the canister wall. Since the same liquid, HPFP, was used throughout the results discussed in Chapter 6 the parameters of greatest interest are ΔG_{132} (energy of interaction of powder-canister immersed in HPFP) and ΔG_{131} (energy of interaction of powder-powder immersed in HPFP) since these parameters describes the likeliness of adhesion in the MDI.

In Figure 6.4 the predicted interactions show that as ΔG_{131} increase ΔG_{132} increase, which means that as the cohesive interactions of particles in HPFP decrease the particles interact more with HPFP and less through adhesive interactions with the canister wall. $\Delta G < 0$ means attraction while $\Delta G > 0$ means repulsion and if looking at ΔG_{131} the hydrophobic powders, BDP and budesonide, interact through attraction ($\Delta G_{131} < 0$) when immersed in HPFP while the hydrophilic ones, PVP, PAA and terbutaline sulphate interact through repulsion ($\Delta G_{131} > 0$). This means that hydrophilic powders interact more with HPFP, probably due to hydrogen bonding. Studies in the literature have shown that repulsive particle-liquid forces have a stronger impact than attractive particle-canister forces in driving particle adhesion to the canister wall (Vervaet and Byron, 1999), hence they are as important to consider as ΔG_{132} when studying adhesion. It has also been shown by others that with lower ΔG_{131} it gets harder to de-agglomerate powders in similar systems (Parsons et al., 1992), which in this study would mean that the ease of de-agglomeration decreases like: terbutaline sulphate > PAA > PVP > budesonide > BDP. Hence, the lower powder-liquid interaction the higher the adhesion becomes.

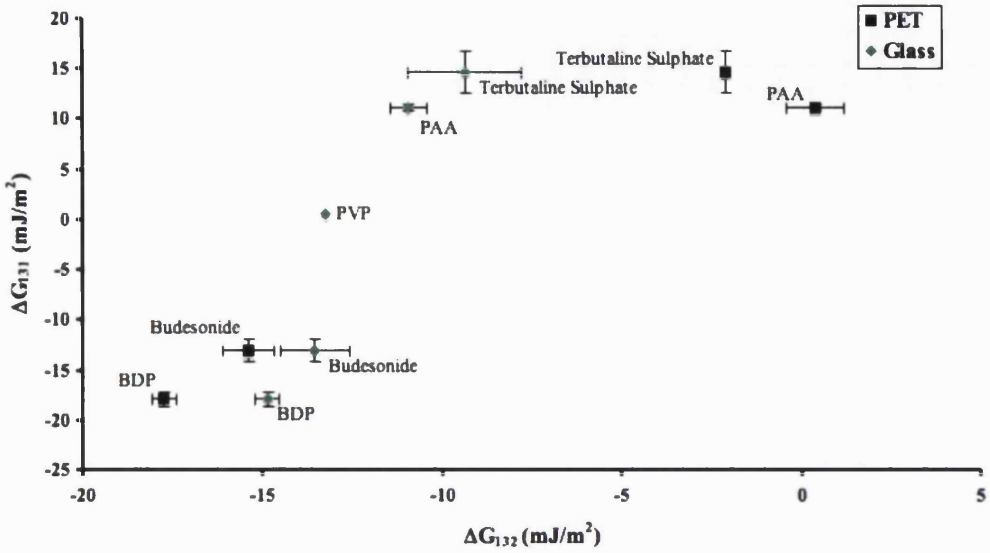

Figure 6.4. Predicted powder-powder interactions in HPFP (ΔG_{131}) against powder-canister interactions in HPFP (ΔG_{132}) of powders: BDP, budesonide, terbutaline sulphate and PAA and canisters: PET and glass.

The results from Figure 6.4 together with the results in Figure 6.2 show that as particle-particle interactions in HPFP decrease (ΔG_{131} increase), particle-canister interactions in HPFP decrease (ΔG_{132} increase) and true particle adhesion decreases for all canister materials involved. A similar correlation was shown by others where adhesion occurred when the particle-canister interactions (ΔG_{132}) were greater than the particle-liquid interactions (ΔG_{131}) and when the particle-canister interactions were lower than the particle-liquid interactions no adhesion occurred (Parsons et al., 1992), which was true for all systems in Figure 6.4 but for PAA to glass. According to Parsons *et al.* PAA should adhere to glass since $\Delta G_{132} < \Delta G_{131}$ but that was not the case in this study. However the adhesion of PAA to glass was only determined visually, so there may have been low adhesion that was not detectable visually. But assume there was no adhesion of PAA to glass as stated earlier, then a possible reason is suggested to explain why no adhesion occur when $\Delta G_{132} < \Delta G_{131}$. The glass surface energy parameters used in the calculations for the ΔG values presented here were not measured but obtained from the literature and may therefore not be the same as for the canisters used, which could have lead to inaccuracies in the calculated interactions.

In Figure 6.5 the extent of true adhesion of three powders (budesonide, terbutaline sulphate and PAA) to four canister materials (PET, AL, ALAN and ALPF) was plotted

as a function of ΔG_{132} (energy of interaction between particle-canister immersed in HPFP) and the graph shows the relationship between true adhesion and predicted adhesive interactions where the true adhesion increases as the predicted particle-canister energy of interaction in HPFP increase. Figure 6.5 also shows that the higher the adhesion to a canister material is the steeper the slope is, which indicates that from limited data of true adhesion and energy of interaction (ΔG_{132}) for three powders only it can be predicted how likely a powder is to adhere to that very canister material. This could be a useful tool in an engineer perspective during development of pMDIs.

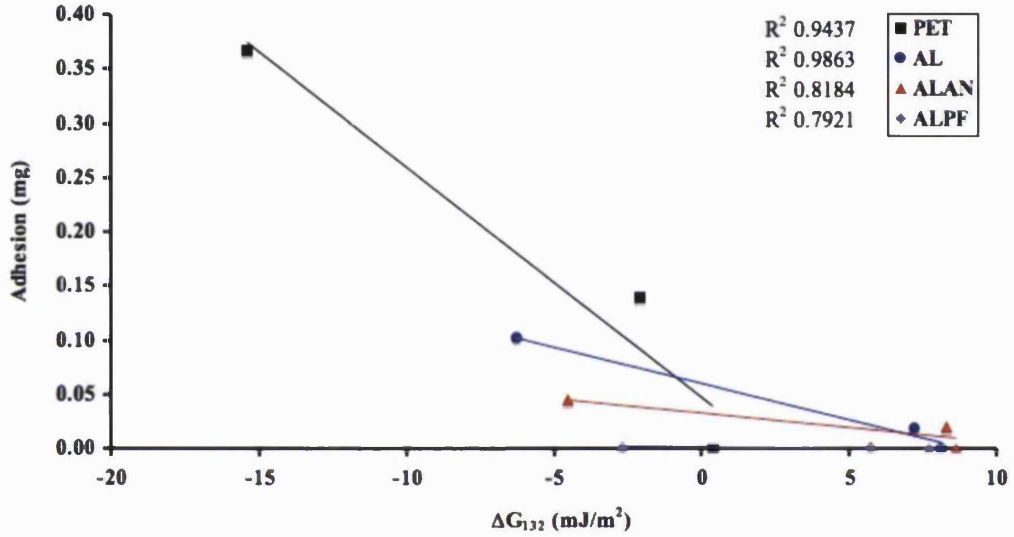

Figure 6.5. True adhesion of powders in HPFP to canisters against predicted particle-canister interaction in HPFP (ΔG_{132}) between particles in HPFP and canisters. Powders: budesonide, terbutaline sulphate and PAA and canisters: PET, AL, ALAN and ALPF. The true adhesion of PAA was not measured but assumed to be zero based on visual observations in Chapter 3.

Figure 6.6 and Figure 6.7 describe the correlation between true adhesion and non-polar and polar energy of interaction of powder-canister immersed in HPFP (ΔG_{132}) respectively and the figures show that the non-polar interactions are attractive ($\Delta G_{132}^{LW} < 0$) and the polar repulsive ($\Delta G_{132}^{AB} > 0$). This shows the importance of considering both polar and apolar interactions when predicting true adhesion since none of them can predict adhesion on its own. The linear correlation between the true adhesion and ΔG_{132}^{LW} was good (R^2 0.8984 - 0.9987) and show that the adhesion increases with higher non-polar interactions. There are also signs of increased adhesion with higher polar interactions but the correlation between true adhesion and ΔG_{132}^{AB} (R^2 0.6855 -

0.9085) was not as good as for ΔG_{132}^{LW}. This contradicts a study from the literature that suggested that the polar interactions are the most important to consider when evaluating force of adhesion measured by AFM (James et al., 2009). They looked at similar systems as the ones studied here and found that when the force of adhesion measured by AFM was correlated with ΔG good linear correlations between the force of adhesion and ΔG_{132} and ΔG_{132}^{AB} were found but not with ΔG_{132}^{LW} (James et al., 2009). However, James *et al.* as well as others (Traini et al., 2006) have based the ΔG_{132} calculations on the assumption that the liquid, HPFP, is non-polar ($\gamma_3^+ = \gamma_3^- = 0$ mJ·m^{-2}), which has been proven wrong by others (Beausang, 2005). In this study the polarity of HPFP was taken into consideration and therefore polar surface energy parameters from Beausang *et al.* were used in the ΔG calculations ($\gamma_3^+ = 2.50$ mJ·m^{-2} and $\gamma_3^- = 1$ mJ·m^{-2}). For comparative reasons the calculations of all ΔG values were repeated using $\gamma_3^+ = \gamma_3^- = 0$ mJ·m^{-2} and the results got very different and did not show the trends presented in this chapter. The equations used in the detailed calculations of ΔG_{132} in Appendix 1.4.1 are also shown here, Equation 4.5 and Equation 4.6, to demonstrate that ΔG_{132} is highly dependant on the polar surface energy parameters of HPFP, γ_3^+ and γ_3^-.

$$\gamma_{13} = \left(\sqrt{\gamma_1^{LW}} - \sqrt{\gamma_3^{LW}}\right)^2 + 2\left(\sqrt{\gamma_1^+\gamma_1^-} + \sqrt{\gamma_3^+\gamma_3^-} - \sqrt{\gamma_1^+\gamma_3^-} - \sqrt{\gamma_1^-\gamma_3^+}\right) \quad (4.5)$$

$$\Delta G_{132} = \gamma_{12} - \gamma_{13} - \gamma_{23} \quad (4.6)$$

Since this study has shown that even though the polarity of HPFP is low it has a large impact on the predicted interactions the polar surface energy parameters for HFAs must be used rather than assuming zero contribution.

In Figure 6.6 and Figure 6.7 the ALPF canisters, where the lowest true adhesion occurred for all powders, show a distinct difference in non-polar as well as polar predicted interactions compared to the other canister materials, the non-polar interactions show low attraction and the polar interactions show low repulsion compared to the other canisters. Since ALPF is the canister material in this study where least adhesion occurred this information could be very useful when evaluating new coatings for pMDI devices.

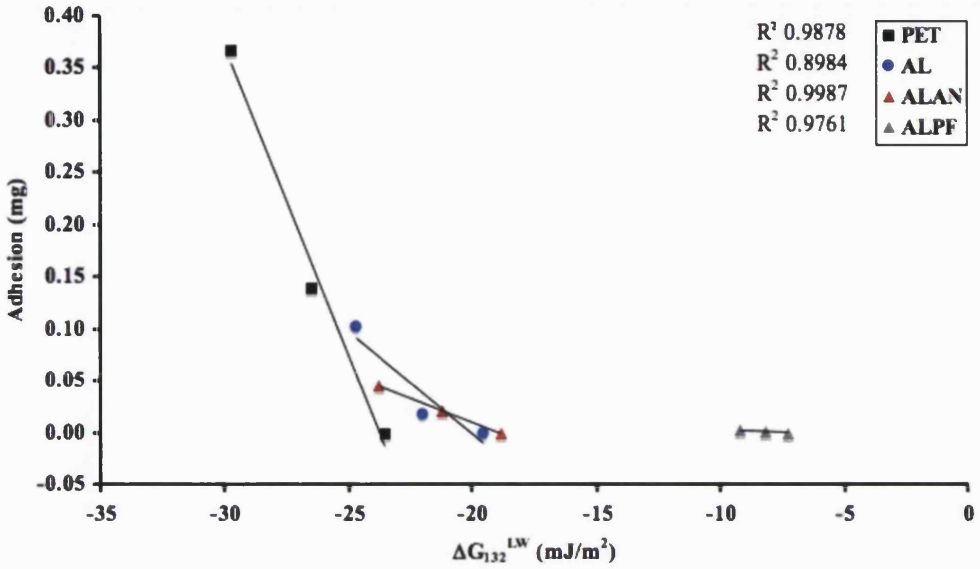

Figure 6.6. True adhesion of powders in HPFP to canisters against predicted non-polar particle-canister interaction in HPFP (ΔG_{132}^{LW}) between particles in HPFP and canisters. Powders: budesonide, terbutaline sulphate and PAA and canisters: PET, AL, ALAN and ALPF. The true adhesion of PAA was not measured but assumed to be zero based on visual observations in Chapter 3.

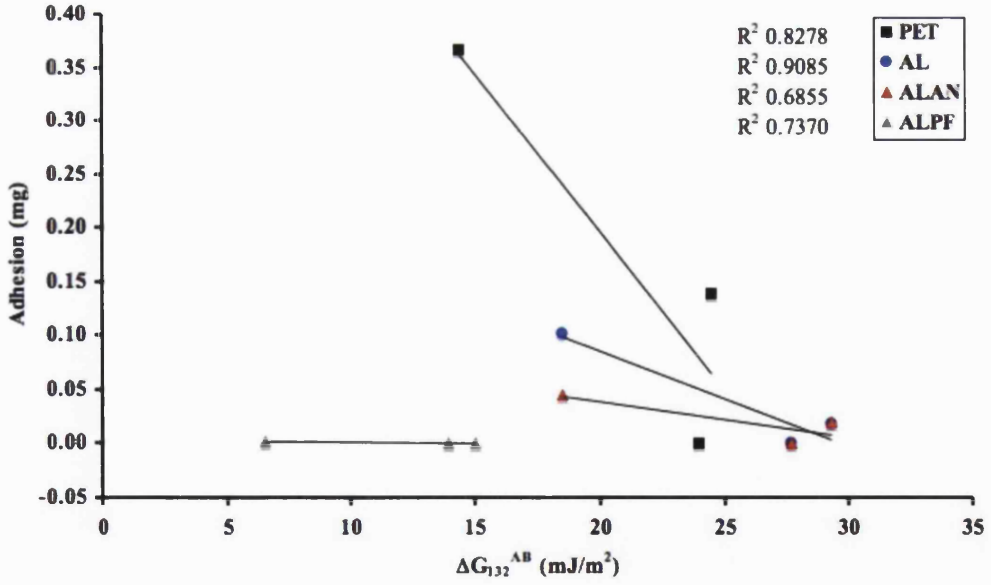

Figure 6.7. True adhesion of particles in HPFP to canisters against predicted polar particle-canister interaction in HPFP (ΔG_{132}^{AB}) between particles in HPFP and canisters. Powders: budesonide, terbutaline sulphate and PAA and canisters: PET, AL, ALAN and ALPF. The true adhesion of PAA was not measured but assumed to be zero based on visual observations in Chapter 3.

Figure 6.8 shows the true adhesion against the predicted particle-canister energy of interaction above the fluid line (ΔG_{12}), which was attractive for all systems and the adhesion decreased as the attractive energy of interactions decreased. Adhesion above the meniscus area occurred for all powders but PAA so the attractive energy of interactions between particles and canister cannot alone explain the true adhesion, other interactions should also be considered.

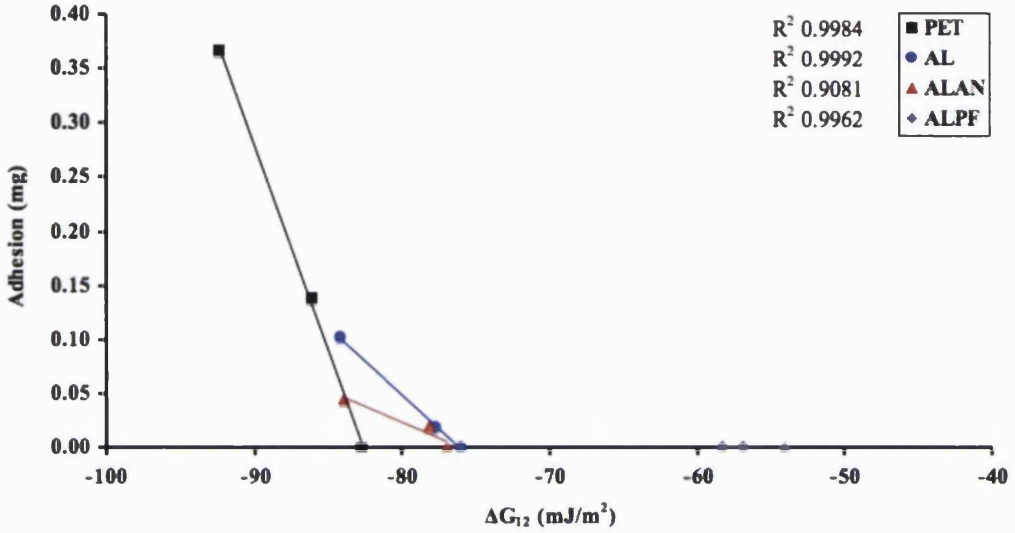

Figure 6.8. The true adhesion of particles in HPFP to canisters against predicted particle-canister interaction (ΔG_{12}) between particles in HPFP and canisters. Powders: budesonide, terbutaline sulphate and PAA and canisters: PET, AL, ALAN and ALPF. The true adhesion of PAA was not measured but assumed to be zero based on visual observations in Chapter 3.

In this section it was found that using ΔG_{132} (energy of interaction of powder-canister immersed in HPFP) predicts the true adhesion in the model MDIs studied better than ΔG_{12} (energy of interaction of powder-canister). With higher ΔG_{132} and higher ΔG_{131} (energy of interaction of powder-powder immersed in HPFP) the adhesion decreased, which showed that as the particles interacts less through adhesion to the canister wall or cohesion to themselves they interact more with the liquid, which leads to less adhesion. It was also shown that as ΔG_{132}^{LW} (apolar energy of interaction powder-canister immersed in HPFP) decreased and ΔG_{132}^{AB} (polar energy of interaction powder-canister immersed in HPFP) decreased the true adhesion increased. There was also evidence that when the particle-canister interactions were attractive, $\Delta G_{132} < 0$, a pronounced adhesion of particles in the meniscus area formed a ring of adhered particles, which did

not occur when the particle-canister interactions were repulsive, $\Delta G_{132} > 0$. Using the free energy of interaction for explaining and predicting the adhesion in model MDIs was shown beneficial since it could predict if more or less adhesion would occur. Also the method allows a good coverage of intermaterial interactions in the model MDI to be calculated, as shown in Figure 6.1. However, it has been shown that other factors than surface energy has an impact on adhesion and therefore ΔG alone cannot perfectly predict true adhesion.

6.2.2 Adhesion by Interaction Parameters Based on Theoretical Solubility Parameters

The ability to predict true adhesion in model MDIs by interaction parameters (ϕ) based on Hansen solubility parameters calculated from Stefanis' group contribution method in Chapter 4 will be looked into in this section.

When powder-canister, powder-liquid and liquid-canister interactions were predicted by ϕ binary systems was looked at, hence the presence of HPFP in powder-canister and powder-powder interactions was not considered. Since Stefanis' solubility parameters were theoretical values based on the molecular structure of organic molecules they could be used for the majority of the materials used in the model metered dose inhaler systems, though not AL, ALAN and glass since they are inorganic materials. In Figure 6.9 the relation between true adhesion and predicted powder-canister interactions (ϕ_{12}) for PET canisters is presented and as ϕ_{12} increased the true adhesion increased, just as for the correlation between true adhesion and ΔG_{12} (free energy of interaction powder-canister) in Figure 6.6. The linearity for PET in Figure 6.9 was good with R^2 0.9018. The theory states that the closer to unity ϕ_{12} is the more likely it is that material 1 and material 2 interact. Since there was no significant difference between the budesonide and terbutaline sulphate true adhesion data points to ALPF in HPFP Figure 6.9 did not show a plot for ALPF.

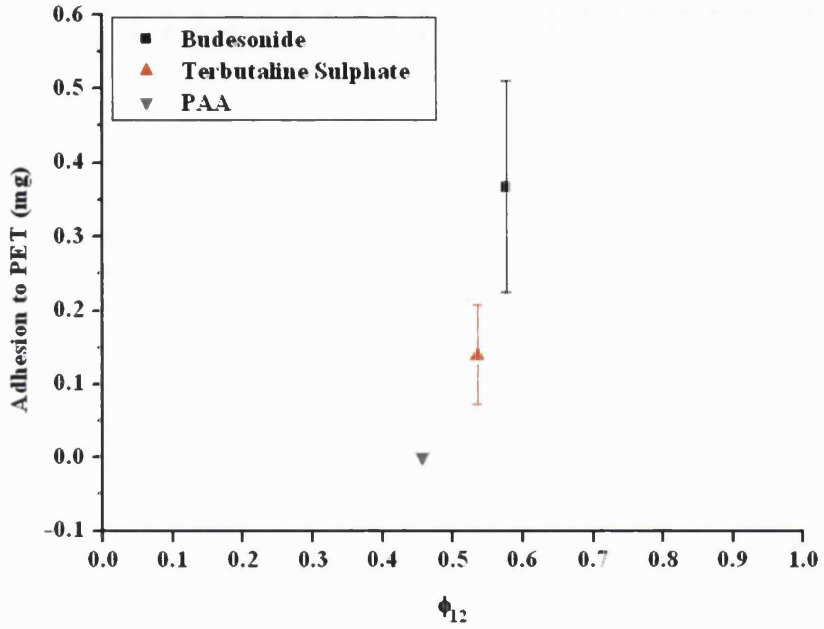

Figure 6.9. True adhesion to PET canisters (n=15) against powder-canister interaction parameter (ϕ_{12}) based on Hansen solubility parameters from Stefanis' group contribution method, powders: budesonide, terbutaline sulphate and PAA. PAA adhesion was not measured but assumed to be zero based on visual observations in Chapter 3.

Figure 6.10 shows the relationship between the true adhesion to PET and predicted particle-HPFP interactions (ϕ_{13}) (R^2 0.6518) and ϕ_{13} was higher when the true adhesion was lower. There was a clear difference in ϕ_{13} between the powder that did not adhere to PET, PAA and the powders that did adhere to PET, budesonide and terbutaline sulphate, showing that a higher predicted interaction parameter between the powder and the liquid lead to a lower adhesion to the canister wall.

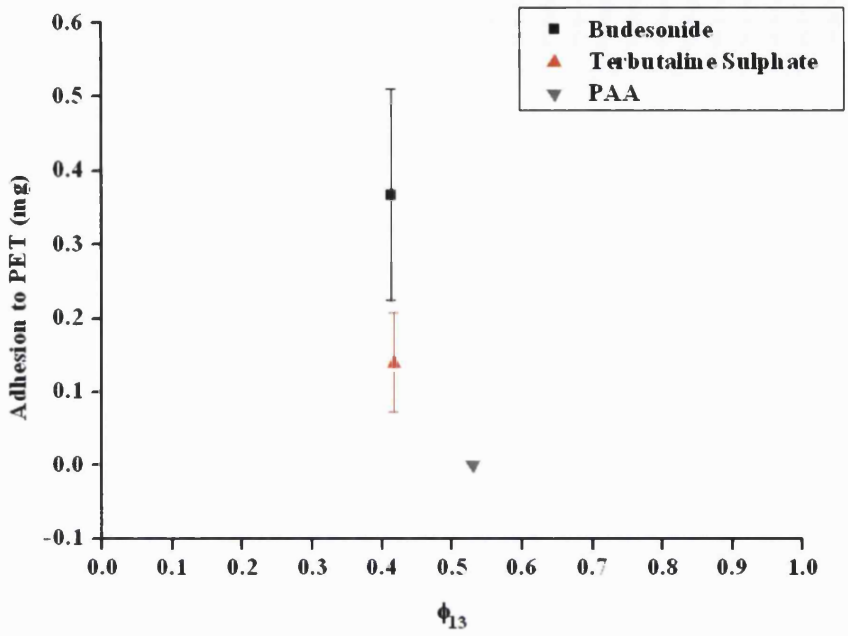

Figure 6.10. True adhesion to PET canisters (n=15) against powder-HPFP interaction parameter (ϕ_{13}) based on Hansen solubility parameters from Stefanis' group contribution method, powders: budesonide, terbutaline sulphate and PAA. PAA adhesion was not measured but assumed to be zero based on visual observations in Chapter 3.

From the data presented in this section it was shown that adhesion could be predicted by calculating ϕ for binary systems, including ϕ_{12} (interaction parameter of powder-canister based on Hansen solubility parameters) and ϕ_{13} (interaction parameter of powder-liquid based on Hansen solubility parameters). For ϕ of binary systems the same correlation was found as for ΔG (energy of interaction) for ternary systems, where lower particle-canister interactions (ϕ_{12}) and higher powder-liquid interactions (ϕ_{13}) lead to lower adhesion. It was found that the powder-liquid interactions assist in any canister adhesion prediction and should be determined together with the powder-canister interactions to give a full picture of the predicted interactions. In Chapter 4, Section 4.2.5.2 it was shown that the true adhesion is lower in a liquid that easier wets the canister wall. For budesonide adhesion to PET canisters the true adhesion from perfluoroheptane was higher than the true adhesion from HPFP and $\phi_{\text{perfluoroheptane-PET}} < \phi_{\text{HPFP-PET}}$. A limited amount of data could be used for the correlations in this section and only PET data was used for the predictions of true adhesion by ϕ. However, the predicted ΔG interactions for AL, ALAN and ALPF followed the same trends as PET

and therefore the same trends would most likely have been shown for ϕ. The main advantage when predicting true adhesion with ϕ is that the interactions are possible to predict based on basic information often available for most compounds (molecular structure, density and molecular weight) but the disadvantage is that the method is limited to organic compounds.

6.2.3 Adhesion by Force of Adhesion from AFM

A minor AFM study was reported in Chapter 5 where the force of adhesion (F_{adh}) was determined for particle-canister interactions at zero per cent relative humidity and its correlations with true adhesion is presented in Figure 6.11 and Figure 6.12, the force of adhesion for PET was not included because it was too large to measure, which agrees with it being the material all powders adhered most to among PET, AL, ALAN and ALPF. However, since so few AFM experiments were carried out F_{adh} by AFM could only be used as a complimentary method to predict true adhesion. The standard deviation of F_{adh} was very large, which is reasonable for canister surfaces of this roughness (Götzinger and Peukert, 2003), still there were significant differences between the F_{adh} measurement where the rank order between powders and canister materials decreased like ${F_{adh}}^{PET} > {F_{adh}}^{ALPF} > {F_{adh}}^{AL} > {F_{adh}}^{ALAN}$ (2 sample t-test, $p < 0.05$).

The correlation between true adhesion of budesonide and F_{adh} is shown in Figure 6.11 and it shows that ${F_{adh}}^{AL} > {F_{adh}}^{AL}$ when the true adhesion for AL was higher, which was expected. ${F_{adh}}^{PET}$ is not correlated with the true adhesion of budesonide to PET in Figure 6.11 as ${F_{adh}}^{PET}$ was to high to measure, but it could still be correlated to the true adhesion of budesonide to PET that was 0.37 mg, the material where budesonide adhered most. However AFM could not describe the true adhesion of budesonide to ALPF as well as it could for PET, AL and ALAN. ${F_{adh}}^{ALPF} > {F_{adh}}^{AL}$ and ${F_{adh}}^{ALPF} > {F_{adh}}^{ALAN}$ did not describe the true adhesion of budesonide that was significantly lower than both AL and ALAN compared to ALPF. The higher ${F_{adh}}^{ALPF}$ is probably due to a larger contact area between the particle and canister surface due to the large peak distance of the ALPF surface, as discussed in Section 5.4.2. It could also be due to the lower hardness of the polymer coating since it has been shown by others that a softer surface results in a higher F_{adh} (James et al., 2007).

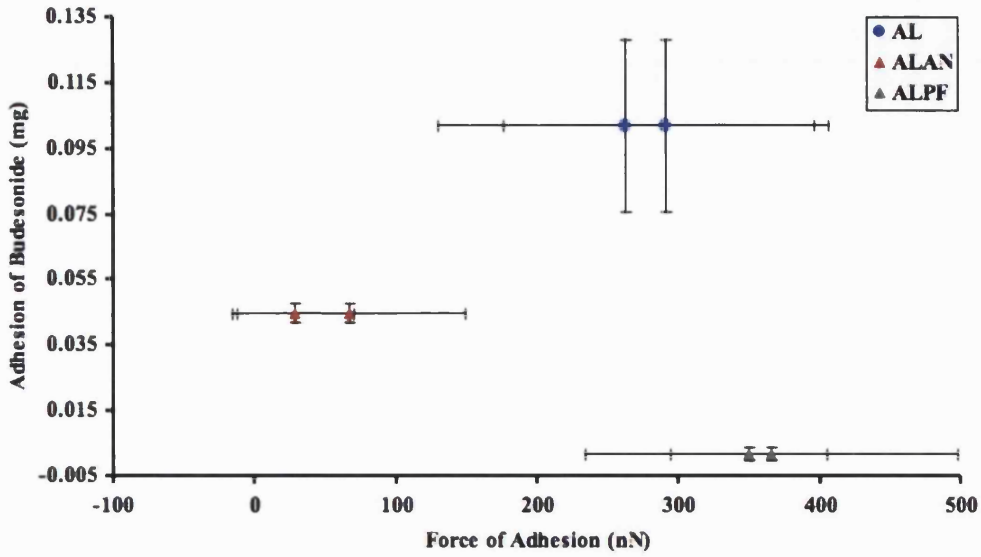

Figure 6.11. True adhesion against force of adhesion measured by AFM for budesonide. Each data point on the x-axes represent a mean of AFM force of adhesion measurements of the same particle to the same surface (n=256).

The correlation of true adhesion with F_{adh} for terbutaline sulphate in Figure 6.12 show that even though $F_{adh}^{AL} > F_{adh}^{ALAN}$ the true adhesion did not differ (2 sample t-test, $p < 0.05$), F_{adh} of more terbutaline sulphate particles than one would have been useful to confirm this. The true adhesion of terbutaline sulphate to ALPF was significantly different and lower than to AL and ALAN and $F_{adh}^{ALPF} > F_{adh}^{AL}$ and $F_{adh}^{ALPF} > F_{adh}^{ALAN}$ (2 sample t-test, $p < 0.05$). Probably the higher contact area between the terbutaline sulphate particle and ALPF was the reason for the higher F_{adh}^{ALPF} compared to F_{adh}^{AL} and F_{adh}^{ALAN} even though the adhesion to ALPF was lower than to AL and ALAN, as for budesonide.

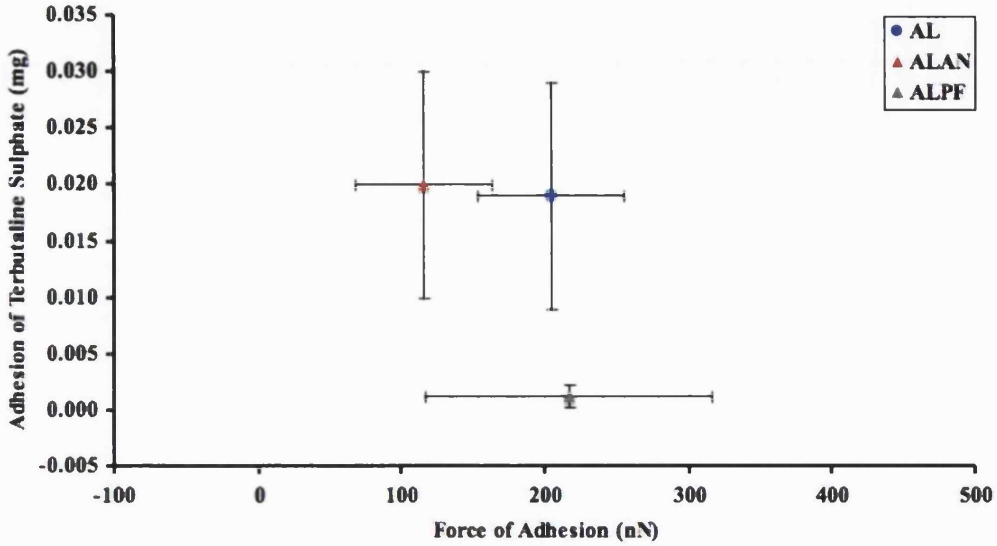

Figure 6.12. True adhesion (n=15) against force of adhesion measured by AFM for terbutaline sulphate. Each data point on the x-axes represent a mean of AFM force of adhesion measurements of the same particle to the same surface (n=256).

To conclude this section the AFM results discussed show that the true adhesion rank decrease of budesonide of PET > AL > ALAN could be described by $F_{adh}^{PET} > F_{adh}^{AL} > F_{adh}^{ALAN}$ but in order to see how F_{adh}^{ALPF} correlated with the true adhesion the canister topography had to be considered. This was also the case when F_{adh}^{ALPF} for terbutaline sulphate was correlated to the true adhesion. F_{adh} could not describe the true adhesion of terbutaline sulphate to AL and ALAN canisters. In general F_{adh} values for more particles per powder would have been useful to show and confirm any trends. Since the importance of particles interaction with the liquid in the suspension as well as the canister wall was shown in the previous two sections it would be useful to measure F_{adh} in HPFP liquid and vapour since it may give a better correlation between true adhesion and F_{adh}. AFM is a useful technique in describing forces of interactions between a particle and a surface since it gives a detailed picture of the interactions involved but since it is sensitive to roughness, peak distance and hardness of the materials involved such parameters must be considered when evaluating AFM data.

6.2.4 Adhesion by Particle Size, Solubility and Roughness

The particle roughness and size impact on adhesion has not been investigated much in pMDI systems but it has in dry powder systems and what has been shown is that

adhesion generally decreases with increased particle and canister roughness due to reduced contact area and number of contact points (Paajanen et al., 2009, Adi et al., 2008b, Adi et al., 2008a). In those studies the chemical nature of the compound was kept the same but the particles surface roughness and size was altered. For a study to show the impact of physicochemical properties such as particle roughness, size and solubility the same or very similar compounds, with very similar physicochemical properties except from the one looked at, should be used. In this study the variation in chemical nature of the powder compounds was wide and the only ones that were considered similar enough to compare were BDP and budesonide where the main difference was in solubility. Unfortunately no quantitative adhesion study in HPFP analysed by HPLC could be performed for BDP due to degradation by time in HPFP so only the values by weight are available for discussion.

Particle roughness impact on adhesion was not specifically looked into in this study but the visual roughness of particles was presented in Figure 2.3, Section 2.2.3 and the spray-dried particles PAA, PVA and PVP were smooth while the micronised particles BDP, budesonide and terbutaline sulphate were rough. Since both smooth and rough particles adhered there was no correlation where lower particle roughness caused higher adhesion in this study, which indicates that surface chemistry had higher impact on adhesion than surface roughness when various materials were compared, as shown by the correlations with adhesion in the previous sections.

When considering the particle size for all the compounds that were partially soluble in HPFP, i.e. PVP, BDP, budesonide and terbutaline sulphate the size could have been modified when in contact with HPFP, therefore the size measurements were done in HPFP and will be used to discuss how size influences true adhesion. In Figure 6.13 the adhesion to glass and AL canisters against particle size is shown and there are indications that larger particles adhere less than small ones. Unfortunately the size of PVP in HPFP could not be measured. When PVP/HPFP suspension was added to HPFP in the diffraction chamber of the Mastersizer, as described in Section 2.4.2, PVP particles instantly got stuck to the chamber wall, probably due to the high solubility in HPFP, which did not make particle size measurements possible. In the literature studies have shown that the diameter of microparticles have an impact on adhesion and a larger diameter leads to lower particle-wall interaction since the contact area is reduced (Jiang

et al., 2008). It has also been shown by others that higher predicted cohesive interactions in HFA suspensions means that de-agglomeration of the powder is harder (Parsons et al., 1992). In Section 4.2.5.1, Table 4.15, it was shown that BDP and budesonide are very cohesive when immersed in HPFP while terbutaline sulphate and PAA are not. This means that since BDP and budesonide are smaller and more cohesive than terbutaline sulphate and PAA they should be more likely to adhere more since the contact area with the canister wall is larger and cohesion to already adhered particles favoured.

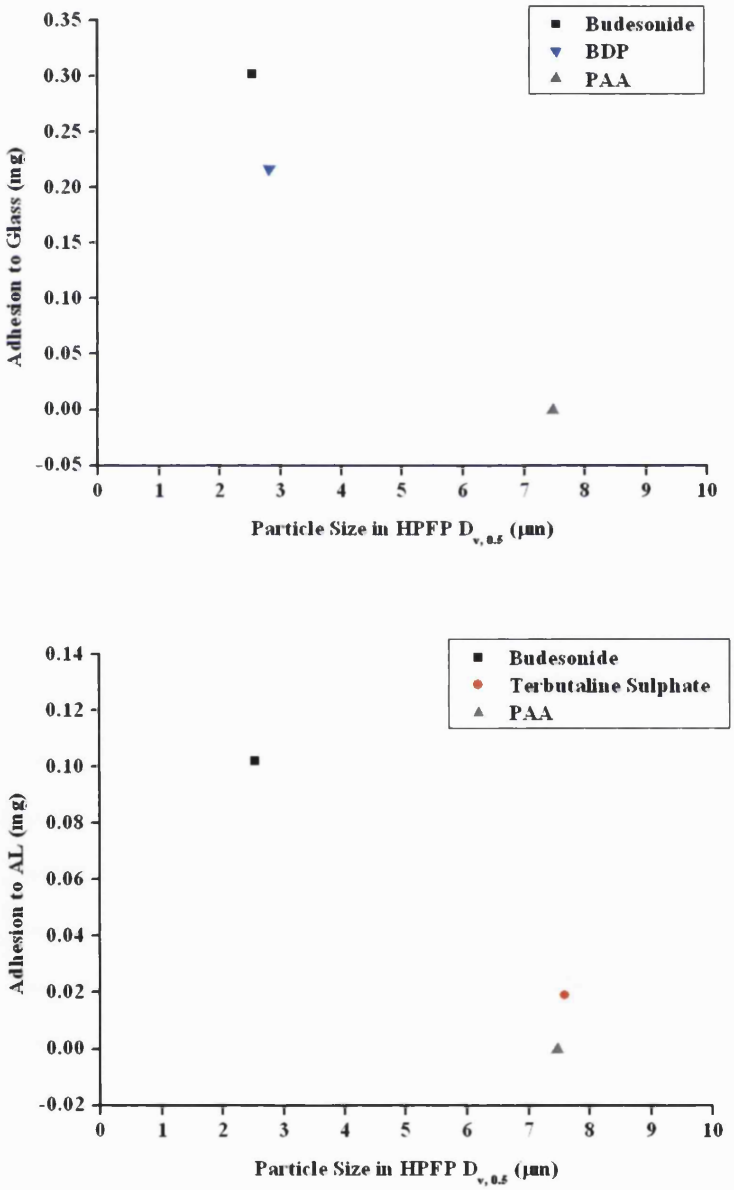

Figure 6.13. Adhesion to glass and AL canisters by particle size ($D_{v,0.5}$) in HPFP. PAA adhesion was not measured but assumed to be zero based on visual observations in Chapter 3.

It was found in Chapter 3 that solubility has an impact on the true adhesion to canisters, where partly soluble compounds adhered and insoluble ones did not. It was not possible to correlate solubility to adhesion for all powder compounds and compare them since they had very different physicochemical properties. However the two corticosteroids with very similar physicochemical properties, apart from solubility, were compared and the adhesion of the more soluble BDP in HPFP was lower than budesonide most likely as a result of adhered particles dissolving in HPFP. This is shown in Figure 6.14, which was originally presented in Chapter 3. When looking at particle interactions in HFA both the surface properties and the solubility of particles has been shown to influence adhesion because when particles are soluble in the HFA a dynamic process of adsorption and desorption can freely occur but if they are not soluble the interactions strongly depend on the surface properties of the particles (Jones et al., 2006a). PVP has been reported to have much lower surface energy (γ) than BDP and budesonide (Cayakara et al., 2006) and should therefore adhere less if only the surface energy was considered, as shown in Figure 6.4, but in Chapter 3 it was shown that PVP adhesion to glass was higher than the adhesion of the higher γ compounds BDP and budesonide. Solubility data for powders in HPFP was presented in Table 2.10 in Section 2.13.3 and showed that PAA and PVA most likely are insoluble in HPFP and the rest of the powder compounds were partly soluble in HPFP, which means that PAA and PVA interactions mainly depend on surface properties while the interactions for the others is a balance of several interactions.

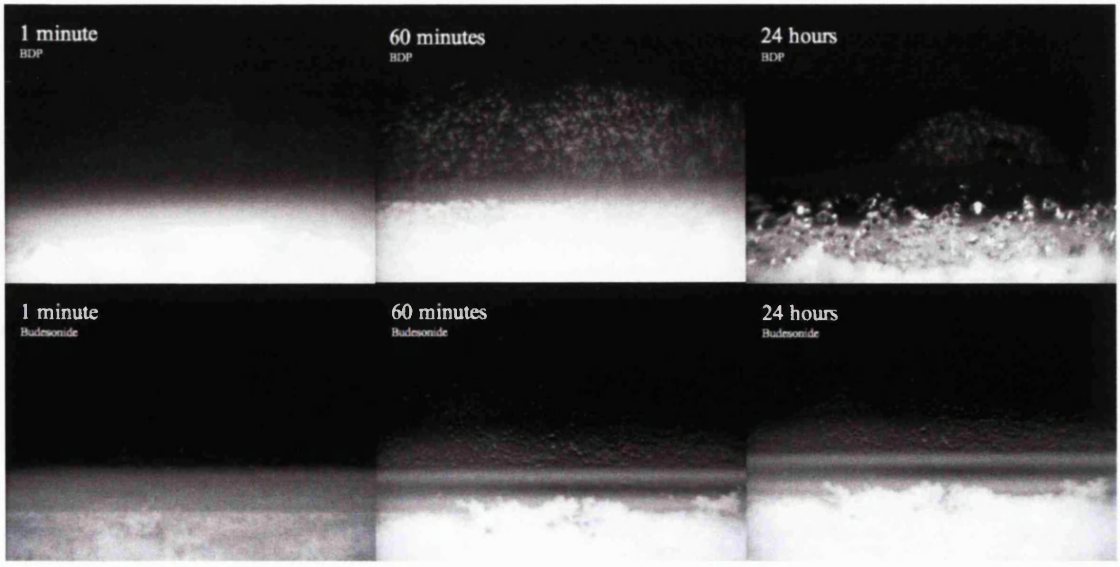

Figure 6.14. Adhesion of BDP and budesonide in HPFP suspension to PET canister, images captured from the outside of the canister.

6.2.5 Adhesion by Canister Heterogeneities

The physical heterogeneities of canister surfaces were looked at by SEM in Chapter 2 and by AFM in Chapter 5 and the chemical heterogeneities were determined by contact angle in Chapter 4. In this section the impact canister heterogeneities had on true adhesion will be looked at. It was shown that there were differences in roughness between the different materials but as the mean roughness was below 100nm it did not have an impact on contact angle measurements that mainly showed chemical heterogeneities.

6.2.5.1 Adhesion by Physical Heterogeneities

In Chapter 5 the root mean squared roughness (R_{RMS}) of the inner canister surfaces was determined by AFM and correlated to the force of adhesion (F_{adh}) measured by AFM. It was shown that not only R_{RMS} had an impact on F_{adh} but also the peak distance in the topography. Generally the impact of canister roughness on adhesion in pMDIs has not been evaluated enough but it has been shown that roughness has an effect on force of adhesion (Audry et al., 2009, Traini et al., 2006, Young et al., 2004, Price et al., 2002). Figure 6.15 show a plot with adhesion against R_{RMS} from AFM and no obvious trends could be seen. It was observed that the smoothest canister surfaces, glass and PET, caused the highest adhesion while the rougher surfaces, AL, ALAN and ALPF, caused lower adhesion, which may be due to higher contact area between the smoother surfaces and particles compared to the rougher surfaces, but since a clearer trend for adhesion by surface chemistry was shown in Section 6.2.1 and Section 6.2.2 the differences were more likely due to surface chemistry than roughness. There was no correlation between adhesion and R_{RMS} for the aluminium based surfaces and also the trend for adhesion of budesonide to the various canister materials was different from that of terbutaline sulphate, which again indicates that other factors than canister roughness has an impact on the adhesion.

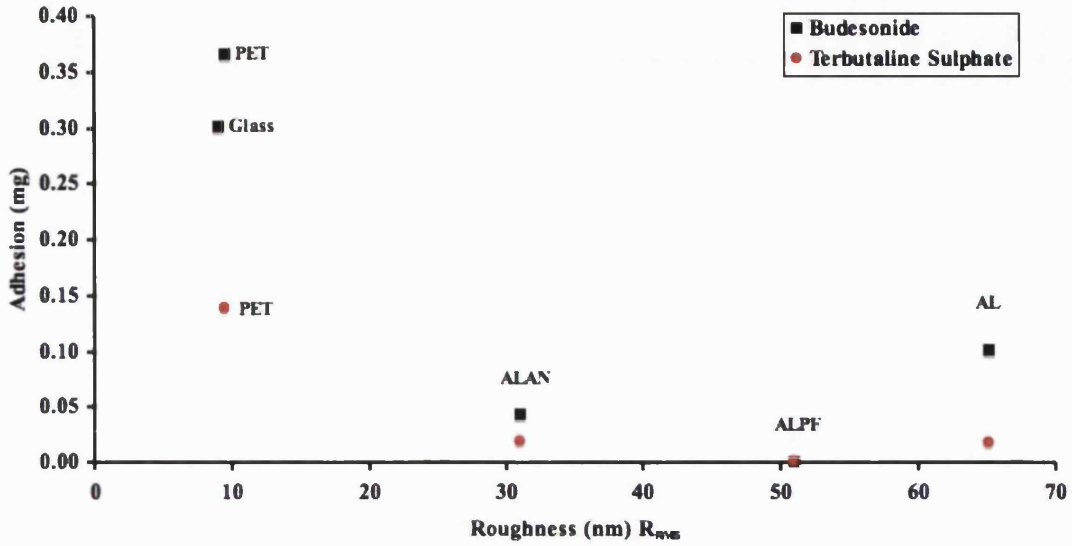

Figure 6.15. Adhesion of budesonide and terbutaline sulphate from HPFP suspensions to canisters against canister roughness (R_{RMS}) measured by AFM tapping mode.

6.2.5.2 Adhesion by Chemical Heterogeneities

The surface heterogeneities of canister materials were determined in Chapter 4, Section 4.3.1, by contact angle measurements of one apolar and two polar liquids on the surfaces. It was found that the canister surface heterogeneities are non-uniformly distributed at the surface and that the surfaces mainly consist of lower surface energy areas containing defects of higher surface energy areas.

In Chapter 3 the adhesion for budesonide and terbutaline sulphate in HPFP suspensions to canister walls was presented and it decreased in the following rank order PET > AL > ALAN > ALPF and PET > ALAN > AL > ALPF respectively (2 sample t-test, $p < 0.05$), as shown in Figure 6.16 The high and wide spread adhesion of powders to PET could be due to the smooth surface shown by the low hysteresis in Figure 6.17, since a smooth surface gives larger contact area and therefore more adhesion, as discussed in Chapter 5. However, if low hysteresis would mean high adhesion the adhesion to ALPF should also be high, which is not the case. Therefore studying the chemical heterogeneities solely could not explain the adhesion.

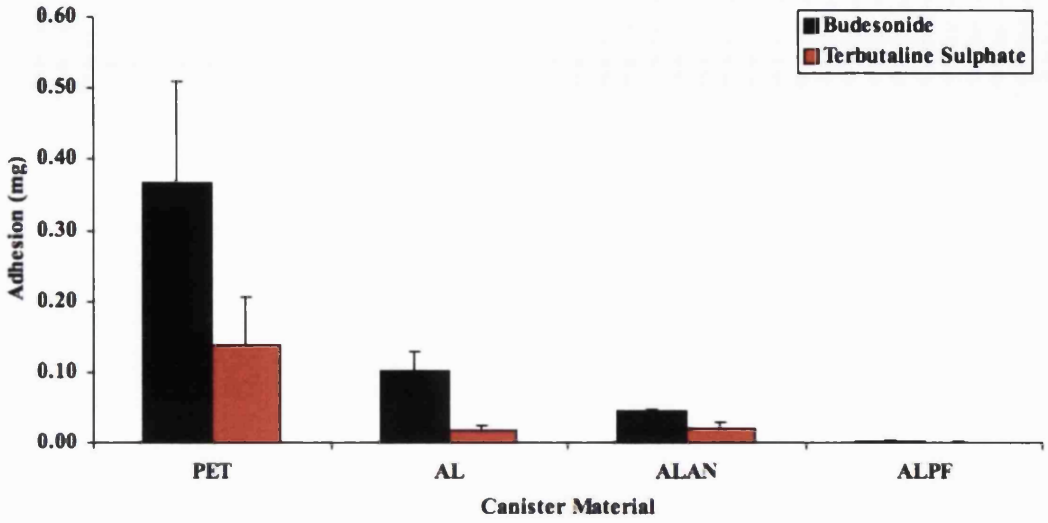

Figure 6.16. True adhesion of budesonide and terbutaline sulphate from HPFP suspensions to canister walls (n=15).

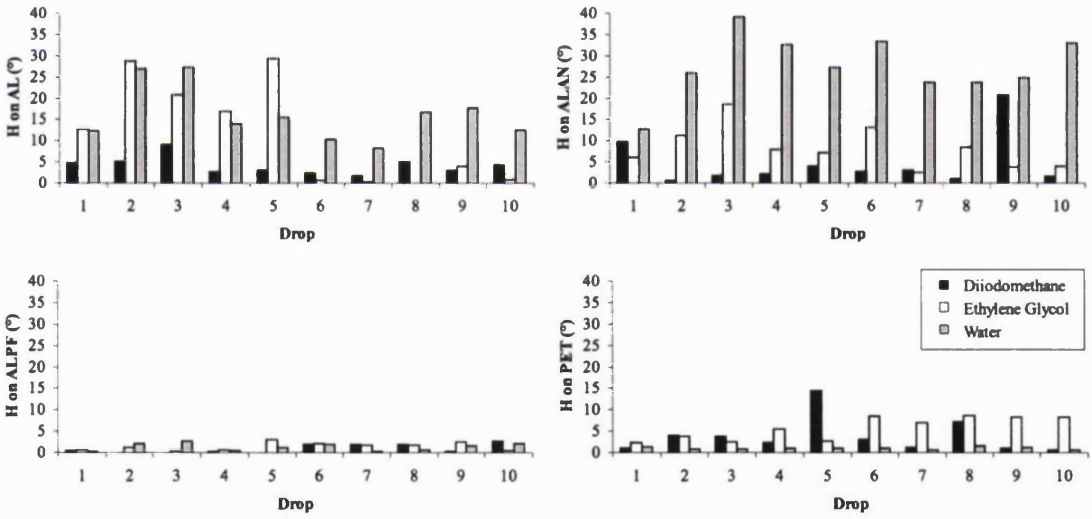

Figure 6.17. Contact angle hysteresis (H) of sessile drops on canisters: AL (top left), ALAN (top right), ALPF (bottom left) and PET (bottom right).

6.3 Conclusions

Three methods were evaluated for their suitability to predict true particle adhesion in model metered dose inhalers: first Gibbs Free energy of interaction (ΔG) based on surface energy parameters from contact angle measurements; secondly a purely theoretical approach, the interaction parameter (ϕ) based on Hansen solubility

parameters from Stefanis' group contribution method and finally a direct approach, the force of adhesion between a particle and the canister surface by AFM measurements. The results of powder-canister interactions determined with the three different methods are summarized in Table 6.1.

Table 6.1. Summary table of adhesive interactions by Gibbs free energy of interaction from surface energy parameters based on contact angle measurements (ΔG), interaction parameter based on Hansen solubility parameters from Stefani's group contribution method (ϕ) and force of adhesion from AFM measurements (F^{adh}), where (1) represents the powder and (2) the canister.

ΔG_{12}				
	BDP	**Budesonide**	**Terbutaline Sulphate**	**PAA**
PET	-93.4	-92.4	-86.2	-82.8
AL	-85.5	-84.2	-77.8	-76.1
ALAN	-85.2	-84.0	-78.2	-77.0
ALPF	-58.3	-58.3	-56.9	-54.1
ϕ_{12}				
	BDP	**Budesonide**	**Terbutaline Sulphate**	**PAA**
PET	0.602	0.576	0.535	0.456
AL	-	-	-	-
ALAN	-	-	-	-
ALPF	0.898	0.876	0.799	0.758
F^{adh}_{12}				
	BDP	**Budesonide**	**Terbutaline Sulphate**	**PAA**
PET	-	-	-	-
AL	-	291.04	204.27	-
ALAN	-	28.32	115.58	-
ALPF	-	349.11	216.36	-

All approaches did predict interactions to some extent though ΔG was considered the best one, followed by ϕ and finally force of interaction from AFM. Generally the true adhesion of powders decreased in the following rank order: PET > AL > ALAN > ALPF. BDP and budesonide adhered more than terbutaline sulphate, PAA did hardly adhere at all. The methods could only predict if more or less adhesion would occur not

how much material would adhere. In overview ΔG and ϕ both told the same story, which was that higher predicted interactions between materials lead to higher true adhesion. ΔG and ϕ showed that the powder-canister interaction as well as the powder-liquid interaction should be considered when predicting true adhesion since adhesion to the canister wall is a balance of the two interactions. Furthermore it was shown that both apolar Liftzich-van der Waals interactions and polar acid-base interactions has an impact on adhesion and should therefore be considered when predicting true adhesion. It was found that a full physicochemical profile of the materials involved when predicting true adhesion was useful as a complimentary tool to ΔG and ϕ. In Figure 6.16 the predicted interactions that were evaluated are shown and the largest number of interactions were determined by ΔG and the fewest by AFM.

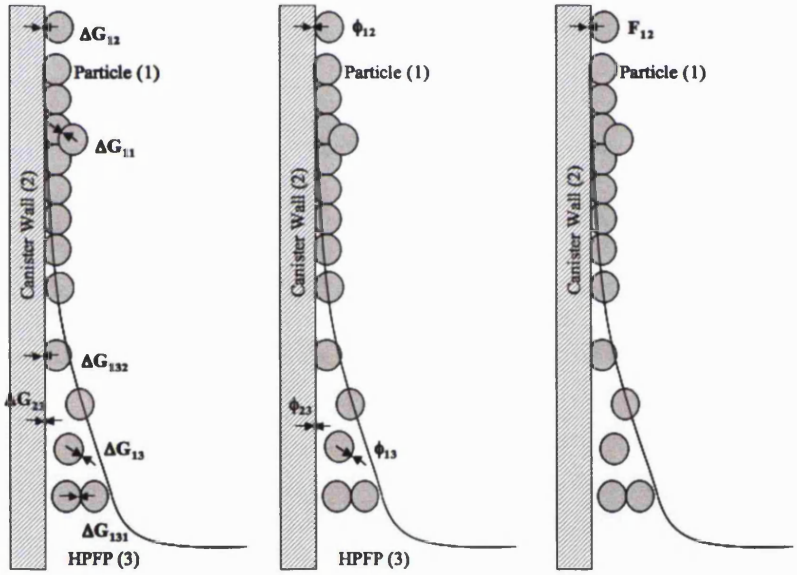

Figure 6.18. The interactions that were predicted with each of the three methods, from left: ΔG from surface energy parameters, ϕ from solubility parameters and AFM from direct adhesion measurements.

Finally it was observed that when raw data from different sources was used it gave variations in the final results shown by trend breaks. Therefore in order to predict adhesion in model MDI systems raw data such as contact angles and solubility parameters should be determined for the very materials used in the true adhesion study, since the surface energy and solubility parameters can vary between batches and various material grades. Also the parameters used should be determined with the same measurement technique, i.e. in this study surface energy was determined by sessile drop

contact angles only and not mixed with surface energy determined by inverse gas chromatography.

Chapter 7: Further Work

The work done in this study has proved valuable to further understand the adhesion occurring in model metered dose inhalers and the parameters with greatest impact on adhesion. Even though several tools for predicting the adhesion in suspension pMDIs has been evaluated in this study several areas could be investigated further for a fuller picture of pMDI systems.

First an expansion of the true adhesion of microparticles in model MDIs performed in Chapter 3 would benefit from further investigations. The purpose of looking at a model propellant in this study was to enable comparison of the true adhesion with the predicted interactions measured with methods not allowing the use of propellants since they must be handled under pressure. However carrying out true adhesion tests of the systems investigated in this study in HFA propellants, looking at both sedimenting and creaming suspensions, would be of great interest to gain a deeper understanding of the impact pressure, changes in physicochemical properties of HFAs and particle density would have on microparticle adhesion. The true adhesion studies would also benefit from looking at the difference in adhesion of physicochemically similar compounds to gain a further understanding on factors that drive adhesion. In this study there were signs of and has been suggested by others that parameters such as particle solubility, canister and particle roughness and canister hardness has an impact on adhesion and this could only be properly investigated if very similar materials are used where only one of the factors mentioned above is what differs them.

Then it would be of great interest to expand the visual study of adhesion by the fluid line, both during the course of adhesion as in Section 3.3.4 and when the adhesion is completed and the canisters are empty with dry adhered material on the canister walls to further understand visually where and how adhesion occur. Furthermore an expansion of the studies in Chapter 4, where predicted interactions by the surface component approach based on sessile drop contact angles and the interaction parameters based on Stefanis' group contribution theory were looked into, would be beneficial to see if the trends in Chapter 6 are applicable to a wider range of systems. These two methods are straight forward compared to the AFM study in Chapter 5 and since it was shown that

the two methods were better predictive methods for true adhesion it would be better to focus on expanding them rather than AFM. However, if AFM studies would be performed the adhesive as well as cohesive interactions between particles and canisters in zero per cent relative humidity, HPFP vapour and HPFP liquid should be looked at. Finally the particle size change in the suspension over time and its effect on adhesion is an area that should be investigated more since it would give extensive information of crystal growth and/or particle agglomeration over time in the suspensions.

In previous studies the theoretical interactions are often determined in a model propellant such as HPFP but directly compared to the true adhesion in propellants such as HFA134a and HFA227. This study has shown that the physicochemical properties of propellant, particles and canister has a great impact on adhesion and therefore the author recommend that theoretical predictions of interactions in pMDIs are confirmed by true adhesion studies in the systems used for predictions as well as real systems to confirm that the true adhesion is not altered by the extra ingredients in the real system.

Appendix 1: Detailed Calculation Examples

A1.1 Surface Energy Parameters from Contact Angles

The surface energy parameters of materials were calculated with Equation 4.12 – Equation 4.14 from Section 4.1.1.1 and here follows a detailed calculation example. The following abbreviations will be used for the compounds in the calculation example:

DIM – diiodomethane
EG – ethylene glycol
WAT – water
BUD – budesonide

If an appropriate set of test liquids has been chosen for the contact angle measurements. It does not matter what polar liquid is chosen as *L1* and *L2* respectively, it should give the same result.

Calculation of γ^{LW}_{BUD}

First γ^{LW}_{BUD} was calculated. The contact angle of diiodomethane on budesonide and the surface energy components of diiodomethane were used. The following values were obtained from Table 4.1 and Table 4.4 for diiodomethane and budesonide respectively:

γ_{DIM}= 51 mJ·m^{-2}
γ^{LW}_{DIM}= 51 mJ·m^{-2}
θ= 24° = (1° = π/180 Rad) 0.42 Rad

$$\gamma^{LW}_{BUD} = \frac{\gamma^2_{DIM}\left(1+\cos\theta_{DIM}\right)^2}{4\gamma^{LW}_{DIM}} = \frac{51^2\left(1+\cos 0.42\right)^2}{4\cdot 51} = \mathbf{47\ mJ\cdot m^{-2}} \qquad \text{(A1)}$$

Secondly the electron acceptor and donor components of the surface energy were calculated. The following values for ethylene glycol, water and the liquids contact angles on budesonide were obtained from Table 4.1 and Table 4.6:

γ_{EG} = 48 mJ·m^{-2} γ_{WAT} = 73 mJ·m^{-2}

γ_{EG}^{LW} = 29 mJ·m^{-2} γ_{WAT}^{LW} = 22 mJ·m^{-2}

γ^{+}_{EG} = 2 mJ·m^{-2} γ^{+}_{WAT} = 26 mJ·m^{-2}

γ^{-}_{EG} = 47 mJ·m^{-2} γ^{-}_{WAT} = 26 mJ·m^{-2}

θ_{EG} = 31 ° = 0.54 Rad θ_{WAT} = 59 ° = 1.03 Rad

γ_{BUD}^{LW} = 47 mJ·m^{-2}

Calculation of γ^{+}_{BUD}

$$\gamma^{+}_{BUD} = \left(\frac{\sqrt{\gamma^{+}_{WAT}}\left(\gamma_{EG}(1+\cos\theta_{WAT}) - 2\sqrt{\gamma^{LW}_{BUD}\gamma^{LW}_{EG}}\right) - \sqrt{\gamma^{+}_{EG}}\left(\gamma_{WAT}(1+\cos\theta_{WAT}) - 2\sqrt{\gamma^{LW}_{BUD}\gamma^{LW}_{WAT}}\right)}{\left(2\sqrt{\gamma^{-}_{EG}\gamma^{+}_{WAT}} - 2\sqrt{\gamma^{-}_{WAT}\gamma^{+}_{EG}}\right)} \right)^2 \quad (4.13)$$

The right side of Equation 4.13 was divided into three parts named A, B and C.

$$A = \sqrt{\gamma^{+}_{WAT}}\left(\gamma_{EG}(1+\cos\theta_{EG}) - 2\sqrt{\gamma^{LW}_{BUD}\gamma^{LW}_{EG}}\right)$$
$$B = \sqrt{\gamma^{+}_{EG}}\left(\gamma_{WAT}(1+\cos\theta_{WAT}) - 2\sqrt{\gamma^{LW}_{B}\gamma^{LW}_{WAT}}\right) \quad (A2)$$
$$C = \left(2\sqrt{\gamma^{-}_{EG}\gamma^{+}_{WAT}} - 2\sqrt{\gamma^{-}_{WAT}\gamma^{+}_{EG}}\right)$$

$$A = \sqrt{\gamma^{+}_{WAT}}\left(\gamma_{EG}(1+\cos\theta_{EG}) - 2\sqrt{\gamma^{LW}_{BUD}\gamma^{LW}_{EG}}\right) = \quad (A3)$$
$$\sqrt{26}\left(48\cdot(1+\cos 0.54) - 2\sqrt{47\cdot 29}\right) = 79$$

$$B = \sqrt{\gamma^{+}_{EG}}\left(\gamma_{WAT}(1+\cos\theta_{WAT}) - 2\sqrt{\gamma^{LW}_{BUD}\gamma^{LW}_{WAT}}\right) = \quad (A4)$$
$$\sqrt{2}\left(73\cdot(1+\cos 1.03) - 2\sqrt{47\cdot 22}\right) = 66$$

$$C = \left(2\sqrt{\gamma^{-}_{EG}\gamma^{+}_{WAT}} - 2\sqrt{\gamma^{-}_{WAT}\gamma^{+}_{EG}}\right) = \quad (A5)$$
$$\left(2\sqrt{47\cdot 26} - 2\sqrt{26\cdot 2}\right) = 55$$

$$\gamma_{BUD}^{+} = \left(\frac{A-B}{C}\right)^2 = \left(\frac{79-66}{55}\right)^2 = \mathbf{0.06\ mJ\cdot m^{-2}} \quad \text{(A6)}$$

Calculation of γ^{-}_{BUD}

$$\gamma_{BUD}^{-} = \left(\frac{\sqrt{\gamma_{WAT}^{-}}\left(\gamma_{EG}(1+\cos\theta_{EG}) - 2\sqrt{\gamma_{BUD}^{LW}\gamma_{EG}^{LW}}\right) - \sqrt{\gamma_{EG}^{-}}\left(\gamma_{WAT}(1+\cos\theta_{WAT}) - 2\sqrt{\gamma_{BUD}^{LW}\gamma_{WAT}^{LW}}\right)}{\left(2\sqrt{\gamma_{EG}^{+}\gamma_{WAT}^{-}} - 2\sqrt{\gamma_{WAT}^{+}\gamma_{EG}^{-}}\right)} \right)^2 \quad \text{(4.14)}$$

In the same way as for Equation 4.13 Equation 4.14 was divided into three parts named D, E and F.

$$D = \sqrt{\gamma_{WAT}^{-}}\left(\gamma_{EG}(1+\cos\theta_{EG}) - 2\sqrt{\gamma_{BUD}^{LW}\gamma_{EG}^{LW}}\right)$$
$$E = \sqrt{\gamma_{EG}^{-}}\left(\gamma_{WAT}(1+\cos\theta_{WAT}) - 2\sqrt{\gamma_{BUD}^{LW}\gamma_{WAT}^{LW}}\right) \quad \text{(A7)}$$
$$F = \left(2\sqrt{\gamma_{EG}^{+}\gamma_{WAT}^{-}} - 2\sqrt{\gamma_{WAT}^{+}\gamma_{EG}^{-}}\right)$$

$$D = \sqrt{\gamma_{WAT}^{-}}\left(\gamma_{EG}(1+\cos\theta_{EG}) - 2\sqrt{\gamma_{BUD}^{LW}\gamma_{EG}^{LW}}\right) =$$
$$\sqrt{26}\left(48\cdot(1+\cos 0.54) - 2\sqrt{47\cdot 29}\right) = 79 \quad \text{(A8)}$$

$$E = \sqrt{\gamma_{EG}^{-}}\left(\gamma_{WAT}(1+\cos\theta_{WAT}) - 2\sqrt{\gamma_{B}^{LW}\gamma_{WAT}^{LW}}\right) =$$
$$\sqrt{47}\left(73\cdot(1+\cos 1.03) - 2\sqrt{47\cdot 22}\right) = 319 \quad \text{(A9)}$$

$$F = \left(2\sqrt{\gamma_{EG}^{+}\gamma_{WAT}^{-}} - 2\sqrt{\gamma_{WAT}^{+}\gamma_{EG}^{-}}\right) =$$
$$\left(2\sqrt{2\cdot 26} - 2\sqrt{26\cdot 47}\right) = -55 \quad \text{(A10)}$$

$$\gamma_{BUD}^{-} = \left(\frac{D-E}{F}\right)^2 = \left(\frac{79-319}{-55}\right)^2 = \mathbf{19\ mJ\cdot m^{-2}} \quad \text{(A11)}$$

Calculation of $\gamma^{AB}{}_{BUD}$

Equation 4.4 gave the polar surface tension parameter

$$\gamma^{AB}_{BUD} = 2\sqrt{\gamma^{+}_{BUD}\gamma^{+}_{BUD}} = 2\sqrt{0.06 \cdot 19} = \mathbf{2\ mJ \cdot m^{-2}} \quad \text{(A12)}$$

Calculation of γ_{BUD}

Equation 4.3 gave the total surface tension

$$\gamma_{BUD} = \gamma^{LW}_{BUD} + \gamma^{AB}_{BUD} = 47 + 2 = \mathbf{49\ mJ \cdot m^{-2}} \quad \text{(A13)}$$

A1.2 K_A and K_D from IGC

Calculations of γ^{LW}, K_A *and* K_D *for BDP*

γ^{LW} was calculated from the results in Figure 4.5 and K_A and K_D from results in Figure 4.6. Equation 4.15 and 4.17 from Section 4.1.1.2 were used.

N = $6.02 \times 10^{23}\ mol^{-1}$

Slope = $2.79 \times 10^{23}\ J^{1/2} \cdot m^{-1} \cdot mol^{-1}$

Calculation of γ^{LW}

$$2N\left(\gamma^{LW}_{BDP}\right)^{\frac{1}{2}} = slope \quad \text{(A14)}$$

$$\gamma^{LW}_{BDP} = \frac{slope^2}{4N^2} = \frac{\left(2.79 \cdot 10^{23}\right)^2}{4\left(6.02 \cdot 10^{23}\right)^2} = \frac{3.63 \cdot 10^{47}}{4 \cdot 7.79 \cdot 10^{46}} = 0.05367\ J \cdot m^{-2} = \mathbf{53.67\ mJ \cdot m^{-2}} \quad \text{(A15)}$$

Calculation of K_A and K_D

Then K_A was obtained from the slope and K_D from the intercept in Figure 4.6 according to

$$\Delta G_A = K_A DN + K_D AN^* \tag{4.16}$$

K_A = **0.107**

K_D = **0.053**

A1.3 Solubility Parameters Calculated by Stefanis' Group Contribution Method

Calculating δ, δ_d, δ_p and δ_h from Stefanis group contribution method.

In the following examples a detailed description of the calculation for the Stefanis group contribution method will be presented. Equation 4.22 – Equation 4.24 in Section 4.1.2.2 will be used but are repeated in this section for convenience. There will be two examples, the first of HPFP and the second of BDP. In order to calculate Hansen solubility parameters with the Stefanis method the molecular structures of the compounds are required, Figure A1. There will be no polymer example but for the polymers one repeating unit was used as the molecular structure.

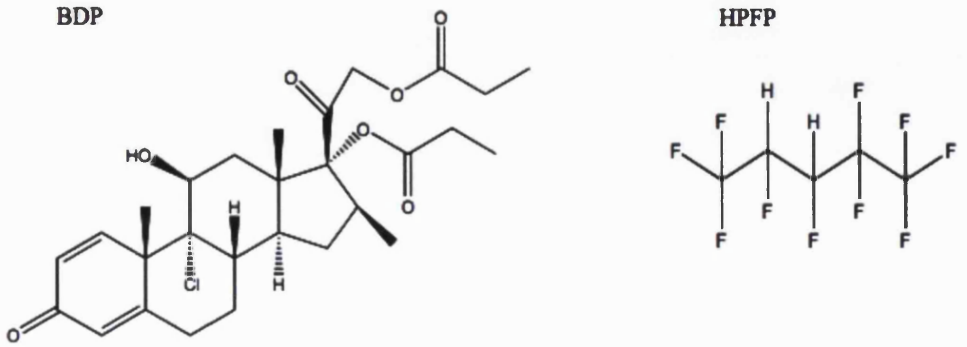

Figure A1. The molecular structure of compounds used in example calculations.

Calculating δ, δ_d, δ_p and δ_h for HPFP

All first and second order groups contributing to the Hansen solubility parameters were localised and counted, Figure A2. Then the group contributions were tabled and the sums of each contribution (ΣNC) was calculated, Table A1. Finally the Hansen solubility parameters were calculated. In Stefanis method there were not yet values available for some polar and hydrogen bonding group contributions (>CF_2 and F in Table 4.11). Therefore the calculated values for HPFP may be less accurate.

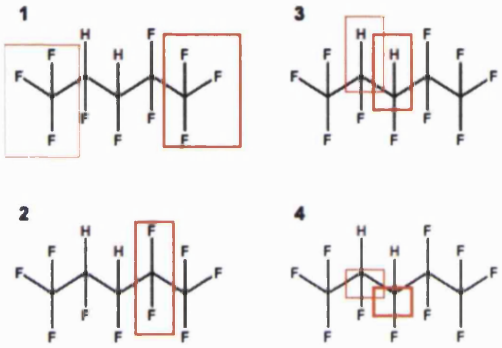

Figure A2. Image of molecular groups included when calculating Hansen solubility parameters with Stefanis group contribution method.

Table A1. Group contributions for HPFP when calculating its Hansen solubility parameters with Stefanis method (Stefanis and Panayiotou, 2008, Stefanis, 2008).

Figure Number	1st Order Groups	Occurrences (N_i)	Contributions (C_i)		
			δ_d	δ_p	δ_{hb}
1	$-CH_3$	2	-0.0921	-2.1318	-1.2997
2	$>CF_2$	1	-0.9628	--	--
3	-CH-	2	0.5982	0.6051	-0.2064
4	F	2	-0.6557	--	--
		$\sum_j N_j C_j$	**-1.2620**	**-3.0659**	**-3.0122**
	2nd Order Groups				
	None				

$$\delta_d = \left(\sum_i N_i C_i + W\sum_j N_j C_j + 16.9981\right) = \{W = 0\} = \quad \text{(A16)}$$

$$(-1.2620 + 16.9981) = 15.7361$$

$$\delta_p = \left(\sum_i N_i C_i + W\sum_j N_j C_j + 7.6134\right) = \{W = 0\} = \quad \text{(A17)}$$

$$(-3.0659 + 7.6134) = 4.5475$$

$$\delta_h = \left(\sum_i N_i C_i + W\sum_j N_j C_j + 7.7004\right) = \{W = 0\} = \quad \text{(A18)}$$

$$(-3.0122 + 7.7004) = 17.0377$$

Calculating δ, δ_d, δ_p and δ_h for BDP

Hansen solubility parameters for BDP were calculated in the same way as for HPFP. First and second order groups contributing to the Hansen solubility parameters were localised and counted, Figure A3 Then the group contributions were tabled and the sums of each contribution (ΣNC) was calculated, Table A2.

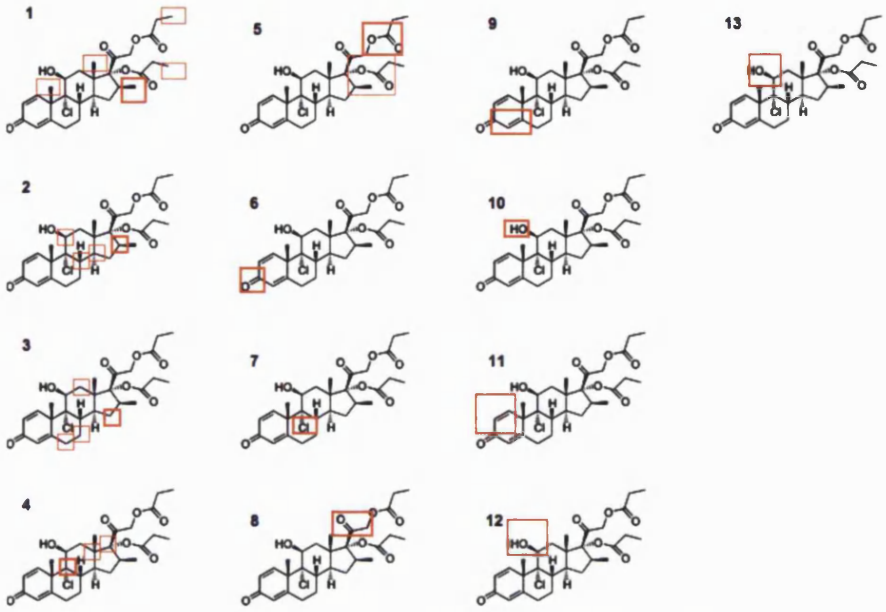

Figure A3. Image of molecular groups included when calculating Hansen solubility parameters with Stefanis group contribution method.

Table A2. Group contributions for BDP when calculating its Hansen solubility parameters with Stefanis' method (Stefanis and Panayiotou, 2008, Stefanis, 2008).

Figure Number	1st Order Groups	Occurrences (N_i)	Contributions (C_i)		
			δ_d	δ_p	δ_h
1	$-CH_3$	5	-0.9328	-1.6444	-0.7458
2	>CH-	4	0.5982	0.6051	-0.2064
3	$-CH_2$	4	0.0089	-0.3141	-0.3877
4	>C<	3	1.2911	2.0249	-0.0113
5	$-CH_2COO-$	2	0.6450	3.4942	1.3893
6	>C=O	1	-0.9022	0.7691	1.7033
7	>CCl-	1	2.8308	1.8196	0.1473
8	$-CH_2CO-$	1	0.8343	3.6101	-0.3929
9	-CH=C<	1	0.4993	-1.1018	-1.7171
10	OH	1	-0.2159	1.0587	7.3609
11	-CH=CH-	1	0.0.2242	-0.5037	-0.1253
		$\sum_i N_i C_i$	**6.1982**	**11.5673**	**3.6155**
	2nd Order Groups				
12	>CHOH-	1	0.1298	0.2366	-0.2453
13	$C_{cyclic}=O$	1	-0.3253	0.1972	-0.4496
		$\sum_j N_j C_j$	**-0.1955**	**0.4338**	**-0.6949**

$$\delta_d = \left(\sum_i N_i C_i + W \sum_j N_j C_j + 16.9981\right) = \{W = 1\} = \quad \text{(A19)}$$

$$(6.1982 - 0.1955 + 16.9981) = 23.0008$$

$$\delta_p = \left(\sum_i N_i C_i + W \sum_j N_j C_j + 7.6134\right) = \{W = 1\} = \quad \text{(A20)}$$

$$(11.6573 + 0.4338 + 7.6134) = 19.7045$$

$$\delta_{hb} = \left(\sum_i N_i C_i + W \sum_j N_j C_j + 7.7004\right) = \{W = 1\} = \quad \text{(A21)}$$

$$(3.6155 - 0.6949 + 7.704) = 10.6209$$

A1.4 Interactions

A1.4.1 Free Energy of Interaction from Surface Energy Parameters Based on Contact Angles

Calculations of energy of interaction between budesonide and PET and also between budesonide and PET submerged in HPFP.

For calculations of interactions between budesonide (1) and PET (2) Equations 4.4 and 4.7 were used and for interactions between the materials submerged in HPFP (3) Equation 4.8 and 4.9 was used. One example of calculations for each of the following parameters will be demonstrated here: ΔG_{12}, γ_{12} and ΔG_{132}. Detailed calculations of γ^{LW}, γ^{+}, γ^{-} and γ was shown in Section 4.1.1.1. The numbers used for these calculations were taken from Table 4.7.

$\gamma_1^{LW} = 46\ mJ{\cdot}m^{-2}$	$\gamma_2^{LW} = 44\ mJ{\cdot}m^{-2}$	$\gamma_3^{LW} = 8\ mJ{\cdot}m^{-2}$
$\gamma_1^{+} = 0.06\ mJ{\cdot}m^{-2}$	$\gamma_2^{+} = 0.003\ mJ{\cdot}m^{-2}$	$\gamma_3^{+} = 3\ mJ{\cdot}m^{-2}$
$\gamma_1^{-} = 19\ mJ{\cdot}m^{-2}$	$\gamma_2^{-} = 6\ mJ{\cdot}m^{-2}$	$\gamma_3^{-} = 1\ mJ{\cdot}m^{-2}$
$\gamma_1 = 49\ mJ{\cdot}m^{-2}$	$\gamma_2 = 45\ mJ{\cdot}m^{-2}$	$\gamma_3 = 11\ mJ{\cdot}m^{-2}$

Calculation of ΔG_{12}

$$\gamma_{12} = \left(\sqrt{\gamma_1^{LW}} - \sqrt{\gamma_2^{LW}}\right)^2 + 2\left(\sqrt{\gamma_1^{+}\gamma_1^{-}} + \sqrt{\gamma_2^{+}\gamma_2^{-}} - \sqrt{\gamma_1^{+}\gamma_2^{-}} - \sqrt{\gamma_1^{-}\gamma_2^{+}}\right) = \quad \text{(A22)}$$

$$\left(\sqrt{46} - \sqrt{44}\right)^2 + 2\left(\sqrt{0.06 \cdot 19} + \sqrt{0.003 \cdot 6} - \sqrt{0.06 \cdot 6} - \sqrt{19 \cdot 0.003}\right) = 0.75$$

γ_{13} and γ_{23} were calculated in the same way but with the surface energy parameters for each specific system and resulted in:

$\gamma_{13} = 7\ mJ{\cdot}m^{-2}$

$\gamma_{23} = 10\ mJ{\cdot}m^{-2}$

$$\Delta G_{12} = \gamma_{12} - \gamma_1 - \gamma_2 = 0.75 - 49 - 45 = \mathbf{-93\ mJ{\cdot}m^{-2}} \quad \text{(A23)}$$

Calculation of ΔG_{132}

$$\Delta G_{132} = \gamma_{12} - \gamma_{13} - \gamma_{23} = 0.75 - 7 - 10 = \mathbf{-16\ mJ{\cdot}m^{-2}} \quad \text{(A24)}$$

Calculation of ΔG_{131}

$$\Delta G_{131} = -2\gamma_{13} = -2 * 7 = \mathbf{-14\ mJ{\cdot}m^{-2}} \quad \text{(A25)}$$

A1.4.2 Interaction Parameter from Solubility Parameters Based on Stefanis Method

Calculation of ϕ of budesonide to PET

A – budesonide

B – PET

${}^{A}\delta = 32$ MPa$^{1/2}$	${}^{B}\delta = 25$ MPa$^{1/2}$
${}^{A}\delta_d = 23$ MPa$^{1/2}$	${}^{B}\delta_d = 19$ MPa$^{1/2}$
${}^{A}\delta_p = 14$ MPa$^{1/2}$	${}^{B}\delta_p = 14$ MPa$^{1/2}$
${}^{A}\rho = 1.3$ g·cm^{-3}	${}^{B}\rho = 1.3$ g·cm^{-3}
${}^{A}M = 431$ g·mol^{-1}	${}^{A}M = 65\,000$ g·mol^{-1}

This equation gives the interaction parameter based on solubility parameters.

$$\phi = 2\left[\frac{{}^{A}x_d \cdot {}^{B}x_d}{{}^{A}x_d \cdot g_1 + {}^{B}x_d \cdot g_2} + \frac{{}^{A}x_p \cdot {}^{B}x_p}{{}^{A}x_p \cdot g_1 + {}^{B}x_p \cdot g_2}\right] \tag{A26}$$

First calculate the fractional non-polarity x_d for both materials.

$${}^{A}x_d = \left[\frac{{}^{A}\delta_d}{{}^{A}\delta}\right]^2 = \left[\frac{23}{32}\right]^2 = 0.5 \tag{A27}$$

$${}^{B}x_d = \left[\frac{{}^{B}\delta_d}{{}^{B}\delta}\right]^2 = \left[\frac{19}{25}\right]^2 = 0.6 \tag{A28}$$

the fractional polarity x_p for both materials.

$${}^{A}x_P = 1 - {}^{A}x_d = 1 - 0.5 = 0.5 \tag{A29}$$

$${}^{B}x_P = 1 - {}^{B}x_d = 1 - 0.6 = 0.4 \tag{A30}$$

the molar volumes are

$$ {}^{A}V = \frac{{}^{A}M}{{}^{A}\rho} = \frac{430}{1.3} = 332 \text{ cm}^3\cdot\text{mol}^{-1} \quad \text{(A31)} $$

$$ {}^{B}V = \frac{{}^{B}M}{{}^{B}\rho} = \frac{65000}{1.3} = 50\,000 \text{ cm}^3\cdot\text{mol}^{-1} \quad \text{(A32)} $$

the constant g^1

$$ g_1 = \frac{{}^{A}\delta_d \cdot {}^{A}V^{\frac{1}{3}}}{{}^{B}\delta_d \cdot {}^{B}V^{\frac{1}{3}}} = \frac{23 \cdot 332^{\frac{1}{3}}}{19 \cdot 50000^{\frac{1}{3}}} = 0.3 \quad \text{(A33)} $$

the constant g_2

$$ g_2 = \frac{1}{g_1} = \frac{1}{0.3} = 3 \quad \text{(A34)} $$

Finally it gives the interaction parameter

$$ \phi = 2\left[\frac{0.5 \cdot 19}{0.5 \cdot 0.3 + 0.6 \cdot 3} + \frac{0.5 \cdot 0.4}{0.5 \cdot 0.3 + 0.4 \cdot 3}\right] = \mathbf{0.6} \quad \text{(A35)} $$

References

ADAMSKA, K. & VOELKEL, A. (2005) Inverse gas chromatographic determination of solubility parameters of excipients. *International journal of pharmaceutics,* 304, 11-17.

ADI, H., TRAINI, D., CHAN, H. K. & YOUNG, P. M. (2008a) The influence of drug morphology on the aerosolisation efficiency of dry powder inhaler formulations. *Journal of pharmaceutical sciences,* 97, 2780-2788.

ADI, S., ADI, H., TANG, H., TRAINI, D., CHAN, H. K. & YOUNG, P. M. (2008b) Micro-particle corrugation, adhesion and inhalation aerosol efficiency. *European Journal of Pharmaceutical Sciences,* 35, 12-18.

ALISON, P., GRIFFITHS, P., JAMES, R., WILLOCK, D. & ROGUEDA, P. (2005) Explaining the phase behaviour of the pharmaceutically relevant polymers poly(ethylene glycol) and poly(vinyl pyrrolidone) in semi-fluorinated liquids. *Journal of Pharmacy and Pharmacology,* 57, 973-980.

ALPAR, O. H., SOMAVARAPU, S., ATUAH, K. N. & BRAMWELL, V. W. (2005) Biodegradable mucoadhesive particulates for nasal and pulmonary antigen and DNA delivery. *Advanced Drug Delivery Reviews,* 57, 411-430.

ASHAYER, R., LUCKHAM, P. F., MANIMAARAN, S. & ROGUEDA, P. (2004) Investigation of the molecular interactions in a pMDI formulation by atomic force microscopy. *European Journal of Pharmaceutical Sciences,* 21, 533-543.

AUDRY, M. C., RAMOS, S. & CHARLAIX, E. (2009) Adhesion between highly rough alumina surfaces: An atomic force microscope study. *Journal of Colloid and Interface Science,* 331, 371-378.

BEAUSANG, E. (2005) Surfactant-mediated surface modification of microparticles for pressurised metered dose inhalation. *Department of pharmaceutics.* London, University of London, School of Pharmacy.

BEGAT, P., MORTON, D. A. V., STANIFORTH, J. N. & PRICE, R. (2004) The Cohesive-Adhesive Balances in Dry Powder Inhaler Formulations II: Influence on Fine Particle Delivery Characteristics. *Pharmaceutical Research,* 21, 1591-1597.

BI, R. & ZHANG, N. (2007) Liposomes as a carrier for pulmonary delivery of peptides and proteins. *Journal of biomedical nanotechnology,* 3, 332-341.

BLONDINO, F. E. & BYRON, P. R. (1998) Surfactant Dissolution and Water Solubilization in Chlorine-Free Liquified Gas Propellants. *Drug Development and Industrial Pharmacy,* 24, 935-945.

BOULET, L. P., BECKER, A., BÉRUBÉ, D., BEVERIDGE, R. & ERNST, P. (1999) Canadian asthma consensus report. IN ASSOCIATION, C. M. (Ed.).

BOUSQUET, J. & KHALTAEV, N. (2007) Global surveillance, prevention and control of chronic respiratory diseases: a comprehensive approach. IN ORGANISATION, W. H. (Ed.) Geneva.

BRITTO, I. L. (2007) Metered dose inhaler. IN GLAXOSMITHKLINE (Ed.) US.

BUCKTON, G. (1990) Contact Angle, Adsorption and Wettability - a Review with Respect to Powders. *Powder Technology,* 61, 237-249.

BUCKTON, G., DARCY, P. & MCCARTHY, D. (1995) The extent of errors associated with contact angles 3. The influence of surface roughness effects on angles measured using a Wilhelmy plate technique for powders. *Colloids and Surfaces A: Physicochemical and Engineering Aspects,* 95, 27-35.

BUCKTON, G. & GILL, H. (2007) The importance of surface energetics of powders for drug delivery and the establishment of inverse gas chromatography. *Advanced Drug Delivery,* 59, 1474-1479.

BYRON, P. R. (1994) Dosing reproducibility from experimental albuterol suspension metered-dose inhalers. *Pharmaceutical Research,* 11, 580-584.

CARR, N. (2008) *The Encyclopaedia Britannica,* Chicago, Encyclopaedia Britannica Inc.

CARTWRIGHT, J. H. E., PIRO, O. & VILLACAMPA, A. I. (2002) Pattern formation in solutal convection: vermiculated rolls and isolated cells. *Physica A: Statistical Mechanics and its Applications,* 314.

CAYAKARA, T., ALASLAN, A., EROGLU, M. S. & GÜVEN, O. (2006) Surface energetics of poly(N-vinyl-2-pyrrolidone)/chitosan blend films. *Applied Surface Science,* 252, 7430-7435.

CDER (1994) Reviewer guidance - validation of chromatographic methods.

CHARSLEY, E. L. & WARRINGTON, S. B. (1992) *Thermal analysis - Techniques and applications,* Cambridge, The Royal Society of Chemistry.

CHEN, R., TAGAWA, M., HOSHI, N., OGURA, T., OKAMOTO, H. & DANJO, K. (2004) Improved Dissolution of an Insoluble Drug Using a 4-Fluid Nozzle Spray-Drying Technique. *Chemical and Pharmaceutical Bulletin,,* 52, 1066-1070.

CHIDAVAENZI, O. C., BUCKTON, G. & KOOSHA, F. (2001) The effect of co-spray drying with polyethylene glycol 4000 on the crystallinity and physical form of lactose. *International Journal of Pharmaceutics,* 216, 43-49.

COLUMBANO, A. (2000) Modification of microparticle surfaces by use of alkylpolyglycoside surfactants. *Pharmaceutics.* London, University of London, School of Pharmacy.

COTE, M., HUGHES, C. E., AUSTIN, T. K., ROGUEDA, P. G. A., PAN, Z. G., HARRIS, K. D. M. & GRIFITHS, P. C. (2008) Characterization of a polymorphic system exhibiting substantial variation of solubility in a fluorinated solvent. *Journal of Physical Chemistry C,* 112, 1470-1478.

COULSON, J. M., RICHARDSON, J. F., HARKER, J. H. & BACKHURST, J. R. (1999) *Chemical engineering,* Oxford, Butterworth-Heinemann.

CROMPTON, G. K. (2004) How to achieve good compliance with inhaled asthma therapy. *Respiratory Medicine,* 98, 35-40.

DALBY, R. & SUMAN, J. (2003) Inhalation therapy: Technological milestones in asthma treatment. *Advanced Drug Delivery Reviews,* 55, 779-791.

DEEGAN, R. D., BAKAJIN, O., DUPONT, T. F., HUBER, G., NAGEL, M. W. & WITTEN, T. A. (2000) Contact line deposits in an evaporating drop. *Physical Review E,* 62, 756-765.

DEEGAN, R. D., BAKAJIN, O., DUPONT, T. F., HUBER, G., NAGEL, S. R. & WITTEN, T. A. (1997) Capillary flow as the cause of ring stains from dried liquid drops. *Nature,* 389, 827-829.

DICKINSON, P. A., SEVILLE, P. C., MCHALE, H., PERKINS, N. C. & TAYLOR, G. (2000) An investigation of the solubility of various compounds in the hydrofluoroalkane propellants and possible model liquid propellants. *Journal of Aerosol Medicine-Deposition Clearance and Effects in the Lung,* 13, 179-186.

DOHMEIER, D. M., HEYWORTH, D. & WILDE, T. (2009) The application of a new high performance dual-layer coating to pressurized metered dose inhaler hardware. IN DALBY, R. N., BYRON, P. B., PEART, J., SUMAN, J. D. &

YOUNG, P. M. (Eds.) *Respiratory Drug Delivery Europe 2009.* Lisbon, Portugal, Davis Healthcare International Publisher.
DOLOVICH, M. (1995) Characterization of medical aerosols: physical and clinical requirements for new inhalers. *Aerosol Science and Technology,* 22, 392-299.
EVERETT, D. H. (1988) *Basic principles of colloid science,* Letchworth, The Royal Society of Chemistry.
FLORIANO, W. B. (2004) Dielectric constant and density of water as a function of pressure at constant temperature. *Brazilian Journal of Physics,* 34, 38-41.
FOWKES, F. M. (1963) Additivity of intermolecular forces at interfaces. I. Determination of the contribution to surface and interfacial tensions of dispersion forces in various liquids. *Journal of Physical Chemistry,* 67, 2538-2541.
FOWKES, F. M., RIDDLE, F. L., PASTORE, W. E. & WEBER, A. A. (1990) Interfacial interactions between self-associated polar liquids and squalane used to test equations for solid - liquid interfacial interactions. *Colloids and Surfaces A,* 43, 367-387.
GAVINI, E., HEGGE, A. B., RASSU, G., SANNA, V., TESTA, C., PIRISINO, G., KARLSEN, J. & GIUNCHEDI, P. (2006) Nasal administration of Carbamazepine using chitosan microspheres: In vitro/in vivo studies. *International Journal of Pharmaceutics,* 307, 9-15.
GÖTZINGER, M. & PEUKERT, W. (2003) Dispersive forces of particle–surface interactions: direct AFM measurements and modelling. *Powder Technology,* 130, 102-109.
GOVIND, N., JINKS, P. A., ROSS, D. L. & WARD, G. H. (2000) Medical inhalation aerosol formulations containing budesonide. US.
GRONEBERG, D. A., PAUL, H. & WELTE, T. (2006) Novel strategies of aerosole pharmacotherapy. *Experimental and toxicologic pathology,* 57, 49-53.
GUTMANN, V. (1978) *The donor-acceptor approach to molecular interactions,* New York, Plenum Press.
HANCOCK, B. C. (1997) The use of solubility parameters in pharmaceutical dosage form design. *International Journal of Pharmaceutics,* 148, 1-21.
HANSEN, C. M. (2000) *Hansen solubility parameters – A user's handbook,* Boca Raton, Florida, CRC Press.
HICKEY, A. J., DALBY, N. & BYRON, P. R. (1988) Effects of surfactants on aerosol powders in suspension. Implications for airborne particle size. *International Journal of Pharmaceutics,* 42, 267-270.
HILDEBRAND, J. H., PRAUSNITZ, J. M. & SCOTT, R. L. (1970) *Regular and related solutions,* New York, Van Nostrand Reinhold.
HINDS, W. C. (1999) *Aerosol technology,* New York, John Wiley and Sons.
HOY, K. L. (1989) Solubility parameter as a design parameter for water borne polymers and coatings. *Journal of Coated Fabrics,* 19, 53-67.
HOYE, J. A., GUPTA, A. & MYRDAL, P. B. (2008) Solubility of solid solutes in HFA-134a with a correlation to physico-chemical properties. *Journal of Pharmaceutical Sciences,* 97, 198-208.
HUU-PHUOC, N., HO, N. T., BUCHMANN, M. & KESSELRING, U. W. (1987a) Determination of partial and total cohesion parameters of caffeine, theophylline, and methyl para-hydroxybenzoate by gas-solid chromatography. *Journal of Pharmaceutical Sciences,* 76, 406-410.
HUU-PHUOC, N., NAM-TRAN, H., BUCHMANN, M. & KESSELRING, U. W. (1987b) Experimentally optimized determination of the partial and total

cohesion parameters of an insoluble polymer (microcrystalline cellulose) by gas-solid chromatography. *International Journal of Pharmaceutics,* 34, 217-223.
HUU-PHUOC, N., PHAN-TAN-LUU, R., MUNAFO, A., RUELLE, P., NAMTRAN, H., BUCHMANN, M. & KESSELRING, U. W. (1986) Determination of partial solubility parameters of lactose by gas solid chromatography. *Journal of Pharmaceutical Sciences,* 75, 68-72.
JAMES, J., CREAN, B., DAVIES, M., TOON, R., JINKS, P. & ROBERTS, C. (2008) The surface characterisation and comparison of two potential sub-micron, sugar bulking excipients for use in low-dose, suspension formulations in metered dose inhalers. *International Journal of Pharmaceutics,* 361, 209-221.
JAMES, J., DAVIES, M., TOON, R., JINKS, P. & ROBERTS, C. (2007) Comparing the surface energetics and mechanical properties of two potential sub-micron sugar bulking excipients for use in low-dose, suspension formulations in metered dose inhalers. *Drug Delivery to the Lungs 18.* Aerosol Society.
JAMES, J., DAVIES, M., TOON, R., JINKS, P. & ROBERTS, C. (2009) Particulate drug interactions with polymeric and elastomeric valve components in suspension formulations for metered dose inhalers. *International Journal of Pharmaceutics,* 366, 124-132.
JIANG, Y., MATSUSAKA, S., MASUDA, H. & QIAN, Y. (2008) Characterizing the effect of substrate surface roughness on particle-wall interaction with the airflow method. *Powder Technology,* 186, 199-205.
JINKS, P. M. (2008) A new high performance dual-layer coating for inhalation hardware. *Drug Delivery to the Lungs 19.* Edinburgh, UK.
JONES, M. D. (2006) An investigation into the dispersion mechanisms of ternary dry powder inhaler formulations by the quantification of interparticulate forces. *Department of Pharmacy and Pharmacology.* University of Bath.
JONES, M. D., GAISFORD, S., CHIOU, H., TANG, P., CHAN, H. K. & BUCKTON, G. (2008) Comparison of methods for the calculation of specific free energy of adsorption from inverse gas chromatography data using pharmaceutical materials. Department of Pharmaceutics, The School of Pharmacy, University of London.
JONES, S. A., MARTIN, G. P. & BROWN, M. B. (2006a) Manipulation of beclomethasone-hydrofluoroalkane interactions using biocompatible macromolecules. *Journal of Pharmaceutical Sciences,* 95, 1060-1074.
JONES, S. A., MARTIN, G. P. & BROWN, M. B. (2006b) Stabilisation of deoxyribonuclease in hydrofluoroalkanes using miscible vinyl polymers. *Journal of Controlled Release,* 115, 1-8.
KANG, J. W., ABILDSKOV, J. & GANI, R. (2002) Estimation of mixture properties from first- and second-order group contributions with the UNIFAC model. *Industry and Engineering Chemistry Research,* 41, 3260-3273.
KELLER, M. (1999) Innovations and perspectives of metered dose inhalers in pulmonary drug delivery. *International Journal of Pharmaceutics,* 186, 81-90.
KRALCHEVSKY, P. A. & NAGAYAMA, K. (2000) Capillary interactions between particles bound to interfaces, liquid films and biomembranes. *Advances in colloid and interface science,* 85, 145-192.
KRÜSS (2002) *DSA1 v 1.80 drop shape analysis user manual,* Hamburg, Krüss GmbH.
LAZGHAB, M., SALEH, K., PEZRON, I., GUIGON, P. & KOMUNJER, L. (2005) Wettability assessment of finely divided solids. *Powder Technology,* 157, 79-91.
LEACH, C. L. (2005) The CFC to HFA transition and its impact on pulmonary drug development. *Respiratory Care,* 50, 1201-1206.

LEWIS, D., GANDERTON, D., MEAKIN, B. J., VENTURA, P., BRAMBILLA, G. & GARZIA, R. (2008) Pressurised metered dose inhalers (MDI). Chiesi Farmaceutici S.p.A.

LEWIS, D. A., GANDERTON, D., MEAKIN, B. J. & BRAMBILLA, G. (2005) Modulite®: a simple solution to a difficult problem. *Respiration,* 72, 3-5.

LEWIS, G. A., MATHIEU, D. & PHAN-TAN-LUU, R. (1999) *Pharmaceutical Experimental Design (Drugs and the Pharmaceutical Sciences),* New York, Marcel Dekker Inc.

LYKLEMA, J. (1991) *Fundamentals of interface and colloid science, volume 1: fundamentals,* San Diego, Academic Press Inc.

LYSENG-WILLIAMSON, K. A. & SIMSON, D. (2008) Budesonide/formoterol pressurized metered-dose inhaler. *Drugs,* 68, 1855-1864.

MASOLI, M., FABIAN, D., HOLT, S. & BEASLEY, R. (2004) The global burden of asthma. IN ASTHMA, T. G. I. F. (Ed.) *Executive summary of the GINA dissemination committee report.* Wellington and Southampton, Medical research institute of New Zealand and University of Southampton.

MCDONALD, K. J. & MARTIN, G. P. (2000) Transition to CFC-free metered dose inhalers - into the new millennium. *International Journal of Pharmaceutics,* 201, 89-107.

MITCHELL, J. P. & NAGEL, M. W. (2004) Particle size analysis of aerosols from medicinal inhalers. *KONA,* 22, 32-65.

MORRIS, C. J. & PARVIZ, B. A. (2006) Self-assembly and characterization of marangoni microfluidic actuators. *Journal of micromechanics and microengineering,* 16, 972-980.

MUKHOPADHYAY, P. & SCHREIBER, H. P. (1995) Aspects of acid-base interactions and use of inverse gas chromatography. *Colloids and surfaces A: Physicochemical and engineering aspects,* 100, 47-71.

NAGAYAMA, K. (1996) Two-dimensional self-assembly of colloids in thin liquid films. *Colloids and Surfaces A: Physicochemical and Engineering Aspects,* 109, 363-374.

PAAJANEN, M., KATAINEN, J., RAULA, J., KAUPPINEN, E. I. & LAHTINEN, J. (2009) Direct evidence on reduced adhesion of salbutamol sulphate particles due to L-leucine coating. *Powder Technology,* 192, 6-11.

PARSONS, G. E., BUCKTON, G. & CHATHAM, S. M. (1992) The use of surface energy and polarity determinations to predict physical stability of non-polar, non-aqueous suspensions. *International Journal of Pharmaceutics,* 83, 163-170.

PAUL, A., GRIFFITHS, P., JAMES, R., WILLOCK, D. & ROGUEDA, P. (2005) Explaining the phase behaviour of the pharmaceutically relevant polymers poly(ethylene glycol) and poly(vinyl pyrrolidone) in semi-fluorinated liquids. *Journal of Pharmacy and Pharmacology,* 57, 973-980.

PHILLIPS, E. M., BYRON, P. R. & DALBY, R. N. (1993) Axial ratio measurements for early detection of crystal growth in suspenion-type metered dose inhalers. *Pharmaceutical Research,* 10, 454-456.

PHILLIPS, E. M., BYRON, P. R., FULTS, K. & HICKEY, A. J. (1990) Optimized inhalation aerosols. II. Inertieal testing methods for particle size analysis of pressurized inhalers. *Pharmaceutical Research,* 7, 1228-1233.

PRICE, R., YOUNG, P. M., EDGE, J. N. & STANIFORTH, J. N. (2002) The influence of relative humidity on particulate interactions in carrier-based dry powder inhaler formulations. *International Journal of Pharmaceutics,* 246, 47-59.

PUREWAL, T. S. & GRANT, D. J. W. (1997) *Metered dose inhaler technology*, Interpharm/CRC.
REHMAN, M., SHEKUNOV, B. Y., YORK, P., LECHUGA-BALLESTEROS, D., MILLER, D. P., TAN, T. & COLTHORPE, P. (2004) Optimisation of powders for pulmonary delivery using supercritical fluid technology. *European Journal of Pharmaceutical Sciences,* 22, 1-17.
RICHTER, K. (2004) Successful use of DPI systems in asthmatic patients - key parameters. *Respiratory Medicine,* 98, 22-27.
RIDDER, K. B., DAVIES-CUTTING, C. & KELLAWAY, I. W. (2005) Surfactant solubility and aggregate orientation in hydrofluoroalkanes. *International Journal of Pharmaceutics,* 295, 57-65.
RILLOSI, M. & BUCKTON, G. (1995) Modelling mucoadhesion by use of surface energy terms obtained by the Lewis acid-Lewis base approach. *International Journal of Pharmaceutics,* 117, 75-84.
ROBERTS, C. J. (2009) AFM or what? A chritical evaluation of surface analytical techniques that predict interparticulate interactions. IN DALBY, R. N., BYRON, P. R., PEART, J., SUMAN, J. D. & YOUNG, P. M. (Eds.) *Respiratory Drug Delivery Europe 2009.* Lisbon, Portugal, Davis Healthcare International Publishing.
ROGUEDA, P. G. A. (2003) HPFP, a model propellant for pMDIs. *Drug Development and Industrial Pharmacy,* 29, 39-49.
ROSENSTOCK, J., CAPPELLERI, J. C., BOLINDER, B. & GERBER, R. A. (2004) Patient satisfaction and glycemic control after 1 year with inhaled insulin (Exubera) in patients with type 1 or type 2 diabetes. *Diabetes Care.*
ROSILIO, V. (2007) Paris.
ROWE, R. C. (1988) Adhesion of film coatings to tablet surfaces - A theoretical approach based on solubility parameters. *International Journal of Pharmaceutics,* 41, 219-222.
RUZER, L. S. & HARLEY, N. H. (2005) *Aerosol handbook: Measurement, dosimetry and health effects,* New York, CRC Press.
SAKAGAMI, M., KINOSHITA, W., SAKON, K., SATO, J. & MAKINO, Y. (2002) Mucoadhesive beclomethasone microspheres for powder inhalation: their pharmacokinetics and pharmacodynamics evaluation. *Journal of Controlled Release,* 80, 207-218.
SHAYA, F. T., DONGYI, D., AKAZAWA, M. O., BLANCHETTE, C. M., WANG, J., MAPEL, D. W., DALAL, A. & SCHARF, S. M. (2008) Burden of contaminant asthma and COPD in a medical population. *Chest,* 134, 14-19.
SKYLER, J. S., JOVANOVIC, L., KLIOZE, S., REIS, J. & DUGGAN, W. (2006) Two-year safety and efficacy of inhaled human insulin (Exubera) in adult patients with type 1 diabetes. *Diabetes Care.*
SMYTH, H. D. C. (2003) The influence of formulation variables on the performance of alternative propellant-driven metered dose inhalers. *Advanced Drug Delivery Reviews,* 55, 807-828.
SOLVAY (2008) IN S.A., S. (Ed.) Brussels, Sovay.
STEFANIS, E. (2008).
STEFANIS, E. & PANAYIOTOU, C. (2008) Prediction of hansen solubility parameters with a new group-contribution method. *International Journal of Thermophysics,* 29, 568-585.
TAJBER, L., CORRIGAN, D. O., CORRIGAN, O. I. & HEALY, A. M. (2009) Spray drying of budesonide, formoterol fumarate and their composites-I.

Physicochemcial characterisation. *International Journal of Pharmaceutics,* 367, 79-85.
TELKO, M. J. & HICKEY, A. J. (2005) Dry powder inhaler formulation. *Respiratory Care,* 50, 1209-1227.
TERZANO, C. (2001) Pressurized metered dose inhalers and add-on devices. *Pulmonary Pharmacology and Therapeutics,* 14, 351-366.
THI, T. H. H., DANÈDE, F., DESCAMPS, M. & FLAMENT, M. (2008) Comparison of physical and inhalation properties of spray-dried and micronized terbutaline sulphate. *European Journal of Pharmaceutics and Biopharmaceutics,* 70, 380-388.
TIWARI, D., GOLDMAN, D., MALICK, W. A. & MADAN, P. L. (1998) Formulation and evaluation of albuterol metered dose inhalers containing tetrafluoroethane (P134a), a non-CFC propellant. *Pharmaceutical Development and Technology,* 3, 163-174.
TONG, H. H. Y., SHEKUNOV, B. Y., YORK, P. & CHOW, A. H. L. (2002) Influence of polymorphism on the surface energetics of salmeterol xinafoate crystallized from supercritical fluids. *Pharmaceutical Research,* 19, 640-648.
TRAINI, D. (2005) Physical properties and interactions in metered dose inhalers. Bath, University of Bath.
TRAINI, D., ROGUEDA, P., YOUNG, P. & PRICE, R. (2005) Surface energy and interparticle force correlation in model pMDI formulations. *Pharmaceutical Research,* 22, 816-825.
TRAINI, D., YOUNG, P. M., ROGUEDA, P. & PRICE, R. (2006) The use of AFM and surface energy measurements to investigate drug-canister material interactions in a model pressurized metered dose inhaler formulation. *Aerosol Science and Technology,* 40, 227-236.
TRAINI, D., YOUNG, P. M., ROGUEDA, P. & PRICE, R. (2007) In vitro investigation of drug particulates interactions and aerosol performance of pressurised metered dose inhalers. *Pharmaceutical Research,* 24, 125-135.
UNEP (2000) The montreal protocol on substances that deplete the ozone layer. IN LAYER, S. F. T. V. C. F. T. P. O. T. O. L. A. T. M. P. O. S. T. D. T. O. (Ed.).
VAN KREVELEN, D. W. & HOFTYZER, P. J. (1997) *Properties of polymers,* Amsterdam, Elsevier.
VAN OSS, C. J. (1994) *Interfacial forces in aqueous media,* New York, Marcel Dekker.
VAN OSS, C. J., CHADHURY, M. K. & GOOD, R. J. (1987) Monopolar surfaces. *Advances in Colloid and Interface Science,* 28, 35-64.
VERVAET, C. & BYRON, P. R. (1999) Drug-surfactant-propellant interactions in HFA-formulations. *International Journal of Pharmaceutics,* 186, 1999.
VERVAET, C. & BYRON, P. R. (2000) Polystyrene microsphere spray standards based on CFC-free inhaler technology. *Journal of aerosol medicine,* 13, 105-115.
VOELKEL, A., STRZEMIECKA, B., ADAMSKA, K. & MILCZEWSKA, K. (2009) Inverse gas chromatography as a source of physiochemical data. *Journal of Chromatography A,* 1216, 1551-1566.
WILLIAMS, R. O., ROGERS, T. L. & LIU, J. (1999) Study of solubility of steroids in hydrofluoroalkane propellants. *Drug development and industrial pharmacy,* 25, 1227-1234.
WOLFF, V., PERWUELZ, A., ELACHARI, A. & CAZE, C. (1999) Determination of surface heterogeneity by contact angle measurements on glassfibres coated with different sizings. *Journal of Materials Science,* 34, 3821-3829.

WORLD HEALTH ORGANIZATION (2008a) Asthma, fact sheet N°307. http://www.who.int/mediacentre/factsheets/fs307/en/print.html.

WORLD HEALTH ORGANIZATION (2008b) Chronic obstructive pulmonary disease (COPD), fact sheet N°315. IN ORGANIZATION, W. H. (Ed.), http://www.who.int/mediacentre/factsheets/fs315/en/print.html.

WU, L., AL-HAYDARI, M. & DAROCHA, S. R. P. (2008a) Novel propellant-driven inhalation formulations: engineering polar drug particles with surface-trapped hydrofluoroalkane-philes. *European Journal of Pharmaceutical Sciences,* 33, 146-158.

WU, L., BHARATWAJ, B., PANYAM, J. & DAROCHA, S. R. P. (2008b) Core-shell particles for the dispersion of small polar drugs and biomolecules in hydrofluoroalkane propellants. *Pharmaceutical Research,* 25, 289-301.

WU, S. (1982) *Polymer interface and adhesion,* New York, Marcel Dekker Inc.

YIN, S. X., FRANCHINI, M., CHEN, J., HSIEH, A., JEN, S., LEE, T., HUSSAIN, M. & SMITH, R. (2005) Bioavailability enhancement of a COX-2 inhibitor, BMS-347070, from a nanocrystalline dispersion prepared by spray-drying. *Journal of Pharmaceutical Sciences,* 94, 1598-1607.

YOUNG, P. M., PRICE, R., LEWIS, D., EDGE, S. & TRAINI, D. (2003) Under pressure: predicting pressurized metered dose inhaler interactions using the atomic force microscope. *Journal of Colloid and Interface Science,* 262, 298-302.

YOUNG, P. M., PRICE, R., TOBYN, M. J., BUTTRUM, M. & DEY, F. (2004) The influence of relative humidity on the cohesion properties of micronized drugs used in inhalation therapy. *Journal of Pharmaceutical Sciences.*

YOUNG, P. M., TOBYN, M. J., PRICE, R., BUTTRUM, M. & DEY, F. (2006) The use of colloid probe microscopy to predict aerosolization performance in dry powder inhalers: AFM and in vitro correlation. *Journal of Pharmaceutical Sciences,* 95, 1800-1809.

YOUNG, T. (1805) An essay on the cohesion of fluids. *Philosophical Transactions of the Royal Society of London A,* 95, 65-87.

ZENG, X. M., MARTIN, G. P. & MARRIOTT, C. (2001) *Particulate interactions in dry powder formulations for inhalation,* London, Informa Healthcare.

ZHOU, H., GÖTZINGER, M. & PEUKERT, W. (2003) The influence of particle charge and roughness on particle–substrate adhesion. *Powder Technology,* 135-136, 82-91.